

Enhancement of the REMix energy system model: Global renewable energy potentials, optimized power plant siting and scenario validation

A thesis accepted by the
Faculty of Energy-, Process- and Bio-Engineering of the
University of Stuttgart
in partial fulfillment of the requirements for the degree of
Doctor of Engineering Sciences (Dr.-Ing.)

by

Daniel Stetter

born in Heidelberg, Germany

First examiner: Prof. Dr.-Ing. habil. DEng/Auckland Hans Müller-Steinhagen

Second examiner: Prof. Dr.-Ing. Alfred Voß

Date of defence: April 10th, 2014

Institute of Thermodynamics and Thermal Engineering
University of Stuttgart

2012

Eines von Papas Lieblingsgedichten:

In Hamburg wohnten zwei Ameisen,
die wollten nach Australien reisen.

In Altona auf der Chaussée,
taten ihnen die Füße weh.

Und so verzichteten sie weise
auf den letzten Teil der Reise.

(Joachim Ringelnatz)

Danksagung

Die vorliegende Dissertation wurde während meiner Tätigkeit als wissenschaftlicher Mitarbeiter am Deutschen Zentrum für Luft- und Raumfahrt Stuttgart und Gastwissenschaftler an der Ecole Nationale Supérieure des Mines de Paris im Zeitraum zwischen 2009 und 2012 angefertigt. Durch vom Umweltbundesamt und Bundesumweltministerium wie auch der EU-Kommission geförderte Projekte war die Finanzierung der Arbeit gesichert und in die wissenschaftliche Community durch die Mitarbeit unter anderem an den Projekten "Weltweites GIS-gestütztes Inventar erneuerbarer Energieressourcen in räumlicher und zeitlicher Auflösung", "EU-EnerGEO", "EU-Endorse" und "EU-ADVANCE" eingebettet. Teile der in dieser Dissertation vorgestellten Ergebnisse basieren auf Beiträgen zu diesen Projekten und sind entsprechend gekennzeichnet. An dieser Stelle möchte ich all jenen meinen herzlichen Dank aussprechen, die zum Gelingen des Projekts "Promotion" beigetragen haben.

Zunächst gilt mein aufrechter Dank meinem Doktorvater Prof. Hans Müller-Steinhagen für die vertrauensvolle Unterstützung, akademische Betreuung, Durchsicht und Begutachtung der Arbeit. Weiterhin danke ich Prof. Jürgen Schmid für sein herzliches Engagement und die Bereitschaft den Zweitbericht für die Arbeit zu übernehmen. Zu meinem großen Bedauern konnte er die Abgabe und Verteidigung der Arbeit nicht mehr erleben. An seiner Stelle konnte ich sehr kurzfristig Prof. Alfred Voß für den Mitbericht der Arbeit gewinnen, für seine spontane Hilfsbereitschaft bedanke ich mich herzlich.

Dr. Wolfram Krewitt danke ich für die Vergabe der Arbeit und Betreuung, die durch seinen viel zu frühen Tod abrupt endete. Seine sehr freundliche, unaufgeregte und professionelle Art wie auch seine weitreichende Expertise bleiben mir in besonderer Erinnerung.

Dr. Christoph Schillings und Dr. Franz Trieb danke ich herzlich sowohl für die sehr angenehme, kollegiale wissenschaftliche Begleitung, als auch für die immerwährende Bereitschaft des sich Zeitnehmens um Fragen aller Art kompetent zu beantworten.

Meiner geschätzten Kollegin Kristina Nienhaus gilt mein besonderer Dank für Hilfe und Unterstützung besonders in der Strukturierungsphase der Promotion. Carsten Hoyer-Klick danke ich für die Hilfsbereitschaft bei jeglichen Fragestellungen hinsichtlich der Prozessierung von Solardaten wie auch der Unterstützung bei der Vorbereitung von Gastaufenthalten am National Renewable Energy Laboratory und der Ecole Nationale Supérieure des Mines de Paris. Eva-Maria Ast danke ich für die Beantwortung unzähliger administrativer Fragen und ihre jederzeit großzügige Unterstützung.

Dr. Dominik Heide gilt mein besonderer Dank für zahlreiche Diskussionen und äußerst wertvolle Beiträge, unter anderem der Unterstützung bei Modellierungsarbeiten für REMix wie auch die Einführung in \LaTeX , unzählige heitere Stunden am DLR und darüber hinaus. In die vorliegende Arbeit flossen des Weiteren viele frische Ideen

meiner ehemaligen Praktikanten und Diplomanden Marco Caffisch, Andrea Weidenfeld, Celia Moreno, Felix Jander und Florian Werner wie auch unseres engagierten Hilfswissenschaftlers Denis Hess ein.

Allen weiteren Kollegen der Abteilung Systemanalyse und Technikbewertung danke ich ebenfalls für die sehr angenehme und familiäre Arbeitsatmosphäre.

Meinen Gastgebern der Ecole Nationale Supérieure des Mines de Paris, besonders Dr. Philippe Blanc, Dr. Bella Espinar und Prof. Lucien Wald, danke ich für die professionelle und sehr freundschaftliche Aufnahme in ihre Arbeitsgruppe wie auch unzählige wissenschaftliche Beiträge und das Aufzeigen neuer Lösungsansätze sowohl zur Prozessierung von Daten der direkten Solarstrahlung als auch zur Untersuchung von Portfolioeffekten volatiler Erzeugung.

Dr. David Renné und Patrick Sullivan des US-amerikanischen National Renewable Energy Laboratory und Prof. Luis Vargas der Universidad de Chile danke ich für die Ermöglichung von Kurzaufenthalten in den Jahren 2008 und 2010 sowie viele interessante Diskussionen und Einblicke beim Thema Solarstrahlung und Energiesystemmodellierung.

In unkomplizierter Weise haben des Weiteren unter anderem Dr. Paul Stackhouse von der National Aeronautics and Space Agency (NASA SRB Daten) und Prof. Petra Döll von der Goethe-Universität Frankfurt (Volumenströme Wasser) Satelliten- und Bodenstationsdaten für das Ressourcenarchiv bzw. Hinweise zu dessen Interpretation zur Verfügung gestellt und weitere Hintergrundinformationen geliefert: Mein besonderer Dank an sie und ihre Arbeitsgruppen.

Abschließend danke ich meiner Familie für die kontinuierliche Unterstützung und Hilfsbereitschaft, die sie mir zu Teil kommen lassen, besonders meinem Bruder Klaus mit Familie, Catherine mit Familie wie auch meinen Schwiegereltern, die in der heißen Abschlussphase durch Ihre spontane, unermüdliche und offenherzige Unterstützung entscheidend den Abschluss der Arbeit ermöglichten.

Mein größter Dank gilt meiner Frau Christine und unseren wundervollen Kindern, für Ihre großzügige Unterstützung zu jeder Zeit und Verständnis, wenn Papa nochmal an der Doktorarbeit etwas ändern musste....

Stuttgart, im Dezember 2012

This document was printed using L^AT_EX.

Abstract

Against the background of depleting fossil resources and strongly desired cuts on CO₂ emissions to mitigate global temperature rise the use of renewable energy conversion technologies is of ever increasing interest for decision makers around the globe. To provide an improved assessment of both technically and economically feasible contributions of these technologies a detailed analysis of the major renewable resources is required. As electricity generation based on these sources is subject to fluctuations, data with high temporal and spatial resolution on their availability is indispensable for integrating large shares of renewable capacities into energy infrastructures.

The original release of the energy system model REMix [Sch12], an abbreviation for Renewable Energy Mix, is capable of performing both renewable energy potential assessments for Europe and simulations of green-field European energy supply systems. The scope of the present doctoral thesis is to enhance the existing modelling environment in terms of

- (i.) extending the geographic coverage of the resources database from a European to a global scale resulting in the new, globally applicable potential assessment tool REMix-EnDaT ("Energy Data Tool"),
- (ii.) adding the plant siting optimization module REMix-PlaSMo, capable of assessing siting effects of renewable power plants on the portfolio output and
- (iii.) adding a new alternating current power transmission model between 30 European countries and CSP¹ electricity imports from power plants located in North Africa and the Middle East via high voltage direct current links to the optimization module REMix-OptiMo ("Optimization module").

With respect to the global potential assessment tool REMix-EnDaT, a thorough investigation is carried out creating an hourly global inventory of the theoretical potentials of the major renewable resources solar irradiance, wind speed and river discharge at a spatial resolution of 0.45°x0.45°². A detailed global land use analysis determines eligible sites for the installation of the corresponding conversion technologies, such as photovoltaic modules on roof tops, concentrating solar power plants in deserts or wind turbines onshore and offshore.

¹CSP: Concentrating Solar Power

²This corresponds to some 50x50 km² at the equator with decreasing grid box sizes as the poles are approached.

In order to relate the theoretical resource potentials to technically feasible power output in a bottom-up approach³, sufficiently detailed power plant models are implemented. The latter allow for the assessment of power output, cost per kWh and respective full load hours taking into account the theoretical potentials, technological as well as economic data.

All of the aforementioned steps are successively implemented into REMix-EnDaT. It is capable of determining the discussed parameters for arbitrary locations around the globe, bearing in mind the restrictions imposed by the spatial resolution of the land use and the resources data. The scope of the global potential assessment tool REMix-EnDaT is twofold:

First, as an assessment tool for arbitrary geographic locations, countries or world regions, deriving either site-specific or aggregated installable capacities, cost as well as full load hour potentials. Second, as a tool providing input data such as installable capacities and hourly renewable electricity generation for further assessments using REMix-PlaSMo and REMix-OptiMo.

The plant siting module tool REMix-PlaSMo yields results as to where the volatile power technologies photovoltaics and wind are to be located within a country in order to gain distinct effects on the aggregated power output. Three different modes are implemented: (a.) Optimized plant siting in order to obtain the cheapest generation cost, (b.) a minimization of the photovoltaic and wind portfolio output variance and (c.) a minimization of the residual load variance. Input data such as installable capacities and hourly power generation data for photovoltaics and wind are provided by the module REMix-EnDaT.

The third fundamental addition to the REMix model within this work is the amendment of the module REMix-OptiMo with a new power transmission model based on the direct current approximation of the alternating current power flow. Moreover, electricity imports originating from concentrating solar power plants located in North Africa and the Middle East are now feasible.

All of the new capabilities and extensions of the original release of the REMix model as summarized above are used and tested in three case studies as follows:

In case study 1, using the module REMix-EnDaT, a global potential assessment is carried out for 10 OECD world regions, deriving installable capacities, cost and full load hours for PV, CSP, wind and hydro power. According to the latter, photovoltaics will represent the cheapest technology in 2050, an average of 1634 full load hours could lead to an electricity generation potential of some 5500 PWh. Although CSP also taps solar irradiance, restrictions in terms of suitable sites for erecting power plants are more severe. For that reason, the maximum potential amounts to some 1500 PWh. However, thermal energy storage can be used, which, according to this assessment, could lead to 5400 hours of full load operation. Onshore wind power could tap a potential of 717 PWh by 2050 with an average of 2200 full load hours while offshore, wind power plants could achieve a total power generation of 224 PWh with an average of 3000 full load hours. The electricity generation potential of hydro power exceeds 3 PWh, 4600 full load hours of operation are reached on average. All results of the potential assessment case study are presented and discussed using graphs and maps.

³In this type of information processing, the information available in sub-systems is grouped and computed to obtain results for the parent system.

In case study 2, using the module REMix-PlaSMo, an assessment for Morocco is carried out as to determine limits of volatile power generation in portfolios approaching full supply based on renewable power. The volatile generation technologies are strategically sited at specific locations to take advantage of available resources conditions. It could be shown that the cost optimal share of volatile power generation using photovoltaic and wind power without considering storage or transmission grid extensions is one third. Moreover, the average power generation cost using a portfolio consisting of PV, CSP, wind and hydro power can be stabilized at about 10 $\frac{\text{€ct}}{\text{kWh}}$ by the year 2050.

In case study 3, using the module REMix-OptiMo, a validation of a scenario based upon an updated framework of TRANS-CSP⁴ [TSK⁺06] is carried out. The original release of TRANS-CSP is updated with more recent figures on electricity supply and demand until 2010 and a new demand projection until 2050. This updated scenario framework is then validated using REMix-OptiMo. Hourly electricity generation potentials are provided by REMix-EnDaT. The optimization is carried out on an hourly basis with respect to minimizing the overall system cost, thereby investigating if the scenario predictions hold under the precondition that electricity production is to meet the demand at all times during one investigated year. This reevaluation is intended to assess the scientific significance of the updated TRANS-CSP scenario framework. It could be shown, that the assumed load can safely be met in all countries for each hour using the scenario's power plant portfolio. Furthermore, it was proven that dispatchable renewable power generation, in particular CSP imports to Europe, have a system stabilizing effect. Using the suggested concept, the utilization of the transfer capacities between countries would decrease until 2050.

⁴TRANS-CSP assesses both renewable electricity potentials in 30 European countries and feasible contributions of renewable electricity imports provided by concentrating solar power plants in North Africa and the Middle East. Economic and social impacts are also highlighted.

Zusammenfassung

Vor dem Hintergrund der Verknappung fossiler Ressourcen und notwendiger Reduktionen der CO₂ Emissionen um einen globalen Temperaturanstieg abzumildern, kommt die Nutzung erneuerbarer Energien weltweit zunehmend in den Interessenfokus von Entscheidungsträgern. Zur Ermöglichung einer verbesserten Untersuchung technisch und ökonomisch umsetzbarer Beiträge dieser Technologien ist eine tiefgreifende Analyse der wichtigsten erneuerbaren Ressourcen von herausragender Bedeutung. Da die Elektrizitätserzeugung auf der Grundlage dieser Ressourcen fluktuierender Natur ist, sind sowohl räumlich wie zeitlich aufgelöste Daten hinsichtlich ihrer Verfügbarkeit unerlässliche Voraussetzung zur Einbindung signifikanter Anteile erneuerbarer Kraftwerkskapazitäten in Energieversorgungsinfrastrukturen.

Die Originalversion des Energiemodells REMix [Sch12], einer Abkürzung für "Renewable Energy Mix" - also der "Versorgungsmix mit erneuerbaren Energien", ermöglicht sowohl die Durchführung von Potenzialuntersuchungen von erneuerbaren Energien auf Europäischer Ebene als auch Simulation von gesamteuropäischen Energieversorgungssystemen basierend auf einem "grüne Wiese" Ansatz. Hauptziele der vorliegenden Dissertation liegen in der Weiterentwicklung der existierenden Modellumgebung hinsichtlich

- (i.) der Erweiterung der geografischen Abdeckung der Ressourcendatenbank von Europäischer hin zu globaler Ebene, resultierend in dem neuen, global anwendbaren Potentialanalysewerkzeug REMix-EnDaT ("Energy Data Tool" - Werkzeug zur Prozessierung energierelevanter Daten)
- (ii.) der Neuentwicklung des Kraftwerksstandortoptimierungswerkzeugs REMix-PlaSMo ("Plant Siting Module" - Kraftwerksstandortoptimierungsmodul), welches in der Lage ist, Effekte der Kraftwerksstandorte auf die Erzeugung des Gesamtportfolios zu untersuchen
- (iii.) des neuen Energieübertragungsmodells zwischen 30 Europäischen Ländern sowie CSP⁵ Elektrizitätsimporten mittels Hochspannungs-Gleichstrom-Übertragung von Kraftwerken in Nordafrika und dem Nahen Osten im Rahmen des Moduls REMix-OptiMo ("Optimization Module" - Optimierungsmodul)

Für das globale Potentialanalysewerkzeug REMix-EnDaT wird auf Basis einer umfassenden Untersuchung ein stündliches globales Inventar der theoretischen Potenziale der wichtigsten erneuerbaren Ressourcen Solarstrahlung, Wind und Volumenabflüsse in einer räumlichen Auflösung von $0.45^\circ \times 0.45^\circ$ ⁶ erstellt.

⁵CSP: Concentrating Solar Power - Solarthermisches Kraftwerk

⁶Dies entspricht in etwa $50 \times 50 \text{ km}^2$ in Höhe des Äquators mit abnehmenden Zellengrößen hin zu den Erdpolen.

Eine detaillierte Landnutzungsanalyse bestimmt nutzbare Flächen zur Installation der entsprechenden Technologien, wie etwa der Photovoltaik auf Dachflächen, solarthermischer Kraftwerke in Wüsten oder Windturbinen auf dem Festland sowie auf hoher See. Um die theoretischen Ressourcenpotenziale mit technisch machbarer Stromerzeugung in Verbindung zu bringen, kommen bottom-up Kraftwerksmodelle zur Anwendung. Diese ermöglichen Untersuchungen der Stromerzeugung, der auftretenden Kosten pro kWh und der damit einhergehenden Volllaststunden unter Einbezug der theoretischen Potenziale, technischer wie auch ökonomischer Daten.

Die zuvor genannten Arbeitsschritte werden sukzessive in das Modul REMix-EnDaT implementiert, welches die eingeführten Größen für beliebige Orte weltweit unter Berücksichtigung der durch die räumliche Auflösung der Landnutzungs- und Ressourcendaten auferlegten Restriktionen bestimmen kann. Das global operable Potenzialanalysewerkzeug REMix-EnDaT verfolgt dabei zweierlei Ziele:

Erstens, die Bereitstellung eines Analysewerkzeugs für beliebige geografische Orte, Länder oder Weltregionen, welches entweder ortsspezifisch oder aggregiert installierbare Kapazitäten, Kosten- wie auch Volllaststundenpotenziale erheben kann.

Zweitens, als ein Werkzeug zur Bereitstellung entscheidungsrelevanter Inputdaten wie installierbarer Kraftwerkskapazitäten und stündlicher erneuerbarer Energieerzeugung für weitergehende Analysen mittels der Module REMix-PlaSMo und REMix-OptiMo.

Das Kraftwerksstandortoptimierungsmodul REMix-PlaSMo untersucht an welchen Orten die volatilen Kraftwerkstechnologien Photovoltaik und Windkraft innerhalb eines Landes platziert werden sollten, um gezielt Einfluss auf die Charakteristik der aggregierten Kraftwerkserzeugung nehmen zu können. Drei unterschiedliche Modi sind implementiert: Die Optimierung der Kraftwerksstandortwahl hinsichtlich (a.) des Erreichens der günstigsten Gesamtlösung, (b.) der Minimierung der Varianz der volatilen Kraftwerkserzeugung durch Photovoltaik und Windkraft sowie (c.) der Minimierung der Varianz der Residuallast. Inputdaten wie etwa installierbare Leistungen und stündliche Energieerzeugung für Photovoltaik- und Windanlagen werden durch REMix-EnDaT bereitgestellt.

Die dritte fundamentale und im Rahmen dieser Arbeit hinzugefügte Neuerung in der REMix-Umgebung ist die Weiterentwicklung des Moduls REMix-OptiMo um ein überarbeitetes Stromübertragungsmodell basierend auf der Gleichstromnäherung des Wechselstromflusses. Des Weiteren sind Elektrizitätsimporte aus solarthermischen Kraftwerken in Nordafrika und dem Nahen Osten jetzt möglich.

Die Gesamtheit der zuvor genannten Neuerungen und Weiterentwicklungen von REMix findet in den drei folgenden Fallstudien Anwendung:

In Fallstudie 1 wird basierend auf dem Modul REMix-EnDaT eine globale Potenzialanalyse für 10 OECD Weltregionen durchgeführt, wobei installierbare Kraftwerkskapazitäten, Kosten und Volllaststunden für PV, CSP, Wind- und Wasserkraft bestimmt werden. Danach wird die Photovoltaik im Jahr 2050 die preisgünstigste Technologie darstellen und in dieser Hinsicht auch vor der Windkraft liegen. Mit durchschnittlich 1634 Volllaststunden könnten rund 5500 PWh an Elektrizitätserzeugungspotenzial durch die Photovoltaik gehoben werden. Obwohl CSP Kraftwerke auch Solarstrahlung nutzen, existieren hinsichtlich ihrer Einsatzorte schärfere Restriktionen. Daher liegt das maximale Potenzial bei rund 1500 PWh, allerdings mit der Option thermischer Energiespeicherung, womit in der Untersuchung knapp 5400 Volllaststunden erreicht werden können.

Die Windkraft stellt onshore im Jahr 2050 ein Potenzial von etwa 717 PWh bei durchschnittlich 2200 Volllaststunden. Offshore Windkraftanlagen erzielen ein Elektrizitätserzeugungspotenzial von 224 PWh bei knapp 3000 Volllaststunden. Das Elektrizitätserzeugungspotenzial der Wasserkraft liegt bei über 3 PWh, wobei durchschnittlich rund 4600 Volllaststunden erreicht werden. Sämtliche Ergebnisse der Potenzialanalyse werden in Form von Schaubildern und Karten präsentiert.

In Fallstudie 2 wird für Marokko eine Untersuchung basierend auf dem Modul REMix-PlaSMo durchgeführt, die das Ziel verfolgt, die Grenzen der volatilen Energieerzeugung in Portfolios mit bis zu 100% erneuerbarer Energie aufzuzeigen. Die volatilen Erzeugungstechnologien werden strategisch platziert, um die vorherrschenden Ressourcenbedingungen optimal ausnutzen zu können um so bestmögliche Ausgleichseffekte zu erzielen. Dabei konnte gezeigt werden, dass der kostenoptimale Anteil volatiler Erzeugung aus Photovoltaik und Wind ohne Berücksichtigung von Speichern und eines potenziellen Netzausbaus bei rund 30% liegt. Außerdem stabilisieren sich die durchschnittlichen Erzeugungskosten eines aus Photovoltaik, CSP, Wind- und Wasserkraft bestehenden Portfolios bei rund $10 \frac{\text{€ct}}{\text{kWh}}$ bis zum Jahr 2050.

In Fallstudie 3 wird mit Hilfe des Moduls REMix-OptiMo die Validierung eines Szenarios basierend auf einem Update des TRANS-CSP⁷ [TSK⁺06] Datengerüsts durchgeführt. Die Originalausgabe von TRANS-CSP wird mit neueren Daten aus dem Jahr 2010 hinsichtlich der Versorgung mit und Nachfrage nach Elektrizität wie auch einer Nachfrageprognose bis zum Jahr 2050 aktualisiert. Dieses verbesserte Szenariengerüst wird mittels REMix-OptiMo validiert. Stündliche Zeitreihen der Elektrizitätserzeugung werden durch REMix-EnDaT bereitgestellt. Die Optimierung wird auf Basis stündlicher Zeitschritte unter der Bedingung der Kostenminimierung des Gesamtsystems durchgeführt, wobei untersucht wird, ob die Szenariovorhersagen eine stündliche Lastdeckung ohne Versorgungsausfall für ein gesamtes untersuchtes Jahr gewährleisten können. Diese Reevaluation soll die wissenschaftliche Aussagekraft des aktualisierten TRANS-CSP Szenariengerüsts überprüfen. Es konnte dabei gezeigt werden, dass die angenommene Last in allen Ländern zu jeder Stunde mittels des im Szenario vorgegebenen Kraftwerksportfolios gedeckt werden kann. Die gesamtsystemstabilisierende Funktion regelbarer erneuerbarer Energie, insbesondere von CSP Importen nach Europa, konnte bewiesen werden. Bei Nutzung dieses Konzepts würde sich die Auslastung der Grenzkuppelleistungen bis zum Jahr 2050 verringern.

⁷TRANS-CSP untersucht sowohl Elektrizitätserzeugungspotenziale in 30 Europäischen Ländern als auch umsetzbare Beiträge erneuerbarer Elektrizitätsimporte von solarthermischen Kraftwerken Nordafrikas und des Nahen Ostens. Ökonomische wie auch soziale Einflüsse werden ebenfalls beleuchtet.

Acronyms

AC	Alternating Current
AM	Air Mass
AP	Application
BHI	Beam Horizontal Irradiance
BNI	Beam Normal Irradiance
BSRN	Baseline Surface Radiation Network
CIA	Central Intelligence Agency
CO ₂	Carbon Dioxide
CSP	Concentrating Solar Power
DC	Direct Current
DHI	Diffuse Horizontal Irradiance
ECMWF	European Centre for Medium-Range Weather Forecasts
EnDaT	Energy Data Tool
ENTSO-e	European Network of Transmission System Operators for Electricity
EUMENA	Europe - Middle East - North Africa
FLH	Full load hours
GAMS	General Algebraic Modeling System
GDP	Gross Domestic Product
GHI	Global Horizontal Irradiance
GIS	Geographic Information System
HVDC	High Voltage Direct Current
IEA	International Energy Agency
ISIS	Irradiance at the surface derived from ISCCP cloud data
MENA	Middle East - North Africa
MERRA	Modern Era Retrospective Analysis for Research and Applications
MESOR	Management and Exploitation of Solar Resource Knowledge
MS	Milestone

NASA	National Aeronautics and Space Agency
NREAP	National Renewable Energy Allocation Plans
O&M	Operation & Maintenance
OECD	Organisation for Economic Cooperation and Development
OptiMo	Optimization Module
PlaSMo	Plant Siting Optimization Module
PV	Photovoltaics
REMix	Renewable Energy Mix
RMSD	Root Mean Squared Deviation
SM	Solar Multiple
SOLEMI	Solar Energy Mining
SRB	Surface Radiation Budget
SRU	Sachverständigenrat für Umweltfragen
SSE	Surface Meteorology and Solar Energy
TMY	Typical Meteorological Year
TRANS-CSP	Trans-Mediterranean Interconnection for Concentrating Solar Power
WEC	World Energy Council
WEO	World Energy Outlook
WEPP	World Electric Power Plants database
WRF	Weather Research and Forecasting

Symbols

a_i, b_i and c_i	$[-]$	PlaSMo installation coefficients
$a_{p,n}$	$[\text{€}]$	annuity
$A_{c,i}$	$\left[\frac{\text{km}^2}{\text{c}\cdot i}\right]$	suitable area per capita c and country i
A_i	$[\text{km}^2]$	area of pixel i
$AF_{p,n}$	$[-]$	annuity factor
B	$[S]$	susceptance
csi	$[-]$	clear sky index
$C_i^{tech, gen}$	$\left[\frac{\text{€ct}}{\text{kWh}}\right]$	generation cost per technology and grid box i
$C_{spec}^{tech, inv}$	$\left[\frac{\text{€}}{\text{kW}}\right]$	specific investment cost per capacity
$C_{spec}^{tech, op}$	$\left[\frac{\text{€}}{\text{kW}}\right]$	specific operational cost per capacity
C_0	$[\text{€}]$	capital value of an investment
$C_{total}^{tech, annual, i}$	$[\text{€}]$	total annual cost per grid box i
Cov	$[-]$	covariance
d_{rotor}^{wind}	$[m]$	diameter wind turbine
day	$[-]$	day of year
$E_{el}^{tech, annual, i}$	$[MWh_{el}]$	total annual electricity yield per grid cell i
$E_{el, i}^{tech}(t)$	$[MWh_{el}]$	average hourly power plant output per grid cell i
$E_{el}^{Demand}(t)$	$[MWh_{el}]$	power demand
$E_{el}^{Residual}(t)$	$[MWh_{el}]$	residual load
$E_{i,j}^{flow}(t)$	$[MWh_{el}]$	net power flow on the line between two nodes i and j
$E_{solar}^{CSP, field, i}(t)$	$[MWh_{th}]$	hourly solar field heat output per pixel i
f_{av}^{tech}	$[\%]$	availability factor
$flh_{country}^{tech}$	$[h]$	full load hours
$f_{distance}^{wind}$	$[-]$	distance factor wind
f_{loss}^{tech}	$[\%]$	loss factor
$f_{solar}^{CSP, multiple}$	$[-]$	solar multiple
$f_{suitability}$	$[-]$	technology dependent suitability factor
f_{tcd}	$\left[\frac{W}{m^2}\right]$	thermal capacity density factor CSP

f_{total}^{cloud}	$[-]$	total cloud fraction
f_{p2s}	$[h]$	ratio of thermal storage capacity to power block size
f_T^{PV}	$[-]$	temperature factor PV
G	$[S]$	conductance
h_{hub}	$[m]$	hub height above ground of a wind turbine
$I(t)$	$[A]$	sinusoidal currents
I_{BNI}	$[\frac{W}{m^2}]$	beam normal irradiance
$I_{BNI}^{clear\ sky}$	$[\frac{W}{m^2}]$	clear sky beam normal irradiance
I_{DHI}	$[\frac{W}{m^2}]$	diffuse horizontal irradiance
I_{GHI}	$[\frac{W}{m^2}]$	global horizontal irradiance
$I_{GHI}^{clear\ sky}$	$[\frac{W}{m^2}]$	clear sky global horizontal irradiance
I_{GHI}^{toa}	$[\frac{W}{m^2}]$	horizontal component of the irradiance at the top of the atmosphere
$I_{module,i}^{PV}(t)$	$[\frac{W}{m^2}]$	hourly average irradiance on the PV module for grid cell i
$I_{normal,i}^{trough}$	$[\frac{W}{m^2}]$	normal irradiance on the CSP trough for grid cell i
I_{toa}	$[\frac{W}{m^2}]$	average extraterrestrial radiation
I_{sc}	$[\frac{W}{m^2}]$	solar constant
k	$[-]$	diffuse fraction
$k_{extinction}$	$[-]$	extinction coefficient
k_t	$[-]$	clearness index
m	$[-]$	height corrected optical mass
n	$[a]$	depreciation period
p	$[\%]$	interest rate
$p_{area}^{tech, inst}$	$[\frac{W_{el}}{m^2}]$	area-specific installable capacity
P	$[W]$	average power
$P_i^{tech, inst}$	$[MW_{el}]$	installed capacity at grid box i
$P_i^{tech, inst_max}$	$[MW_{el}]$	maximum installable capacity for each grid box i
$P_{mod,i}^{tech, inst}$	$[MW_{el}]$	modernized installed capacity at grid box i
$P_{new,i}^{tech, inst}$	$[MW_{el}]$	new installed capacity at grid box i
$P_{nominal}^{wind}$	$[MW_{el}]$	nominal capacity wind turbine

q^{PV}	[%]	q-factor PV
Q_{sf}	[W_{th}]	effective heat output of the CSP solar field at standard testing conditions
Q	[W]	reactive power
r	[m]	radius
$T_{node}^{tech, normed}(t)$	[MWh]	input time series normed to one MWh
T_{sun}	[K]	temperature at the sun's surface
$U(t)$	[V]	sinusoidal voltages
$v_{resulting}^{wind}(h_{hub})$	[$\frac{m}{s}$]	resulting wind speed
v_{u-wind}, v_{v-wind}	[$\frac{m}{s}$]	u- and v-directed wind velocities
$X_{technical, country}$	[TWh]	country specific technical potential
Y	[$\frac{1}{\Omega}$]	complex admittance
z_0	[m]	surface roughness length
η^{tech}	[%]	technology specific efficiency
ϵ_{solar}	[—]	solar excentricity factor
ω	[Hz]	frequency
$\phi_{module, i}^{PV}(t)$	[K]	hourly ambient temperature PV module
ϕ_{STC}^{PV}	[K]	PV module temperature at standard testing conditions
$\phi_{U, I}$	[—]	phase
ρ	[$\frac{kg}{m^3}$]	density of air
σ^2	[—]	standard expression for the variance
τ_z	[—]	optical thickness of the atmosphere
\underline{S}	[W]	complex power
φ	[o]	difference between the current's and the voltage's phases

Contents

1. Introduction and Outline	1
1.1. Motivation	1
1.2. Major goals and structure of this work	2
2. Review and structure of the energy modeling environment REMix	7
2.1. Model development history	7
2.2. Enhancements within this work	10
3. REMix-EnDaT: Model enhancements and application in a global potentials study	13
3.1. Outline	13
3.2. Overall structure of and enhancements to REMix-EnDaT	14
3.2.1. Global land use assessment to identify installable capacities for power plant installations	14
3.2.1.1. Suitable sites	16
3.2.1.2. Suitable areas	18
3.2.1.3. Area-specific installable capacities	20
3.2.1.4. Installable capacities	21
3.2.2. Setting up a global inventory of renewable resources	22
3.2.2.1. Solar Irradiance	23
3.2.2.1.1. Available data on GHI and BNI	23
3.2.2.1.2. Processing of Global Horizontal Irradiance	24
3.2.2.1.3. Processing of Beam Normal Irradiance	29
3.2.2.2. Wind	39
3.2.2.2.1. Available data on wind	39
3.2.2.2.2. Wind speed processing	40
3.2.2.3. River run-off	42
3.2.2.3.1. Considered run-off data sets and data processing	42
3.2.3. Power plant technology modeling	44

3.3.	Application of REMix-EnDaT: Global assessment of renewable energy potentials	48
3.3.1.	Further background	48
3.3.1.1.	Potential definitions	48
3.3.1.1.1.	From capital budgeting to generation cost and cost potentials	50
3.3.1.1.2.	From annual electricity yield and installed capacities to full load hours	53
3.3.1.2.	Determination of a typical meteorological year	53
3.3.1.3.	Impact of the layout of CSP plants with different solar multiples on the full load hours	56
3.3.2.	Results	58
3.3.2.1.	Full load hour and cost potentials	58
3.3.2.2.	Sensitivity Analysis	70
3.4.	Discussion	74
3.4.1.	Accuracy of the resources data	74
3.4.1.1.	General remarks	74
3.4.1.2.	Impact of the spatial resolution	75
3.4.2.	Evaluation of the global potential assessment's results	78
3.4.2.1.	General remarks	78
3.4.2.2.	Areas of improvement	78
4.	REMix-PlaSMo: Overall structure and study on portfolio effects of volatile generation	81
4.1.	Outline	81
4.1.1.	Motivation and goals	81
4.1.2.	Approach	83
4.2.	Algebraic formulation	84
4.3.	Application of REMix-PlaSMo: Assessment of portfolio effects in Morocco	89
4.3.1.	Setup of the optimization	89
4.3.2.	Results	93
4.3.2.1.	Overall cost	93
4.3.2.2.	Discussion on the top performing optimization modes	97
4.3.3.	Summary	100

5. REMix-OptiMo: Enhancements and application in a scenario validation study	105
5.1. Overview on REMix-OptiMo	105
5.2. Enhancing REMix-OptiMo: A new power transmission model	107
5.3. Application of REMix-OptiMo:	
Validation of an updated TRANS-CSP scenario	112
5.3.1. Approach and major outcomes of the new TRANS-CSP scenarios	112
5.3.2. Configuration of REMix-OptiMo for the validation simulations . .	115
5.3.2.1. Installed capacities, power generation, load and trans-	
mission	115
5.3.2.2. Integration of CSP power from North African sites via	
HVDC links	119
5.3.2.3. Optimization process and objective	122
5.3.3. Simulation results	124
5.4. Summary	136
6. Key results, concluding remarks and outlook	137
Bibliography	141
A. Annex	157
A.1. Physical principles of solar irradiance	157
A.2. Global potential assessment in terms of 10 OECD regions	161
A.3. Setup and major outcomes of the original TRANS-CSP release	173
A.4. REMix-OptiMo equations and boundary conditions used in this work . .	179
A.5. ENTSO-e net transfer capacities	191
A.6. Model parameters for HVDC transmission from MENA to Europe	193
A.7. Parameter discussion	195
List of Figures	203
List of Tables	213

1. Introduction and Outline

1.1. Motivation

An ever increasing demand for energy since the beginning of the industrial revolution until today has so far primarily been met by fossil energy vectors and uranium. Their advantages are obvious: easy transport at normal pressure and ambient temperatures, up until nowadays comparatively cheap access and eligibility for instantaneous energy conversion on demand due to ideally chemically stored and thus extremely precious forms of energy. However, political tensions due to depleting fossil resources triggering soaring prices in conjunction with expected sharp increases of power demand, increasing risks caused by anthropogenic climate change and the technological maturity of renewable energy technologies are leading to a steeply rising interest in sustainable energy resources as well as state of the art research for sustainable future energy supply systems. In order to provide a scientifically based framework for decision makers concerned with feasible transition paths towards low-carbon energy systems, both scenario development and energy system modelling are key factors and of major importance in contemporary energy research. Input parameters to energy system assessments influencing their quality and significance such as cost and technology specific figures, and resources data in particular, are the predominant factors to obtain accurate results.

Although available globally, data on the availability of the major renewable resources solar irradiance, windspeed and river run-off has not yet been presented in one single consistent potential tool with complementary temporal and spatial resolutions, thereby making it accessible to site, country or region-specific assessments operable on a global scale. Such a tool is capable of delivering enhanced analyses on renewable technology potentials as desired e.g. in order to broaden the knowledge foundation for regional and global energy scenarios or incentive programs. Since renewable power generation is subject to volatile spatial and temporal availability, the potential assessment can be improved by using

- (i.) data with high temporal and spatial resolution,
- (ii.) bottom-up technology models,
- (iii.) optimized power plant siting in order to profit from portfolio effects and
- (iv.) energy system models eligible of simulating the effects of fluctuations, transport and storage.

Each of the former aspects are taken into account in this work and are elaborated in the following sections.

1.2. Major goals and structure of this work

Against the aforementioned background within this thesis the original release of the energy modelling suite REMix, an abbreviation for Renewable Energy Mix, developed by Yvonne Scholz within her PhD thesis [Sch12] and amended by Luca de Tena in his ongoing PhD thesis [Ten12], is further enhanced. Three major innovations partly interacting with each other are added, in turn significantly improving the capabilities of the model as a whole:

First, the establishment of a flexible globally applicable tool both for the determination of renewable energy potentials and for the provision of hourly power generation time series for selected renewable power plants is intended. Within the REMix model this module is called REMix-EnDaT (Energy Data Tool). Considered technologies comprise photovoltaic¹, concentrating solar thermal power², wind on- and offshore and hydro power. All technologies but hydro power are modelled employing a bottom-up approach and build upon an extensive, spatially resolved and hourly resources inventory for solar irradiance, windspeed and river discharge. These resources data are derived from various sources indicated and discussed separately. Interpolations are performed where necessary to obtain the intended format. The processed data has a spatial resolution of $0.45^\circ \times 0.45^\circ$, corresponding to some $50 \times 50 \text{ km}^2$ at the equator. Solar irradiance and wind speeds are incorporated with a temporal resolution of one hour, comprising a time frame from 1984 through 2005, monthly means interpolated to hourly values are implemented for river discharge. On the one hand, this framework is used independently as a tool for the assessment of theoretical, technical, cost and full load hour potentials. On the other hand it is capable of providing input data for additional analysis steps using two further modules of the REMix modelling suite, REMix-PlaSMo (Plant Siting Module) and REMix-OptiMo (Optimization Module).

REMix-PlaSMo is an optimization tool at country level capable of identifying best sites for volatile renewable power plant installation for three optimization modes: Least cost of the portfolio, portfolio output variance minimization and residual load variance minimization. It is a completely new feature of the REMix energy modelling suite, added within the framework of this thesis.

Finally REMix-OptiMo, the energy system optimization tool, is enhanced in terms of adding both a new alternating current³ transmission model for power flows between countries and the option of importing electricity from CSP plants located in North African and Middle Eastern countries via high voltage direct current links. For both REMix-PlaSMo and REMix-OptiMo, input data on installable capacities and hourly electricity generation potentials can be provided by REMix-EnDaT. The two enhanced tools REMix-EnDaT and REMix-OptiMo and the new development REMix-PlaSMo are employed in case studies as follows: REMix-EnDaT is used for a global potential

¹Photovoltaic: Hereafter referred to as PV.

²Concentrating solar power: Hereafter referred to as CSP.

³Alternating current: Hereafter referred to as AC.

assessment⁴ of PV, CSP, wind and hydro power. REMix-PlaSMo is employed for a case study on portfolio effects in Morocco. REMix-OptiMo is finally used within a validation of a new scenario for 30 European countries based upon an update of the TRANS-CSP⁵ [TSK⁺06] framework.

Overall, the following milestones summarize the intended work load for this doctoral thesis, an overview is given in figure 1.1 along with the respective chapters where the approaches for and results of these milestones are presented and discussed:

- MS 1. Global land use analysis to identify suitable sites for the installation of renewable energy power plants.
- MS 2. Creation of a global hourly database containing spatially and temporally resolved information on the renewable energy resources solar irradiance, wind and river runoff on a 0.45° spatial grid.
- MS 3. Enhancement of the original release of REMix-EnDaT by developing a globally applicable tool capable of determining installable capacities, hourly power generation, full load hours and cost potentials.
- MS 4. Development of the new REMix module PlaSMo, capable of optimizing power plant siting within a country or region of interest. Three different assessment modes are implemented.
- MS 5. Enhancement of the original release of REMix-OptiMo⁶ by adding a new power transmission model and enabling electricity imports via high voltage links.
- MS 6. Implementation of CSP electricity imports via high voltage direct current links from North African and Middle Eastern countries to Europe.

After the methodological work in milestones MS 1 through MS 6, the enhanced REMix modules EnDaT and OptiMo and the newly added module PlaSMo are run in case study applications AP A to AP C:

- AP A. Application A: Global assessment of renewable energy potentials employing REMix-EnDaT.
- AP B. Application B: Determination of best installation sites for PV and wind in order to derive the effects on the portfolio output for the cases overall cost minimization, portfolio power output variance and residual load variance minimization. The case is made for Morocco employing REMix-PlaSMo.
- AP C. Application C: Validation of a new scenario based on an updated TRANS-CSP framework by incorporating its installed capacities in a dynamical (hourly resolved) linear optimization employing REMix-OptiMo.

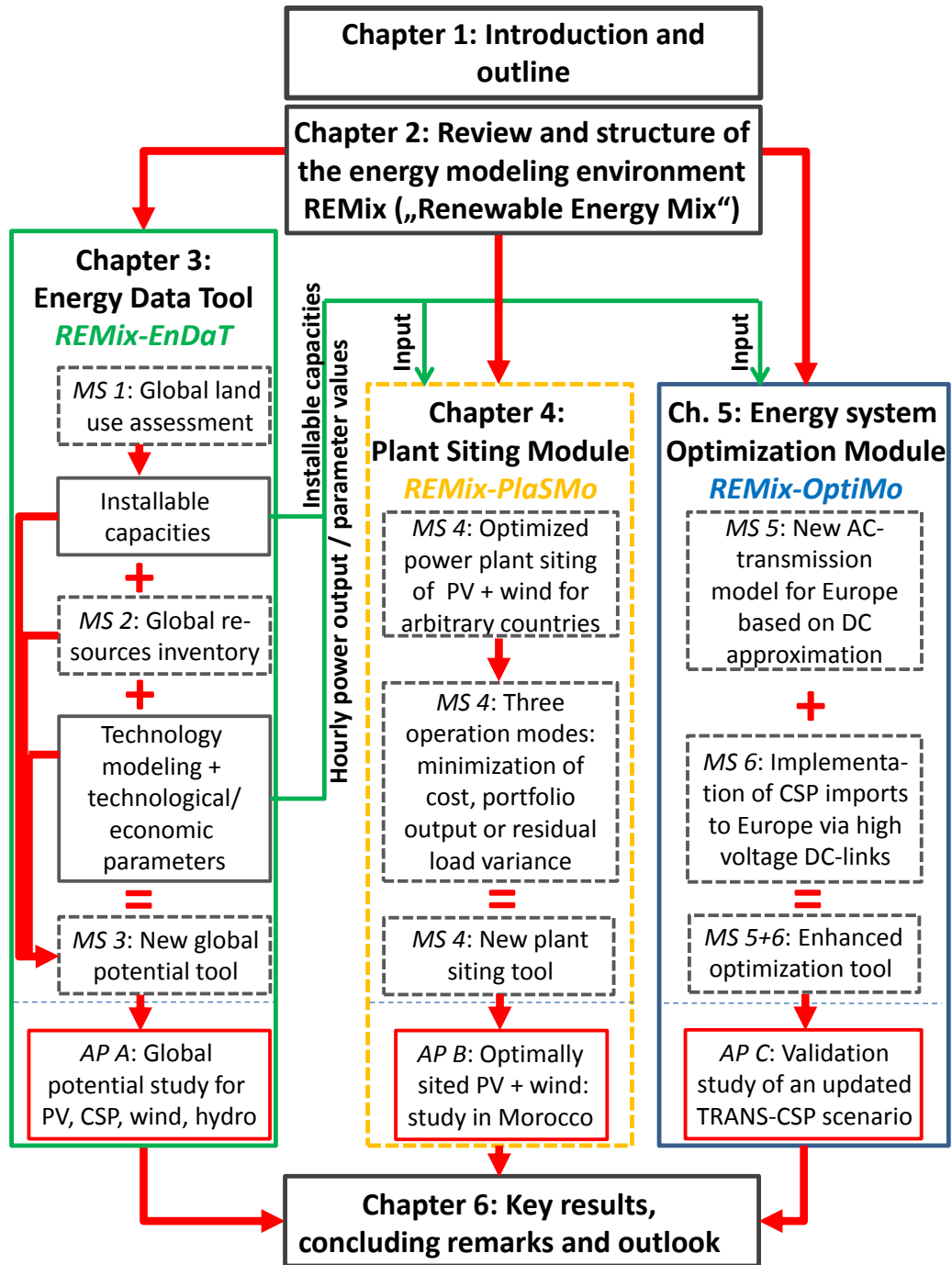


Figure 1.1.: Outline of the intended workflow for this thesis. Dashed boxes indicate amendments or new developments (milestones MS 1 to MS 6). Enhancements to the tools REMix-EnDaT and REMix-OptiMo are made. REMix-PlaSMo is a new feature within the REMix modelling environment. These three REMix modules are eventually employed in three applications (AP A to AP C).

In the following the principal composition of the thesis and the implementation of the milestones is presented. The present document shall enable the reader to gain a general idea of the achievements obtained during the thesis and the overall pathways of the assessment process. It is structured as follows:

The present chapter 1 gives a motivation for, an introduction to and outline on the key goals anticipated in this thesis.

Chapter 2 reviews the energy system modelling suite REMix, briefly giving a historic overview on the model and addressing the various interactions of the distinct modules it is comprised of. It is intended to provide a solid foundation allowing for a thorough understanding of the status quo of the modelling environment and where new features have been amended within this present work. Hence this chapter is a prerequisite for the understanding of the discussions conducted in the following chapters either contributing to or employing REMix.

Chapter 3 covers all items of work related to the enhanced globally applicable potential assessment module REMix-EnDaT⁷, capable of deriving installable capacities, hourly power output and potential assessments: A global land use assessment is carried out to identify suitable sites for renewable power installation (MS 1). Furthermore the creation of the global resources database as a prerequisite for any further assessments of REMix-EnDaT is presented (MS 2). A brief introduction is given on the physical background of the resources, along with data processing issues and a discussion on the significance of the data with respect to its spatial resolution. In particular, an extensive approach is presented with respect to algorithms for the determination of beam normal irradiance data using global downward fluxes. Theoretical potentials are derived and presented using maps which indicate the long term annual means of solar irradiance, wind speed and river run-off. These steps finally yield the global assessment tool for renewable energy potentials (MS 3). This resulting version of REMix-EnDaT is used to compute results of a global assessment of technical, cost and full load hour potentials for the technologies PV, CSP, on- and offshore wind and hydro power (AP A). These calculations are performed using typical meteorological years of the resources data on a grid box level. Also outcomes from a sensitivity analysis both in terms of varying the installation cost and technical parameters are presented.

Chapter 4 presents the newly implemented plant siting module REMix-PlaSMo⁸ (MS 4), designed with three optimization modes to use effects of directed power plant siting on a portfolio: Minimization of the overall cost, the portfolio's power output variance and the portfolio's residual load. A sound algebraic formulation is given. The module is applied in a case study for Morocco (AP B). Technologies concerned for volatile feed-in are PV and wind power, the overall optimization will moreover be set up with hydro

⁴subdivided into the world regions OECD Europe, OECD North America, OECD Pacific, India, China, Latin America, Transition Economies, Africa and Middle East

⁵The original release of TRANS-CSP is a scenario for an electricity supply of Europe with high shares of both domestic and -where necessary - imported renewable power.

⁶A REMix-OptiMo release by Luca de Tena [Ten12] is used.

⁷Energy Data Tool

⁸Plant Siting Module

power, CSP as the complementary technology and an hourly resolved power demand. Three major cases are investigated in line with the three available optimization modes described above. In this respect, the results obtained from minimizing the portfolio's power output variance and the portfolio's residual load are the extreme boundaries for the setup of a CSP power plant. It can be designed accordingly, providing either base or peak load. The overall results in terms of cost and the performance of each technology as well as the entire portfolio are discussed.

Chapter 5 opens with the presentation of the specifics of the energy system optimization module REMix-OptiMo⁹. Moreover the addition of a new power transmission model including its mathematical framework of the direct current approximation of the alternating current power flow is discussed (MS 5). The so-obtained enhanced version of REMix-OptiMo is used for a validation study of a scenario based upon an updated TRANS-CSP [TSK⁺06] framework. This update of the original TRANS-CSP framework, which is the foundation for a new scenario used for the validation process in the results section of this chapter, is discussed. For the validation process, the setup of the optimization is presented: how data provided by REMix-EnDaT, load data and the new transmission model are used and in particular, how CSP power plants in North Africa linked to various European countries using high voltage direct current links are implemented (MS 6).

Finally a summary of the results of dynamically simulating the energy system comprised of 30 countries according to the scenario framework of the updated TRANS-CSP study is discussed (AP C).

Chapter 6 concludes this doctoral thesis' results and gives an outlook on desired future work.

The appendix contains discussions, data and figures which are referred to throughout the thesis. Particular attention is drawn to the presentation of the results of the global potentials assessment in terms of 10 OECD world regions in annex A.2 and a brief summary on the key findings and methodological approach of the original TRANS-CSP study as a leading assessment for a future supply of Europe based on high shares of renewable energies in annex A.3.

⁹Optimization Module

2. Review and structure of the energy modeling environment REMix

For the determination of potentials of both renewable energy resources and technologies, to assess the characteristics, general feasibility and performance of future energy systems as well as to investigate closely related fields, the original release of the energy modeling environment REMix has been established within the framework of a doctoral thesis by Scholz [Sch12]. REMix, abbreviating Renewable Energy Mix, provides a sound variety of tools and capabilities, addressing the aforementioned area of research. The major focus of the present thesis is to enhance this existing framework, add new features to it and finally, to apply and test this amended version in case studies.

2.1. Model development history

Contemporary energy modeling software solutions can primarily be distinguished both in terms of focusing on different temporal horizons, i.e. short-term vs. long-term, and the approaches used (top-down versus bottom-up) [GEMF09]. Short term models covering periods of up to one year use existing power plant portfolios which are exogenously implemented to determine optimum resources scheduling, e.g. using merit order approaches, while simulations aiming at the determination of optimized portfolio transformations, e.g. from fossil to renewable-based power, analyse investment decisions and are thus naturally being laid out to cover longer time frames. Due to the wide array of scientific questions and possible input parameters, energy system models are inherently interdisciplinary [Str11], with an emphasis on contributions from economics and engineering. Unger [Ung10] gives a broad overview on the different kinds of models, sub-dividing them into engineering economic, computational general equilibrium, macroeconomic, input-output, hybrid and integrated assessment models. The modeling environment REMix has originally been established by Scholz [Sch12] to provide a tool closing the gap between existing long-term models¹ and - at the time - very few short-term energy system models².

¹such as MARKAL [SGS01], PRIMES [Cap01], EFOM [Voo82], MESSAGE [MGG96], TIMES [LCV+05a] or ReMIND [SKB12].

²Only models with related goals such as [Czi05; Bib04] were available.

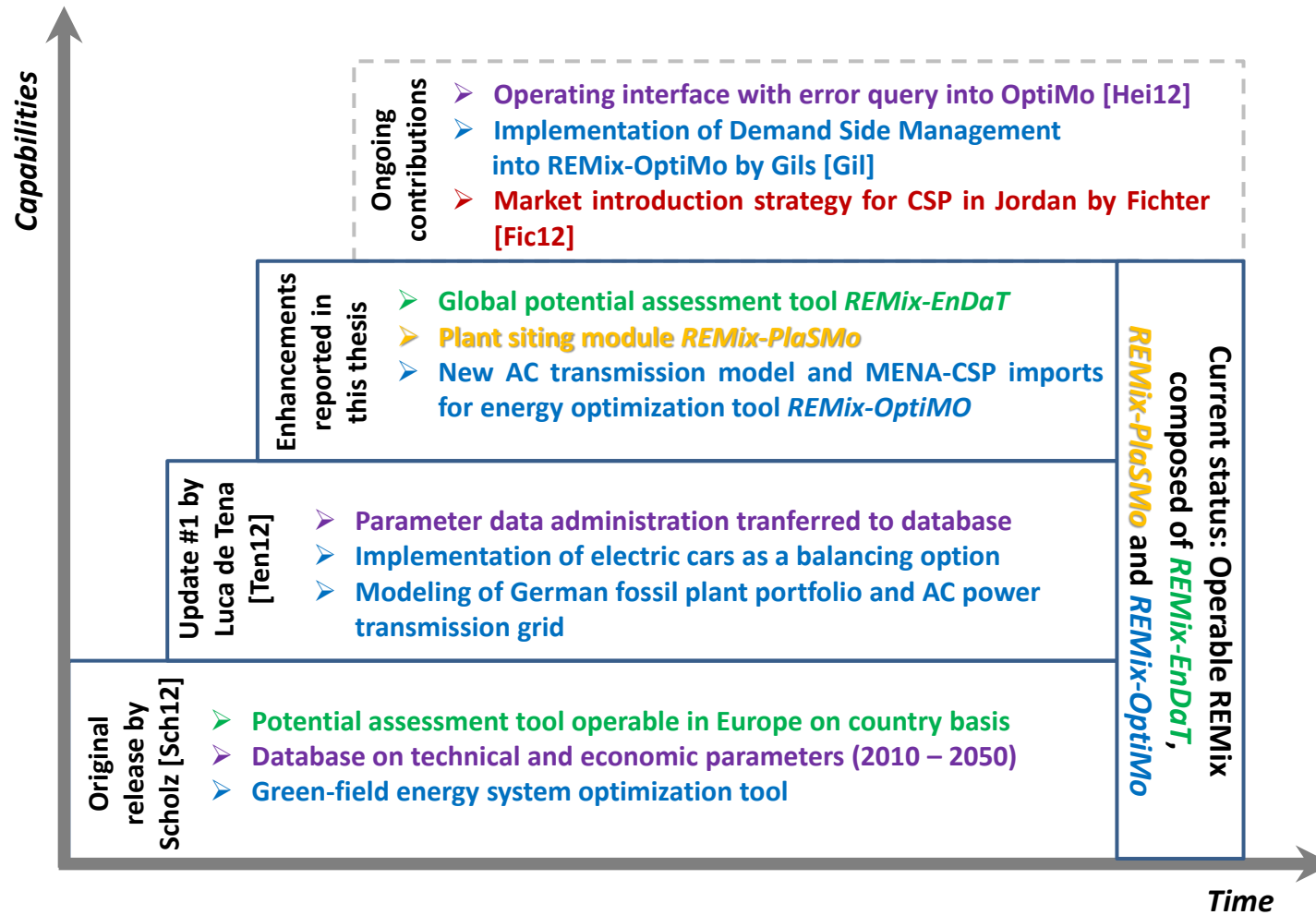


Figure 2.1.: Historical development of the energy modeling environment REMix (Renewable Energy Mix). It is composed of the three major modules EnDaT, PlaSMo and OptiMo. Major contributions to these modules are highlighted in green (EnDaT), yellow (PlaSMo) and blue (OptiMo). Adjacent components are highlighted in purple and red.

To better understand the REMix energy modeling tool's contents and capabilities, its historical development as indicated in figure 2.1 is briefly discussed in the following:

Original release of the REMix model

In the first release by Scholz [Sch12] the focus of REMix is laid on potential assessments and on optimized green-field and least cost power plant portfolios in Europe. Considered technologies for the potential assessments are photovoltaic, concentrating solar, wind, hydro, geothermal and biomass power. A vast database including technical and economic parameters and their anticipated evolution between 2010 and 2050 is included. The determination of figures for maximum installable power plant capacities and hourly power generation time series using bottom-up power plant models is feasible on a country basis. This is due to the fact that the energy system optimization is also run for nodes which comprise one country. The optimization in turn uses hourly data of electricity demand and potential renewable power generation. Power transmission between countries is implemented using high voltage direct current links. Compressed air, hydrogen and pumped hydro technologies are included as storage options.

Update #1

Within the framework of the PhD thesis by Luca de Tena [Ten12] electric cars as a means of balancing power are introduced to the optimization model. A thorough database is established to automate parameter data input to the optimization tool. Also, a new AC-transmission model is established using power transfer distribution factors. However, the latter is merely operatable in Germany, which is divided into subregions to better assess regional effects. Also for Germany, the current conventional power plant portfolio is assessed and modeled in great detail.

Ongoing contributions

Demand side management is being introduced into the model by Gils [Gil]. Potentials for demand shifting are assessed and modeled within the energy system optimization. Furthermore a complete overhaul of the overall structure of the operating interface, including input error query and scenario run administration, are currently being included by Heide [Hei12]. A side branch of the model deals with a short term optimization of renewable energy capacity expansion in order to investigate market introduction strategies for CSP in Jordan [Fic12].

2.2. Enhancements within this work

Within the present work the potential assessment tool of Scholz [Sch12] is enhanced by enabling operability on a global scale. For arbitrary locations on earth maximum installable capacities and potential hourly power generation time series can be derived for the technologies photovoltaics, concentrating solar, on- and offshore wind and hydro power. Moreover, the effects of optimized power plant siting on the portfolio output of photovoltaics and wind can now be assessed. Finally, a new power transmission model for Europe and the option of CSP electricity imports from countries of the Middle East and North Africa are implemented within the energy system optimization model, enhancing a version from Luca de Tena [Ten12].

Figure 2.2 gives a summary of the resulting energy modeling environment REMix. Amendments added to REMix within the framework of this thesis are highlighted in red. Building upon the existing framework and considering the amendments resulting from the present work, REMix is now composed of three partially interdependent sub-modules. These constituting components of the REMix energy modeling suite are:

- A The energy data tool REMix-EnDaT ("Energy Data Tool"):
REMix-EnDaT is capable of providing (i.) stand-alone potential assessments as well as data such as hourly generation profiles and demand time series or (ii.) installable capacities of selected volatile renewable technologies.
- B The plant siting optimization module REMix-PlaSMo ("Plant optimization tool"):
REMix-PlaSMo is capable of determining optimum siting of PV and wind power plants against the background of minimizing (i.) the overall volatile portfolio cost, (ii.) the portfolio's output variance and (iii.) the portfolio's residual load variance.
- C The energy system optimization module REMix-OptiMo ("Optimization module"):
REMix-OptiMo is capable of (i.) deriving optimized least-cost and green-field supply portfolios and (ii.) determining optimized power plant dispatch.

REMix-EnDaT, REMix-PlaSMo and REMix-OptiMo are elaborated in greater detail in chapters 3, 4 and 5 respectively. In each chapter, the methodology of the corresponding REMix module along with its major capabilities is presented. Enhancements made to the model within this work are discussed in great detail there. Each of the aforementioned chapters closes with an application of the amended REMix module in a case study: REMix-EnDaT is used to compute cost and full load hour potentials on a global scale for the technologies photovoltaics, concentrating solar, on- and offshore wind and hydro power. REMix-PlaSMo is operated to assess portfolio effects of photovoltaics and wind generation in Morocco. REMix-OptiMo is used to validate an updated TRANS-CSP [TSK⁺06] scenario.

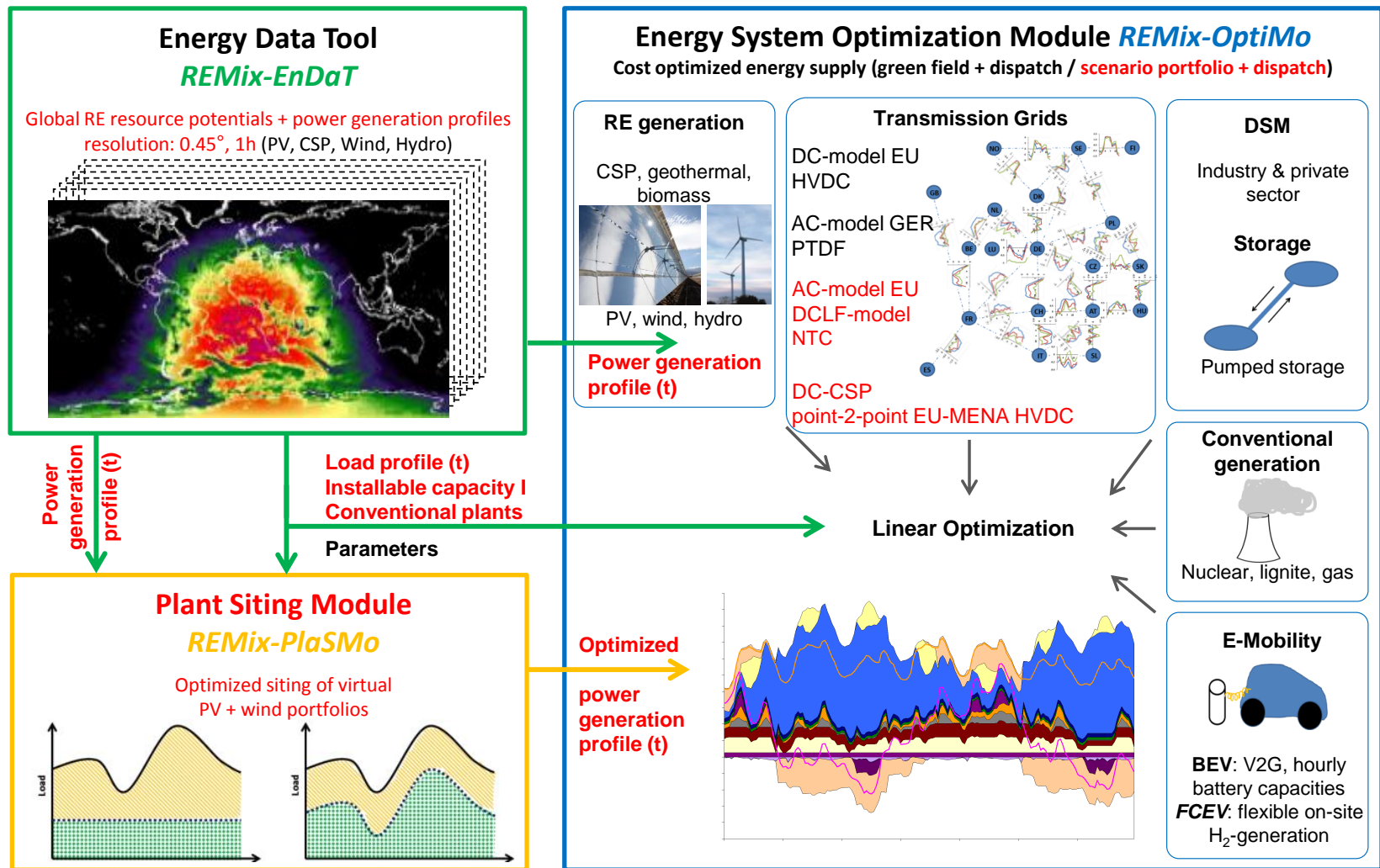


Figure 2.2.: Setup of the energy modeling environment REMix (Renewable Energy Mix). It is composed of the three major modules EnDaT, PlaSMo and OptiMo. Enhancements to REMix added within the present work are highlighted in red. Credits: CSP plant photo [DLR14b], wind plant photo [DLR14a], portfolio dispatch graph [Sch09a].

3. REMix-EnDaT: Model enhancements and application in a global potentials study

3.1. Outline

Within the REMix modeling suite, REMix-EnDaT¹ is capable of providing both, on the one hand, independent investigations to determine different potentials² of renewable energy conversion and, on the other hand, time series data for the technologies PV, CSP, wind, and hydro power which eventually serve as input to the modules PlaSMo and OptiMo. One major innovation compared to prior existing work and its core competence is the capability to carry out potential assessment calculations for arbitrary sites on a global level. The general methodology as presented in this chapter is indicated in figure 3.1. After this outline, the chapter is composed of three additional sections: First of all, the work to enhance the model, which is embedded into the core structure of the existing tool. The components, installable capacities, resources availability and hourly power output, discussed in section 3.2, constitute the enhanced tool REMix-EnDaT. Reference is made to items which have not been developed as part of this thesis, but are to be presented nonetheless to enable an understanding of the new overall workflow. An application of this enhanced version of REMix-EnDaT is presented in section 3.3, elaborating on a global assessment of renewable energy potentials. A discussion and outlook are given in section 3.4.

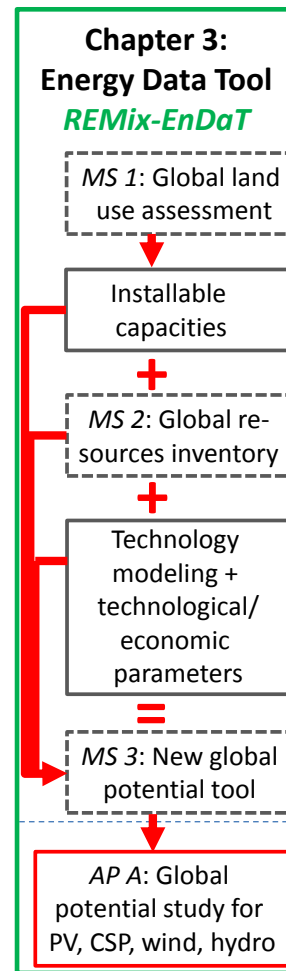


Figure 3.1.: Structure of the present chapter.

¹Energy Data Tool

²In this work, theoretical, technical, economic and full load hour potentials are assessed. For the definitions used, please see section 3.3.1.1 for further reference.

3.2. Overall structure of and enhancements to REMix-EnDaT

The tool REMix-EnDaT works on a pixel-basis, i.e. for each pixel installable capacities (see subsection 3.2.1) and hourly resources data (see subsection 3.2.2) are derived. These two components are used in power plant models (see subsection 3.2.3) to determine feasible hourly power generation. The enhanced version of REMix-EnDaT is now presented in this section, focusing on the following items:

A Identification of installable capacities

In order to derive installable capacities on a global scale, a world-wide land use assessment is carried out within this work. The approach is presented in subsection 3.2.1 in terms of the exclusion criteria and further assumptions applied. The general objective is the determination of suitable areas and subsequently installable capacities for renewable power plants.

B Establishment of a global resources database

Within this work a global resources database is set up for solar irradiance, wind speed and river discharge. The data is processed to meet the requirements of the pixel based approach in this work with its spatial resolution of 0.45° . All resources data are available hourly. A discussion on the establishment of this database is given in subsection 3.2.2.

C Determination of hourly power output using power plant models

Bottom-up power plant models for the technologies PV, CSP and wind are used in this work as presented in subsection 3.2.3. For each grid box, the approach yields hourly power generation based on the installable capacity, technology parameters and resource availability. This output can be aggregated to conglomerations of interest (e.g. on country levels). For hydro power plants a top-down approach is used to derive hourly power output.

The aforementioned workflow is now elaborated and discussed in greater detail and results in the establishment of a global potential assessment tool. The overall approach for the determination of suitable sites and installable capacities as well as the power plant technology models are based on Scholz [Sch12]. The amendments to REMix-EnDaT have been developed by the author within the framework of the publicly funded project [SGS11], the discussion in the following sections is partly excerpted from that work.

3.2.1. Global land use assessment to identify installable capacities for power plant installations

To enable a brief outline on the approach, a summary of the methodology for the identification of installable capacities is depicted in figure 3.2. First of all, the eligibility of

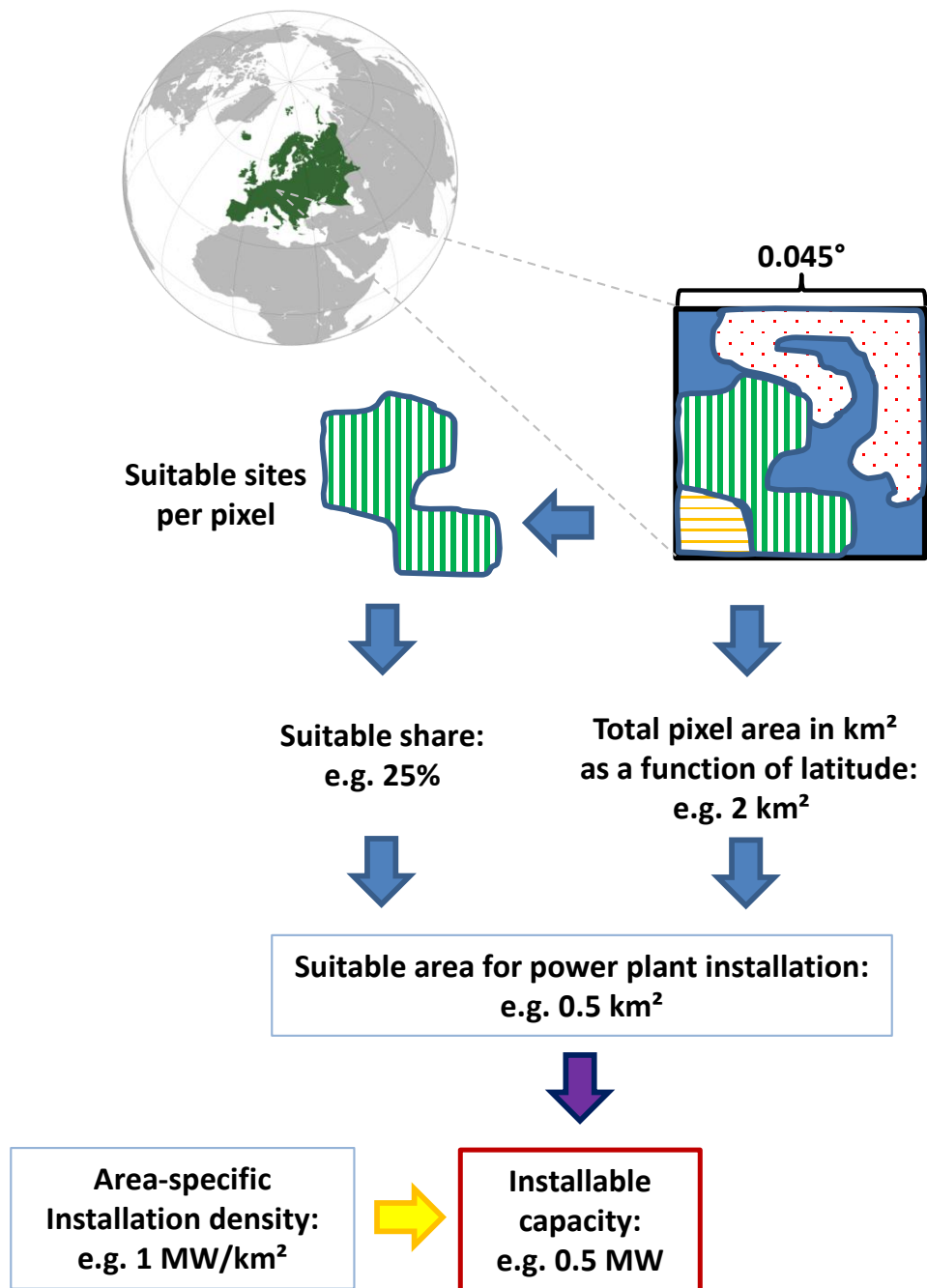


Figure 3.2.: Processing chain in order to determine the installable capacity of one specific technology for a given pixel. First of all the suitable sites are found and their total share of the pixel is derived. Second, the area of the pixel is calculated as a function of its geographic position (latitude). Third, these two items are combined to come up with the suitable area for power plant installation. Using the latter along with the area-specific installation density yields the installable capacity (source for globe image: [Eur]).

each respective pixel for power plant installation has to be determined in terms of the suitable share taking into account land use data and further restrictions. This suitable share is the segment of each pixel, which can be used for power plant installation. Once the suitable share is derived, each pixel's area as a function of the geographic latitude is of interest in order to obtain the suitable area for power plant installation. Considering an installation density in $[\frac{W}{m^2}]$, determined for each technology in a preceding step, and combining it with the suitable area yields the installable capacity per pixel for each respective technology. This approach holds for PV, CSP, onshore and offshore wind. For hydro power a different approach is used: From the WEPP³ database [WEP09] the hydro power plants have been geo-referenced to allocate existing installed capacities to each grid box. A discussion of the approach for the determination of installable capacities is now given.

3.2.1.1. Suitable sites

As a prerequisite to assess installable capacities, the determination of suitable areas for the installation of power plants is of major interest. For the assessments presented in this study, suitable sites have to be identified for open-area PV, CSP, on- and offshore wind power plants.

In order to limit calculation and rounding errors to a minimum, first of all suitable pixels are identified on a 300x300 m² grid, which is the maximum resolution these land use data are available on a global scale [BB05]. The results of this first step are projected to obtain suitable shares per pixel of a 0.045° raster.

A short discussion on the land use criteria assumed for the installation of different technologies will follow, concluded by the mathematical expression used in this assessment for the determination of the installable capacity. Figure 3.2 summarizes the entire process while figures 3.3 and 3.4 indicate various georeferenced data maps used for the assessment.

Suitable sites for open area Photovoltaics, Concentrating Solar Power and Onshore Wind

For the identification of suitable sites for the installation of open area PV, CSP and wind onshore, the Global Land Cover database [BB05] is employed, containing 23 different land use classes, out of which four are considered to be eligible for renewable power plant installations. In order to avoid any conflicting land uses, such as the installation of power plants on agricultural land, merely the following land use categories are considered:

- Closed to open (>15%) shrub land (<5 m: broadleaved or needle leaved, evergreen or deciduous)
- Closed to open (>15%) herbaceous vegetation (grassland, savannas or lichens)
- Sparse (<15%) vegetation and bare areas

³World Electric Power Plants database

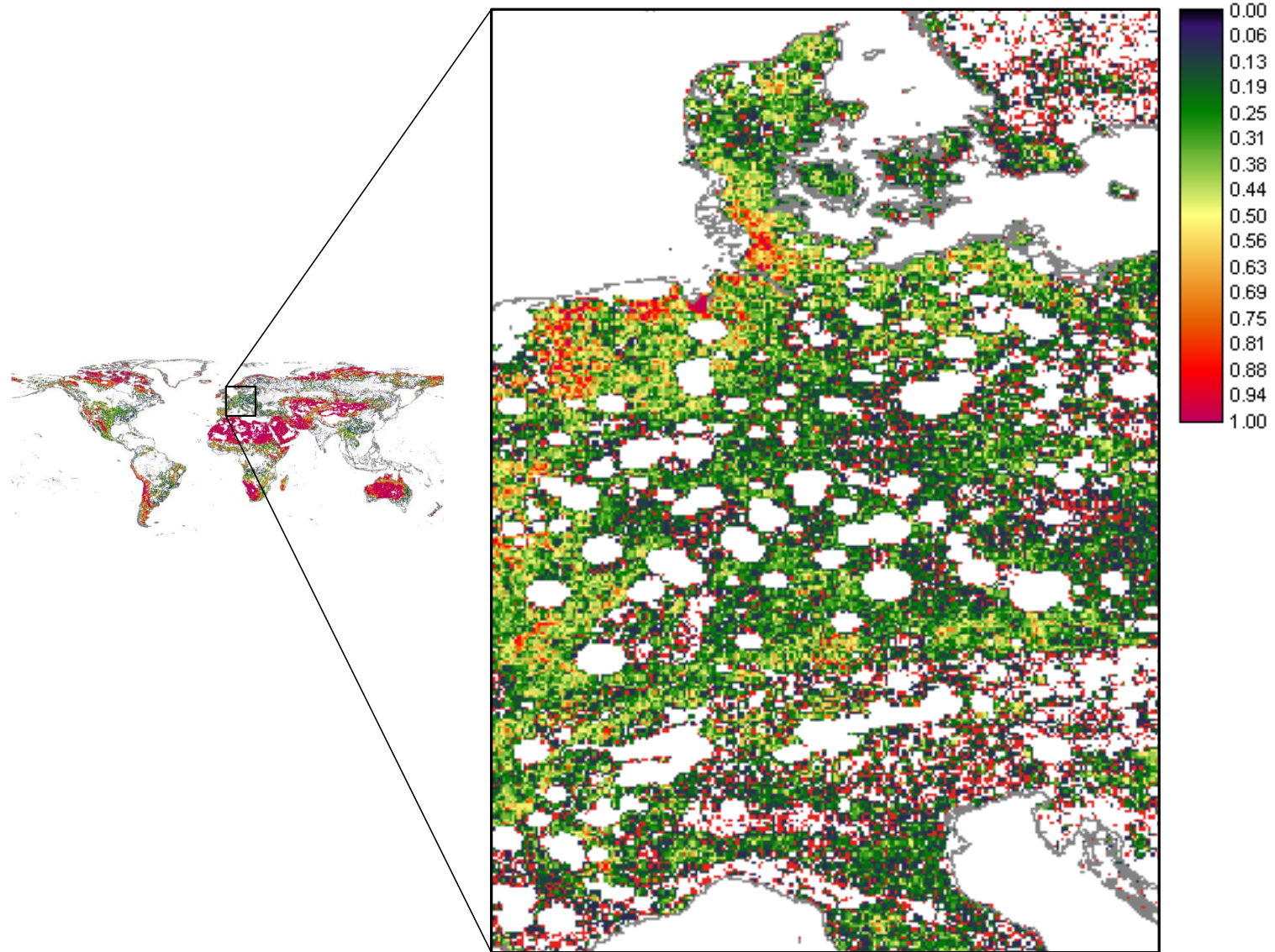


Figure 3.3.: Results for suitable shares for power plant installation using the approach discussed in this section. The color code ranges from 0 (0% suitable) to 1 (100% suitable). White areas are completely excluded.

Moreover the areas occupied by the latter land use categories are further reduced by glaciers (plus a security zone of 10 km), sand dunes (plus a security zone of 10 km for shifting dunes) and saltpans (all of the former according to the Digital Soil Map of the World [DSM07]), any hydrological areas such as lakes, reservoirs, rivers, freshwater marsh, floodplain, swamp and flooded forest, pan, coastal brackish or saline wetland, bog, fen, mire, intermittent wetland (corresponding to the Global Lakes and Wetlands Database [GLW04]). Protected areas (according to the World Database on Protected Areas [WDP10]) as well as all surfaces within a 1 km buffer around settled areas are also not considered for any power plant installation. For the remaining surfaces - indicated in figure 3.3 - final criteria are established according to table 3.1 to determine the resulting suitable sites for PV, CSP and onshore wind. Figure 3.4 shows distances to settlement and elevations with respect to sea level and slopes. All of these parameters can be chosen according to the user's preferences.

	open area PV	CSP	onshore wind
minimum resource		1800 kWh/a	4 m/s
maximum slope [°]	45	2.1	15
maximum elevation [km]	2.5	2.5	2.5
minimum distance to settlement [km]	1	1	1

Table 3.1.: Overview on the final exclusion criteria to determine suitable areas for power plant installation.

Suitable sites for offshore wind

For offshore wind, in a first step only exclusive economic zones are considered (the zones up to 200 nautical miles from the coasts, please see top map in figure 3.4). Furthermore, depths of up to 40 m are considered. Protected areas reduce the eligible sites. Taking into account unaccounted technical constraints and sea use competition (e.g. military zones, shipping routes, fishery areas), in accordance to [Fel] 75% of each pixel of the remaining seabed between 5 and 40 km are considered for installations. Near shore areas less than 5 km off shore are utterly excluded.

3.2.1.2. Suitable areas

In order to determine each pixel's area in terms of its suitable share, hereafter referred to as suitable area for power plant installation, the grid boxes considered suitable (their shares as indicated in figure 3.3) are multiplied by the area of each pixel. In case of decentralized roof-top PV systems in settlement areas, the determination of suitable areas is carried out using an approach initially proposed by Hoogwijk [Hoo04], where a link is established between the suitable surface for installation of modules in [m²] and the GDP⁴ per capita in the respective country. According to this approach, the suitable surface for installation of decentralized photovoltaic systems per capita c in country i

⁴GDP: Gross Domestic Product

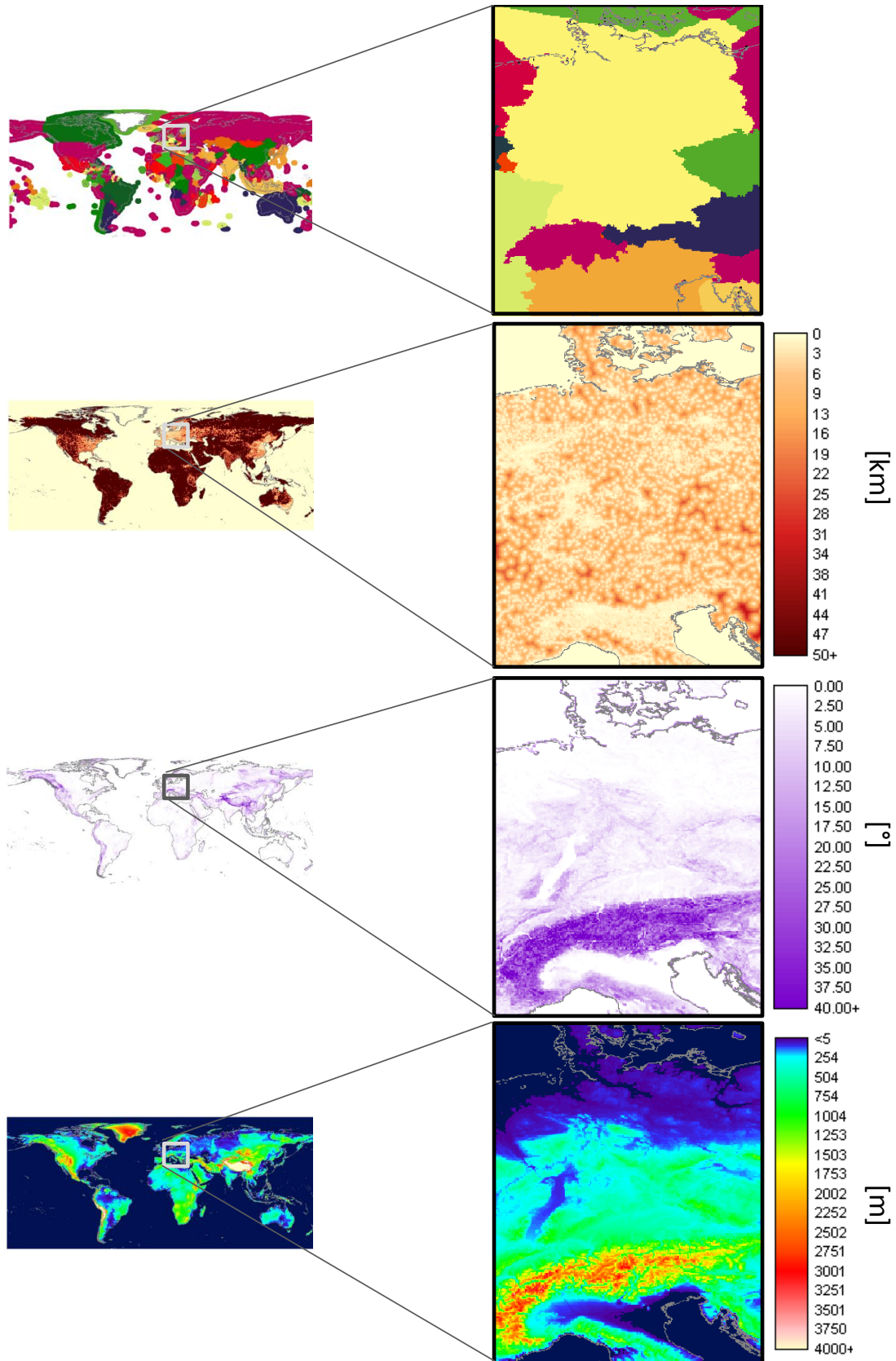


Figure 3.4.: Various global maps used within the tool REMix-EnDaT, from top to bottom: Identification of countries and their exclusive economic zones, distances to settlements [km], terrain slopes [$^{\circ}$] and elevations [m] with respect to sea level.

$A_{c,i}$ is expressed by:

$$A_{c,i} = 0.06 \cdot GDP_i^{0.6} \quad (3.1)$$

Data on the GDP per capita was used from the CIA factbook [CIA10]. Together with population density data [Lan10] a georeferenced map is created stating the suitable area for decentralized photovoltaic power plants per pixel.

3.2.1.3. Area-specific installable capacities

In the following, the area-specific installable capacity expressed in $[\frac{MW}{km^2}]$ for PV, CSP, on- and offshore wind is discussed according to Scholz [Sch12], who uses data as indicated in table 3.2:

<i>Parameter</i>	2010	2020	2030	2040	2050
PV module efficiency η^{PV} [%]	16.1	17.3	18	18	18
PV q-factor q^{PV} [%]	81.1	82	82.9	83.8	84.7
CSP thermal capacity factor f_{icf}^{CSP} [MW_{th}/km^2]	176.2	176.2	176.2	176.2	176.2
Onshore wind nominal capacity turbine $P_{nominal}^{onshore}$ [kW]	1950	3400	4400	5000	5500
Offshore wind nominal capacity turbine $P_{nominal}^{offshore}$ [kW]	3000	6000	8000	10000	12000
Onshore wind rotor diameter $d_{rotor}^{onshore}$ [m]	77.5	102.3	116.4	124.1	130.1
Offshore wind rotor diameter $d_{rotor}^{offshore}$ [m]	96.1	135.9	156.9	175.4	192.2
Onshore and offshore wind distance factor $f_{distance}^{wind}$ [m]	6	6	6	6	6
PV area-specific installable capacity [MW/km^2]	130.6	141.9	149.2	150.8	152.5
CSP solar field area-specific installable capacity [MW_{th}/km^2]	176.2	176.2	176.2	176.2	176.2
Onshore wind area-specific installable capacity [MW/km^2]	10.4	10.4	10.4	10.4	10.4
Offshore wind area-specific installable capacity [MW/km^2]	10.4	10.4	10.4	10.4	10.4

Table 3.2.: Data used for the determination of the area-specific installation capacities (top) and the resulting values (bottom) according to Scholz [Sch12].

Photovoltaic

In case of photovoltaic, the area-specific installable capacity $p_{area}^{PV, inst}$ is derived at standard testing conditions⁵ from the efficiencies of the modules expressed in [%] η^{PV} and the efficiencies q^{PV} of the remaining plant components, such as DC-AC converters:

$$p_{area}^{PV, inst} = \eta^{PV} \cdot q^{PV} \cdot 1000 \frac{MW}{km^2} \quad (3.2)$$

Concentrating Solar Power

In this work, parabolic troughs are used as the reference technology. CSP plants using parabolic troughs transform the radiation energy twice, the first transformation from

⁵The standard testing conditions for devices tapping global horizontal irradiance (GHI) imply normal pressure of 1bar, a global horizontal irradiance of $1000 \frac{W}{m^2}$ at an ambient temperature of 25°C [Ste07].

radiation into heat occurs in the troughs of the solar field and the second transformation in the steam turbines transforming heat into electricity. Therefore, for the derivation of the area-specific thermal installable capacity of CSP $p_{area}^{CSP, inst_{th}}$, the expression of a thermal capacity density factor f_{tcd} , derived from the Luz System 3 collectors used in the SEGS VII solar field [PLK⁺02] is introduced as

$$f_{tcd} = \frac{Q_{sf}}{A} \quad (3.3)$$

$$p_{area}^{CSP, inst_{th}} = f_{tcd} \quad (3.4)$$

with the effective heat output of the solar field at standard testing conditions⁶ Q_{sf} . Hence, the area-specific thermal installable capacity of CSP, referring to the solar field, also implies areas used for service roads or the power block. Moreover, the trough rows are built with a minimum distance to minimize shadowing for small solar elevation angles. Furthermore optical impurities, tracing errors and heat loss of the first cycle medium during circulation are considered in this factor.

Wind Power

For the installation of wind turbines interference effects of wind plants closely constructed next to one another have to be taken into account. The area-specific installable capacity $p_{area}^{wind, inst}$ is defined by the nominal capacity $P_{nominal}^{wind}$ of a single wind turbine over its area demand A . The latter is determined using a distance factor $f_{distance}^{wind}$ and the turbine diameter d_{rotor}^{wind} , and yields the fact, that turbines should be placed with an adequate distance to one another in order to minimize interference:

$$p_{area}^{wind, inst} = \frac{P_{nominal}^{wind}}{A} \quad (3.5)$$

$$= \frac{P_{nominal}^{wind}}{\sqrt{0.75} \cdot (d_{rotor}^{wind} \cdot f_{distance}^{wind})^2} \quad (3.6)$$

3.2.1.4. Installable capacities

PV, CSP and wind power

Eventually the information gathered in the preceding steps is merged to determine the different technologies' maximum installable capacities for each grid box i $P_i^{tech, inst_{max}}$ [MW]. According to the first development by Scholz [Sch12], they are a function of the technology dependent area-specific installation density $p_{area}^{tech, inst}$ [$\frac{MW}{km^2}$], the area A_i of the grid box i [km^2] and a dimensionless technology dependent suitability factor $f_{suitability}$

$$P_i^{tech, inst_{max}} = p_{area}^{tech, inst} \cdot A_i \cdot f_{suitability} \quad (3.7)$$

⁶The standard testing conditions for devices tapping beam normal irradiance (BNI) imply normal pressure of 1bar, a beam normal irradiance of $800 \frac{W}{m^2}$ at an ambient temperature of 25°C [Ste07].

The area suitability factor $f_{suitability}$ is set equal to one for all technologies onshore, i.e. PV, CSP and onshore wind, and to 0.75 for offshore wind. The area of each grid box is determined as a function of its geographic latitude.

Hydro Power

For hydro power, an approach differing from the proposed land-use and GDP based analyses discussed before is carried out. This is particularly due to the fact that hydro power is a very mature technology, which inherently involves the fact of all major sites for installation already being used. Moreover, an estimate as to which areas are available for the construction of new plants, dams or reservoirs using detailed land use data is beyond the scope of this work. For these reasons, the WEPP⁷ database [WEP09] is used to derive contemporarily installed hydro capacities along with the added information of their geographic location. To take account of the temporal evolution from 2010 until 2050 in decade steps, both modernization and new construction are considered:

For modernizations an approach presented by Scholz [Sch12] is used, proposing a modernization factor of 15%, i.e. over the course of an estimated lifetime of 60 years, today's installed capacity increases by that figure: If 300 MW were installed in 2010, in 2020 $\frac{10}{60}$, in 2030 $\frac{20}{60}$ etc. of the installed capacity $P_i^{hydro, inst}$ would be modernized: In this example, $\frac{1}{6} \cdot 300 \text{ MW} = 50 \text{ MW}$ of which 15% amount to 7.5 MW and $\frac{1}{3} \cdot 300 \text{ MW} = 100 \text{ MW}$ of which 15% amount to 15 MW leading to modernized capacities $P_{mod, i}^{hydro}$ of 307.5 MW and 315 MW in 2020 and 2030 respectively.

For new constructions figures on the technical potentials $X_{technical, country}$ [TWh] on country levels provided by [WEC10] are used. The following relation is employed to come up with potentials for new installations $P_{new, i}^{hydro, inst}$:

$$P_{new, i}^{hydro, inst} = \frac{X_{technical, country}}{flh_{country}^{hydro}} - (P_i^{hydro, inst} + P_{mod, i}^{hydro}) \quad (3.8)$$

Each country's full load hours $flh_{country}^{hydro}$ are derived by the quotient current annual hydro power generation over installed hydro capacity.

3.2.2. Setting up a global inventory of renewable resources

In this chapter the general approach to establish a global resources database for solar irradiance, wind and river discharge is presented⁸. Physical backgrounds of each resource, major processing steps and the theoretical potential are presented separately for each resource in the following sections.

⁷World Electric Power Plants database

⁸Within this work, corresponding data sets for temperature and the solar elevation angle have also been processed.

3.2.2.1. Solar Irradiance

The potential assessment for electricity generation using photovoltaics requires both global horizontal (GHI) as well as beam normal irradiation (BNI) data, whereas for electricity output calculations of concentrating solar power plants BNI data is the most important resource needed. In this section, the data sets used and their main characteristics will be presented along with a discussion of other resource data currently available. Processing steps and obtained data quality are then presented and discussed. Due to the wealth of physical background related to solar irradiance, an overview on the latter is given in annex [A.1](#).

3.2.2.1.1. Available data on GHI and BNI

For the purpose of this work, data is desired that fulfills the requirements of featuring both a global geographical coverage and sufficient temporal resolution⁹. Only very few data sets meet the latter specifications and will henceforth be discussed according to an excerpt of work conducted by the author within [\[SGS11\]](#):

- **ISIS**

The ISIS data set is available on a global scale with a temporal resolution of three hours and a spatial resolution of 280x280 km² providing GHI and BNI data. It covers a time period of 21 years from 1984 through 2004, enabling the calculation of stable long-term averages, the evaluation of the variability of irradiance from year to year and the study of extreme atmospheric conditions on the irradiance at the surface, e.g. after a volcano eruption [\[Loh06\]](#). Yielding physical and optical properties of the atmosphere, DLR-ISIS irradiances are derived through radiative transfer calculations based on the ISCCP data set provided by the National Aeronautics and Space Agency NASA. Details of the radiative transfer model and the atmospheric properties data sets can be found on the DLR-ISIS website [\[SI12\]](#).

- **SRB**

The NASA/GEWEX Surface Radiation Budget (SRB) releases 2.5 and 3.0 [\[SSE12; SRB12\]](#) cover the entire globe with a spatial resolution of 1°x1° and time steps of three hours. The data pool contains a wide variety of short wave, long wave and cloud property parameters. The data quality of the three hourly values has been verified by cross-checking with measurements from various sites of the Baseline Surface Radiation Network (BSRN) covering a period of thirteen years (1992-2005). After aggregation of short wave data from release 3.0 for all sites and years, the mean bias was determined to be 5.2 $\frac{W}{m^2}$ (e.g. the model fluxes being lower by 1.9%) and the root mean square difference is 88.2 $\frac{W}{m^2}$. Furthermore, errors for the ground measurements are estimated within an interval of 8-20 $\frac{W}{m^2}$ [\[SRB12\]](#). The authors have not done any independent validation of the parameters provided in these files. Release 2.5 provides optical depth and cloud cover data as a prerequisite for flux computations to obtain beam normal irradiance data. No cross validation assessment has been carried out, therefore, the processed BNI data will be cross-checked in this work.

⁹Further assessments in this work are aiming at hourly values on a global scale as input.

Table 3.3 summarizes the introduced data sets as far as their spatial and temporal resolution as well as their regional coverage are concerned:

	ISIS	SRB (2.5 & 3.0)
temporal resolution	3h	3h
spatial resolution	280 km	1° (approx. 110 km)
regional coverage	global	global
temporal coverage	21 years	22 years

Table 3.3.: Summary of the different data sets presented above. The Solar Radiation Budget data sets (releases 2.5 and 3.0) [SRB12] provided by NASA were chosen for the further analyses.

The demands of the project are best met by NASA’s SRB data sets, since they provide an excellent combination of temporal and spatial resolution quality on a global scale.

3.2.2.1.2. Processing of Global Horizontal Irradiance

As indicated above, raw data on GHI is provided by NASA¹⁰ with three hourly time steps. Therefore an interpolation is carried out and discussed here as part of an excerpt of work conducted by the author within [SGS11] eventually yielding hourly data. For its determination, first of all hourly clear sky global horizontal irradiation data is calculated at a spatial resolution of $0.45^\circ \times 0.45^\circ$. The data originates from a clear sky model developed by Bird [BH81] and modified by Iqbal [Iqb83]. The model includes atmospheric parameters such as aerosols, moisture and others. The processing chain for computation of GHI data is depicted in figure 3.5. The NASA data set contains a large variety of meteorological parameters. Out of this pool, the parameter ”all sky surface downward flux” from release 3.0 is spatially projected from $1^\circ \times 1^\circ$ to $0.45^\circ \times 0.45^\circ$ using a nearest neighbor approach. This approach relates each data value of the final 0.45° grid to the original 1° mesh. A linear spatial interpolation is not carried out due to very high processing effort. For the temporal resolution, an interpolation is performed as follows: Each time step (3h) is divided by its respective counterpart of clear sky GHI data, yielding a clear sky index (GHI)¹¹ data set at a three hourly temporal resolution. The data obtained this way is almost independent of solar geometry and atmospheric path length. The clear sky index is therefore easier to interpolate. It is used in a linear interpolation in order to get hourly data for the clear sky index (GHI). By multiplying the latter with hourly clear sky GHI data provided by Hoyer-Klick [HK12], hourly global horizontal irradiance meeting the spatial and temporal resolution demands is processed.

¹⁰For GHI the parameter ”all sky surface downward flux” was used.

¹¹A similar expression for the clear sky index of BNI can be found, therefore GHI is stressed in parenthesis.

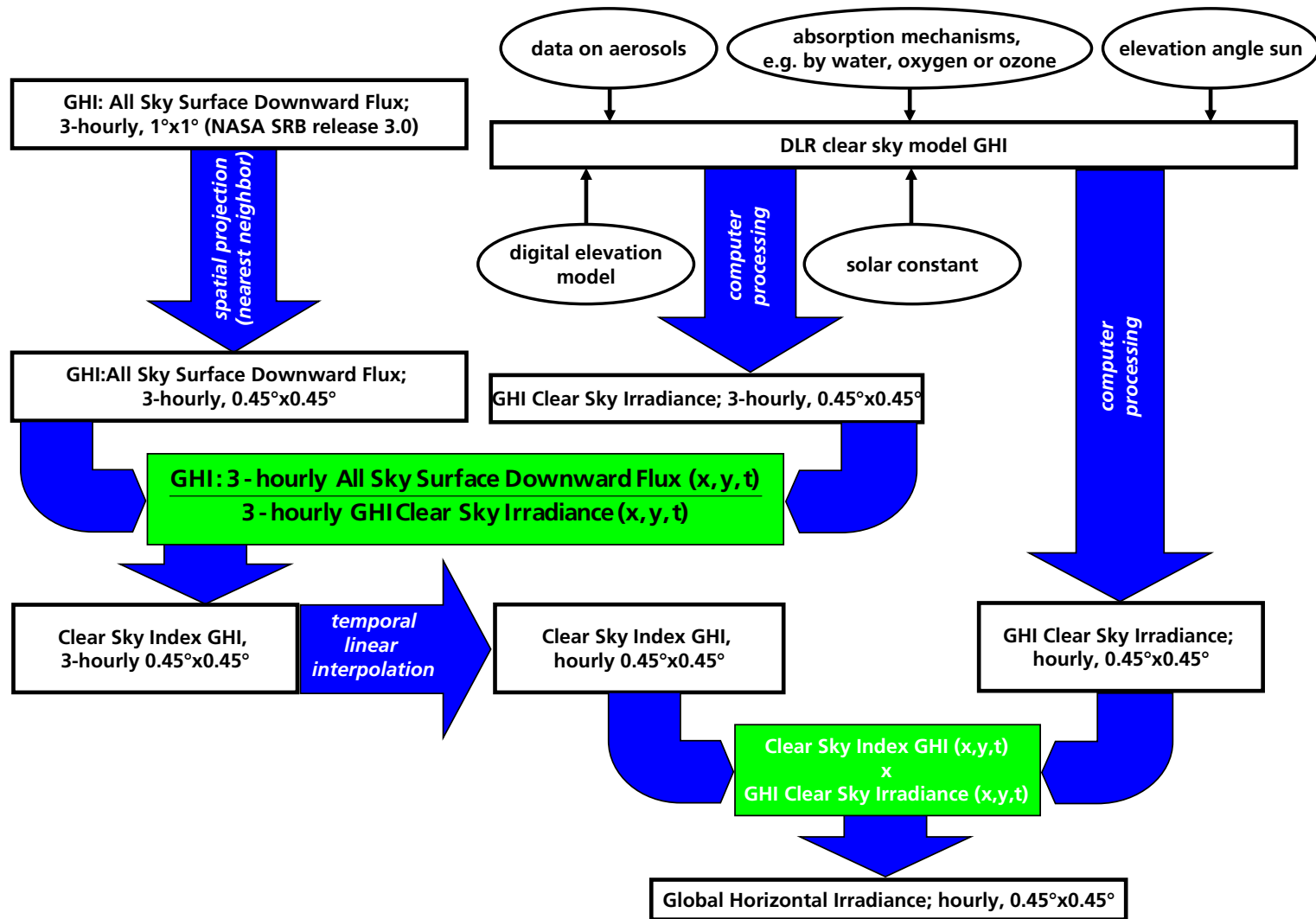


Figure 3.5.: Processing chain for computation of GHI data. Clear sky GHI data, provided by DLR and data from NASA SRB release 3.0 [SRB12] were combined in order to determine hourly global horizontal irradiance data with a spatial resolution of 0.45°x0.45°.

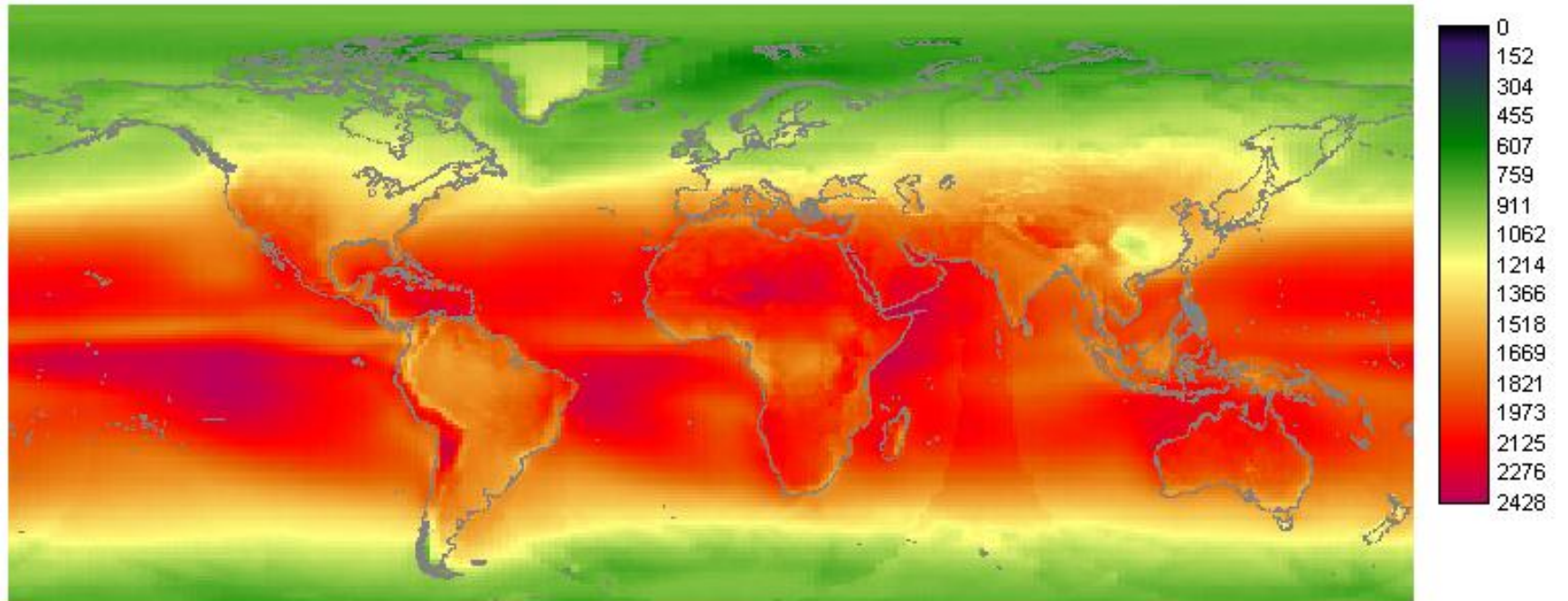


Figure 3.6.: Annual average of global horizontal irradiance resulting from the 22 year data set processed in this work, covering a time frame from 1984 through 2005. The values presented are displayed in $\left[\frac{kWh}{m^2 \cdot a}\right]$. Overall, solar irradiance is naturally higher the closer the site is located to the equator. Furthermore, the height above sea level and regional weather patterns also impact on the incident irradiance at ground level.

For all sun elevations smaller than 3° the clear sky GHI values are set equal to zero, in order to avoid values out of range and to account for early morning and late evening shading and blocking by obstacles on the horizon, which is not calculated in detail. Figure 3.6 displays the average annual global horizontal irradiance obtained by this approach. In order to validate the approach described before, 18 ground station data sets of the BSRN network [BSR12] as indicated in figure 3.7 are used to cross-check the interpolated GHI NASA data¹². For this cross-check, a script developed by Hoyer-Klick [HK12] based on benchmarking approaches from Beyer et al. [BMS⁺09] is used. The stations of the Baseline Radiation Network BSRN provide high quality data with temporal resolutions ranging from one to three minutes for different periods between 1992 and today¹³ on various atmospheric parameters, inter alia temperature, pressure, precipitation and, of capital importance regarding this thesis, solar irradiance [BSR12]. Being geographically spread over the entire globe and situated at different latitudes and elevations, their area of coverage lies in different climatic zones thus offering the possibility of comparing satellite derived irradiance data as used in this work with a wide range of high end ground data. For the purpose of this thesis, out of the pool of existing and candidate stations, 18 stations are chosen in order to be capable of cross-checking the processed satellite data originally obtained through [SRB12]. The selection of the stations is primarily based on the temporal coverage of the available data. Since this work's satellite based data covers a time frame from 1984 through 2005, only stations with both partially and utterly coinciding time periods are considered. The scatter plot resulting from cross-checking BSRN data with the processed GHI data is presented in figure 3.8. BSRN data has been quality checked to eliminate values out of range (negative, greater than $1000 \frac{W}{m^2}$), or inconsistent data (the beam horizontal (BHI) and diffuse horizontal irradiances (DHI) have to equal the global horizontal irradiance (GHI)). The cross-check yields a correlation of 0.9 between the ground measurements and the interpolated hourly satellite data and an average root mean bias deviation of -3.94%, indicating that the interpolated values are slightly lower than ground data, but nonetheless qualitatively very good. Furthermore, comparisons to annual GHI sums based on monthly means provided by NASA [SRB12] are carried out. The latter indicate an average absolute deviation of -1.8% for all sites globally. Therefore, both comparisons of the processed satellite data are considered to be in very good agreement with ground measurements.

¹²According to figure 3.7, the stations chosen for the cross-check are Bermuda (BER), Billings (BIL), Cambourne (CAM), Carpentras (CAR), Cocos Islands (COC), Darwin (DAR), Desert Rock (DRA), Florianopolis (FLO), Fort Peck (FPE), Kwajalein (KWA), Momote (MAN), Palaiseau Cedex (PAL), Rock Springs (PSU), Regina (REG), Sede Boquer (SBO), Sioux Falls (SXF), Tamanrasset (TAM) and Toravere (TOR).

¹³The stations do not cover identical time periods, they vary from site to site.

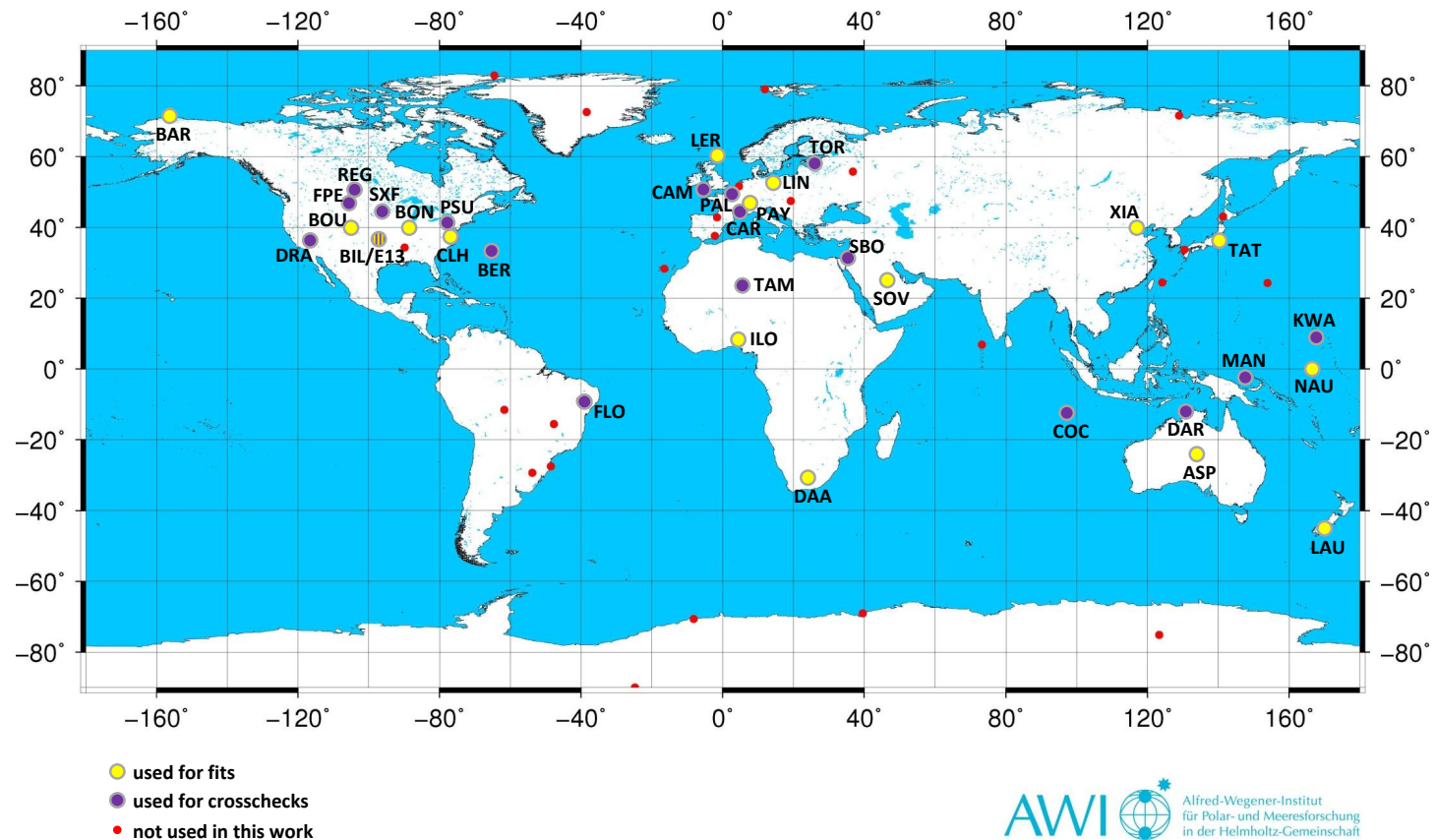


Figure 3.7.: Map indicating the stations used for cross-checks of both processed GHI and BNI data as well as for the generation of hourly BNI data using an empirical approach. Data is kindly provided by the Baseline Surface Radiation Network BSRN [BSR12]. Abbreviations represent Alice Springs (ASP), Barrow (BAR), Bermuda (BER), Billings (BIL), Bondville (BON), Boulder (BOU), Cambourne (CAM), Carpentras (CAR), Chesapeake Light (CLH), Cocos Islands (COC), De Aar (DAA), Darwin (DAR), Desert Rock (DRA), South Great Plains (E13), Florianopolis (FLO), Fort Peck (FPE), Ilorin (ILO), Kwajalein (KWA), Lauder (LAU), Lindenberg (LIN), Lerwick (LER), Momote (MAN), Nauru Island (NAU), Palaiseau Cedex (PAL), Payerne (PAY), Rock Springs (PSU), Regina (REG), Sede Boqer (SBO), Solar Village (SOV), Sioux Falls (SXF), Tamanrasset (TAM), Tateno (TAT), Toravere (TOR), Xianghe (XIA).

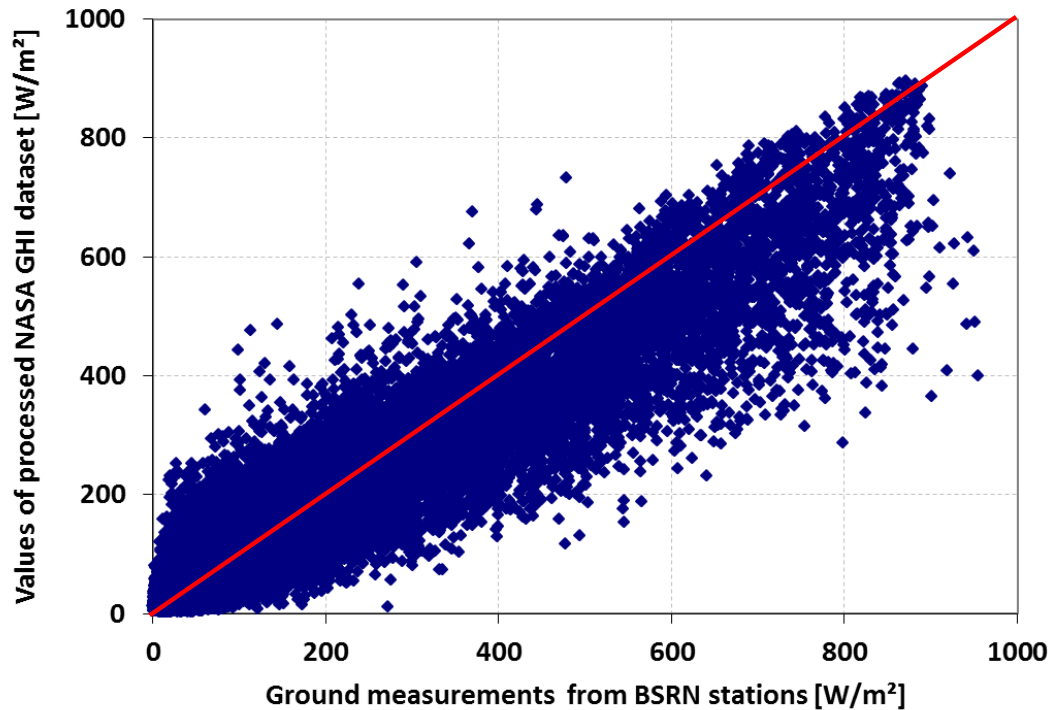


Figure 3.8.: Scatter plot derived from cross-checking the processed NASA GHI data set with ground station measurements of the BSRN network. A correlation coefficient of 0.9 and a root mean bias deviation of -3.94% are achieved, indicating very good agreement between the assessed data.

3.2.2.1.3. Processing of Beam Normal Irradiance

Determination of BNI data using physical and empirical approaches

Since representative data on the beam normal irradiance on a global scale is merely available for monthly or annual means [SRB12], this discussion gives an overview on the approach to establish an hourly global BNI data set. It will also be published in a report of the EU-funded project Endorse [End12]. Although providing data based on a three hourly temporal resolution, ISIS [ISI12] is not employed in this work. Comparisons of the distribution functions of annual BNI sums to both NASA SRB [SRB12] and SOLEMI¹⁴ [SOL12] carried out by Hoyer-Klick [HKSS] for a window

¹⁴SOLEMI offers high quality irradiance maps with temporal resolutions of 30 minutes and a spatial resolution of 2.5 km². It is based on satellite data derived from both Meteosat positions located at 0° and 63° east. Almost 50% of earth's surface is accounted for. The data is processed using a clear sky model to determine theoretical clear sky irradiation at surface level considering multiple absorption and scattering mechanisms. Information on the transmission of the broad band irradiance as well as cloud cover data provided by Meteosat satellites is used to calculate the irradiance at earth's surface. For further details please see [SOL12].

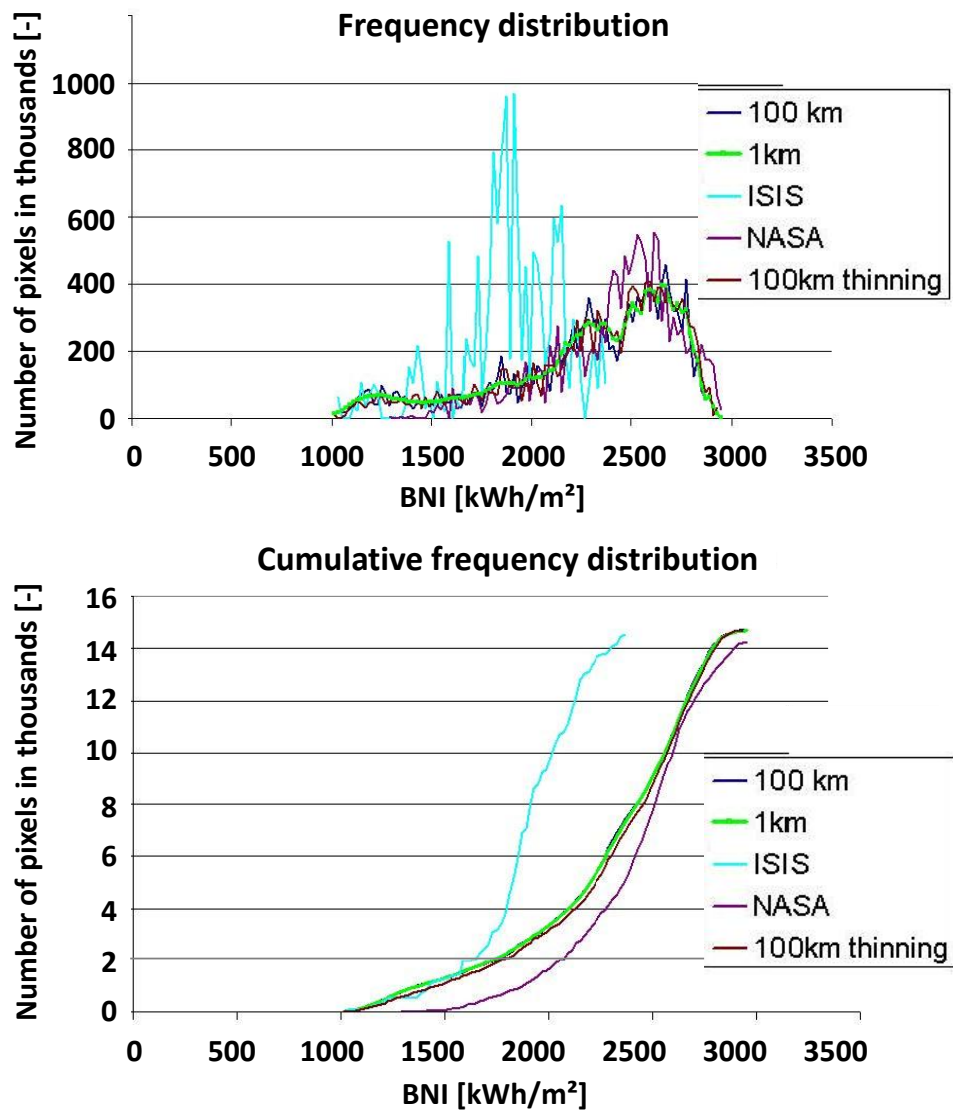


Figure 3.9.: Distribution functions of BNI annual sums for a window comprising Southern Europe and the Middle East / North Africa provided by Hoyer-Klick [HKSS]. High resolution data provided by SOLEMI [SOL12] is aggregated from 1 km to 100 km in order to obtain comparable values. A qualitative agreement can be observed between NASA [SRB12] and SOLEMI data [SOL12]. However, ISIS data [ISI12; Loh06] yields distributions which are out of the range of the other benchmarks.

comprising Southern Europe, North Africa and the Middle East yield significant underestimations, as shown in figure 3.9. Due to the very good agreement between NASA SRB data [SRB12] and SOLEMI, the annual BNI sum provided by NASA is taken as reference in this work. Different methods are now conducted to develop a representative BNI data set based on hourly values. All results are cross-checked both to NASA’s annual BNI sum and to ground measurements of the BSRN network [BSR12]. Overall two fundamentally differing approaches are feasible:

Physical approach

Sophisticated broadband radiative transfer models [BH81; Iqb83; RBW00; RAA+10] simulating the effects occurring in earth’s atmosphere are generally based on long term climatological and reanalysis data of the various constituents of the atmosphere such as ozone, aerosol and water vapour. A considerable improvement can be obtained by using the elevation of each site and the introduction of the Linke turbidity factor [RBW00]. This way of modeling of the atmospheric processes provides accurate results for high clearness values [RAA+10], i.e. particularly under clear sky conditions. In order to obtain data which is temporally resolved and capable of representing atmospheric conditions with lower clearness conditions, the Heliosat method was first proposed by Cano et al. [CMA+86] and subsequently improved by Beyer et al. [BCH96] and Hammer et al. [HHH+03]. It builds upon the aforementioned clear sky data and uses both satellite imagery on clouds and information on the ground albedo to determine a cloud index, which is in turn correlated to the clear sky index csi , where

$$csi = \frac{I_{GHI}}{I_{GHI}^{clear\ sky}} \quad (3.9)$$

with the ordinary and clear sky global horizontal irradiances I_{GHI} and $I_{GHI}^{clear\ sky}$, respectively. Multiplying data from a GHI clear sky model with GHI clear sky index information results in global horizontal irradiance (GHI) data at the ground, as indicated in the processing chain of figure 3.5.

Empirical approach

Another way of obtaining data on the beam normal irradiance is based on an empirically determined split of the global horizontal irradiance¹⁵ into its diffuse and direct (beam) components. Rather than using models which represent the atmospheric effects, a fundamental statistical relationship between the diffuse fraction k and the clearness index k_t is used: The former describes the ratio between the diffuse horizontal irradiance I_{DHI} and the global horizontal irradiance I_{GHI} :

$$k = \frac{I_{DHI}}{I_{GHI}} \quad (3.10)$$

The clearness index k_t is a means of expressing the atmospheric transmissivity using the quotient of the global horizontal irradiance at the ground I_{GHI} over the horizontal component of the irradiance at the top of the atmosphere I_{GHI}^{toa} :

¹⁵also referred to as all sky short wave downward flux

$$k_t = \frac{I_{GHI}}{I_{GHI}^{toa}} \quad (3.11)$$

By plotting ground data on the diffuse fraction over the clearness index for a given site, a fundamental relationship is observed as shown in figure 3.11: Low values of the clearness index involve high diffuse irradiance shares and vice versa. By fitting a function which best represents the aforementioned relation for a given sample, the diffuse fraction can be derived for arbitrary values of the clearness index. Various authors propose such an approach, the major difference in their assessments is either using piecewise regression equations for determined clearness index intervals [RBD90; LJ60; OH76; ESJ82; JTAK06] or using one regression term, yielding a function over the entire range of clearness values concerned [CMD⁺07; MM06; MYM06; RAA⁺10].

In this work, both physical (i.) and empirical approaches (ii.+ iii.) are carried out to obtain a total of five hourly BNI data sets on a global scale, all of which comprising the time frame from 1984 to 2005. The physical approach yields results where the global and beam irradiance components are decoupled, whereas the results from the empirical approaches formally merely split up the global irradiation component: The smaller the direct (beam) component, the larger the diffuse component and vice versa, therefore resulting in an unaffected global sum. In the following paragraphs the respective approaches will be discussed including deviation and cross-checks with the NASA annual BNI sum as well as BSRN¹⁶ data:

- **BNI data set i (A+B): Physical approach using Bird clear sky model plus ratio between I_{GHI} and $I_{GHI}^{clear\ sky}$ (i-A) and Bird clear sky model plus NASA total cloud fraction (i-B):**

The first method presented uses beam normal irradiance clear sky data processed by Hoyer-Klick [HK12], originating from a model originally developed by Bird [BH81] and modified by Iqbal [Iqb83], taking into account the suns elevation, aerosols and water vapor. The elevation angle is determined according to Iqbal [Iqb83]. Both data sets, i.e. (i-A) and (i-B) are based on the latter clear sky data. The fundamental idea to establish the link between clear sky beam normal irradiance and beam normal irradiance values at the ground is to consider the clearness of the atmosphere. In case (i-A), this clearness is represented by the ratio between I_{GHI} and $I_{GHI}^{clear\ sky}$, whereas in case (i-B) an expression using cloud fraction data provided by NASA SRB release 2.5 is used. The relations for both cases respectively are given below:

¹⁶According to figure 3.7, stations chosen for the cross-check are Bermuda (BER), Billings (BIL), Cambourne (CAM), Carpentras (CAR), Cocos Islands (COC), Darwin (DAR), Desert Rock (DRA), Florianopolis (FLO), Fort Peck (FPE), Kwajalein (KWA), Momote (MAN), Palaiseau Cedex (PAL), Rock Springs (PSU), Regina (REG), Sede Boqer (SBO), Sioux Falls (SXF), Tamanrasset (TAM) and Toravere (TOR).

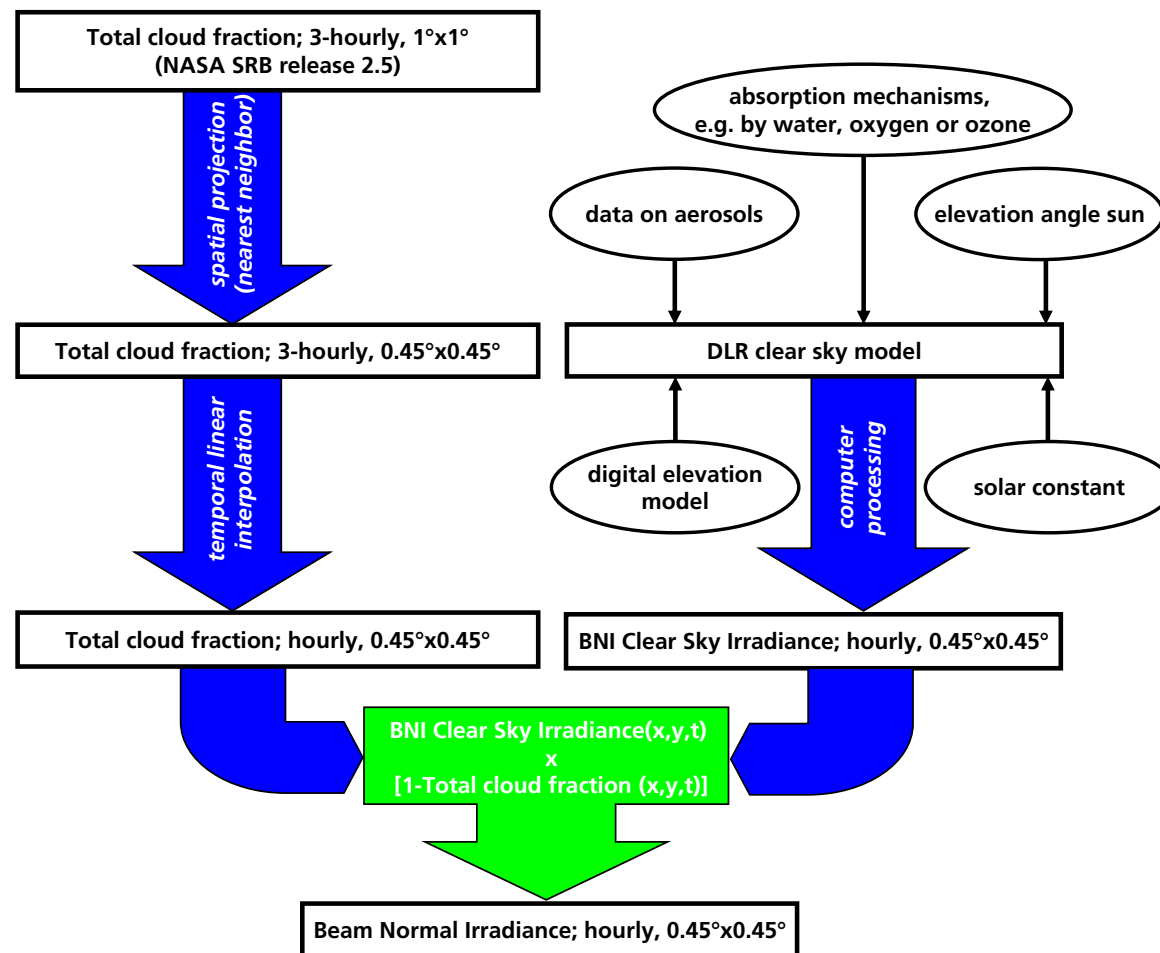


Figure 3.10.: Processing chain for computation of BNI data as used in approach (i-B). Clear sky BNI data, provided by DLR and data from NASA's SRB release 2.5 [SRB12] are combined in order to determine hourly beam normal irradiance data with a spatial resolution of $0.45^\circ \times 0.45^\circ$.

$$I_{BNI} = I_{BNI}^{clear\ sky} \cdot \frac{I_{GHI}}{I_{GHI}^{clear\ sky}} \quad (3.12)$$

$$I_{BNI} = I_{BNI}^{clear\ sky} \cdot (1 - f_{total}^{cloud}) \quad (3.13)$$

with the BNI clear sky irradiance $I_{BNI}^{clear\ sky}$, the ratio between I_{GHI} and $I_{GHI}^{clear\ sky}$ and the total cloud fraction f_{total}^{cloud} .

The processing chain carried out is exemplified for case (i-B) in figure 3.10. Raw data on the cloud fraction from NASA SRB release 2.5 [SRB12] is used based on three hourly values which are interpolated linearly to yield hourly data.

- **BNI data sets ii (A+B): Empirical approach using global fits:**

For this item a regressive model is used in order to derive BNI data from the hourly GHI data I_{GHI} derived in section 3.2.2.1.2. The general idea of such models is discussed above. Ruiz et al. [RAA⁺10] propose two sigmoid fit functions¹⁷ building upon the clearness index plus four fit parameters - being used in approach (ii-A) and expressed by relation (3.14) - and the clearness index and a height corrected optical mass m plus six fit parameters - as used in approach (ii-B) and expressed by equation (3.15).

$$k(k_t) = a_0 - a_1 \exp[-\exp(a_2 + a_3 k_t)] \quad (3.14)$$

$$k(k_t, m) = a_0 - a_1 \exp[-\exp(a_2 + a_3 k_t + a_4 k_t^2 + a_5 m + a_6 m^2)] \quad (3.15)$$

with the clearness index k_t and the optical air mass m . In this work the optical air mass is derived according to Kasten and Young [KY89].

The respective fit values for the variables are indicated in the following table:

model	a0	a1	a2	a3	a4	a5	a6
ii-A	0.952	1.041	2.3	-4.702			
ii-B	0.944	1.538	2.808	-5.759	2.276	-0.125	0.013

Table 3.4.: Fitting coefficients according to Ruiz et al. [RAA⁺10] for the models (ii-A) and (ii-B).

The authors checked their model results with five other models for 21 ground stations situated in the US and Europe.

- **BNI data set iii: Empirical approach using fits from 16 BSRN ground stations:**

The basic idea justifying this third empirical approach is to take into account climatic and regional patterns of the relationship between diffuse fraction and

¹⁷In this work reference is made to their proposed models G0 and G2.

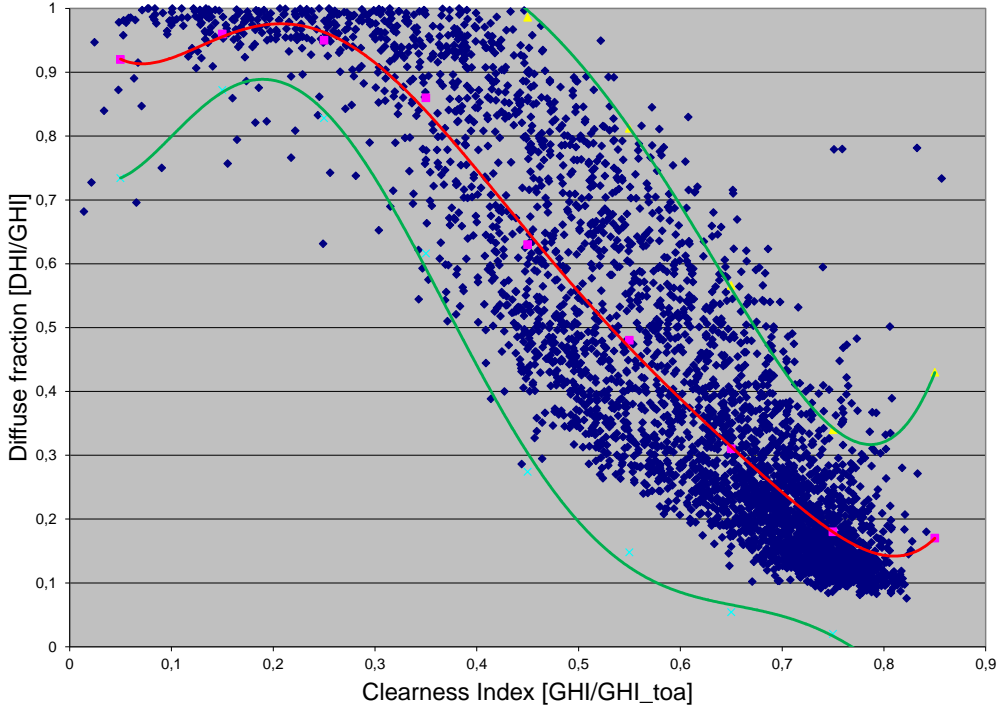


Figure 3.11.: Exemplary scatter plot of clearness index over diffuse fraction for the BSRN station Billings. Means (indicated in red) and standard deviations of the diffuse fraction are determined and interpolated for ten bins, yielding a corridor of quality checked data between the lower and upper boundaries indicated in green.

clearness index by using data of the latter variables from 16 globally distributed BSRN stations as indicated in figure 3.7. First of all, each station's scatter plot is quality checked according to Younes et al. [YCT05] by determining averages and standard deviations of the diffuse fraction for each of ten bins in the entire range of clearness values from zero to one. Data passing the quality check is comprised within an interval of the bin's mean diffuse fraction $\pm 2\sigma$, interpolating finally yields a corridor of quality checked data. Please see figure 3.11 for further insight. The latter is eventually fitted for each station individually using equation (3.14) from Ruiz et al. [RAA⁺10] introduced above and the software tool GAMS [GAM12] in a non linear programming optimization mode to determine a set of coefficients a_i for each station and equation. In order to validate the approach, the fits are in turn employed using ground station global horizontal irradiance data I_{GHI} to determine beam normal irradiance I_{BNI} , which is cross-checked with the actual BNI ground measurements. BNI data for all sites not covered by a BSRN station are interpolated by using a normed inverse distance¹⁸ weighted share of each BSRN station's diffuse fraction value for a given clearness index.

¹⁸Distances on earth are determined using the formulae for the Great Circle Distance, indicating the shortest trajectory on a sphere.

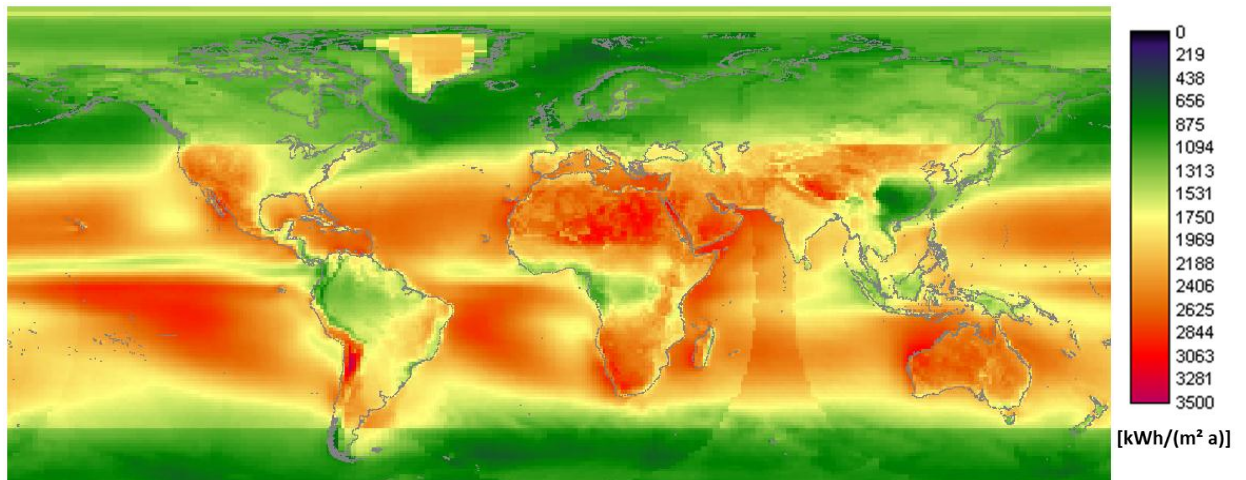


Figure 3.12.: BNI long term annual average provided by NASA SRB 3.0 [SRB12]. This map is used as reference for the cross-check to the five BNI data sets established in this work.

Results obtained from the different approaches

The results for BNI using the various approaches discussed above are cross-checked both to the average annual beam normal irradiance sum provided by NASA SRB 3.0 [SRB12] indicated in figure 3.12 as a means of relative benchmarking and to an ensemble of 18 BSRN ground stations. An overview of the results is given in figure 3.13. Data set (ii-B) is the best performer both in terms of its mean deviation to NASA's annual sum (-7.8 %) and its mean root mean bias deviation averaged over 18 ground station sites (-1.86 %). The enlarged figure 3.14 presents this resulting data set. Results for (ii-A) provide somewhat resembling figures, however, in this model the air mass is not used as a predictor. Results for the other data sets are discarded either due to unreasonably high values - please see (i-A) and (iii) - or due to annual sums which are too inferior, as in case (i-B). For the latter data set this seems to be primarily due to the fact that the attenuation of the clear sky irradiation is merely represented by a cloud fraction term, which reduces the incident light linearly, which does not hold in reality: Even if the sky is - slightly - overcast, direct (beam) components can occur. Overall, data set (ii-B) derived with an empirical approach as discussed in the previous paragraphs is chosen for any further assessments using beam normal irradiance data in this work.

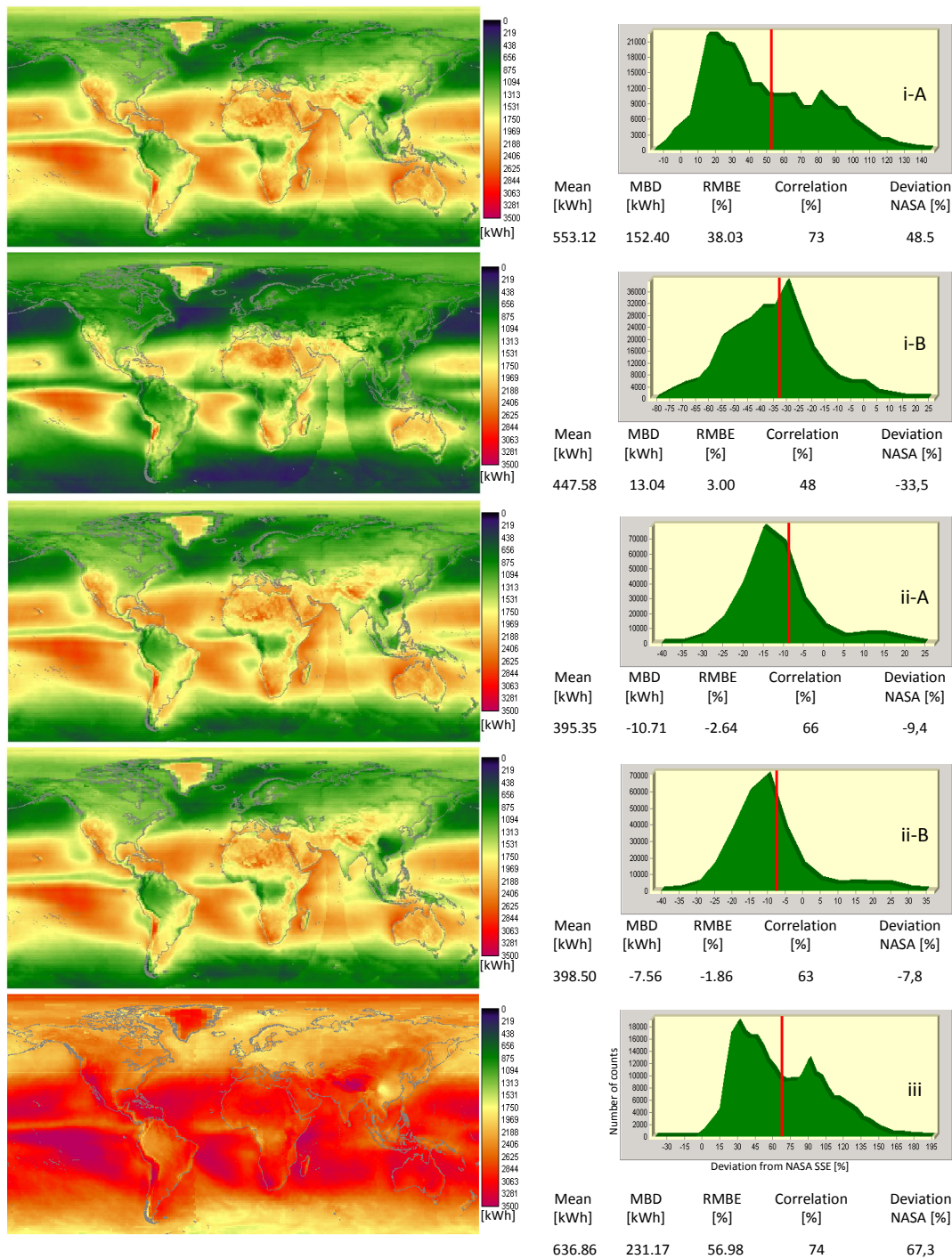


Figure 3.13.: Comparison of the five processed beam normal irradiance data sets (physical (i-A), physical (i-B), empirical (ii-A), empirical (ii-B), empirical (iii)) to 18 BSRN ground stations and to NASA SSE 6.0/SRB 3.0 annual BNI sum [SRB12]. For the former the four indicated figures beneath the distribution graphs on the left are derived as an average for the 18 sites: Satellite data mean, mean bias deviation, root mean bias error and correlation. For the latter the overall map deviation is determined. It is indicated beneath the distribution graphs on the very right. Data set (ii-B) is chosen for further assessments in this work.

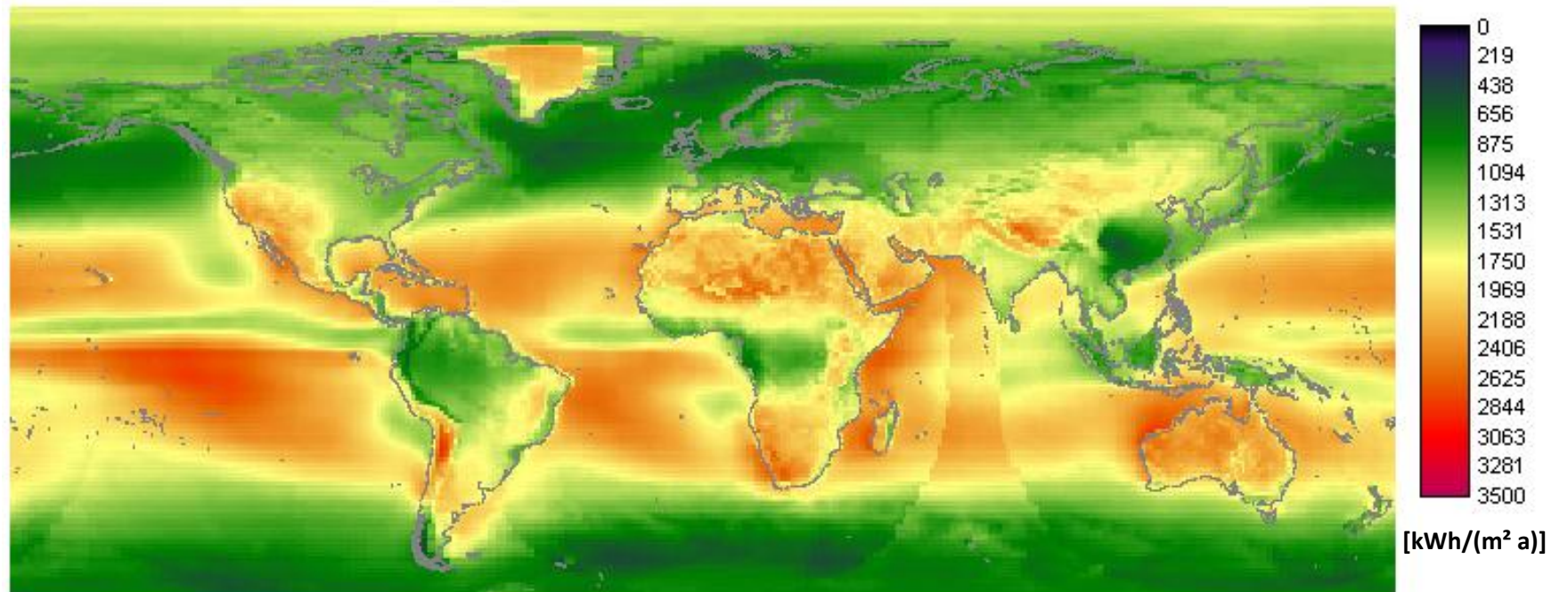


Figure 3.14.: Final BNI long term annual average as obtained by empirical approach ii-B. This data set is the best performer in cross-checks with BSRN ground measurements and NASA BNI annual average.

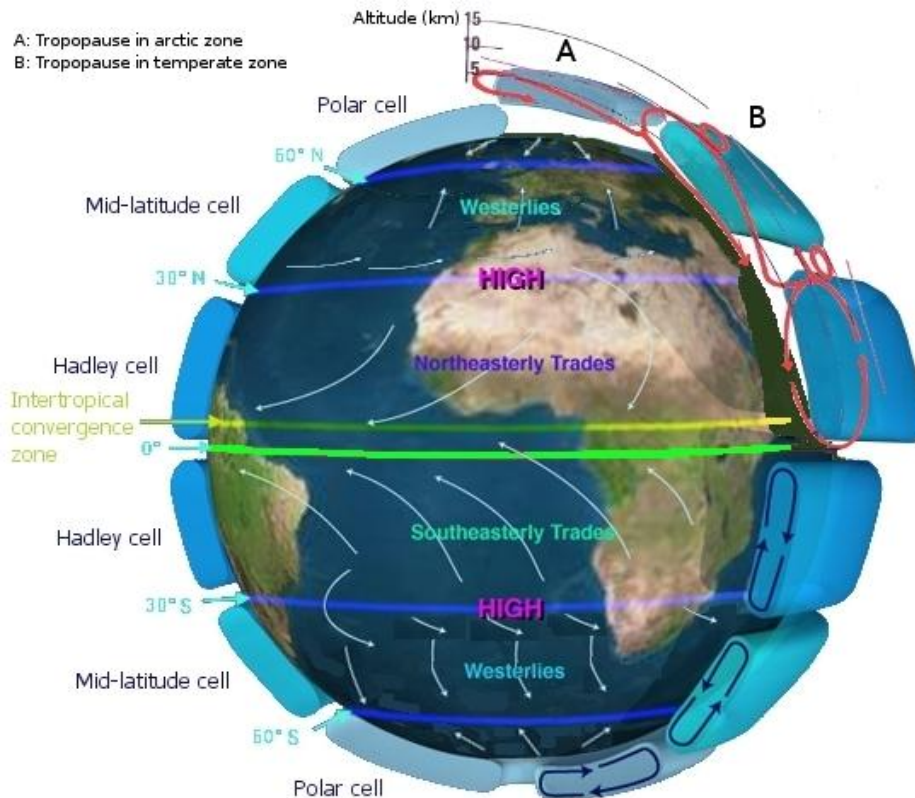


Figure 3.15.: Illustration of earth’s major wind systems according to [WIN12]

3.2.2.2. Wind

In this section the approach and processing to obtain hourly wind data at the desired spatial resolution of 0.45° are discussed. The items in the following are excerpted from work conducted by the author within [SGS11].

After solar irradiation, wind is the renewable resource with the second largest theoretical global potentials. The principle origin of wind is driven by the uneven solar irradiation of earth, thus heating up the atmosphere heterogeneously. This results in different high and low pressure systems, the gradient between these systems entails a balancing air current observed as wind. Local wind systems are caused for instance by temperature differences induced by differing heat capacities of earth’s surface, e.g. the sea-land breeze. An overview of global wind systems is given in figure 3.15.

3.2.2.2.1. Available data on wind

Several regional data sets on wind speeds are available. On a global scale, however, well resolved data both in terms of high spatial as well as hourly temporal resolution is not available or incomplete, which is why retrospective analysis¹⁹ data is used to fill the gap with long-term continuous data records [BRC11]. To obtain such data, sophisticated

¹⁹The term retrospective analysis is also referred to as reanalysis.

	MERRA	NCEP	ERA	ERA-interim	CFSR	GLDAS
temporal resolution [h]	1	6	6	6	6	3
spatial resolution	0.5°x0.66°	210km	125km	80km	38km	1°x1°
temporal coverage [a]	1979-present	1948-2009	1957-2002	1989-present	1979-present	1948-present

Table 3.5.: Overview of existing reanalysis data sets. Wind speed data from the Modern Era Retrospective-analysis for Research and Applications - MERRA - product [MER12] is used in this work.

models study weather and climate variability over the course of climatological time scales. Results are widely used in the earth science community to “drive various models concerned with atmospheric effects, blending the continuity and breadth of output data of a numerical model with the constraint of vast quantities of historical observational data records” [MER12]. A good overview on state-of-the-art reanalysis data is given by Decker et al. [DBW⁺12], who evaluate and rank the performance of six products - indicated in table 3.5 - in terms of their correlation, standard deviation, mean bias and root mean squared error to flux tower observations of, inter alia, temperature and wind speed.

In summary Decker et al. [DBW⁺12] conclude, that the ERA-Interim data set performs slightly better than the rest, however, the usefulness and advantage for this work’s purpose of an hourly temporal resolution as offered by the Modern Era Retrospective-analysis for Research and Applications (MERRA) is obvious. Furthermore, MERRA offers data periods which coincide with the irradiance data from NASA’s SRB products, which are also used in this work as discussed in the previous sections. For these reasons a processed MERRA data set is used for all analyses related to wind power in this work.

3.2.2.2.2. Wind speed processing

Wind speed data from MERRA is available at different heights above ground or for 72 vertical pressure levels. For this work, data with a height of 50 m above ground in both a west-east (u-wind) and a north-south (v-wind) component is used. In analogy to the irradiation data, the MERRA data set is processed in order to meet the desired temporal and spatial specifications. As far as the temporal resolution is concerned, no interpolation is carried out since the MERRA data set comes with hourly values. However, a spatial projection from the original resolution of $\frac{1}{2}^\circ \times \frac{2}{3}^\circ$ to the desired $0.45^\circ \times 0.45^\circ$ is conducted. Moreover, according to the trigonometric relation

$$v_{resulting\ wind}(50\ m) = \sqrt{v_{u-wind}^2 + v_{v-wind}^2} \quad (3.16)$$

a resulting wind speed at a height of 50 m $v_{resulting\ wind}(50\ m)$ is calculated using the wind’s u and v directed velocities v_{u-wind} and v_{v-wind} respectively. Overall, the database contains global wind data from January 1st, 1984 through December 31st, 2005 at hourly time steps. Figure 3.16 displays the long term annual average of the processed data from 1984 through 2005 for a hub height of 50 m using the approach presented in this section.

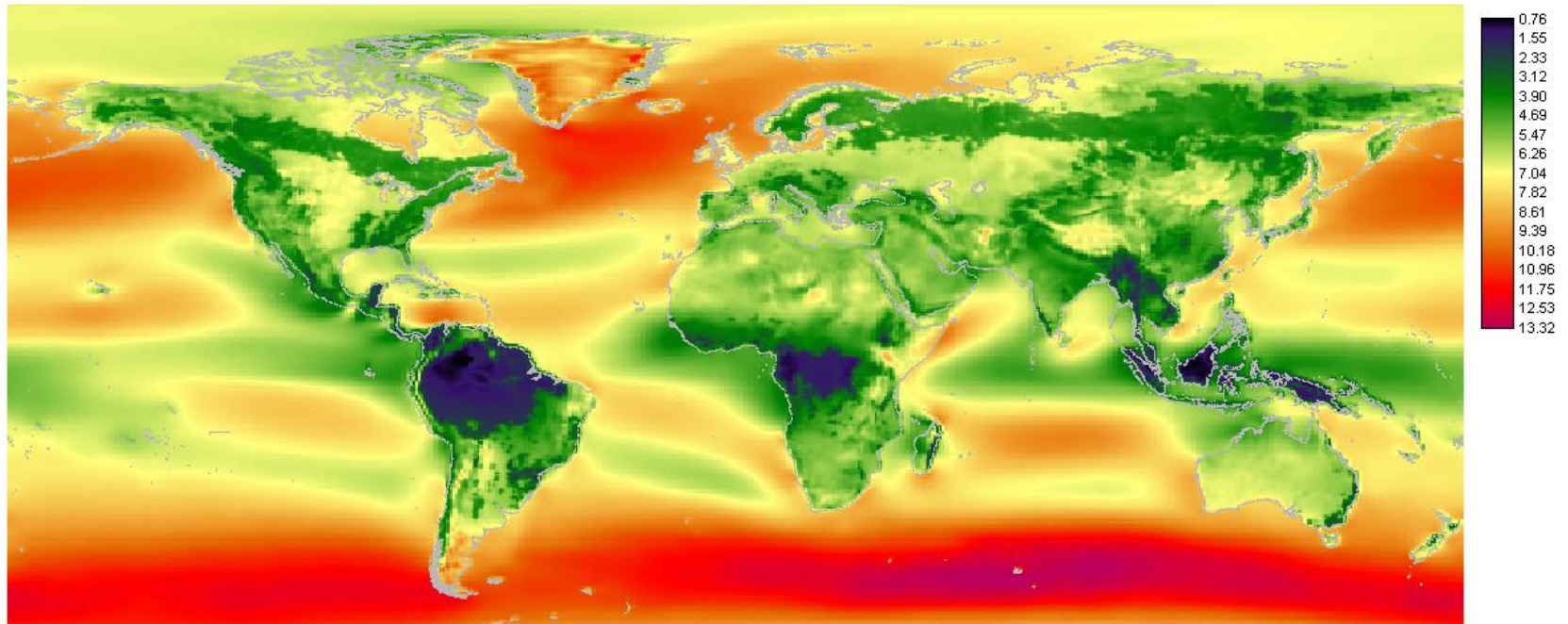


Figure 3.16.: Annual average of the resulting wind speed at a height of 50 m out of the 22 year wind speed data set processed within this work. Indicated values are displayed in $\left[\frac{m}{s}\right]$. Good average wind speeds are generally found in regions with little roughness lengths such as water bodies or deserts. On the other hand, regions with high surface roughness length values, e.g. forests, result in inferior average wind speeds.

3.2.2.3. River run-off

In this section the approach and processing to obtain hourly values for river run-off data at the desired spatial resolution of 0.45° are discussed. Parts of the here presented line of action are excerpted from work conducted by the author within [SGS11].

The world's water cycle is initially driven by the energy provided through solar irradiation which causes evaporations from surface water bodies like lakes and rivers, the soil and the oceans. The water vapor ascends with the heated air, which contains a limited amount of vapor as described by the vapor pressure curve. Once the air cannot accept any additional humidity - which is mainly due to decreasing temperatures of rising air masses - the water vapor condenses which is manifested by the formation of atmospheric clouds. The latter are transported by large scale wind systems as discussed in subsection 3.2.2.2. As soon as the water density exceeds a critical limit, the water precipitates as rain towards the ground. Parts of the precipitation evaporate right away; the remainder will rest on earth's surface, is absorbed by the soil and eventually flows towards the oceans due to the gravitational field. On its way, this run off can be converted into electricity.

3.2.2.3.1. Considered run-off data sets and data processing

There is basically only one data set of river run-off containing both, globally and temporally resolved data. This data is generated by the WaterGap 2.1g model [HD07; DFZ09], which has been developed at the Center for Environmental Systems Research at the University of Kassel in Germany in cooperation with the National Institute of Public Health and the Environment of the Netherlands. The aim of the model is first of all to provide a basis to compare and assess current water resources and water use in different parts of the world, and secondly, to provide an integrated long-term perspective of the impacts of global change on the water sector.

WaterGap comprises two main components, a global hydrology and a global water use model. The former simulates the characteristic macro-scale behavior of the terrestrial water cycle to estimate water resources, while the global water use model computes water use for the sectors households, industry, irrigation, and livestock. The calculations cover the entire land surface on a global scale (with the exception Antarctica) and are performed on a $0.5^\circ \times 0.5^\circ$ spatial resolution [LCV05b]. Döll [Doe10] kindly provides river discharge in $\left[\frac{km^3}{month} \right]$ for each grid cell covering the time frame from 1984 through 2008.

In order to process the files provided by WaterGap, the data is extracted and projected to the desired spatial resolution of $0.45^\circ \times 0.45^\circ$. The monthly averages of electricity output - not the resources data - are interpolated to obtain hourly values, with the boundary condition that the integral over the entire year for both the monthly and hourly data be identical.

Figure 3.17 indicates the long term annual average of the river discharge. An enlargement for the region Europe, North Africa, Middle East is included. The major river drainage systems can be seen.

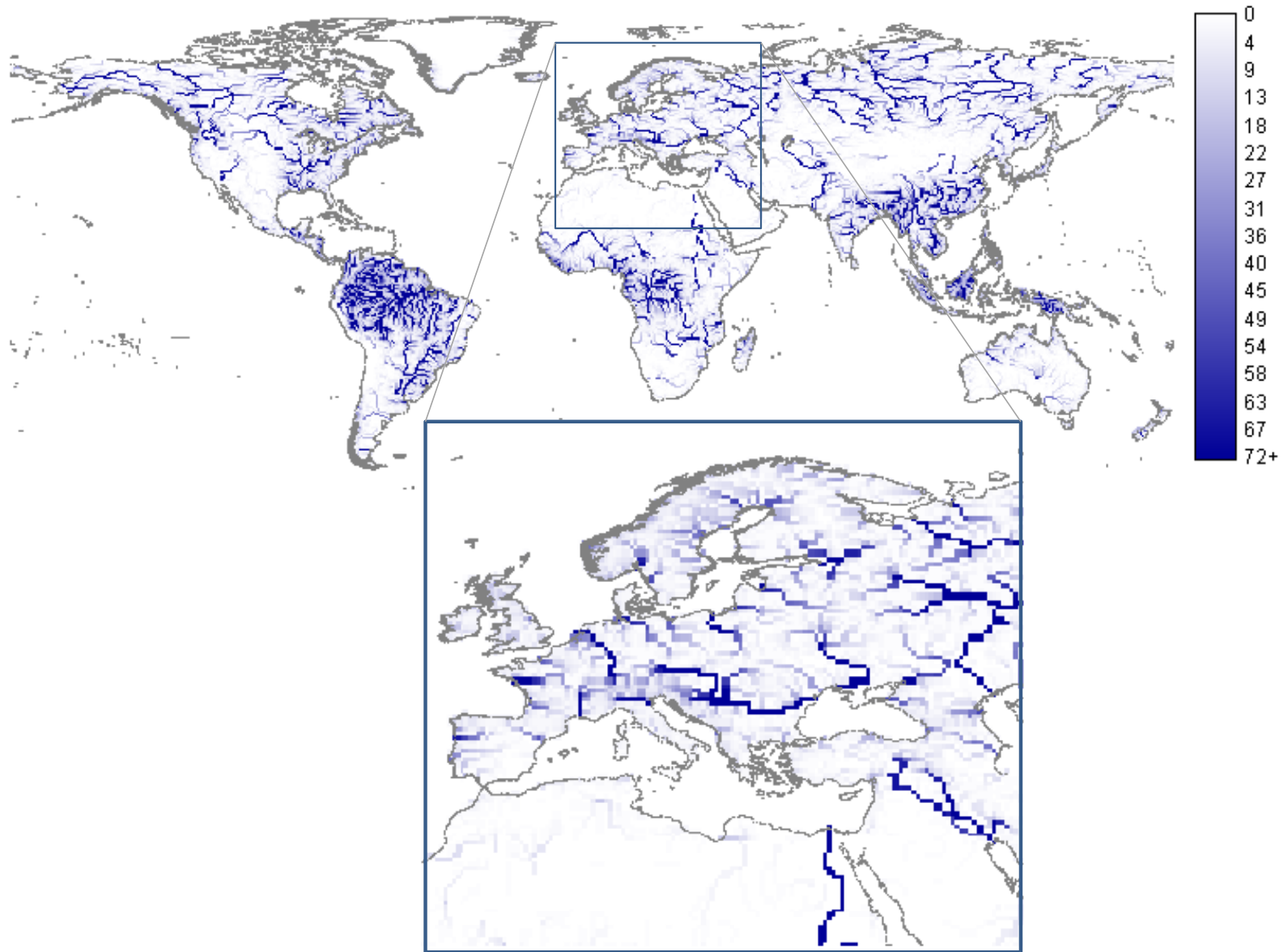


Figure 3.17.: Annual long term average of the river discharge in $\left[\frac{km^3}{a}\right]$ based on data of the WaterGap model [HD07; DFZ09] and processed within this work. The major river systems can be identified.

<i>Parameter</i>	<i>2010</i>	<i>2020</i>	<i>2030</i>	<i>2040</i>	<i>2050</i>
loss factor centralised PV [%]	10	10	10	10	10
loss factor decentralised PV [%]	15	15	15	15	15
availability factor PV [%]	98	98	98	98	98
Temperature coefficient PV [1/°C]	-0.005	-0.0045	-0.0045	-0.004	-0.004
availability factor CSP [%]	0.95	0.95	0.95	0.95	0.95
efficiency of the power block CSP [%]	0.37	0.37	0.37	0.37	0.37
efficiency of thermal storage CSP [%]	0.95	0.95	0.95	0.95	0.95
turbine diameter onshore [m]	77.5	102.3	116.4	124.1	130.1
turbine diameter offshore [m]	96.1	135.9	156.9	175.4	192.2
loss factor wind [%]	0.15	0.15	0.15	0.15	0.15
availability factor wind [%]	0.95	0.95	0.95	0.95	0.95

Table 3.6.: Technical parameters used in this work, according to Scholz [Sch12].

3.2.3. Power plant technology modeling

For the enhanced version of REMix-EnDaT power plant models originally set up by Scholz [Sch12] are used. The parameters of the considered technologies for the year 2010 and assumptions for their development until 2050 are based upon Leitstudie [Lei10]. These parameters, listed in table 3.6, have been updated and reviewed by several German research institutes and have also been used for the SRU study [SRU10]. A discussion of the parameters used in the models is provided in annex A.7. The general approach to obtain hourly power output is discussed below for each technology considered in this work based on excerpts from [SGS11]. The presented equations represent the power output for each pixel i . In subsection 3.2.1 the maximum installable capacity per pixel is derived. Also, in subsection 3.2.2 an hourly resources database is established for each pixel. These two elements of preparatory work are now integrated into the expression for the hourly power outputs per pixel i , $E_{el,i}^{tech}(t)$:

Photovoltaic

Although many semi-conducting materials are eligible for use in photovoltaic modules, mono and multicrystalline silicon based solar cells have gained the largest market impact in recent years and are expected to dominate the markets for the time being. Therefore, technical parameters of silicon based photovoltaic power plants have been applied as modeling input.

For the assessment both decentralized systems, which can be installed in settled areas on roof tops and façades, and centralized systems, i.e. large scale deployment on bare areas, are considered. For the former a normal distribution is assumed for the azimuth angle to consider roofs not directly pointing south (north) on the northern (southern) hemisphere. All open-areas plants are assumed to be optimally directed. The hourly electricity output for grid box i is obtained by using:

- the maximum installable PV capacity $P_i^{PV, inst-max}$, as derived in subsections 3.2.1.3 and 3.2.1.4
- the hourly average irradiance on the module $I_{module,i}^{PV}(t)$ taking into account satellite derived data for global horizontal and beam normal irradiance from a database presented in subsection 3.2.2, the module's tilt and azimuth as well as data on the sun's elevation as a function of location and time according to Quaschnig [Qua06]
- the loss factor f_{loss}^{PV} , which is a function of the module direction, accounting for shadowing and dirt
- the hourly average of the difference of the module temperature $\phi_{module,i}^{PV}(t)$ and the module temperature at standard testing conditions ϕ_{STC}^{PV} (25 °C) multiplied by the temperature factor f_T^{PV} representing the temperature dependence of the modules performance
- the availability factor f_{av}^{PV} taking into account break down or maintenance periods

The average of the hourly power plant output $E_{el,i}^{PV}(t)$ is determined per grid cell i using

$$E_{el,i}^{PV}(t) = P_i^{PV, inst-max} \cdot \frac{I_{module,i}^{PV}(t)}{1000 \frac{W}{m}} \cdot f_{av}^{PV} \cdot (1 - f_{loss}^{PV}) \cdot [1 + f_T^{PV} \cdot (\phi_{module,i}^{PV}(t) - \phi_{STC}^{PV})] \quad (3.17)$$

To obtain the final output per cell, the respective outputs for each direction and for centralized as well as decentralized plants are summed up. Integration over the entire year yields the total annual electricity production of the considered grid cell.

Concentrating solar power

Different setups for concentrating solar power plants have been developed over the past decades. However, linear concentrating parabolic troughs have proven to be a reliable technology in recent years - even in commercial operation - which is why this technology option is used in the modeling.

Hence a CSP plant using solar troughs mounted on an axis directed in north/south direction is considered [Sok04]. Due to this setup, the sun's elevation angle in north/south direction cannot be followed and hence the effective irradiance exploitable by the trough system is reduced due to cosine losses. However, this concept has proven its technical and economic maturity and is therefore used.

The approach is separated into two steps. At first, the heat output of the solar field is derived, the second step comprises the determination of electricity output:

- Heat output of the solar field

To determine the heat output of the solar field per pixel i , data is needed on

- (i.) the maximum installable thermal capacity of the solar trough per pixel i , $P_i^{CSP, inst.max_{th}}$, derived in subsections 3.2.1.3 and 3.2.1.4
- (ii.) the direct (beam) irradiance on the trough taking into account satellite derived data for the beam normal irradiance from a database presented in subsection 3.2.2, the location of the solar field and the solar elevation angle. This ensures a proper representation of the system, also considering the cosine losses due to the single axis design and north-south arrangement of the trough. An in-depth discussion on the calculation of the normal irradiance on the trough is given by Caffisch [Caf09].

Using the maximum thermal installable capacity for each grid box i $P_{th, i}^{CSP, inst.max}$, the beam normal irradiance on the trough $I_{normal, i}^{trough}$ and the standard beam normal irradiance $800 \frac{W}{m^2}$, the total solar field heat output per pixel i $E_{th, solar\ field, i}^{CSP}(t)$ is determined by

$$E_{th, solar\ field, i}^{CSP}(t) = P_{th, i}^{CSP, inst.max} \cdot \frac{I_{normal, i}^{trough}(t)}{800 \frac{W}{m^2}} \quad (3.18)$$

- Electricity output

The electricity output for each pixel i $E_{el, i}^{CSP}(t)$ is derived from the heat output of the solar field $E_{th, solar\ field, i}^{CSP}(t)$ using the availability factor f_{av}^{CSP} and the efficiencies η_{st} and η_{pb} of the thermal storage and the power block, respectively. The thermal storage efficiency is weighted using the solar multiple $f_{solar\ multiple}^{CSP}$:

$$E_{el, i}^{CSP}(t) = E_{solar\ field, i}^{CSP}(t) \cdot f_{av}^{CSP} \cdot \eta_{pb} \cdot \left(1 - \frac{f_{solar\ multiple}^{CSP} - 1}{f_{solar\ multiple}^{CSP}} \cdot (1 - \eta_{st})\right) \quad (3.19)$$

Wind power

Wind electricity output can be derived separately for offshore and onshore sites using data on

- the maximum installable capacity of onshore and offshore plants per pixel i , $P_i^{wind, inst.max}$, as derived in subsections 3.2.1.3 and 3.2.1.4 and
- the velocity of wind at the respective hub height. For this value, satellite derived data for wind speeds at a height of 50 m above the ground from the database presented in subsection 3.2.2 is used. Moreover, the resulting wind speed $v_{resulting\ wind}$ for any hub height above ground h_{hub} of a turbine can be derived according to the vertical wind profile:

$$v_{resulting\ wind}(h_{hub}) = v_{wind}(50\ m) \cdot \frac{\ln \frac{h_{hub}}{z_0}}{\ln \frac{50}{z_0}} \quad (3.20)$$

z_0 indicating the surface roughness, which is also included into the established database. Figures of the surface roughness change slightly throughout the year and are also part of the resources database. For the hub heights used, please see table 3.7.

Parameter	2010	2020	2030	2040	2050
hub height onshore [m]	112	122	127	131	132
hub height offshore [m]	80	102	116	128	140

Table 3.7.: Hub heights used for the calculation of the resulting wind speed according to Scholz [Sch12].

Hourly electricity output per pixel i $E_{el, i}^{wind}(t)$ using wind turbines is then determined as follows:

$$E_{el, i}^{wind}(t) = \frac{P_i^{wind, inst_max}}{P_{rated\ power, i}^{wind}} \cdot f_{av}^{wind} \cdot (1 - f_{loss}^{wind}) \cdot \frac{1}{2} \cdot \rho \left(\frac{d_{rotor}^{wind}}{2} \right) \cdot \Pi \cdot [v_{resulting\ wind}(h_{hub})]^3 \cdot c_p \quad (3.21)$$

The nominal capacity $P_{rated\ power, i}^{wind}$, the installable capacity $P_i^{wind, inst_max}$ and the Betz power coefficient $c_p = 0.593$ indicating the maximum of power exploitation from a moving air mass using a wind turbine in accordance to the ENERCON plant E 82 [Tur12] are used. The ratio of the nominal capacity $P_{rated\ power, i}^{wind}$ and the installable capacity $P_i^{wind, inst_max}$ scales the output of the reference plant. Loss caused by interfering flow fields, i.e. if turbines are sited closely to one another, and during transmission according to Ohm's law are accounted for by a global loss factor f_{loss}^{wind} . Finally, the availability factor f_{av}^{wind} considers periods for maintenance or brake downs. ρ indicates the density of air ($1.225 \frac{kg}{m^3}$), d_{rotor}^{wind} the diameter of the turbine and v the resulting wind speed at the hub height. In order to determine the electricity output of individual wind turbines three wind speed regimes are considered:

- (i.) $0 \frac{m}{s} < v < 12 \frac{m}{s}$ (wind speed at which nominal capacity is approached)
- (ii.) $12 \frac{m}{s} < v < 26 \frac{m}{s}$ (wind speed at which nominal capacity is reached: blades are gradually pitched to keep the output constant and to protect against damage)
- (iii.) $v > 26 \frac{m}{s}$ (wind speed limit: if exceeded turbines are gradually switched off for protection against damage, resulting in a power output of zero)

Hydro power

In contrast to the other technologies discussed above, for hydro power a top-down approach is used to assess electricity generation potentials. As introduced in section 3.2.1.4, a land-use based assessment of installable capacities is replaced by an approach building upon existing run off power plants and their capacities according to the data provided by the World Electric Power Plants Database [WEP09]. Further processing steps include geo-referencing each plant in order to be able to refer all existing capacities to a specific grid box i . Both modernization and new constructions are taken into account. In order to derive power output from the installed capacities, an approach proposed by Czisch [Czi05] is employed considering monthly means of resources data on river run off as presented in section 3.2.2.3.1: The second largest monthly mean run off per pixel is considered to yield the maximum power output of the capacity installed in grid box i , the largest monthly mean yields the same figure while all other months are scaled according to their monthly means. For instance, if in grid box i an installed run off power plant capacity of 100 MW were available, the second largest run-off (and the largest) would lead to an hourly power generation according to this model of 100 MWh. For a monthly mean of merely 50% of the second best performing month the output would be estimated to attain 50 MWh.

3.3. Application of REMix-EnDaT: Global assessment of renewable energy potentials

As discussed above, one of the enhanced capabilities resulting from the developments within REMix is the assessment of technical, economic and full load hour potentials on a global scale, as carried out in this section using the enhanced REMix module EnDaT. This section is divided into two subsections: The first subsection 3.3.1 gives further background for a better understanding of how results are computed. It is made up of discussions on the definitions of the potentials, a mathematical formulation for cost and full load hours, how typical meteorological years are created and a short introduction on the solar multiple of CSP plants.

Building upon this further background, in the results subsection 3.3.2 REMix-EnDaT is employed for the computation of full load hour and cost potentials for PV, CSP, on- and offshore wind and hydro power on a global scale. Also, a sensitivity study is performed for the major parameters used within the assessments.

3.3.1. Further background

3.3.1.1. Potential definitions

Using the approach discussed in the previous sections, both installable capacities and hourly resolved renewable power generation can be determined. According to Kaltschmitt et al. [KSW05], the following definitions for the potential classes displayed in figure 3.18 are used²⁰:

²⁰Definition according to [KSW05] for theoretical, technical and cost potentials, the latter is referred to as economic potential in [KSW05].

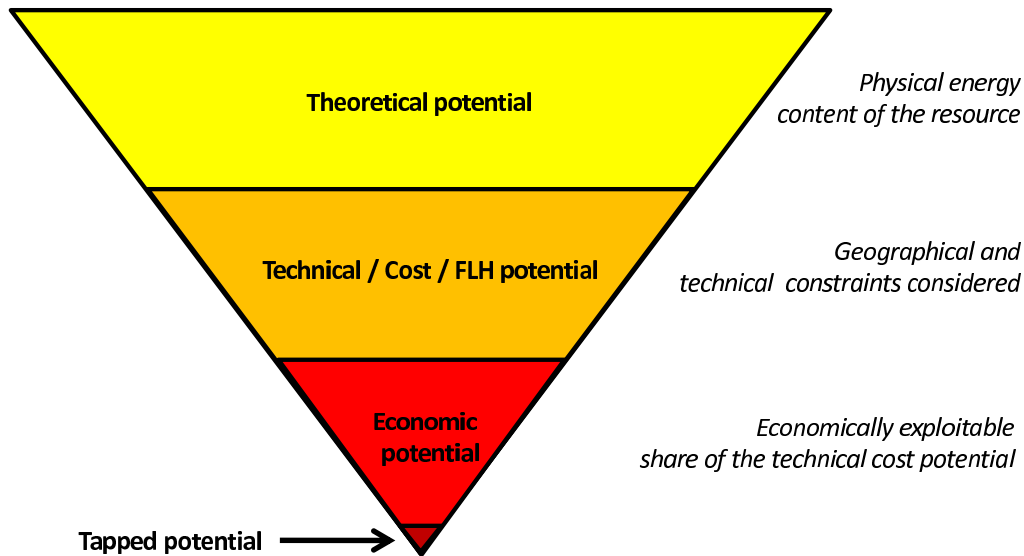


Figure 3.18.: Cascade of different potential classes, all of which being assessed in this work except for economic and tapped potentials. It can be seen how the energy content narrows down from theoretical towards tapped potentials.

A Theoretical potential

→ **Physical energy content or average values of renewable resources:** The theoretical potential of a renewable resource is the amount of the physical energy flow - i.e. solar irradiance in $[\frac{W}{m^2}]$ or wind speed in $[\frac{m}{s}]$ - which could potentially be used at a specific site and during a specific period (e.g. over the course of one entire year). Examples are the electromagnetic energy of solar irradiation, the mean kinetic energy of wind or the potential energy of water. Due to the fluctuating nature of many renewable resources, long term averages are most suitable to derive the theoretical potentials. Determinations of the latter using the resources database established in this work are given in subsection 3.2.2.

B Technical potential

→ **Consideration of geographical and technological limitations, e.g. land availability and restrictions as well as technological parameters, all of the latter yielding sustainability criteria:** Geographical and technical restrictions limit the theoretical potentials. Geographical restrictions used in this work are protected areas, shifting sand dunes, glaciers, areas with large slopes etc. Any technical power conversion is subject to energy losses, since the physical energy content of the renewable resource is never utterly converted into usable electricity or heat. Taking these aspects into consideration, the total amount of potentially converted renewable electricity is defined as the technical potential.

C Cost potential

→ **Establishment of the relationship between technical power generation potentials and the related cost:** Bearing in mind that renewable power has to compete on existing markets, an analysis of the cost per generated (more precisely converted) energy unit is performed. In this work the cost associated with renewable power generation will be derived in subsection 3.3.2.1 for selected technologies according to the discussion in the following subsection 3.3.1.1.1. Moreover a sensitivity analysis is carried out in section 3.3.2.2 in order to assess the impact of deviations from the anticipated cost levels on the economic potentials.

D Full load hour potential

→ **Establishment of the relationship between technical installation potentials and the generated electricity:** Using the annual sum of the hourly power generation and the capacities used for the latter, the ratio of these two figures yields an expression for the full load hours of a technology. A discussion of this type of potential is particularly useful since it is independent of any price levels, merely relating physical figures. It is also derived in subsection 3.3.2.1 according to the definition provided in subsection 3.3.1.1.2.

E Economic potential

→ **The economically exploitable share of the cost potential is referred to as the economic potential.** It is certainly dependent on the market environment which share of the cost potential becomes competitive. Moreover, market incentive programs might increase the demand for potentials which otherwise would not be considered.

F Tapped potential

→ **The actual potential being used in energy conversion systems to generate electricity.** Historically, the major part of the tapped renewable potential is made up of hydro power, nowadays particularly wind power and ever increasing solar power contribute to a real usage of the potential.

3.3.1.1.1. From capital budgeting to generation cost and cost potentials

This paragraph gives an overview as to how cost figures are derived within this work's potential assessment. All cost values used are indicated in table 3.8. They are presented in terms of inflation-adjusted € for the year 2010 in order to maintain comparability with other sources. Furthermore, lifetimes and interest rate are depicted.

Capital budgeting is a classical approach for the determination of the arising annual cost of an investment as a function of the interest rate p and amortisation period n . The approach is straight forward: The captial value of an investment C_0 , in our case the specific investment cost per capacity $c_{spec}^{tech, inv}$ multiplied by the installed capacity of the respective power plant²¹ $P_i^{tech, inst}$, is allocated over the entire depreciation period by using the annuity factor $AF_{p,n}^i$ eventually yielding the annual cost which is referred to as the annuity $a_{p,n}$:

²¹For the potential assessments, the latter coincides with the maximum installable capacity per pixel i $P_i^{tech, inst-max}$, as derived in section 3.2.1.4.

Parameter	2010	2020	2030	2040	2050
specific investment cost open-area PV [€/kW]	2420	948	766	711	696
specific investment cost roof-top PV [€/kW]	2874	1331	1109	1059	1028
specific investment cost solar field CSP [€/kW _{th}]	693	383	272	226	202
specific investment cost power block CSP [€/kW]	1150	1018	905	827	777
specific investment cost thermal storage CSP [€/kW]	52	36	26	22	20
specific investment cost offshore [€/kW]	3327	2117	1815	1512	1311
specific investment cost onshore [€/kW]	1331	1039	988	948	907
specific investment cost modernized plants hydro [€/kW]	1386	1469	1507	1539	1565
specific investment cost new plants hydro [€/kW]	4662	4830	4899	4968	5030
relative fixed operational costs PV [%]	1	1	1	1	1
relative fixed operational costs SF, TS, PB CSP [%]	2.5	2.5	2.5	2.5	2.5
Relative fixed operation cost onshore [%]	4	4	4	4	4
Relative fixed operation cost offshore [%]	5.5	5.5	5.5	5.5	5.5
Relative fixed operation cost hydro [%]	5	5	5	5	5
lifetime of the power plant PV [a]	20	20	20	20	20
lifetime of the power plant CSP [a]	25	25	25	25	25
lifetime of the power plant wind [a]	18	18	18	18	18
lifetime of the power plant hydro [a]	60	60	60	60	60
Interest rate i [%]	6	6	6	6	6

Table 3.8.: Values used in this thesis for the determination of the arising cost based on Scholz [Sch12].

$$a_{p,n} = C_{0,i}^{tech} \cdot AF_{p,n} \quad (3.22)$$

where

$$C_{0,i}^{tech} = c_{spec}^{tech, inv} \cdot P_i^{tech, inst} \quad (3.23)$$

and

$$AF_{p,n} = \frac{(1+p)^n \cdot p}{(1+p)^n - 1} \quad (3.24)$$

In addition to the investment cost, expenses for operation and maintenance are considered by introducing the installation-specific operational cost $c_{spec}^{tech, op}$. In summary, the total annual cost $C_{total\ annual,i}^{tech}$ per grid box i amounts to the sum of investment and operation related expenditures:

$$\begin{aligned} C_{total\ annual,i}^{tech} &= a_{p,n} + C_{0,i}^{tech} \cdot c_{spec}^{tech, op} \\ &= c_{spec}^{tech, inv} \cdot P_i^{tech, inst} \left[\frac{(1+p)^n \cdot p}{(1+p)^n - 1} + c_{spec}^{tech, op} \right] \end{aligned} \quad (3.25)$$

The latter expression holds for all considered technologies with the exception of Concentrating Solar Power, where the total cost for each grid box is derived as the sum of the three different constituting elements of a CSP plant solar field ($C_{total\ annual,i}^{sf}$), power block ($C_{total\ annual,i}^{pb}$) and thermal storage ($C_{total\ annual,i}^{st}$):

$$C_{total\ annual,i}^{CSP} = C_{total\ annual,i}^{sf} + C_{total\ annual,i}^{pb} + C_{total\ annual,i}^{st} \quad (3.26)$$

The solar field's annual cost $C_{total\ annual,i}^{sf}$ is defined by equation (3.25), using the specific installation cost for the thermal capacity. In contrast, the annual cost of the power block $C_{total\ annual,i}^{pb}$ is calculated by the additional factor $f_{solar\ multiple}$ referring to the amount of installed solar fields per power block:

$$C_{total\ annual,i}^{pb} = \frac{c_{spec}^{pb, inv} \cdot P_i^{pb, inst}}{f_{solar\ multiple}} \left[\frac{(1+p)^n \cdot p}{(1+p)^n - 1} + c_{spec}^{pb, op} \right] \quad (3.27)$$

The costs for the storage capacities additionally depend on the ratio of thermal storage capacity to power block size f_{p2s} :

$$C_{total\ annual,i}^{st} = \frac{c_{spec}^{st, inv} \cdot P_i^{st, inst}}{f_{solar\ multiple}} \left[\frac{(1+p)^n \cdot p}{(1+p)^n - 1} + c_{spec}^{st, op} \right] \cdot f_{p2s} \quad (3.28)$$

The installation-specific investment cost of the power block $c_{spec}^{pb, inv}$ and the thermal energy storage $c_{spec}^{st, inv}$ are expressed in terms of electric capacities $\left[\frac{\text{€}}{\text{kW}_{el}} \right]$.

The generation cost per kWh of electricity, technology and grid box i $c_i^{tech, gen}$ are determined by dividing each technologies' total annual cost $C_{total\ annual,i}^{tech}$ by the total annual electricity yield $E_{el\ annual,i}^{tech}$:

$$c_i^{tech, gen} = \frac{C_{total\ annual,i}^{tech}}{E_{el\ annual,i}^{tech}} \quad (3.29)$$

where the total annual electricity output per pixel i $E_{el\ annual, i}^{tech}$ is the accumulation of the hourly electricity output $E_i^{tech, el}(t)$:

$$E_{el\ annual, i}^{tech} = \sum_{t=1}^{8760} E_i^{tech, el}(t) \quad (3.30)$$

The generation cost is derived for each grid box i separately. By accumulating all occurring costs, cost-potential graphs can finally be obtained as shown in section 3.3.2.1.

3.3.1.1.2. From annual electricity yield and installed capacities to full load hours

In order to derive each technologies' full load hours flh_i^{tech} for a given grid box i , the ratio of the total annual electricity output $E_{el\ annual, i}^{tech}$ as derived in equation (3.30) and the installable capacity in grid box i , $P_i^{tech, inst}$ ²², are determined:

$$flh_i^{tech} = \frac{E_{el\ annual, i}^{tech}}{P_i^{tech, inst}} \quad (3.31)$$

The full load hours are derived for each grid box i separately. Integration eventually yields full-load-hour graphs as presented in section 3.3.2.1.

3.3.1.2. Determination of a typical meteorological year

Since the long term renewable resources presented in subsection 3.2.2 vary in terms of the annual mean, probability distributions of the irradiances, wind speeds or river run offs and the exact hourly occurrence of the latter, the question arises which of the available years shall be used for the determination of potentials. In this respect, some authors and institutions propose the establishment of an artificially generated data set, best representing reality in terms of plausibility and probability, taking the aforementioned criteria as quantifying parameters to select real world monthly data for various years to compose one artificial year [WM08], [SOD], [Kal03]. The approach is based on Hall et al. [HPAB78] and determines the most representative month out of the long term data available. The minimum of the summed up differences of the cumulated distribution function of the hourly values of one candidate month (e.g. June) and the long term average cumulated distribution function of all available identical periods (June 1984, June 1985, etc.) is used as the selection criterion, also referred to as the Finkelstein-Schafer statistics [FS71]. The procedure is carried out for every month separately to eventually come up with the typical meteorological year. As this approach is based on a monthly analysis, the annual sum of the so-obtained typical meteorological year differs from the mean annual sum of all years under consideration.

²²The latter coincides with the maximum installable capacity per pixel i , $P_i^{tech, inst.max}$, as derived in section 3.2.1.4 for the potential assessments.

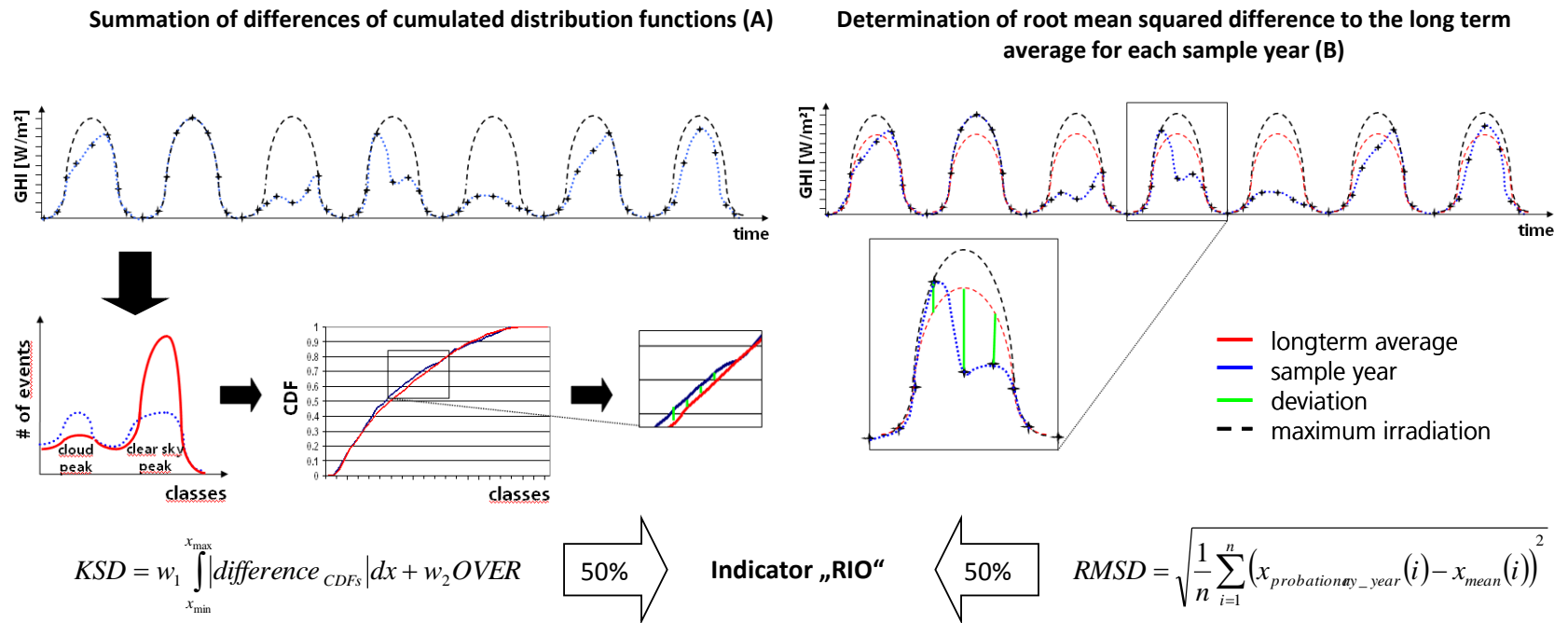


Figure 3.19.: Approach used in this work to determine the typical meteorological year for one site.

In contrast to the procedure discussed above, in this work a modified approach is employed. It is based on an excerpt from work conducted by the author [SGS11], which is further developed here. The approach is indicated in figure 3.19. Its main advantage is the selection of the most representative complete year for each pixel. For this objective, first an analysis of the total energy yield (merely the theoretical potential is considered - no power plant for conversion is used at this point) and the comparison to the long term average at each site (pixel) of the assessed data set, i.e. GHI, BNI, wind speed and river runoff, is carried out. Secondly, the deviation of each time step from the long term average of the resource data for each site (pixel) is considered. The procedure is based on the Kolmogorov-Smirnov-Test proposed within the MESOR project [BMS+09] dealing with these two cases and determining a reference year out of a long term data set for one site using the following approach: On the one hand, all resource data are grouped into classes and a cumulated distribution function is generated both for each sample year and the long time average. The deviations for each class between the two distribution functions (sample year vs. long term average) are then summed up in line with the Finkelstein-Schafer statistics [FS71] introduced above. Two cases are then considered: each class deviation is greater or smaller than a critical threshold value, corresponding to a confidence interval of 99%. All differences of classes exceeding the threshold are summed up and a linear combination of the latter with the deviation of the cumulative functions using weighting factors yields the first indicator called “KSD”. On the other hand the root mean squared difference to the long term average is determined for each sample year, also leading to a second indicator, called “RMSD”. The mean value of both indicators is then derived to obtain the final indicator, called “RIO”. This approach is carried out for the entity of all sample years available. The sample year with the smallest final indicator (“RIO”) gets rated first and is used for the respective pixel. In other words: The result in each pixel is a real, unmodified year. The approach is carried out for all pixels separately, resulting in a data set containing complete real-world resources years, however, neighboring pixels might differ in the year used. This line of action is justified here as in the present chapter potentials are assessed. When it comes to determining hourly mean power output aggregated for a region of concern, e.g. for a country to serve as input for an energy system simulation as carried out in chapters 4.3 and 5.3, a typical meteorological year needs to be derived for the entire region as carried out by the author in [SGS11]. This is due to the fact that portfolio effects of distributed renewable generation are to be investigated using one common year for the entire region considered.

In summary two different fundamental criteria for the selection of a typical year are combined: both hourly and annual cumulated distribution deviation of the sample sum in contrast to the long term average. This approach is particularly advantageous as it considers the annual sum, which is the predominant factor for the cost and full load hour potential, and the hourly occurrence, which is very important when it comes to using the resources data in power plant models using hourly resolution.

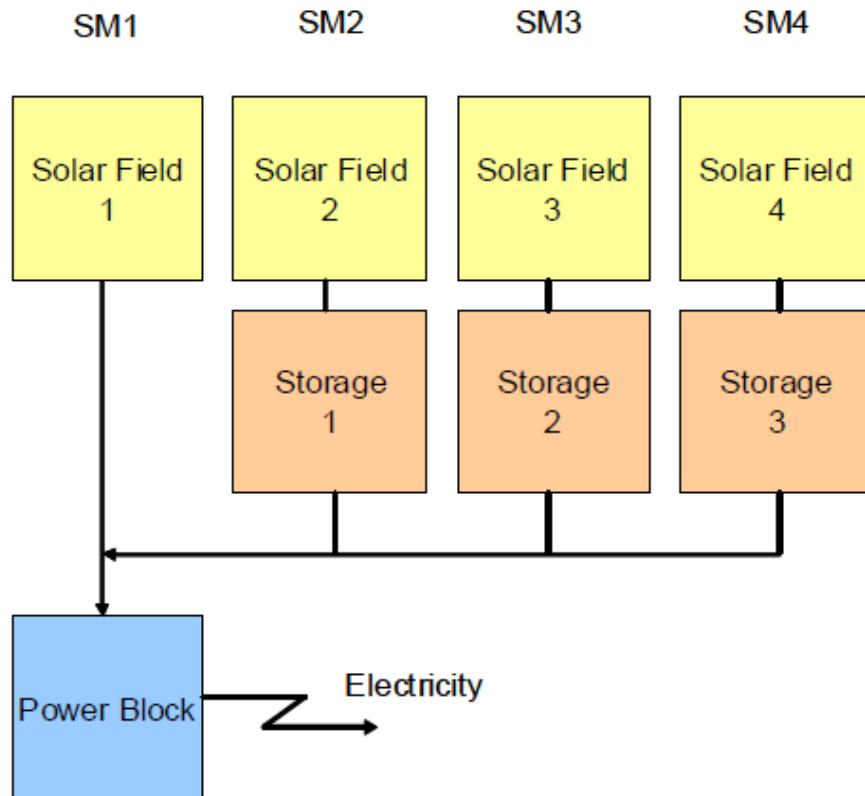


Figure 3.20.: Different possible plant layouts of a CSP plant can be expressed in terms of the solar multiple [TSO⁺09].

3.3.1.3. Impact of the layout of CSP plants with different solar multiples on the full load hours

CSP plants have the great advantage of being capable of providing power which can be dispatched on demand. This stands in clear contrast to other technologies tapping volatile resources. The configuration of CSP plants can be specifically designed for their field of operation. An indicator for the layout is the solar multiple. Figure 3.20 gives an overview on different plant layouts and their respective solar multiples.

A solar multiple of 1 corresponds to a setup without storage. In this configuration, the solar field is designed to provide the turbine's rated capacity for a beam normal irradiance of $800 \frac{W}{m^2}$. A plant with similar rated power of the turbine but a solar multiple of 2 is equipped with two solar fields and one thermal storage. During daytime, solar field 1 directly drives the turbine while solar field 2 charges the thermal energy storage. The latter can be discharged during nighttime to enable an operation of the plant. As indicated in figure 3.21, generally the higher the solar multiple and the better the irradiance conditions, the more the plant is designed to provide base load. The full load hours increase with increasing solar multiples and decreasing geographical latitudes, which in turn leads to improved overall irradiance conditions. For identical irradiance conditions, the performance decreases with increasing latitude due to cosine losses.

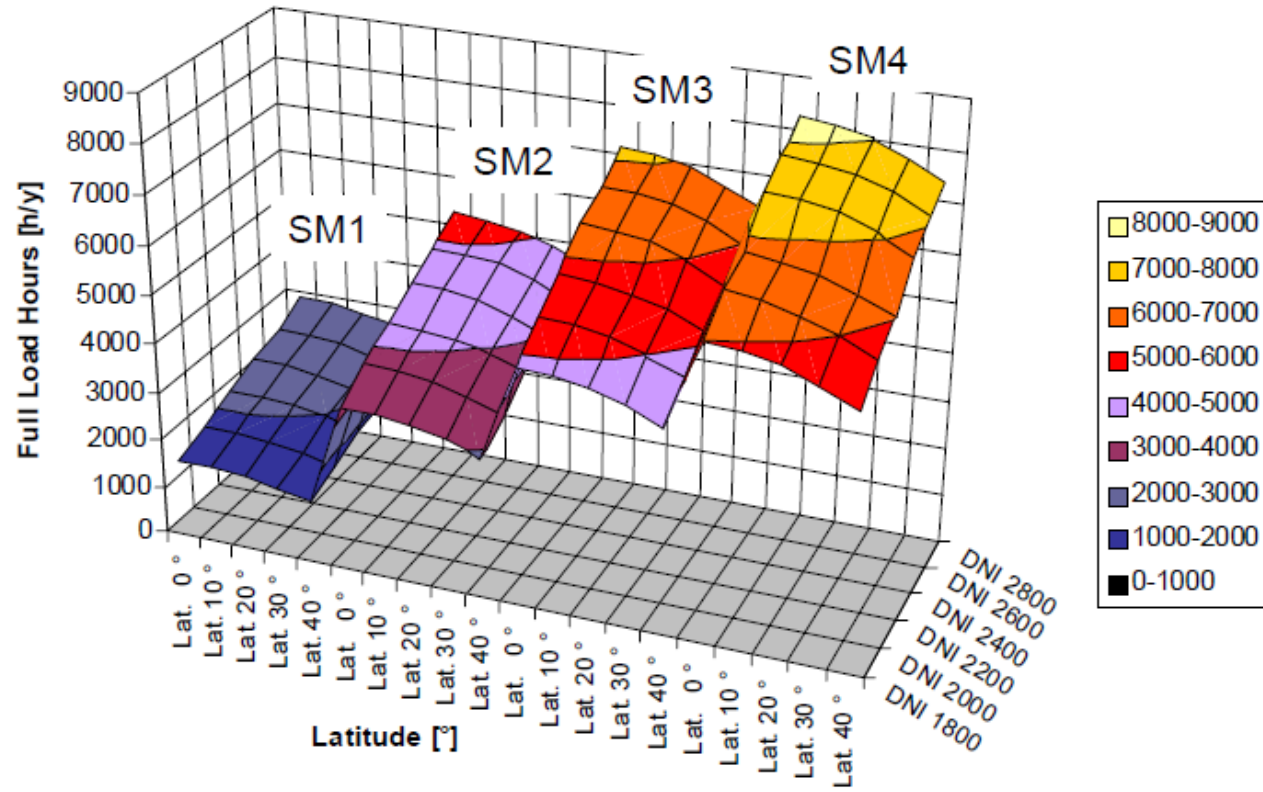


Figure 3.21.: The full load hours of a CSP plant are a function of the irradiance and the solar multiple [TSO+09].

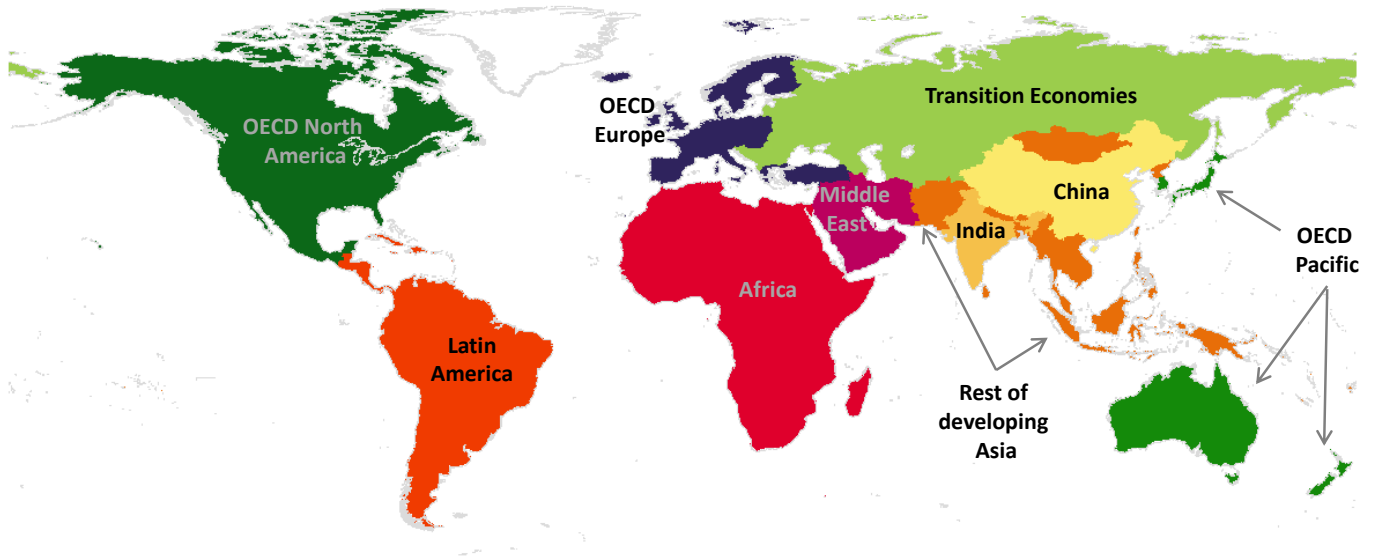


Figure 3.22.: World regions for which the assessments are carried out.

3.3.2. Results

3.3.2.1. Full load hour and cost potentials

In this section the globally applicable potential assessment tool REMix-EnDaT is used to compute both full load hour and cost potentials for a world-wide investigation. The assessments are conducted in terms of 10 world regions, for each of which both full load hour and cost potentials are derived: OCED Europe, OECD North America, OECD Pacific, Transition Economies, China, India, Rest of developing Asia, Latin America, Africa and Middle East. An overview of the assessed regions is given in figure 3.22. While for the determination of regional power output the cumulation yields a smoothed hourly mean generation curve, full load hour and cost potential graphs generally contain the information of the entire region, as each pixel yields a value which is depicted in the graph. Although the assessment is carried out for the three time steps 2010, 2030 and 2050, all graphs presented in this section are only based on the results of the 2010 runs. However, for each world region and in the global summary, all assessments are included as tables. For the special case of CSP, potentials are derived for three different plant layouts ranging from a solar multiple of 1.5 over 2.5 to 3.5, thus representing peak, medium and base load plants, respectively.

Figures 3.23 through 3.25 indicate the resulting full load hours on a global scale for the technologies PV, CSP and wind power. For CSP (figure 3.24), the indicated full load hours refer to the solar field, not the turbine.

The full load hours in each pixel of the presented graphs are derived according to the relation introduced in subsection 3.3.1.1.2. For the calculations typical meteorological years for each pixel as dicussed in subsection 3.3.1.2 are used. Each of the aforementioned figures comes without and with applied land exclusion.

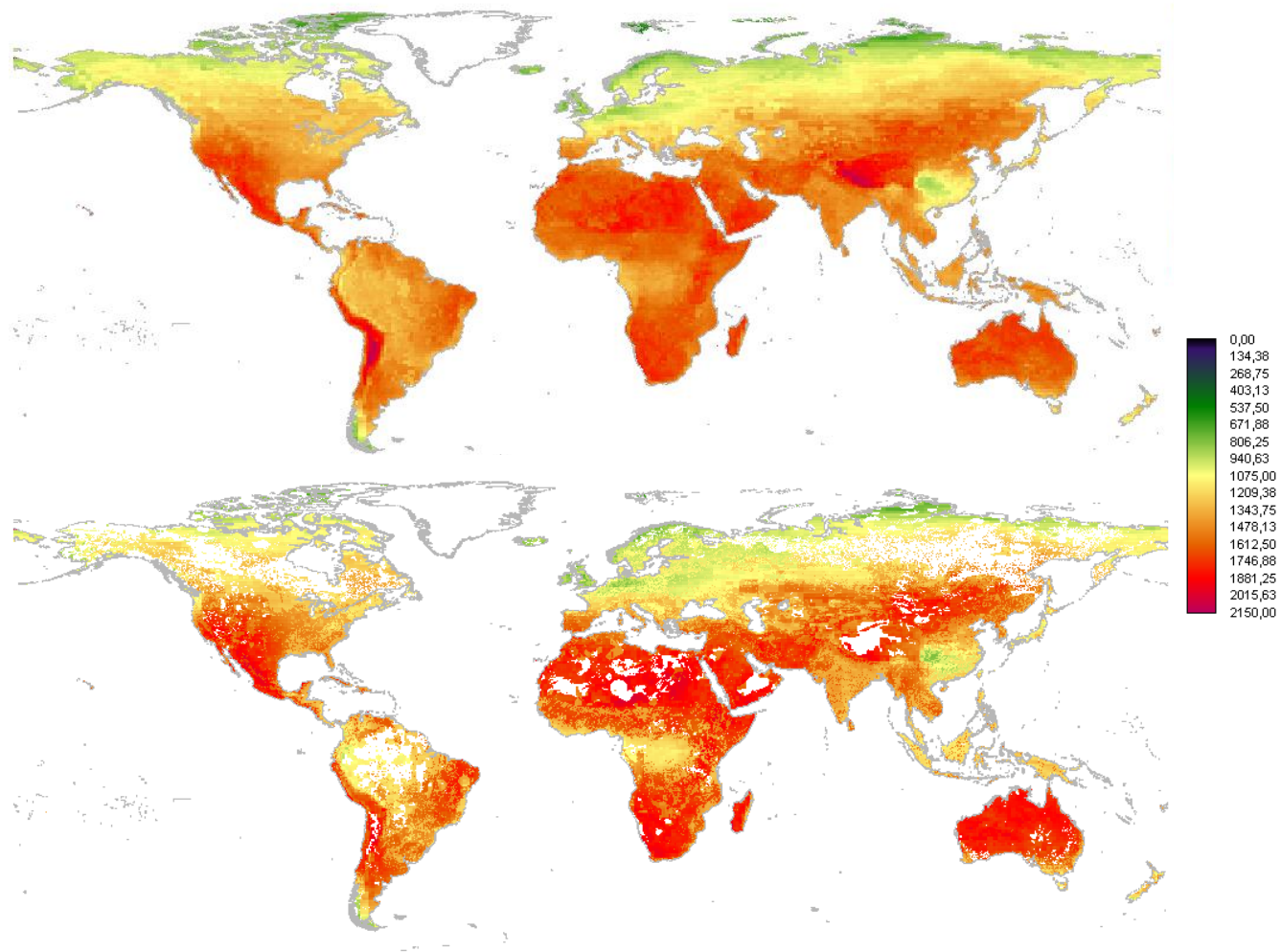


Figure 3.23.: Results for full load hours for photovoltaic power plants in 2010. Top: Theoretically achievable full load hours without any land exclusion criteria. Bottom: Remaining surfaces with respective full load hours after land exclusion.

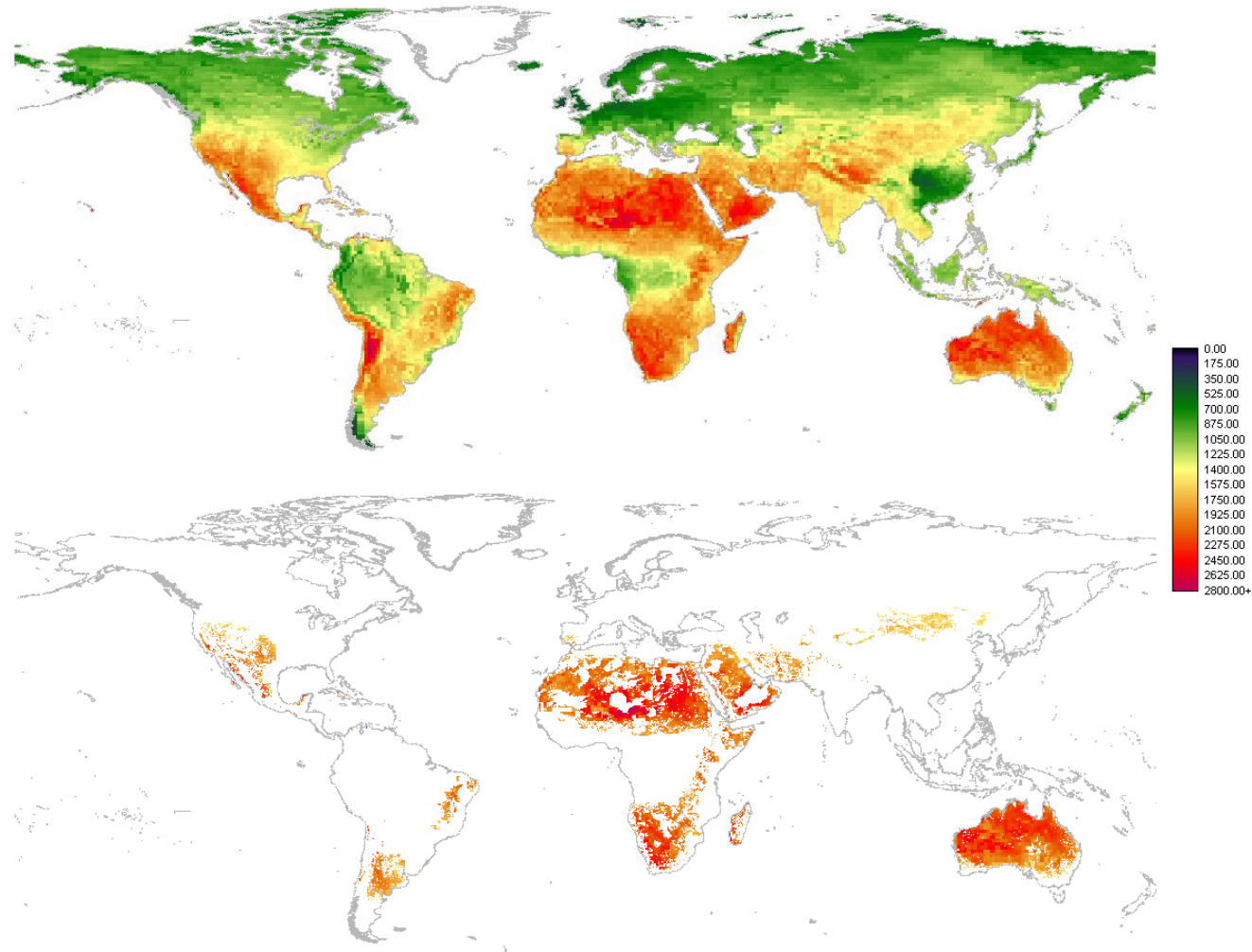


Figure 3.24.: Results for full load hours for concentrating solar power plants in 2010. The figures refer to the full load hours of the solar field. Top: Theoretically achievable full load hours without any land exclusion criteria. Bottom: Remaining surfaces with respective full load hours after land exclusion and minimum resource boundary condition of an annual beam normal irradiance (BNI) sum of $1800 \frac{kWh}{m^2 \cdot a}$.

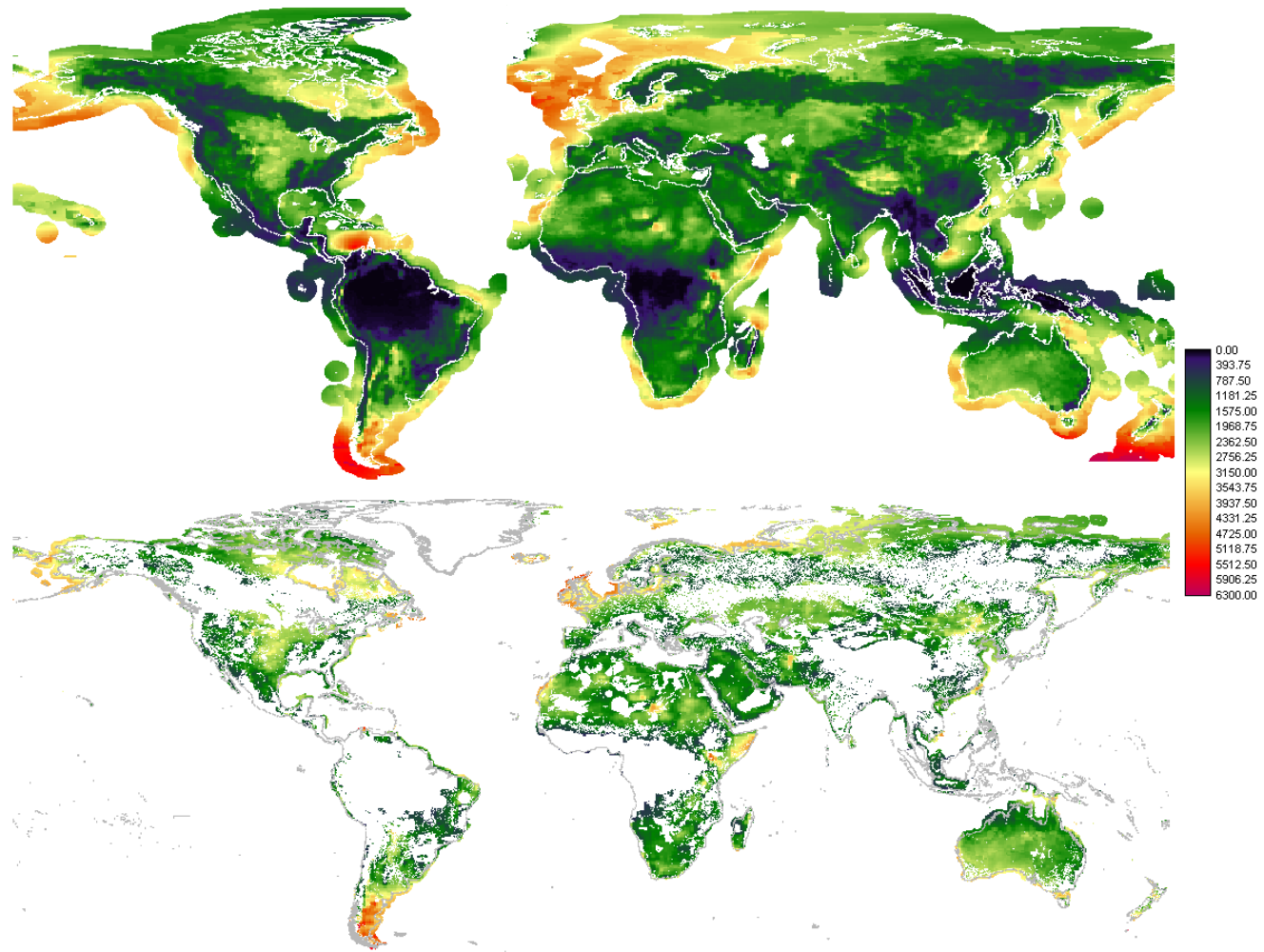
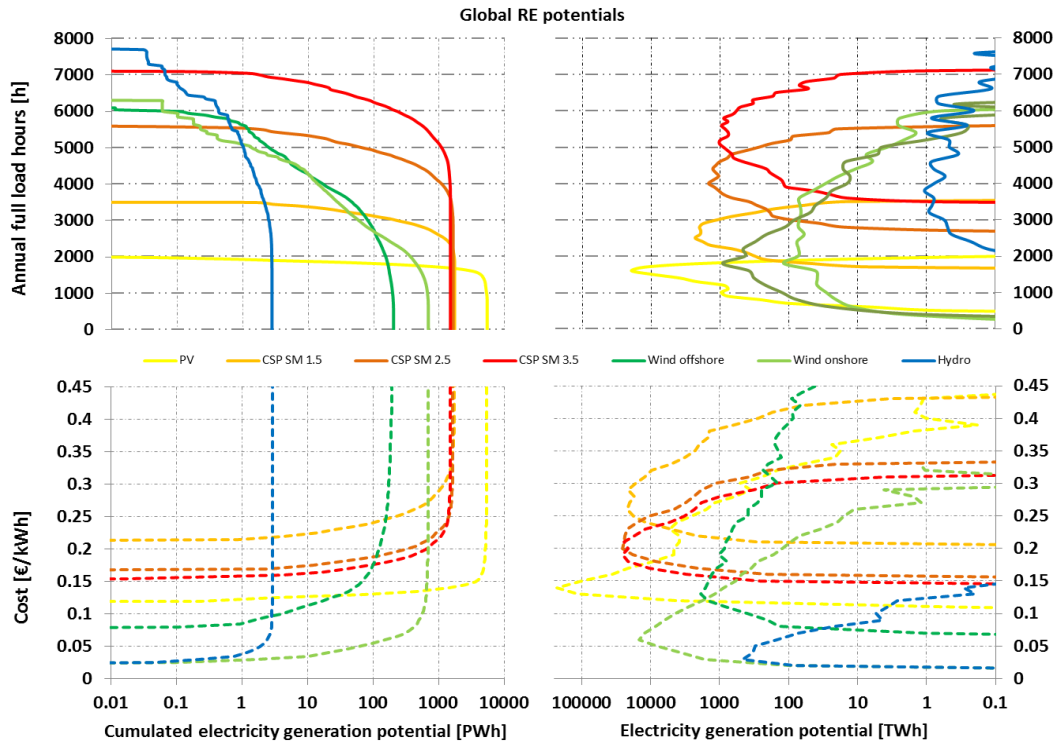


Figure 3.25.: Results for full load hours for onshore and offshore wind power plants in 2010. Top: Theoretically achievable full load hours without any land exclusion criteria. Bottom: Remaining surfaces with respective full load hours after land exclusion and minimum resource boundary condition of an annual mean wind speed of $4 \frac{m}{s}$.

Figure 3.26 indicates the results for full load hours and cost potentials aggregated for the entire globe. They are displayed in terms of both cumulated and non-cumulated electricity generation. In the cumulated graphs, vertical asymptotic behavior indicates the upper limit of the potentials, while horizontal asymptotes are approached for the maximum full load hours and the least cost. The non-cumulated graphs indicate the electricity generation in terms of full load hours and cost. Peak values of the electricity generation in the non-cumulated graph result in an inflection from flat to steep behavior in the cumulated graph. For PV this inflection point can be seen at some 1600 full load hours and $14 \frac{\text{€ct}}{\text{kWh}}$ of generation cost. Moreover, the graphs indicate for instance that hydro power is the technology which can reach the highest full load hours, it is also among the cheapest technologies. Graphs for CSP in this figure are derived in terms of electricity generation for three different solar multiples. Onshore and offshore wind is differentiated between. Similar graphs according to figure 3.26 for each of the 10 OECD world regions are presented in annex A.2. Overall, the following items can be concluded on a global scale:

- Solar irradiance is the predominant resource. Global annual electricity generation potentials using PV as the conversion technology reach between 5404 and 5529 PWh for the years 2010 until 2050. This slight increase of some 2.3% is primarily due to a rise in the module efficiency from 16.1 to 18% and the q-factor from 81.1 to 84.7%, implicitly affecting the full load hours. Global averages of the latter reach 1545, 1614 and 1634 hours or 17.6, 18.4 and 18.7% in terms of the capacity factor in 2010, 2030 and 2050 respectively. Average cost decreases sharply over the considered time span from 15.3 over 4.6 to $4.1 \frac{\text{€ct}}{\text{kWh}}$.

Tapping solar irradiance for the case of concentrating solar power results in less potentials on first sight. This is primarily due to the fact that for CSP plants all surfaces with annual beam normal irradiance sums inferior to $1800 \frac{\text{kWh}}{\text{m}^2 \cdot \text{a}}$ are excluded. For the three investigated plant setups with solar multiples of 1.5, 2.5 and 3.5 electricity generation potentials are estimated to amount to 1719, 1629 and 1482 PWh respectively. The slightly decreasing figures - overall some 14% from solar multiple 1.5 to 3.5 - can be attributed to losses which occur during the thermal storage charging and discharging processes including parasitics. In summary, on the one hand enabling flexible power plant dispatch comes at the expense of decreasing generation potentials, on the other hand global averages of full load hours increase as a function of the solar multiple from 2673 (SM 1.5) to 5383 (SM 3.5) - or expressed in terms of capacity factors - figures for solar multiples 1.5 and 3.5 more than double from 30.5% to 61.4%. Average cost primarily depend on the plant layout: High solar multiples invoke additional investments for both solar field and thermal storage, which are on the other hand more than over-compensated by an increased capacity utilisation of the steam turbine, resulting in a rise of the full load hours of the plant as a whole. For that reason and due to the learning curves, cost decrease from 20.8 to $11.3 \frac{\text{€ct}}{\text{kWh}}$ of fed-in power for a SM 3.5 plant from 2010 to 2050 respectively, for SM 1.5 a decrease from 28.7 to $17.4 \frac{\text{€ct}}{\text{kWh}}$ and for SM 2.5 a decrease from 22.4 to $12.7 \frac{\text{€ct}}{\text{kWh}}$ are observed. These values are rather high compared to recent CSP projects, for instance in Morocco.



	Photovoltaics			CSP				Wind Onshore			Wind Offshore			Hydro		
	2010	2030	2050	SM	1.5	2.5	3.5	2010	2030	2050	2010	2030	2050	2010	2030	2050
Electricity generation potential [PWh]	5404	5466	5529		1719	1629	1482	684	709	717	201	217	224	2.80	2.94	3.13
Average full load hours [h]	1545	1614	1634	2010-2050	2673	4222	5383	2111	2183	2206	2730	2900	2979	4557	4561	4613
Average capacity factor [%]	17.6	18.4	18.7		30.5	48.2	61.4	24.1	24.9	25.2	31.2	33.1	34.0	52.0	52.1	52.7
Average cost [€/kWh]	15.3	4.6	4.1	2010	28.7	22.4	20.8	8.1	6.5	5.9	21.1	10.6	7.4	4.7	4.7	4.8
				2030	19.0	14.1	12.6									
				2050	17.4	12.7	11.3									

Figure 3.26: Results of global electricity generation potentials for the technologies photovoltaic, concentrating solar power, on- and offshore wind and hydro power. The two figures on the left are expressed in terms of cumulated potentials, the top graphs are indicated as a function of full load hours, the bottom graphs as a function of cost. All graphs refer to the year 2010.

This is partly due to the choice of the interest rate and the depreciation period (as indicated in table 3.8 in this work rather moderate values of 6% and 25 years are assumed, respectively). Moreover, strong influence on the CSP generation cost can be attributed to the resource data used. As discussed in paragraph 3.2.2.1.3 and figure 3.13, the annual sums of the beam normal irradiance data used in this work are on average 8% below NASA annual sums, which are taken as reference. This also leads to higher power generation cost.

The noticeable difference in the results between photovoltaics and concentrating solar power particularly in terms of electricity generation potentials can partly be explained by the fact the PV is capable of harvesting the global irradiance sum, i.e. both direct (beam) and diffuse components²³, whereas CSP is limited to the direct (beam) component.

²³Please see section 3.2.2.1 for further insight on global and beam irradiances.

Secondly an inferior area-specific installation density of CSP versus PV causes less potentials: The thermal installation density of a CSP plant is estimated with $173.2 \frac{MW_{th}}{km^2}$. For the conversion from heat to electricity a generator efficiency of 37% is estimated, yielding $65.2 \frac{MW_{el}}{km^2}$. Please note that no storage efficiency is considered at this point and these figures are assumed to remain stable throughout the time period of consideration, i.e. 2010 through 2050. For PV the area-specific installation density ranges from $130.6 \frac{MW_{el}}{km^2}$ in 2010 to $152.5 \frac{MW_{el}}{km^2}$ in 2050. Last, the potentials for CSP already exclude sites which cannot be used economically by a CSP plants using the boundary condition of a minimum annual irradiance sum of $1800 \frac{kWh}{m^2 \cdot a}$. No such exclusion is implemented for PV, as it is also feasible to be implemented in small, decentralized systems. Moreover, high cost per kWh due to unfavorable resource conditions is justifiable in remote areas without access to power grids.

- Wind potentials are the second largest resource according to this assessment's results. Global electricity generation potentials of onshore wind power plants are in the range from 684 to 717 PWh, for offshore plants these figures amount to 201 and 224 PWh for the period between 2010 and 2050. In terms of full load hours, onshore plants see a modest increase from 2111 to 2206 hours, offshore plants from 2730 to 2979 hours - a clear sign for better resource conditions offshore. The latter are due to the fact that surface roughness is far less over water compared to land. Expressed in capacity factors, this adds up to ranges from 24.1 to 25.2% and 31.2 to 34% for onshore and offshore applications, respectively. The moderate increase is caused by the assumption of taller hub heights (112 to 132 m onshore and 80 to 140 m offshore), larger rotor diameters (77 to 130 m onshore and 96 to 192 m offshore) and higher ratings for the nominal power of an individual plant (1950 to 5500 kW onshore and 3 to 12 MW offshore). Despite the increase of the latter figures, the area-specific installable capacities remain constant at $10.4 \frac{MW_{el}}{km^2}$ for both on- and offshore plants in accordance with equation (3.6) in section 3.2.1.4. Average cost for onshore power generation decreases over the period of concern, from 8.1 to 5.9 $\frac{\text{€ct}}{\text{kWh}}$. Since the installation of wind power plants offshore involves much higher efforts which are reflected by higher cost, the average cost evolves on a higher level from 21.1 to 7.4 $\frac{\text{€ct}}{\text{kWh}}$ until 2050.
- Hydro power potentials are far less than those discussed above for photovoltaics, concentrating solar and wind power. The figures found appear to reflect objective physical reasons, however it shall be born in mind that a top-down approach as discussed in sections 3.2.1.4 and 3.2.3 is employed in contrast to the bottom-up approaches for the aforementioned technologies tapping wind and solar resources. In summary, global hydropower electricity generation potentials estimated in this work amount to 2.8 to 3.13 PWh for the considered time period from 2010 through 2050. The moderate increase of some 330 TWh is caused by a considered rise in installed capacities by virtue of modernization of existing plants and new constructions.

These figures are below the actual hydropower generation which amounts to 3.43 PWh in 2010 according to the Worldwatch Institute [Wor12]. This underestimation is due to the used top-down approach, as discussed in section 3.2.3, using monthly run off sums instead of hourly data.

Hydro power is the renewable resource, which has already played a considerable role in generation portfolios since the very beginning of electricity consumption, which can be attributed to the high number of full load hours the plants can be operated with. According to this assessment, full load hours between 4557 and 4613 hours, or in terms of capacity factors, between 52 and 52.7% are reached between 2010 and 2050. Average cost remains at a constant level of $4.7 \frac{\text{€ct}}{\text{kWh}}$ for all assessed scenario years.

In the following discussion, the results are presented in terms of 10 OCED world regions. The goal is to give a general idea as to where good potentials of a certain resource are available along with their quantity. Data provided in figures 3.27 and 3.28 give an overview of the results for each world region²⁴. Since the world regions are made up unevenly in terms of their total surface and resource conditions, a direct comparison is difficult. Therefore, for each region a small discussion follows, using full load hours as the prime indicator:

OECD Europe

Good photovoltaic potentials with full load hours greater than 1400 hours can be found around the Mediterranean Sea in countries such as Spain, Southern France, Italy and Greece. Portugal also has considerable photovoltaic potentials. Central and Northern Europe, at latitudes above some 45°N, still allow for the use of photovoltaic, however, other renewable technologies, wind in particular, generally show much higher full load hours and less cost per kWh. As CSP is only implemented in areas with beam normal irradiance (BNI) annual sums exceeding $1800 \frac{\text{kWh}}{\text{m}^2 \cdot \text{a}}$, merely between 1.3 and 1.5 PWh - depending on the solar multiple of a potential plant - are derived as electricity generation potentials. The sites where it can be deployed show full load hours between 2200 and 4500 hours, for solar multiples 1.5 and 3.5, respectively. Hydro power is widely used in Europe, its potential is assessed to amount to about 550 TWh in 2010, with approximately 4500 hours of full load operation. The best offshore wind sites are found off the coasts of the British isles and in the North Sea, good onshore sites in places such as Denmark, the Netherlands and Northern Germany.

OECD North America

Between latitudes of 65°N to 20°N, full load hours for photovoltaics reach values in the range starting from 1000 hours in Canada and increasing up to 1800 hours in central Mexico. Generally, a gradual increase is observed from northeast to southwest of the assessed region. CSP potentials are visible in the southeastern portion of the United States and all over Mexico, full load hours being observable starting from 1700 hours to 3300 and from 3500 to a maximum of some 6700 hours for solar multiples 1.5 and 3.5, respectively.

²⁴As indicated before, the corresponding graphs are presented in annex A.2

	Photovoltaics			CSP			Wind Onshore			Wind Offshore			Hydro			
	2010	2030	2050	SM	1.5	2.5	3.5	2010	2030	2050	2010	2030	2050	2010	2030	2050
	OECD Europe	97.1	97.4	97.8	2010	1.5	1.4	1.3	20.5	21.3	21.5	23.0	24.4	25.1	0.55	0.58
	1202	1257	1264	2050	2209	3490	4450	2373	2448	2471	3499	3675	3755	4501	4501	4495
	13.7	14.3	14.4		25.2	39.8	50.8	27.1	27.9	28.2	39.9	42.0	42.9	51.4	51.4	51.3
	20.1	6.1	5.5	2010	34.5	26.9	25.1	7.5	6.1	5.5	15.3	7.8	5.5	4.7	4.8	4.8
				2030	22.9	16.9	15.2									
				2050	20.9	15.3	13.6									
OECD North America	462.0	464.1	466.3	SM	53	50	46	89.5	92.7	93.7	44.7	48.0	49.5	0.57	0.60	0.68
	1406	1466	1476	2010	2460	3886	4955	2213	2285	2307	2947	3124	3205	4931	4931	5109
	16.0	16.7	16.8	2050	28.1	44.4	56.6	25.3	26.1	26.3	33.6	35.7	36.6	56.3	56.3	58.3
	17.1	5.2	4.7	2010	31.1	24.3	22.6	7.6	6.2	5.7	18.3	9.3	6.5	4.3	4.3	4.4
				2030	20.7	15.3	13.7									
				2050	18.9	13.8	12.2									
OECD Pacific	831.3	843.3	855.3	SM	451.7	428.0	389.7	106.6	110.9	112.0	27.6	29.8	30.9	0.16	0.16	0.17
	1620	1693	1717	2010	2725	4304	5487	2147	2230	2256	2718	2902	2988	5170	5232	5232
	18.5	19.3	19.6	2050	31.1	49.1	62.6	24.5	25.5	25.7	31.0	33.1	34.1	59.0	59.7	59.7
	14.4	4.3	3.9	2010	28.0	21.8	20.3	7.4	6.0	5.4	20.4	10.3	7.1	3.9	3.9	4.0
				2030	18.6	13.7	12.3									
				2050	17.0	12.4	11.0									
Transition Economies	341.0	341.3	341.6	SM	0.6	0.6	0.5	88.4	91.5	92.5	38.0	40.8	42.2	0.30	0.31	0.33
	1226	1279	1281	2010	2244	3544	4519	2177	2249	2271	2619	2796	2879	4253	4253	4253
	14.0	14.6	14.6	2050	25.6	40.5	51.6	24.8	25.7	25.9	29.9	31.9	32.9	48.5	48.5	48.5
	19.3	5.9	5.4	2010	33.9	26.4	24.6	7.6	6.1	5.6	19.6	9.9	6.9	5.1	5.2	5.2
				2030	22.5	16.6	14.9									
				2050	20.6	15.0	13.3									
China	220.5	221.2	222.0	SM	32.7	30.9	28.2	25.8	26.8	27.1	48.4	9.2	9.6	0.50	0.44	0.46
	1486	1542	1547	2010	2063	3259	4155	1858	1922	1941	2325	2500	2581	4445	4444	4445
	17.0	17.6	17.7	2050	23.6	37.2	47.4	21.2	21.9	22.2	26.5	28.5	29.5	50.7	50.7	50.7
	15.8	4.8	4.3	2010	36.8	28.7	26.7	9.4	7.6	6.9	22.3	11.2	7.8	4.7	4.8	4.8
				2030	24.5	18.1	16.2									
				2050	22.3	16.3	14.4									

Figure 3.27: Results of the potential assessment for the regions (from top to bottom) OECD Europe, OECD North America, OECD Pacific, Transition Economies and China. Figures for electricity generation, average full load hours and capacity factors as well as cost are displayed. The analysis is carried out for the years 2010, 2030 and 2050.

	Photovoltaics			CSP			Wind Onshore			Wind Offshore			Hydro			
	2010	2030	2050	SM	1.5	2.5	3.5	2010	2030	2050	2010	2030	2050	2010	2030	2050
	India	22.4	22.7	23.0		0.2	0.2	0.2	1.3	1.3	1.3	3.7	4.0	4.2	0.09	0.08
	1428	1496	1516	2010-2050	2490	3933	5014	1431	1484	1500	1891	2052	2128	3016	3016	3016
	16.3	17.1	17.3		28.4	44.9	57.2	16.3	16.9	17.1	21.6	23.4	24.3	34.4	34.4	34.4
	16.2	4.9	4.4	2010	30.6	23.8	22.2									
				2030	20.3	15.0	13.4	11.6	9.4	8.6	27.4	13.7	9.5	6.9	7.0	7.1
				2050	18.5	13.5	12.0									
Rest of developing Asia	Photovoltaics			CSP			Wind Onshore			Wind Offshore			Hydro			
	2010	2030	2050	SM	1.5	2.5	3.5	2010	2030	2050	2010	2030	2050	2010	2030	2050
	277.2	279.2	281.2		40.4	38.2	34.8	27.1	27.9	28.2	19.9	21.6	22.4	0.13	0.14	0.15
	1523	1586	1597	2010-2050	2129	3362	4287	1942	2005	2024	1798	1929	1990	4163	4163	4163
	17.4	18.1	18.2		24.3	38.4	48.9	22.2	22.9	23.1	20.5	22.0	22.7	47.5	47.5	47.5
	15.3	4.6	4.2	2010	35.8	27.9	26.0	8.8	7.2	6.5	33.9	16.9	11.7	5.1	5.1	5.2
				2030	23.8	17.6	15.7									
				2050	21.7	15.8	14.0									
Latin America	Photovoltaics			CSP			Wind Onshore			Wind Offshore			Hydro			
	2010	2030	2050	SM	1.5	2.5	3.5	2010	2030	2050	2010	2030	2050	2010	2030	2050
	399.5	403.4	407.6		66.4	62.9	57.3	45.8	47.5	48.0	23.0	25.0	25.9	0.52	0.54	0.57
	1479	1545	1561	2010-2050	2448	3866	4929	2750	2825	2848	3117	3302	3388	4722	4722	4722
	16.9	17.6	17.8		27.9	44.1	56.3	31.4	32.2	32.5	35.6	37.7	38.7	53.9	53.9	53.9
	15.8	4.8	4.3	2010	31.1	24.3	22.6	7.2	5.9	5.3	19.1	9.6	6.7	4.6	4.6	4.7
				2030	20.7	15.3	13.7									
				2050	18.9	13.7	12.2									
Africa	Photovoltaics			CSP			Wind Onshore			Wind Offshore			Hydro			
	2010	2030	2050	SM	1.5	2.5	3.5	2010	2030	2050	2010	2030	2050	2010	2030	2050
	2167.7	2199.6	2231.6		871.8	826.1	750.5	224.9	233.8	236.5	9.0	9.8	10.2	0.07	0.07	0.08
	1623	1696	1721	2010-2050	2751	4345	5540	2046	2119	2142	2427	2600	2680	3912	3911	3912
	18.5	19.4	19.6		31.4	49.6	63.2	23.4	24.2	24.5	27.7	29.7	30.6	44.7	44.7	44.7
	14.4	4.3	3.9	2010	27.8	21.7	20.2	8.2	6.7	6.0	26.6	13.4	9.3	5.5	5.6	5.7
				2030	18.5	13.6	12.2									
				2050	16.8	12.3	10.9									
Middle East	Photovoltaics			CSP			Wind Onshore			Wind Offshore			Hydro			
	2010	2030	2050	SM	1.5	2.5	3.5	2010	2030	2050	2010	2030	2050	2010	2030	2050
	585.7	594.1	602.5		200.7	190.2	173.2	53.7	55.8	56.5	3.9	4.2	4.3	0.01	0.01	0.01
	1584	1655	1679	2010-2050	2561	4045	5158	1607	1665	1683	1704	1830	1888	3238	3238	5332
	18.1	18.9	19.2		29.2	46.2	58.9	18.3	19.0	19.2	19.5	20.9	21.5	37.0	37.0	60.9
	14.7	4.4	4.0	2010	29.8	23.3	21.7	10.1	8.2	7.5	32.2	16.2	11.3	5.0	5.1	5.1
				2030	19.8	14.6	13.1									
				2050	18.1	13.2	11.7									

Figure 3.28: Results of the potential assessment for the regions (from top to bottom) India, Rest of developing Asia, Latin America, Africa and Middle East. Figures for electricity generation, average full load hours and capacity factors as well as cost are displayed. The analysis is carried out for the years 2010, 2030 and 2050.

Excellent wind resources can be found off the Pacific coasts of Alaska, Canada and the continental US, off the shoreline of New England and Eastern Canada up to latitudes of some 50°N and generally in the southern part of the Hudson Bay. Onshore, particularly the Great Plains in the United States stand out with up to 3700 full load hours.

OECD Pacific

Great potentials for photovoltaics can be found almost all over Australia, particularly in the north with up to 1750 full load hours. However this value does not decrease significantly going further south up to latitudes of some 35°S, where full load hours still reach at least a value of 1200. Japan has evenly distributed values close to 1000 full load hours, New Zealand slightly higher with some 1200 hours. The benchmark of $1800 \frac{kWh}{m^2 \cdot a}$ of beam normal irradiance is easily reached in Australia, CSP full load hours are in the range from 1800 to 3500 for solar multiple 1.5 and from 3600 to 7100 for solar multiple 3.5. Good wind sites can be found off the coasts of south Australia and in parts of New Zealand with values around 3000 full load hours.

Transition Economies

The best photovoltaic potentials are found in southeastern parts of Russia, Kazakhstan and Mongolia with values up to 1750 full load hours. Mongolia is - according to this assessment's results - the only country in this region with significant beam normal irradiance potentials exceeding $1800 \frac{kWh}{m^2 \cdot a}$, full load hours being in the range from 1900 to 2600 and 3800 to 5300 for solar multiples 1.5 and 3.5, respectively. Good wind sites can be found off shore in the Barents Sea with some 3800 full load hours and off the coasts of Kamchatka with values up to 3000 hours.

China

Outstanding photovoltaic resource sites can be found in the northern parts of China in the region around the city of Lanzhou with up to 1700 full load hours, CSP potentials range from 1700 to 2400 and 3600 to 4900 full load hours for solar multiples 1.5 and 3.5, respectively, the latter being located in northwestern China in proximity to the city of Urumqi. Good onshore wind sites with up to 3400 full load hours can be found in the north of the cities Beijing, Shenyang and Harbin, the best offshore potential can be found between Quanzhou and Taiwan with up to 4400 full load hours.

India

Good photovoltaic potentials ranging from 1300 to 1500 full load hours can be found throughout the country, particularly in the northwestern regions Gujarat and Rajasthan with up to 1700 full load hours. According to this assessment's land use exclusion criteria and minimum resource boundary condition, very little CSP potential can be found in India: for the remaining suitable sites, full load hours are in the range from 1900 to 2800 and 3900 to 5900 for solar multiples 1.5 and 3.5, respectively. Overall, very little good wind sites with full load hours exceeding 2500 full load hours can be found, for instance in the ocean between India and Sri Lanka.

Rest of developing Asia

For its equatorial vicinity and a day time climate with considerable precipitation, PV full load hours in countries such as Papua New Guinea, Indonesia, Malaysia do not exceed values of 1200. Best sites can be found the region bordered by Vietnam in the southeast and Myanmar in the northwest with up to 1600 full load hours. Due to its geographic location, beam normal irradiances are not tappable in large amounts, though, where available full load hours are in the range between 1800 and 2800 and 3500 to 5900 for solar multiples 1.5 and 3.5, respectively. The best wind potentials can be found off the coast of south Vietnam and in the Timor and Arafura Seas with up to 4300 and 3900 full load hours respectively.

Latin America

The best PV sites can be found westbound of and within the Andes mountains in Chile, Peru, Argentina and Bolivia with up to 1800 full load hours. The eastern tip of Brasilia around the city of Recife also sees good potentials up to 1600 full load hours. CSP potentials are predominantly located in the Atacama desert and central parts of Argentina between Buenos Aires and Mendoza, with 1800 to 3500 and 3700 to 6400 full load hours for solar multiples 1.5 and 3.5, respectively. Some of the best wind spots of the world can be found in the very south of Chile with values approaching up to 6000 full load hours and off the coast of Venezuela with some 5900 full load hours. Onshore, particularly the south of Argentina is rich in high wind speeds, resulting in up to 5000 full load hours.

Africa

Africa sees the world's best potentials for PV and CSP both in terms of quantity and quality: Except for a wide strip around the equator excellent photovoltaic potentials are seen in almost all North and South African countries with up to 1900 full load hours, the top performing sites located in places such as Niger, Tchad, Libya, Somalia, South Africa and Namibia. The best CSP potentials are also found in these locations with 1700 to 3500 and 3600 to 7100 full load hours for solar multiples 1.5 and 3.5, respectively. Excellent onshore wind sites are found in North Kenia close to Lake Turkana with up to 5000 full load hours, Somalia in proximity to Muqdishu and northern Tchad with up to 4200 full load hours and off the coasts of Morocco and Western Sahara with up to 4400 full load hours.

Middle East

In general a region with high solar potentials, top performing PV locations are found in Yemen with up to 1800 full load hours. CSP can also broadly be implemented in all countries of this region with full load hours ranging from 1700 to 3400 and 3500 to 6900 for solar multiples 1.5 and 3.5, respectively. In contrast to the abundant solar potentials, this region sees rather moderate wind potentials, with the best sites attaining just about 2200 full load hours. However, sites of some 2000 full load hours are evenly distributed over the entire Arabic peninsula.

3.3.2.2. Sensitivity Analysis

To analyse the impact of deviations of the major parameters used for the assessment in subsection 3.3.2, sensitivity analyses are carried out for selected parameters in order to determine both, the effects on the full load hours and the cost. For the former an arbitrary site in Niger at the position 10°E and 18°N with both good solar and wind resources is used. For this site data on global horizontal and beam normal irradiances, resulting wind speed and surface roughness length, temperature and solar elevation angle are retrieved from the data sets presented and discussed in subsection 3.2.2 for a time period from 1984 through 2004. The values corresponding to the 100% cases - that is the reference data for the parameters used in this work - are presented in table 3.9. As expected from the relations presented in subsection 3.2.3 to determine power output, a variation of the reference parameter values used in this chapter's assessment has a linear impact on the full load hours for all cases, except for the case of both onshore and offshore wind power, where the hub height and the rotor diameter show a different behavior due to the logarithmic and cubic behavior of equations (3.20) and (3.21) respectively. These results are indicated in figure 3.29.

Conducting the sensitivity analyses in terms of cost - as carried out e.g. by Wissel et al. [WFBV10] - yields much different results. For this case the parameters investment cost per kW, interest rate, depreciation period, fixed operation cost and full load hours are varied, as indicated in figure 3.30. While investment cost, interest rate and fixed operation cost show linear behavior during a single parameter variation, variation of depreciation period and full load hours results in a non-linear impact. Full load hours have the highest sensitivity for all assessed technologies, followed by the depreciation period. For photovoltaics and wind power, these parameters are followed, in terms of their sensitivity, by investment cost, interest rate and fixed operation cost. For hydro power, the impact of the interest rate for both modernized and new plants is considered. Both are less sensitive than the fixed operation cost, characterized by relatively high values. In case of concentrating solar power plants, a distinction is made between the depreciation periods of solar field and power block, the former being more sensitive than the latter. Also, the interest rate is more sensitive for CSP than for the other technologies.

Parameter	Value
investment cost PV [€/kW]	2470
interest rate PV [%]	6
depreciation period PV [a]	20
fixed operation cost PV [%]	1
flh PV	1545
investment cost SF [€/kW]	630
investment cost PB [€/kW]	1150
investment cost ST [€/kW]	52
interest rate CSP [%]	6
depreciation period CSP [a]	25
fixed operation cost CSP [%]	2.5
flh CSP	4222
solar multiple	2.5
investment cost onshore [€/kW]	1160
investment cost offshore [€/kW]	3300
interest rate wind [%]	6
depreciation period wind [a]	18
fixed operation cost onshore [%]	4
fixed operation cost offshore [%]	5.5
flh onshore	2111
flh offshore	2730
investment cost hydro old [€/kW]	4000
investment cost hydro mod [€/kW]	1386
investment cost hydro new [€/kW]	4662
interest rate hydro [%]	6
depreciation period hydro [a]	60
fixed operation hydro old [%]	5
fixed operation hydro mod [%]	1
fixed operation hydro new [%]	5
flh hydro	4557

Table 3.9.: Initial parameters used for the sensitivity analysis, corresponding to the 100% cases.

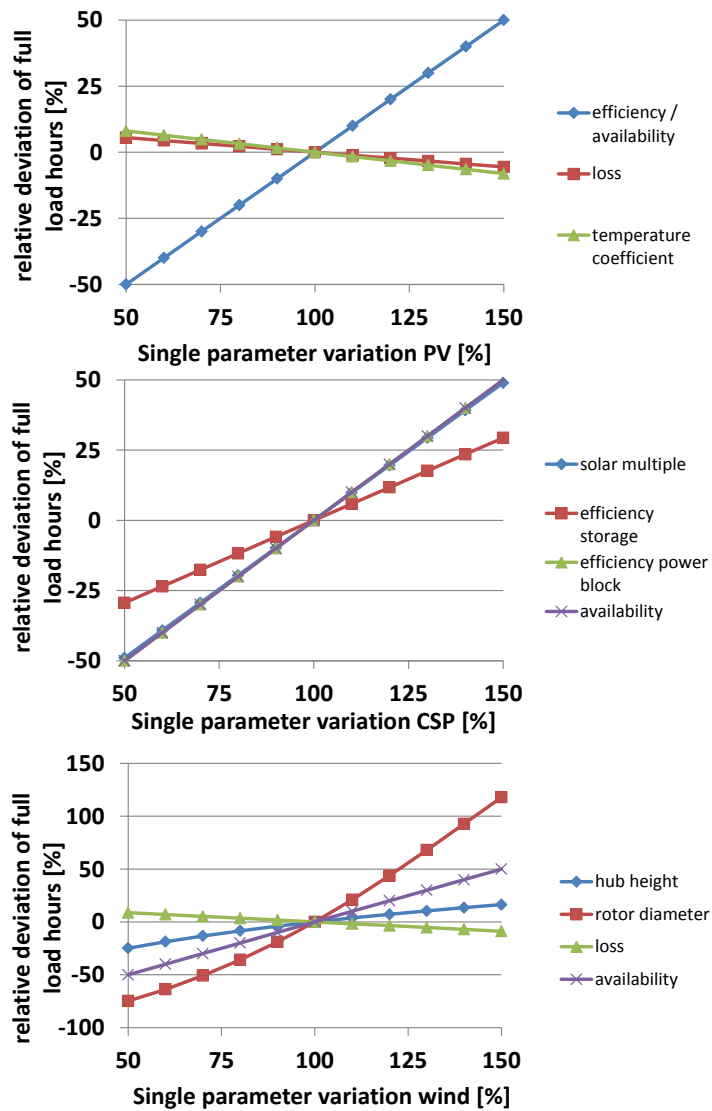


Figure 3.29.: Sensitivity analysis focusing on the deviations of the resulting full load hours after performing a single technical parameter variation. All parameters except for the rotor diameter of wind plants show a linear behavior. For CSP, an initial solar multiple at 100% of 2.5 is considered.

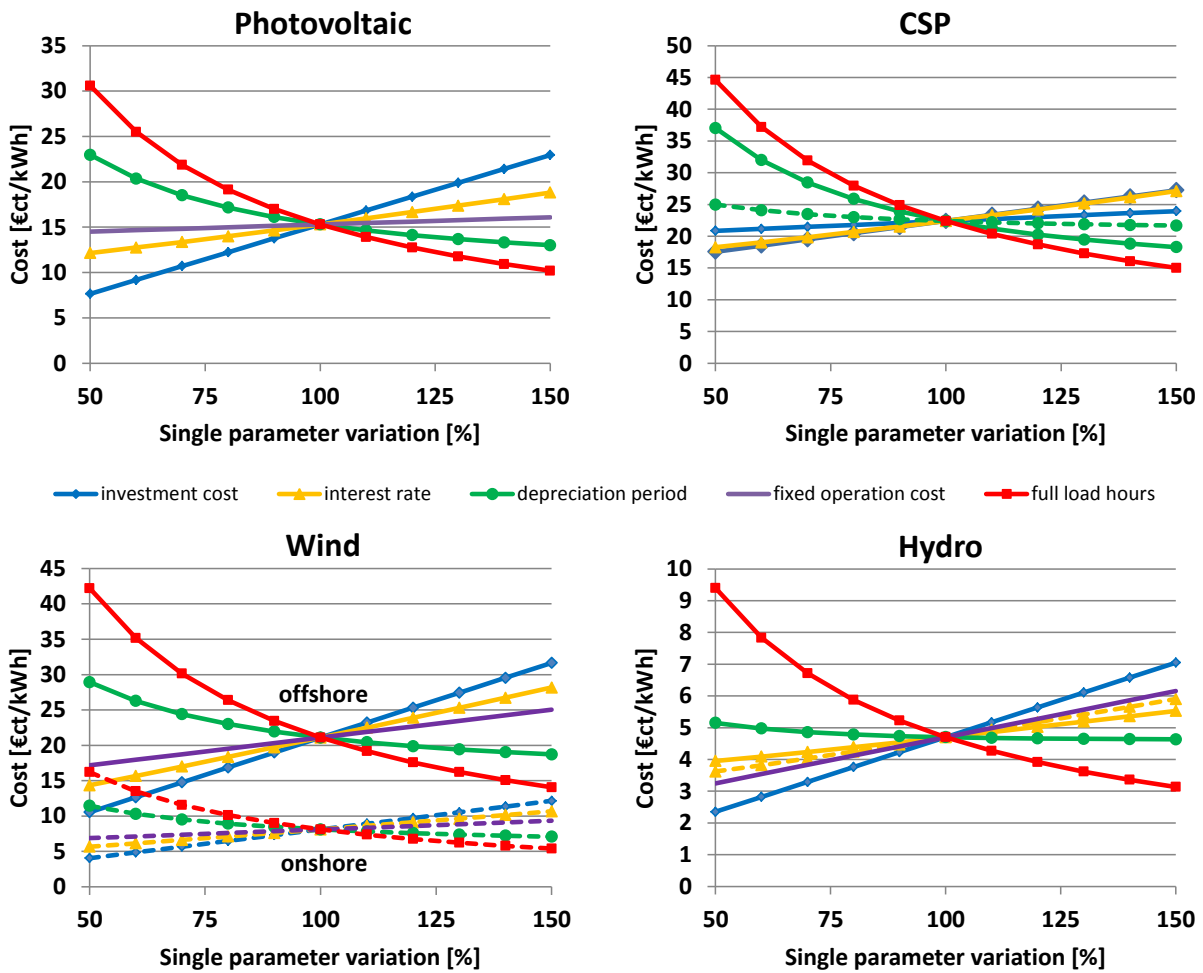


Figure 3.30.: Results of multiple sensitivity analyses focusing on the deviations of the resulting cost per kWh after performing a single economic parameter variation. Particularly full load hours have the greatest impact on the resulting cost estimations.

3.4. Discussion

Within the present chapter, the REMix module EnDaT²⁵ is enhanced in terms of establishing a globally operable potential assessment tool for renewable energies. This new version of REMix-EnDaT is in turn used for a global potential study as conducted in section 3.3. Moreover, potential power output time series, which serve as input for investigations dealing with siting effects and scenario validation - as discussed in sections 4.3 and 5.3, respectively - can be obtained for arbitrary sites globally. A thorough overview on the methodological workflow is given covering the items

- global land use assessment leading to the determination of installable capacities
- establishment of a global resources database on solar irradiance, wind speed and river run off
- power generation using plant models

Major results are the capability to determine installable capacities and hourly power output for the technologies PV, CSP, on- and offshore wind and hydro power on a global scale. These data can in turn be used to derive cost and full load hour potentials, either for single sites or for entire countries or arbitrary regions as cumulated values. The resources database spans a period from 1984 to 2005, any of these years can be used to compute results.

Building upon this framework, full load hour and cost potentials on a global scale are derived. Their regional distribution and occurrence is discussed in detail. The predominant resource is solar irradiance, followed by wind. Although it has only little potential - compared to solar and wind - hydro is the technology which has been using the available resources for decades.

The accuracy of the obtained results is limited with respect to hourly time steps, the spatial resource resolution of 0.45° and the initial land use resolution of $300 \times 300 \text{ m}^2$.

Special focus in this discussion is now given to the representativity of the resources data and the results of the global potentials assessment.

3.4.1. Accuracy of the resources data

3.4.1.1. General remarks

The most critical aspects with respect to resources data is their accuracy. Since the creation of fundamentally new, more sophisticated data sets is beyond the scope of the present work, existing databases are used and further extended.

In terms of solar irradiance, considerable efforts are devoted to the creation of hourly data both on the global horizontal (GHI) and beam normal irradiances (BNI). Very good agreement of the processed hourly resolved solar irradiance data with NASA's annual GHI sum [SRB12] is achieved with an average absolute deviation of -1.8%. For BNI, the

²⁵EnDaT abbreviates "Energy Data Tool".

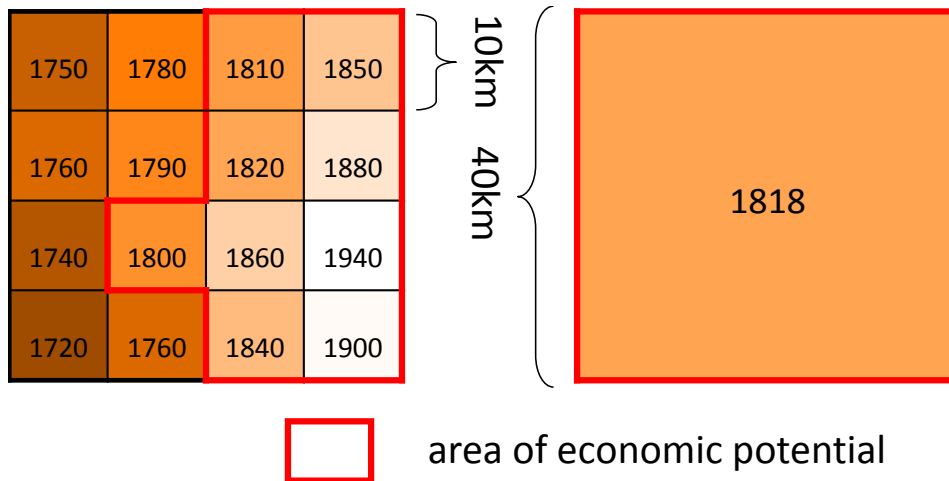


Figure 3.31.: Accumulation of highly resolved data to a coarse pixel according to Hoyer-Klick [HKSS], displayed values in $\left[\frac{kWh}{pixel-a}\right]$. Since solar annual irradiance sums behave rather homogeneous over great distances, the average value of a coarse pixel represents well the distribution of its highly resolved counterparts.

comparison to NASA’s annual sum yields an average absolute deviation of -7.8%. Thus, the resulting irradiance data sets appear to well-represent reality, although regional underestimations can occur. An update of NASA’s irradiance data [SRB12] is expected for summer 2013 with a spatial resolution of 10x10 km².

Wind data used in this work is provided by MERRA [MER12] at an hourly temporal resolution. As no temporal interpolation is carried out, merely spatial resolution effects are discussed below. Ongoing activities focus on the establishment of a high (spatial) resolution wind data set using the WRF model [WRF12] in combination with reanalysis data. Since the impact of spatial resolution effects is particularly important for wind data, a severe improvement in its accuracy is expected for wind potential assessments. Regarding river discharge, on a global scale the data used can be considered to be state-of-the-art. However, during the interpolation to hourly values, the monthly means can merely be considered as good indicators. Nonetheless, the approach is assumed to be justified against the background of run-off regimes varying with rather low frequencies.

3.4.1.2. Impact of the spatial resolution

Since the spatial representativity of the data is of great importance - particularly against the background of using rather coarsely resolved data as performed in this work - the following discussion is dedicated to this issue. As far as solar irradiance is concerned, it appears to behave fairly homogeneously in terms of the resource availability when accumulating data of high spatial resolution to a coarse pixel as indicated in the scheme of figure 3.31 and in the relief of figure 3.32. The average value appears to well-represent the distribution of annual irradiance sums. However, if a minimum threshold

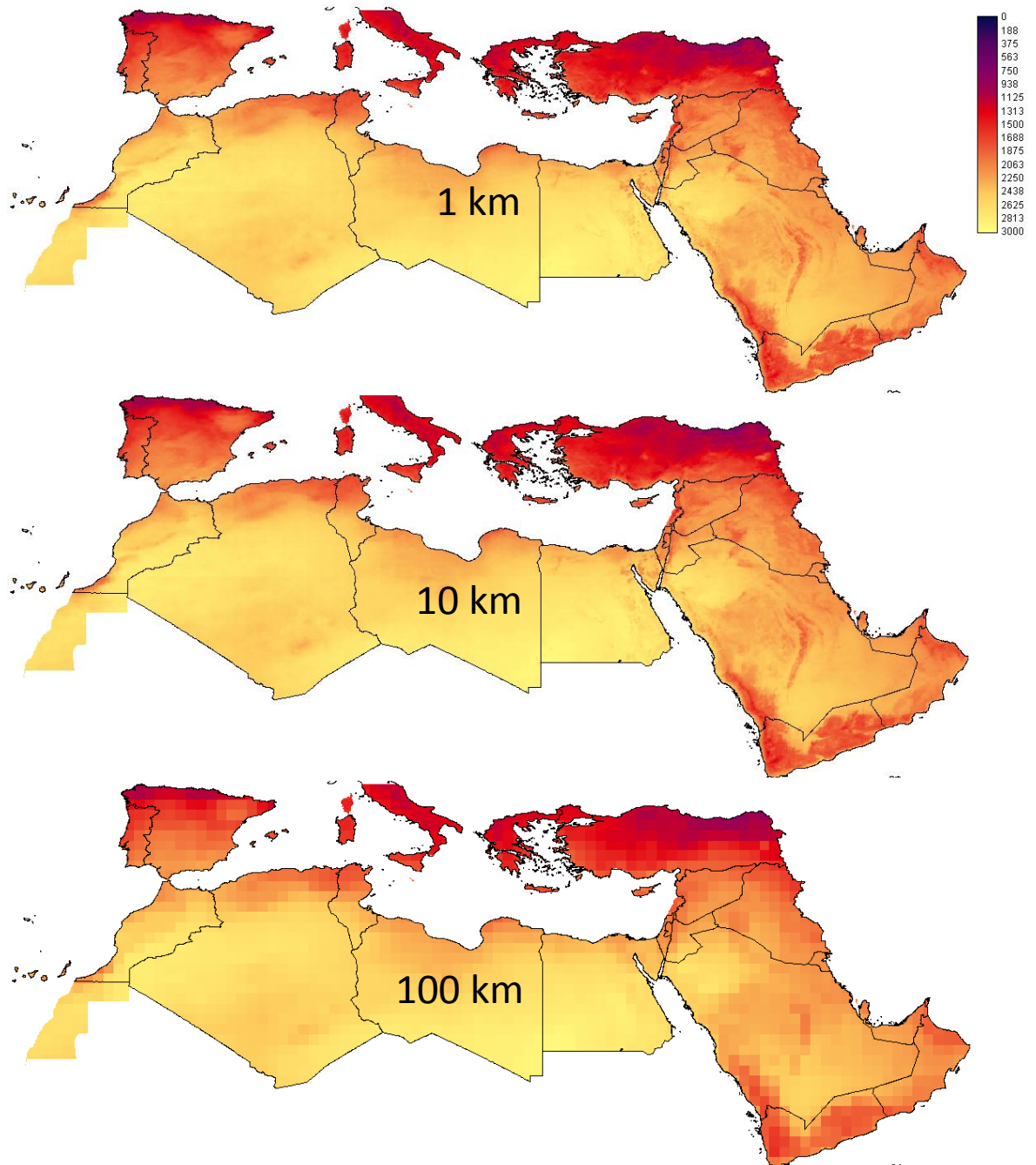


Figure 3.32.: Comparison of the effect of accumulation on the annual beam normal irradiance sums provided by Hoyer-Klick [HKSS]. The coarser the data - from top to bottom - the more details are lost.

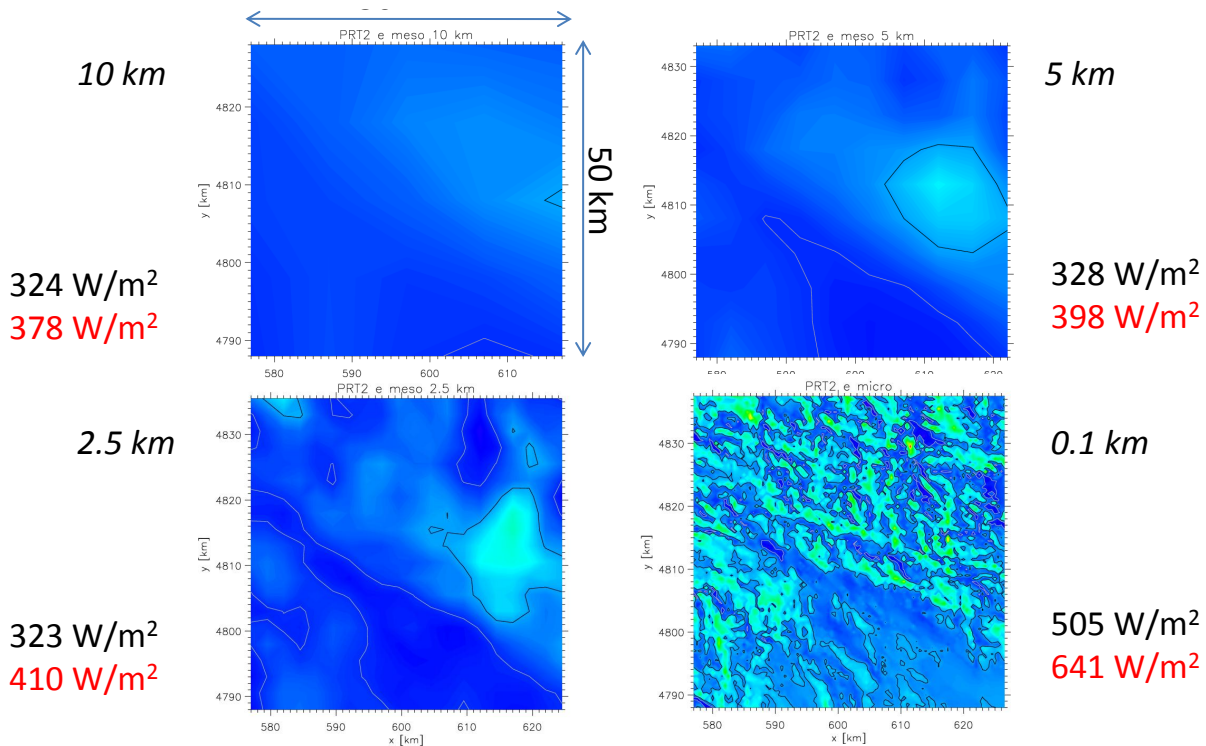


Figure 3.33.: Comparison of coarsely and highly resolved wind data according to Badger [Bad12]. The resolution is indicated in italic figures. Next to each graph, the average value and the mean of the windiest 50% are displayed, the latter in red. With increasing spatial resolution, i.e. from 10 km to 100 m, the mean values increase.

of $1800 \frac{kWh}{m^2 \cdot a}$ of beam irradiance is implemented, particularly in regions with values around this figure, the area for the technical potential might be underrepresented. In terms of the distribution functions, the impact of the pixel resolution is negligible as can be seen in figure 3.9 which was part of the discussion in subsection 3.2.2.1.3.

This picture entirely changes for wind data. As indicated in figure 3.33, the impact of the resolution quality is not negligible for the case of wind speed. With increasing spatial resolution from 10 km up to 100 m, it is eye-catching how advantageous sites become visible and the average power density values substantially rise. Also, the topology of the region becomes obvious, as it has a severe impact on the wind speeds due to funneling and surface roughness effects. Overall, this result underlines that using coarsely resolved wind data generally results in an underestimation of the potential.

For river discharge, a discussion to assess the spatial resolution is not performed due to the lack of data with an improved spatial resolution.

3.4.2. Evaluation of the global potential assessment's results

3.4.2.1. General remarks

The global assessment of cost and full load hour potentials carried out in this chapter gives an insight into both qualitative and quantitative aspects of the potential of feasible power generation using PV, CSP, wind and hydro power. While there are many assessments dealing with deriving renewable energy potentials, only very few cover the entire globe using GIS based spatially resolved data as done in this thesis. The following paragraph is based on and partly excerpted from a discussion carried out by the author within the framework of the project [SGS11]: The two major works dealing with global potentials of renewable technologies are from Hoogwijk [Hoo04] and Czisch [Czi05]. The former focuses on an analysis of the possible competitive contributions of the renewable energy technologies PV, onshore wind and biomass power (using energy crops) to the electricity supply in 17 world regions using cost supply curves. The monthly and annual averages derived in a spatial resolution of 0.5° are eventually used for the IMAGE 2.2 model. The latter focuses on the determination of the most economic energy system in the region Europe - North Africa - West Asia using ECMWF reanalysis data (ERA) with a spatial resolution of 1.125° . In this respect, for solar irradiance three-hourly data, for all other fluctuating resources 6 hourly data is used. In order to be able to model the availability of resources, a potential assessment is carried out before hand for all major renewable conversion technologies, i.e. PV, CSP, wind, biomass, hydro and geothermal power.

Other assessments not using spatially resolved data such as [Rog00], [S99], [WEC10] and [Fel] for wind and [Rog00], [S99] and [Hof02] for solar energy and [BHB03], [Rog00] for biomass give a regionally aggregated overview for the potentials. However in most cases merely theoretical potentials or only one potential type is assessed. As the approaches and regional boundaries differ from this work, comparing the results is difficult. Moreover, production cost or economic potentials are only represented by [WEC10], [Fel] and [Hof02].

Overall and in sharp contrast to this analysis, the aforementioned works altogether use top-down rather than bottom-up approaches. For all assessments including the present investigation, the renewable energy potentials exceed the current and future anticipated global electricity demand by several orders of magnitude.

3.4.2.2. Areas of improvement

In order to come up with more significant results and to determine indisputable figures for the respective potentials, the following discussion deals with areas of improvement that go beyond this work, but should be anticipated for future activities. They are now listed in terms of their immediate impact on the respective potential:

Improvement of theoretical potentials

The first source of error already occurs at the data generation for the resources, e.g. solar irradiance or wind speed. Future satellites using higher spatial resolutions will enable the establishment of resources data in much higher quality. According to the previous discussion, this is important due to the fact that using a mean value for a pixel with a size of up to 50x50 km² does not effectively represent the variation which occurs inside that pixel. Using average values overestimates some sites and - vice versa - underestimates others. Since deployment will happen at the best available sites, higher spatial resolution is desired.

In order to assess the effects of using spatially coarse data, a comparison with regionally available high quality data sources should be performed to derive the error bands and major error mechanisms when using coarsely resolved data. Due to the pixel based approach, the model design is already able to accommodate highly resolved data in the future.

Improvement of technical potentials

The identification of suitable sites for renewable power plants could be enhanced by using land cover data with a spatial resolution below 300x300 m². On a global scale, this resolution is state-of-the-art, thus yielding the best available results. However, further assessments considering forecasted land use changes will improve the data base for suitable sites for any assessment beyond today, as the data used in this work reflects contemporary land use patterns.

The power plant models can be enhanced by several measures: As a first step various conversion technologies within one branch, i.e. the use of various wind turbine models with differing rated capacities (heights, rotor diameters etc.) will lead to more differentiated and elaborate figures. In turn, resources data with higher temporal resolution will enable more realistic modeling results in terms of better representing the fluctuation within each assessed hour. The use of several photovoltaic technologies will also improve the results. The CSP model can be improved by considering other receiver types and heat transfer fluids.

Improvement of economic potentials

The determination of correct economic potentials heavily depends on the error made while estimating the technical potential. Thus, any steps taken for an improvement of the technical potential will also improve the economic one (the same holds for theoretical and technical potentials). Further assessments as to which resource should be tapped in specific regions are to be conducted by energy systems modeling, thus indicating the feasible (or best practice) power plant portfolios and leading to the economically tappable potential.

Predominantly, regionally disaggregated data on cost (installation, O&M, interest) and on depreciation times will enable the determination of potentials which are more representative in the respective regions. In order to address this issue, a sensitivity analysis is performed within this work. Moreover the economic potentials do not represent the need for reserve power plants or the construction of new power lines in order to profit from regionally anticorrelated renewable power generation.

Overall, any research aiming at investigating balancing effects, the potentials of regionally distributed power generation (using virtual power plants) or capacity factor analyses desire renewable potentials data in high temporal resolution. Therefore, the present approach and obtained data within REMix-EnDaT serve as valuable input for energy modeling approaches as carried out in chapters 4.3 and 5.3, since temporal resolutions of one hour are apt of sufficiently reflecting feasible balancing effects. For policy consultancy purposes, the data can be used to shape goals and scenarios for future energy systems and to assess associated cost of a transition from today's supply to a future renewable plant portfolio. Using temporally resolved data strongly enhances the significance of scenarios, as volatile effects of renewable power generation can be represented in great detail. Furthermore based on this work's database, analyses on the complementary role of a blend of renewable technologies can be carried out in identifying potentials for secure base load, as carried out by a joint work of the author and colleagues in [GSSB11]. However, the data is not suitable for energy modeling approaches, which focus on the determination of critical conditions in the power transmission and distribution grids, e.g. deviations from the anticipated voltages and frequencies. For the latter aspect data in much higher temporal and spatial resolution is required.

4. REMix-PlaSMo: Overall structure and study on portfolio effects of volatile generation

4.1. Outline

4.1.1. Motivation and goals

The identification of the maximum power plant capacity $P_i^{tech, inst-max}$ along with the subsequent determination of hourly power output data per grid box $E_{el, i}^{tech}(t)$ for various technologies are among the major goals of REMix-EnDaT discussed in the previous chapter. Building upon these data for the volatile technologies PV, on- and offshore wind as input, in the present chapter an analysis as to where specifically PV and wind power plants should be installed in order to gain distinct effects on their cumulated output and generation cost is performed.

Optimized siting of volatile capacities is of particular interest since - theoretically speaking - in contrast to uncoordinated installation directed balancing effects are expected to considerably improve the performance of the portfolio as a whole both in terms of supply security and the reduction of capital intensive residual load power capacities. This is the main focus of the plant siting module REMix-PlaSMo, which is a newly developed feature of the REMix energy modeling suite. The link between the REMix-EnDaT and REMix-PlaSMo and the content of this chapter are summarized in figure 4.1.

Within REMix-PlaSMo, the siting of the highly volatile portion of the generation portfolio (PV, on- and offshore wind) is optimized on a green-field, i.e. it is assumed that no power plants are installed at the beginning of the optimization process. The so-obtained PV and wind capacities are capable of providing a certain cumulated power output, thereby satisfying the load to a certain extent. The remaining residual load is to be met with other technologies. In this work PlaSMo is designed to meet this residual load with hydro power and CSP, as carried out in a case study later in this chapter. The CSP plants are specially designed in terms of their solar multiple¹.

Such an investigation is of particular interest, since CSP - due to the option of thermal energy storage and co-firing - is capable of electricity power generation on demand whereas PV and wind power cannot provide dispatch power to meet load requirements or for secure grid operation as far as tension and frequency stabilization are concerned. Particulary due to the sharp recent decline in cost for PV-modules, CSP is increasingly

¹For a brief background on the solar multiple please see section 3.3.1.3 in the previous chapter

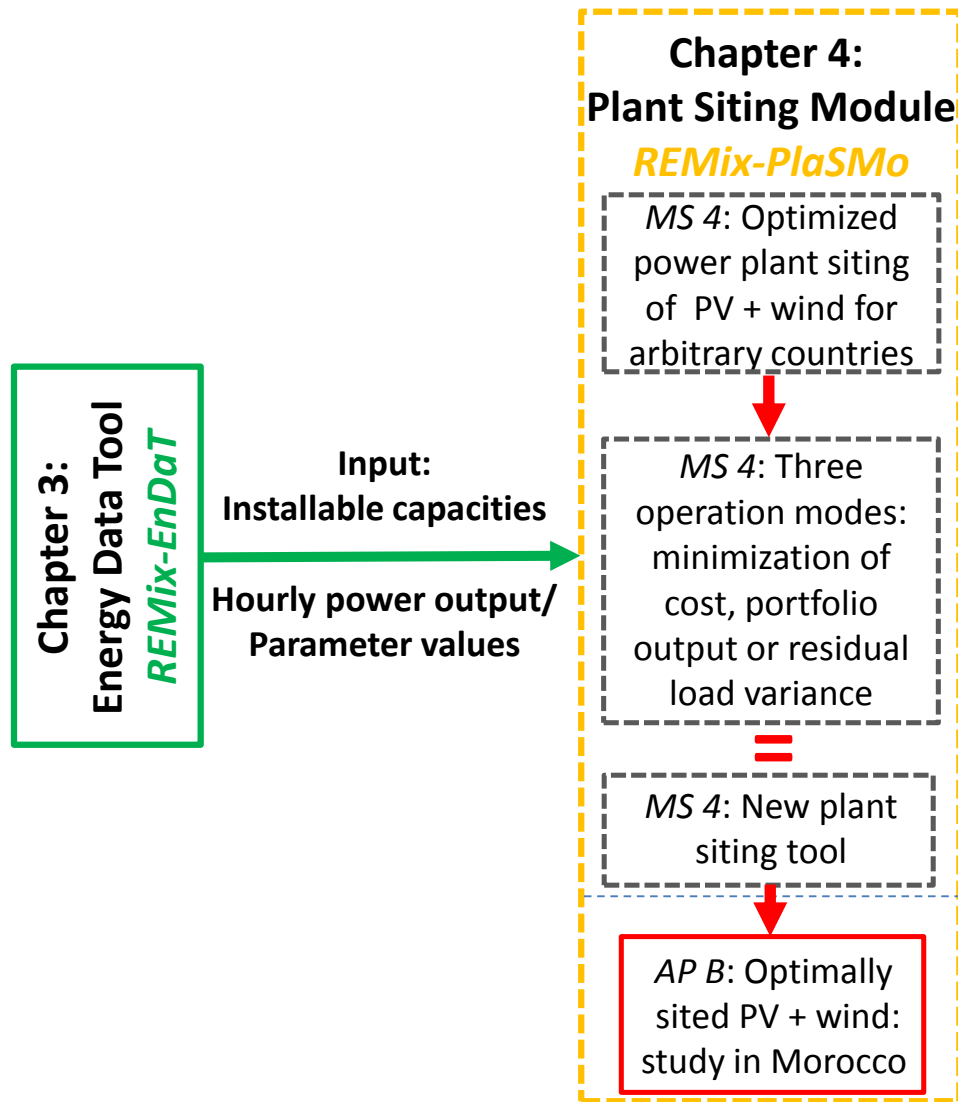


Figure 4.1.: Structure of the present chapter.

being questioned in direct economic comparisons, as it taps the same resource at higher capital cost. Depending on the market structure of the power system, this has a heavy influence on the implementation and usage of CSP plants: In markets merely driven by the generation cost, CSP will not be able to compete with PV in the long run [DM11]. The only justification for CSP is the capability of power dispatch on demand, i.e. supplying capacity when it is needed. That means that in markets (partly) rewarding capacity allocation, the higher generation cost is justified as it is (partly) covered by revenue from providing firm capacity. Moreover, besides economic considerations, this is also a technical imperative.

In the present work a market structure merely taking into account the generation cost is considered, the capital investment, operation and interest cost being distributed over the entire depreciation period. Against this background, the central question to be assessed

is the following: **How can volatile (PV and wind) and firm capacities (CSP and hydro) be best combined to achieve the least overall cost of the entire system and what is the resulting optimum share of volatile power generation?** To investigate this issue, the volatile generation portfolio is optimized with respect to minimizing

- a.) its generation cost
- b.) its portfolio output variance
- c.) the resulting residual load variance

Clearly, options b.) and c.) incur higher volatile annual electricity generation cost as the portfolio is more expensive than in case a.). Therefore it is of prime interest if the resulting residual loads allow for CSP plant configurations which lead to less firm capacity generation cost compared to case a.). In the following the approach to answer this question is discussed.

4.1.2. Approach

The overall approach employed for the development of REMix-PlaSMo is based on a discussion presented by Palmintier and Levine [PL08] who conduct a study on the minimization of the variability of volatile renewable power generation through optimized spatial distribution of the power plants using the standard deviation as the quantifying parameter. The key idea in the present thesis is to extend that approach which uses the installation coefficients a_i , b_i and c_i , taking values in the interval $[0, \dots, 1]$ for each grid box i and the technologies PV, on- and offshore wind respectively in terms of optimizing the overall cost and residual load variance. The investigation is only carried out for the aforementioned technologies, as CSP is capable of providing dispatched energy and hydro power output is not subject to extreme fluctuations, particularly against the background of using fits to obtain hourly values based on monthly means as done in this work. The installation coefficients indicate the share of the maximum installable capacity $P_i^{tech, inst.max}$ as determined by EnDaT (see chapter 3) which eventually should be used in each grid box according to one of the following operation modes:

A Cost minimization mode

In this mode the installation coefficients for the volatile portfolio consisting of PV, onshore and - where available - offshore wind are greater zero for the best performing sites, resulting in the highest tappable full load hours. The residual load - after deduction of hydro power generation - is to be met by CSP.

B PV+wind output variance minimization mode

The cumulated hourly output of PV, onshore and - where available - offshore wind is smoothened in terms of minimizing its portfolio output variance, i.e. hourly virtual power plant output standard deviation throughout an entire year under consideration. After subtraction of hydro power generation the residual load is intended to be met by CSP with low solar multiples, i.e. designed for medium to peak load.

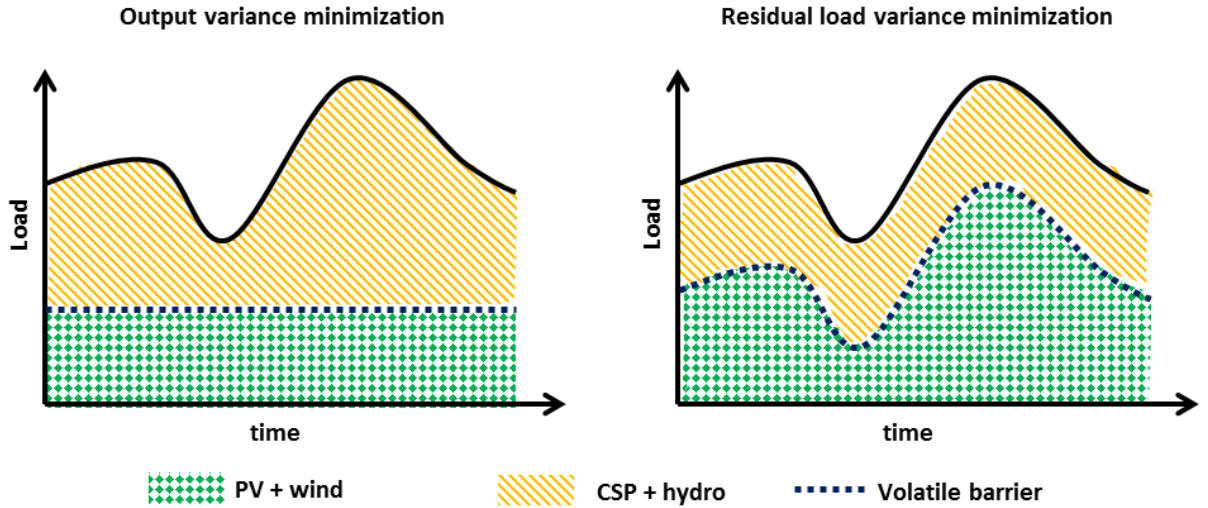


Figure 4.2.: Anticipated effects on the residual load using the optimization modes for variance minimization of the output (left) and the residual load (right).

C Residual load variance minimization mode

In this mode the residual load's standard deviation is minimized after PV, onshore and - where available - offshore wind power generation have been considered and subtracted from the hourly load profile. It is intended to be met using power provided by hydro and CSP with high solar multiples, i.e. designed for base to medium load.

Figure 4.2 indicates the basic effects on the residual loads for cases B and C. Any of the above modes is implemented and operable in any country for which hourly resolved demand data is available.

4.2. Algebraic formulation

The present mathematical framework for REMix-PlaSMo gives an overview as to how the installable capacities and the hourly power output, provided by REMix-EnDaT as presented in chapter 3 for each grid box i and the technologies PV, on- and offshore wind, are used to obtain the coefficients a_i , b_i and c_i , each in the range between $[0, \dots, 1]$. At this stage merely the volatile part of the generation portfolio, i.e. PV and wind, is considered.

For the implementation of the problem within the software tool GAMS [GAM12], the following equations and constraints are introduced to enable the modeling and solving of complex linear optimization problems. All relations imposing a boundary condition are denoted with the equality symbol " $\stackrel{!}{=}$ ", all others with the ordinary symbol " $=$ ":

Annual power output

The overall hourly output of the volatile portfolio $E_{el}^{Portfolio}(t)$ is composed of the hourly contributions derived in subsection 3.2.3, equation (3.17) and (3.21) for photovoltaic, on- and offshore wind $E_{el}^{PV}(t)$, $E_{el}^{onshore}(t)$ and $E_{el}^{offshore}(t)$, respectively. Their overall sum is obtained by the following relation, using the coefficients a_i , b_i and c_i :

$$\begin{aligned} E_{el}^{Portfolio}(t) &= E_{el}^{PV}(t) + E_{el}^{onshore}(t) + E_{el}^{offshore}(t) \\ &= \sum_i^N a_i \cdot E_{el,i}^{PV}(t) + \sum_i^N b_i \cdot E_{el,i}^{onshore}(t) \\ &\quad + \sum_i^N c_i \cdot E_{el,i}^{offshore}(t) \end{aligned} \quad (4.1)$$

Integrating the latter figure over the total number of hours per year results in the portfolio's annual power output $E_{el, annual}^{Portfolio}$:

$$E_{el, annual}^{Portfolio} = \sum_0^{8759} E_{el}^{Portfolio}(t) \quad (4.2)$$

This total power output is limited according to the user: For instance, if a share of 10% of the total electricity demand is to be covered with generation from PV and wind, the following expression holds:

$$E_{el, annual}^{Portfolio} \leq \frac{1}{10} \cdot \sum_t E_{el}^{Demand}(t) \quad (4.3)$$

Residual load

The residual load $E_{el}^{Residual}(t)$ is determined as the difference between power demand $E_{el}^{Demand}(t)$ and hourly power yield of the portfolio $E_{el}^{Portfolio}(t)$:

$$E_{el}^{Residual}(t) = E_{el}^{Demand}(t) - E_{el}^{Portfolio}(t) \quad (4.4)$$

Negative values of the residual load $E_{el}^{Residual}(t)$ indicate surpluses. They can be transported to neighboring countries using the transmission grid. This option is subject to the available net transfer capacities.

Installed capacity

According to the discussion in subsection 3.2.1.4, maximum installable capacities for each pixel i $P_i^{PV, inst_max}$, $P_i^{onshore, inst_max}$ and $P_i^{offshore, inst_max}$ are derived for photovoltaic and wind power using equations (3.7), (3.2) and (3.5). The installed capacities for each technology and site i yield the following boundary conditions, as they must not exceed the installable capacities:

$$P_i^{PV, inst} \leq a_i \cdot P_i^{PV, inst_max} \quad (4.5)$$

$$P_i^{onshore, inst} \leq b_i \cdot P_i^{onshore, inst_max} \quad (4.6)$$

$$P_i^{offshore, inst} \leq c_i \cdot P_i^{offshore, inst_max} \quad (4.7)$$

Integrating over all sites N , the overall installed capacities for each technology $P_{overall}^{PV, inst}$, $P_{overall}^{onshore, inst}$ and $P_{overall}^{offshore, inst}$ are obtained:

$$P_{overall}^{PV, inst} = \sum_i^N P_i^{PV, inst} \quad (4.8)$$

$$P_{overall}^{onshore, inst} = \sum_i^N P_i^{onshore, inst} \quad (4.9)$$

$$P_{overall}^{offshore, inst} = \sum_i^N P_i^{offshore, inst} \quad (4.10)$$

The portfolio's total capacity of photovoltaic, onshore and offshore wind $P^{Portfolio, inst}$ then amounts to:

$$P^{Portfolio, inst} = P_{overall}^{PV, inst} + P_{overall}^{onshore, inst} + P_{overall}^{offshore, inst} \quad (4.11)$$

Cost

The cost of the portfolio is a function of the installed capacities and their annuities. In subsection 3.3.1.1.1, equations (3.22) and (3.24) represent expressions for the annuity $a_{p,n}$ and the annuity factor $AF_{p,n}$:

$$a_{p,n} = C_0^{tech} \cdot AF_{p,n} \quad (4.12)$$

$$AF_{p,n} = \frac{(1+p)^n \cdot p}{(1+p)^n - 1} \quad (4.13)$$

with the initial total investment cost C_0^{tech} , the interest rate p and the depreciation period n .

According to the latter, the annual total cost for the technologies photovoltaic, onshore and offshore wind $C_{total\ annual}^{PV}$, $C_{total\ annual}^{onshore}$ and $C_{total\ annual}^{offshore}$ are set up as follows:

$$C_{total\ annual}^{PV} = P_{overall}^{PV, inst} \cdot (a_{p,n} + c_{spec}^{PV, op}) \quad (4.14)$$

$$C_{total\ annual}^{onshore} = P_{overall}^{onshore, inst} \cdot (a_{p,n} + c_{spec}^{onshore, op}) \quad (4.15)$$

$$C_{total\ annual}^{offshore} = P_{overall}^{offshore, inst} \cdot (a_{p,n} + c_{spec}^{offshore, op}) \quad (4.16)$$

$c_{spec}^{tech, op}$ indicate the technology specific operation cost. The overall cost is then obtained as:

$$C_{total\ annual}^{overall} = C_{total\ annual}^{PV} + C_{total\ annual}^{onshore} + C_{total\ annual}^{offshore} \quad (4.17)$$

Variance

The standard expression for the variance σ^2 of the portfolio using the covariance Cov as proposed for instance by Palmintier and Levine [PL08]

$$\sigma^2 = \sum_{i=1}^N \sum_{j=1}^N a_i a_j Cov(E_i^{tech}(t), E_j^{tech}(t)) \quad (4.18)$$

with the coefficients a_i , a_j and the hourly output series $E_i^{tech}(t)$, cannot be employed for the present problem, as numerical difficulties result in small or even negative Eigenvalues which object the constraint of positive semi-definiteness [Wer12]. Therefore the following solution is introduced²: A reformulation of equation (4.18) is proposed according to Werner [Wer12] as

$$\sigma^2 = x^T M x \quad (4.19)$$

where x is a vector with dimension i containing the asset shares for all sites i and M the covariance matrix. Using

$$M = Q^T Q \quad (4.20)$$

and

$$y = Q x \quad (4.21)$$

eventually the expression

$$\sigma^2 = x^T Q^T Q x \quad (4.22)$$

$$= y^T y \quad (4.23)$$

is obtained. A matrix Q is now sought satisfying the above stated relation (4.20) for the covariance matrix M . Each of the latter's entries are derived using the standard expression for the covariance Cov of a random set of variables x and y for a given number of data points. In this case, x and y are the hourly power generation at sites i and j , $E_i^{tech}(t)$ and $E_j^{tech}(t)$ respectively, with $T=8760$ time steps:

$$Cov(i, j) = \frac{1}{T} \cdot \sum_{t=0}^{8759} \left(\left(E_i^{tech}(t) - \frac{1}{T} \cdot \sum_{t=0}^{8759} E_i^{tech}(t) \right) \cdot \sum_{t=0}^{8759} \left(E_j^{tech}(t) - \frac{1}{T} \cdot \sum_{t=0}^{8759} E_j^{tech}(t) \right) \right) \quad (4.24)$$

Defining an $i \times T$ matrix D , with the entries

$$d_i(t) = E_i^{tech}(t) - \frac{1}{T} \cdot \sum_{t=0}^{8759} E_i^{tech}(t) \quad (4.25)$$

and multiplying the latter with its transverse D^T gives the quadratic $N \times N$ matrix B , where

$$B = D \cdot D^T \quad (4.26)$$

and N is the total number of sites. In order to obtain a relation similar to equation (4.24), each arbitrary entry of B is divided by the total number of hours of the considered time period T :

$$\frac{1}{T} \cdot B = \frac{1}{T} \left(\sum_{t=0}^{8759} (d_i(t) \cdot d_j(t)) \right) \quad (4.27)$$

²The implementation of the solution into the present mathematical framework for the computation of the variance is one of the major results of the Master thesis conducted by Werner [Wer12] under the author's supervision.

Thus D satisfies relation (4.24) and is employed for the computation of the overall variance $y(t)$ taking into account photovoltaic, onshore and offshore wind with their respective site coefficients a_i , b_i and c_i :

$$y(t) = \sum_i a_i \cdot d_i^{PV}(t) + \sum_i b_i \cdot d_i^{onshore}(t) + \sum_i c_i \cdot d_i^{offshore}(t) \quad (4.28)$$

Eventually, the final total variance σ^2 according to relation (4.23) is obtained:

$$\sigma^2 = \frac{1}{T} y^T \cdot y \quad (4.29)$$

$$= \frac{1}{T} \sum_t (y(t))^2 \quad (4.30)$$

Residual load variance

Expression 4.25 is used to compute the portfolio's overall variance along with equations (4.28) and (4.29) taking into account all sites i of an area of investigation and all time steps t desired. If the residual load's overall variance is to be minimized, 4.28 changes to:

$$y(t) = \sum_i a_i \cdot d_i^{PV}(t) + \sum_i b_i \cdot d_i^{onshore}(t) + \sum_i c_i \cdot d_i^{offshore}(t) - E_{el}^{Demand}(t) \quad (4.31)$$

$$= E_{el}^{Residual}(t) \quad (4.32)$$

Objective constraints

The three operation modes introduced in section 4.1 apply the following objective functions:

A Cost minimization mode

Minimize equation (4.17):

$$\min C_{total\ annual}^{overall} \quad (4.33)$$

B PV+Wind output variance minimization mode

Minimize equation (4.29), using relations (4.25) and (4.28) as inputs:

$$\min \sigma^2 \quad (4.34)$$

C Residual load variance minimization mode

Minimize equation (4.29), using relations (4.25) and (4.31) as inputs:

$$\min \sigma^2 \quad (4.35)$$

In summary, the above approach enables the determination of the installation coefficients a_i , b_i and c_i of the volatile generation portfolio made up of PV, on- and offshore wind for three different optimization objectives. Each of the latter operation modes is used in a case study on Morocco discussed in the following sub-chapter.

4.3. Application of REMix-PlaSMo: Assessment of portfolio effects in Morocco

4.3.1. Setup of the optimization

Exemplarily, the tool REMix-PlaSMo is employed for an assessment of the least overall generation cost in Morocco, only using the technologies PV, wind, hydro and CSP. An overview on the workflow to determine the portfolio's overall cost is given in figure 4.3. The setup of the workflow, additional constraints and assumptions are elaborated in the following:

(i.) Green-field approach and considered years

A green-field approach is used, referring to the fact that no existing power plants at all are considered at the beginning of the optimization and that all capacities resulting from the calculations are new constructions. This approach is carried out separately for the years 2010, 2030 and 2050. These years are chosen to obtain results for feasible supply configurations using contemporary economic and technological data (2010), and data of an anticipated medium and long range development (2030 and 2050, respectively). The determination of an optimized pathway between 2010 and 2050 is not part of the optimization objective.

(ii.) Load data used

Hourly load data for the years indicated before is approximated based on an empirical approach by Paul [Pau07], who uses available data on power consumption for typical days, on population and economic growth and specific cultural patterns to create hourly load profiles. This framework is used along with projections on the demand development from 2010 to 2050 from the MENA Water Outlook [MEN11], forecasting a tremendous increase in annual electricity consumption from some 34 TWh in 2010 to more than 190 TWh in 2050. The data provided by Paul [Pau07] is scaled accordingly to obtain the respective annual consumption. The resulting load duration curves of the three investigated years are presented in figure 4.4 as dashed lines.

(iii.) Security margin of firm power - "10% rule"

For each assessed case, a security margin of the total generation provided by firm capacity is considered to represent contributions of indispensable secure power plant capacities for grid stability. No further backup capacities are considered. In figure 4.3 this is indicated as the "10% rule". In this investigation, hydro and CSP plants are used for that purpose, both being capable of quickly adjusting their output, thus enabling grid management in terms of voltage and frequency stabilization. Hence the boundary condition is implemented that at least 10% of the peak load demand be met each hour by hydro or CSP. An hourly hydro power generation time series as provided by REMix-EnDaT is used to determine the necessary amount of hourly gap energy which has to be met by CSP and indicated in figure 4.3 as "CSP load A" - to achieve a total of at least 10% of secure power. The resulting load profiles - in figure 4.3 and hereafter referred to as 90% loads - are also indicated in terms of their load duration in figure 4.4 as solid lines.

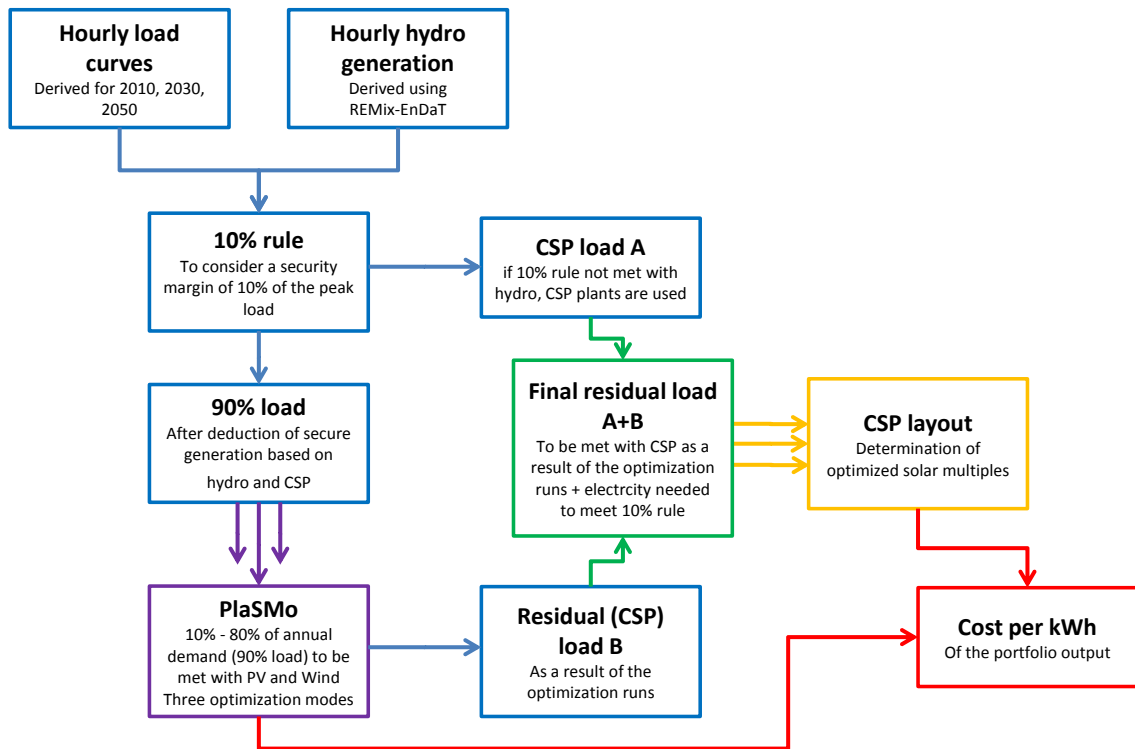


Figure 4.3.: Processing chain for the determination of the overall cost of a portfolio only consisting of PV, CSP, wind and hydro power. Hourly load and hydro power generation data (top left and right) are used to determine a "90% load" and a "CSP load A" according to the "10% rule". These 10% are intended to be met by firm capacity provided by hydro and - if necessary - by CSP, to ensure stable power grid operation. The "90% load" data serves as input to the volatile "PlaSMo" runs (bottom left), which are carried out with cumulated PV and wind shares in the range of 10 to 80% of annual (90%) power demand using three modes: least cost, output variance and residual load variance minimization. "CSP load A" resulting from the "10% rule" and the residual load curves of each respective run - "Residual (CSP) load B" - are summed up to obtain a "Final residual load A+B", in turn being met with an optimized "CSP layout" (center right). Eventually, for each run the overall "cost per kWh" are determined (bottom right).

(iv.) Range of the volatile power generation shares

The impact of the share of volatile annual electricity generation on the power system as a whole in terms of cost and residual load requirements is of high interest. As indicated earlier, in this assessment the volatile technologies PV and wind on the one hand and the firm power technologies CSP and hydro power on the other hand are available. The volatile annual electricity generation share is defined as the portion of the total annual electricity generation which is met with PV, onshore and offshore wind. In this work five different cases for the volatile annual electricity generation shares are investigated. It can take values between

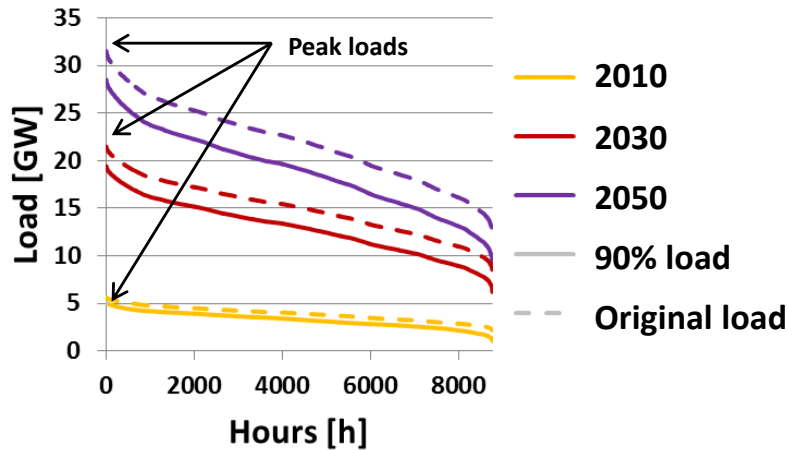


Figure 4.4.: Load duration curves for Morocco for the years 2010, 2030 and 2050. A sharp increase in peak load demand is visible. For the original load cases, it rises from about 5.6 GW in 2010 to more than 31 GW projected for 2050. Also, annual electricity consumption, i.e. the integral of each of the curves presented, rises from about 34 TWh in 2010 to approximately 190 TWh in 2050. 10% of this load is to be met with firm capacity provided by hydro and - for all cases when hydro cannot provide sufficient power - CSP.

10% and 80% in terms of the 90% load. In terms of the original load, these share values take smaller figures. After deduction of the volatile annual electricity generation from the 90% load, "residual (CSP) load B" in figure 4.3 is obtained.

(v.) Final residual load

Combining "CSP load A" as a result of the 10% rule with "residual (CSP) load B" as indicated in figure 4.3, the final "residual load A+B" is obtained. The latter is to be met using CSP plants with specifically designed plant layouts, i.e. solar multiples. They are derived using a second optimization step according to Moser [Mos12], during which the best-suited CSP plant in terms of the least net electricity generation cost is determined.

(vi.) Maximum surplus generation

For all cases the maximum hourly power generation surplus is limited. The only technical options to accommodate surplus are storage³ or power transmission to neighboring power grids. Within the assessment in this chapter electricity storage is not taken into account. However power transmission from Morocco to both Algeria and Spain are considered. Figures for these transmission capacities, hereafter referred to as net transfer capacities, are taken from Brand and Zingerle [BZ10], who give net transfer capacities to Algeria and Spain summing up to 2650 MW in 2010 and 3350 MW from 2015 onward. These values limit the surplus for the 2010 simulations to 2650 MW, and for the 2030 and 2050 simulations to

³Storage is a means of load shifting, as the energy stored is released to the grid at a later stage, with respective conversion losses.

3350 MW. The optimistic assumption is made that the power grids in the neighboring countries are always capable of accomodating any power from Morocco, with the net transfer capacity representing the upper hourly boundary.

(vii.) Overall net generation cost of the portfolio

As discussed earlier, three optimization modes are used. Within each optimization mode, five values are taken for the anticipated volatile share, as introduced above. Therefore, overall 15 simulations are performed. Each run results in a "final residual load A+B" to be met by CSP (please see figure 4.3). The CSP plants' solar multiples are optimized according to each respective "final residual load A+B" using the tool provided by Moser [Mos12].

For each of the aforementioned 15 simulation runs, the portfolio's overall net generation cost per kWh of consumed electricity $c_{overall, net}^{portfolio, gen}$ is determined. The generation cost is derived as annuities for each technology, according to the values and discussion within the framework of REMix-EnDaT, as presented in subsection 3.3.1.1.1. Moreover, hydro power is not included in the cost calculations, as the assumption is made, that all plants are completely depreciated. For the option of co-firing CSP plants with gas, resource prices of 22, 47 and 59 $\frac{\text{€}}{\text{MWh}_{th}}$ according to [IEA12] are used for 2010, 2030 and 2050 respectively.

Eventually, the portfolio's overall net generation cost per kWh of consumed electricity $c_{overall, net}^{portfolio, gen}$ is derived according to the following relation, using the share-weighted⁴ specific net generation cost c_{net} [$\frac{\text{€ct}}{\text{kWh}}$], the hourly power generation $E_{el}^{tech}(t)$ and the surplus $E_{el}^{surplus}(t)$:

$$\begin{aligned} c_{overall, net}^{portfolio, gen} = c_{net}^{PV+wind, gen} \cdot \sum_t \frac{E_{el, net}^{PV+wind, gen}(t)}{E_{el, net}^{PV+wind, gen}(t) + E_{el}^{CSP, gen}(t)} \\ + c_{net}^{CSP, gen} \cdot \sum_t \frac{E_{el}^{CSP, gen}(t)}{E_{el, net}^{PV+wind, gen}(t) + E_{el}^{CSP, gen}(t)} \end{aligned} \quad (4.36)$$

where the net volatile electricity generation is defined as the sum of the gross generations reduced by the sum of the surplus generation, which is transferred to Algeria and Spain:

$$\begin{aligned} \sum_t E_{el, net}^{PV+wind, gen}(t) = \sum_t E_{el, gross}^{PV, gen}(t) + E_{el, gross}^{onshore, gen}(t) \\ + E_{el, gross}^{offshore, gen}(t) - E_{el}^{surplus}(t) \end{aligned} \quad (4.37)$$

The most important questions are: which out of the 15 performed simulations has the least overall net annual electricity generation cost per kWh, which configurations of CSP are used in the different residual load cases, and what is the optimum share of volatile annual electricity generation.

⁴contributions of PV and wind on the one hand and CSP on the other hand.

4.3.2. Results

Employing the mathematical framework discussed in section 4.2 in the workflow introduced in subsection 4.3.1, results are computed for the three different optimization modes.

4.3.2.1. Overall cost

Figure 4.5 summarizes the results for the net annual electricity generation cost of the portfolio as a function of the volatile annual electricity generation share. Key findings according to this figure are:

- Optimum volatile annual electricity generation share

The top performing volatile annual electricity generation share for all simulations assessed is 34%. Other approaches which also present data on the most economic contributions of volatile power give conservative values of 25% [TSK⁺06] up to exhausting 42% [Tri12].

The remaining 66% in this work are met by hydro and CSP. The obtained optimum average portfolio cost figures remain relatively constant throughout the assessed period between 10.1 and 10.5 $\frac{\text{€ct}}{\text{kWh}}$ ⁵ of (net) generated electricity. The anticipated increase of cost for natural gas appears to be entirely compensated by decreasing installation cost for all renewable technologies.

- Effect of the optimization mode and role of CSP

The top performing optimization modes are: least cost in 2010 and 2030 and output variance minimization in 2050. For 2050, the least cost and output variance minimization modes perform almost equally at the optimum volatile share (compare 10.39 to 10.35 $\frac{\text{€ct}}{\text{kWh}}$ respectively). To clarify the reason for this behavior, figure 4.7 gives an insight into the contributions to the portfolio's net overall cost - indicated in figure 4.5 - of its constituting elements net annual CSP generation cost and net volatile annual electricity generation cost. For 2050, it can be seen that the volatile annual electricity generation cost for the cost minimization case is inferior to the variance minimization case. This is due to the fact that in the cost minimization case, sites with high full load hours are tapped using the cheapest available technologies. In contrast, CSP generation in the variance minimization case is cheaper compared to the cost minimization case. The improved overall behavior is therefore solely due to the contributions of CSP. The key figures of the plants for the two optimization cases are indicated in figure 4.6. In the variance minimization case less peak load has to be covered (compare 29098 MW to 30245 MW in the cost minimization case), less capacity is installed in terms of the solar field and the thermal energy storage, thereby reducing initial investment cost. Moreover the renewable share of the plant is higher, less electricity is produced

⁵in 2010 price levels

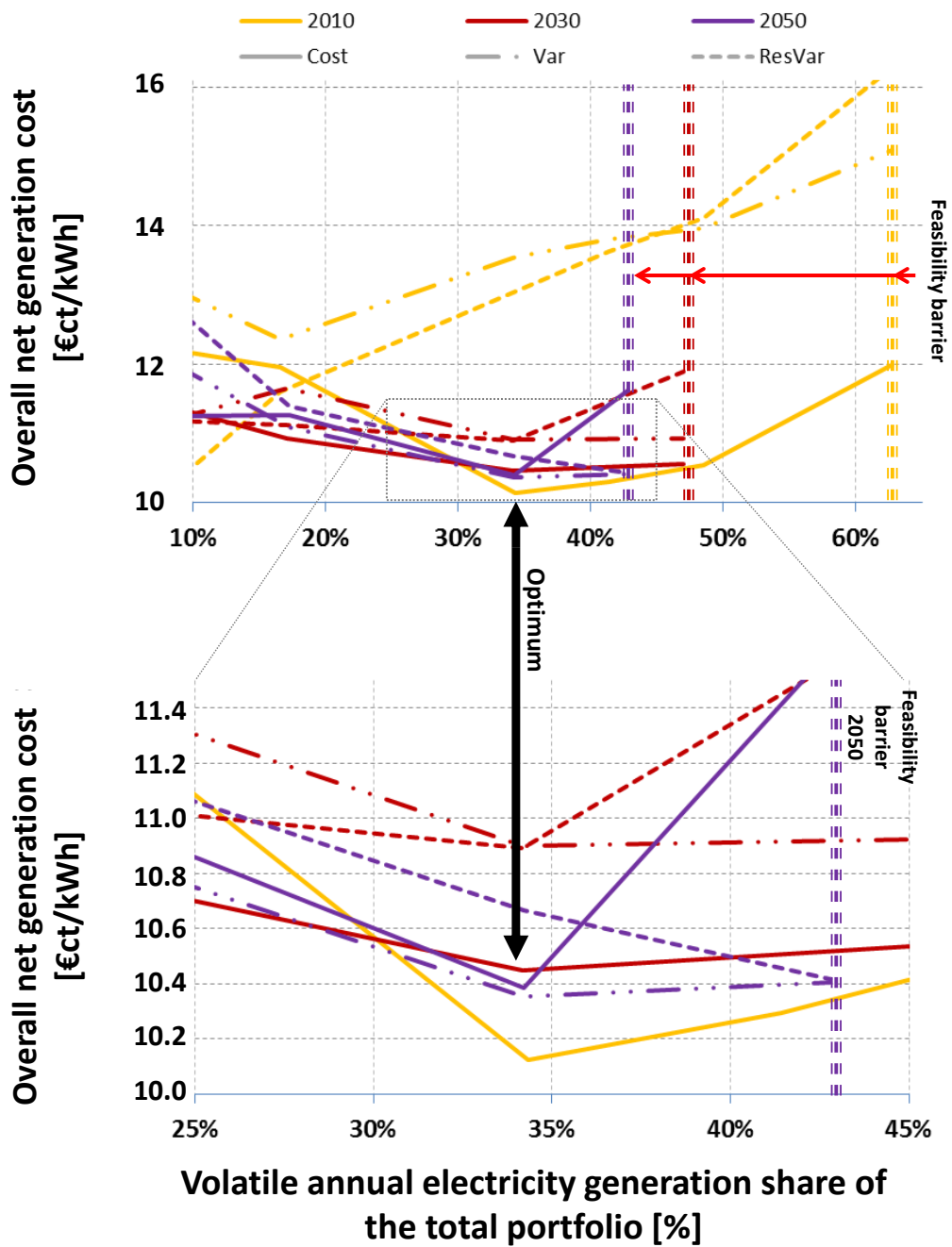


Figure 4.5.: Net generation cost of the portfolio comprised of PV, wind, CSP and hydro as a function of the volatile annual electricity generation share.

Comparison for 2050: 34% volatile generation share

	least cost case	variance minimization case
Peak load [MW]	30245	29098
Solar Multiple	1.79	1.73
TES [h]	8.52	6.71
Net generation cost [€ct/kWh]	13.65	12.74
Renewable share [%]	73.60	75.30
Area solar field [m²]	328535562	307891261
Q_{TES}[MWh]	811607	619909
Backup boiler [MW_{th}]	35716	34175
Net electricity solar [GWh/a]	89675	91459
Net electricity fossil [GWh/a]	33212	31172

Figure 4.6.: Comparison of the CSP plant layouts for the optimum volatile annual electricity generation in the case least cost and variance minimization in 2050. The latter case has higher net generation cost.

using gas. This represents an additional cost advantage for the variance minimization case. For these reasons, the net generation cost is cheaper than in the least cost case: Compare 12.74 to 13.65 $\frac{\text{€ct}}{\text{kWh}}$.

In summary, the minimization of the output variance compared to a minimum cost optimization is only beneficial in 2050, and the difference in the net electricity generation cost is marginal. The residual load can be covered at less cost compared to the cost minimization case. Moreover, there is no point in optimizing the output of the volatile portfolio in terms of obtaining a smoothed residual load curve for CSP, using the residual load variance minimization. The benefit of high full load hours for a CSP plant designed with high solar multiples cannot compensate for the higher cost of the volatile generation portfolio.

- General feasibility limited by surplus constraint

Not all runs are feasible in terms of the setup of the optimization discussed in the previous subsection 4.3.1. Feasible solutions are found to the left of the feasibility barriers indicated as vertical lines in figure 4.5. The principal reason for infeasibility is the restriction of hourly surplus generation which is limited to 2650 MW in 2010 and 3350 MW in 2030 and 2050. As the share of volatile annual electricity generation increases, surplus generation also occurs more often. At a certain point, no more surplus can be accommodated by the (neighboring) grid. These points are the feasibility barriers. In figure 4.5 they move to the left for

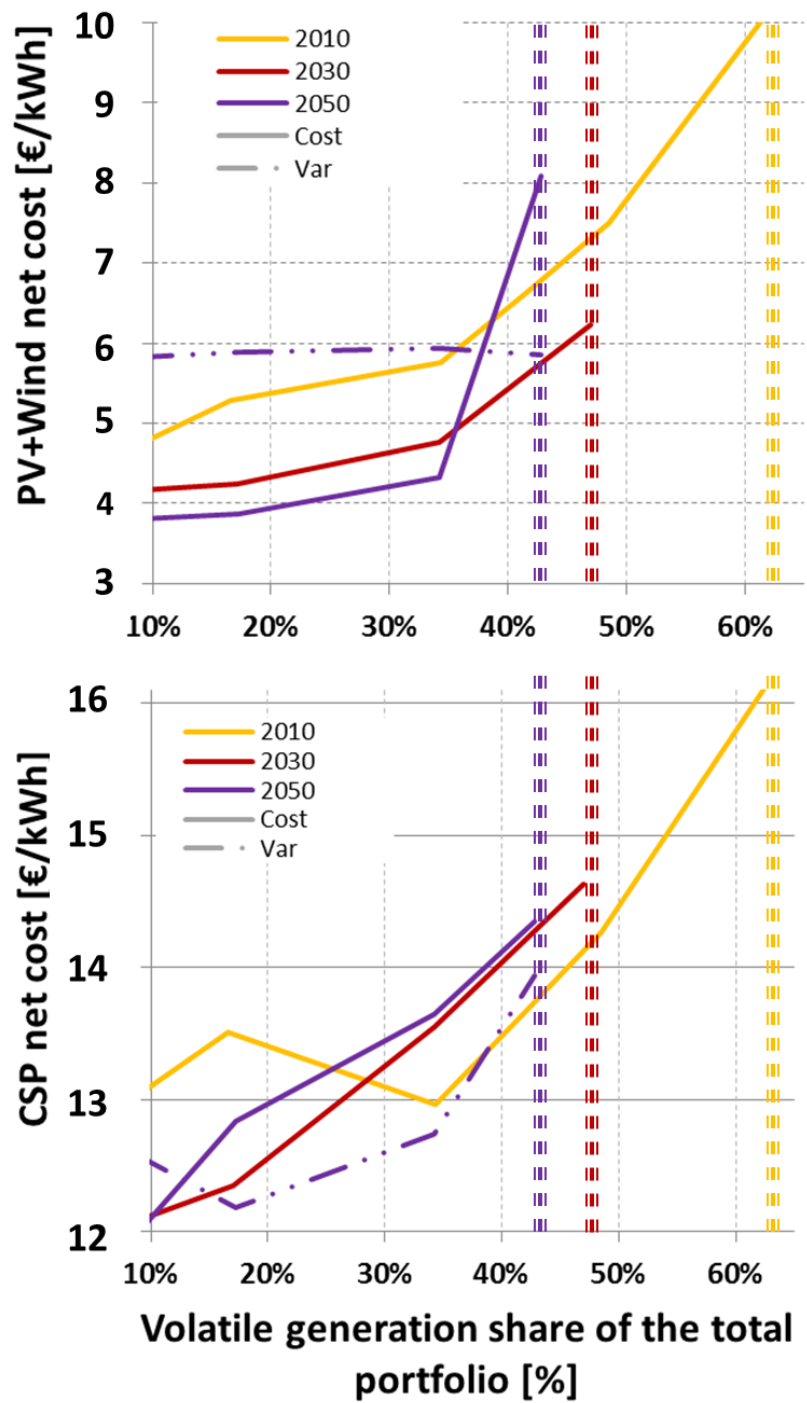


Figure 4.7.: Net generation cost of the volatile portfolio (top) and CSP (bottom).

the years 2010 to 2050. This is due to the fact that the net transfer capacities are assumed to remain constant while a drastic increase in demand and peak load occurs over that period. The relation of possible surplus limited by the existing transmission capacities and peak load drops from 0.47 over 0.16 to 0.11 for the years 2010, 2030 and 2050 respectively. Covering this increased demand with volatile generation is therefore more difficult as the surplus limit remains constant.

4.3.2.2. Discussion on the top performing optimization modes

In this section the top performing optimization modes, i.e. cost minimization in 2010 and 2030 and output variance minimization in 2050 are presented in more detail. The discussion is carried out according to the overview for these three best performing optimizations given in figure 4.8. It indicates the development of the single technology shares (on the ordinate) of both the installed capacities and power generation as a function of the volatile annual electricity generation share (plotted on the abscissa). The volatile annual electricity generation share is the portion of the total annual electricity generation provided by PV, on- and offshore wind. The installed capacities are indicated as dashed lines and power generation as solid lines for CSP (red), hydro (blue), PV (yellow), on- and offshore wind (light and dark green, respectively).

The differences between generation and installed capacity shares are due to different full load hours of the considered technologies. Higher generation shares compared to installed capacity shares indicate better full load hours. In the plot this results in the following observation: CSP, hydro and offshore wind are characterized by full load hours above the portfolio's average, while PV and onshore wind are below that value. For that reason the respective installed capacity shares are smaller than the generation shares for CSP, hydro and offshore wind and larger for PV and onshore wind.

Overall it can be concluded for all three cases that the contributions of CSP both in terms of installed capacities and power generation naturally decline as the volatile shares (PV, on- and offshore wind) increase, as CSP, besides a constant input by hydro power, is the complementing technology in this assessment. For this reason the solid red line in figure 4.8 indicating the CSP generation share of the portfolio's total generation descends linearly in all three cases.

The portfolio's power output becomes increasingly renewable over the course of the assessed years for two reasons: installation cost for all CSP components decrease (as indicated in subsection 3.3.1.1.1) and natural gas prices increase, both facts in turn resulting in an increased solar share. Consequently the portfolio's renewable share also increases towards 2050.

The shares of hydro power decrease from 2010 to 2050, which is due to the fact that only modernization of existing installations and no new constructions are considered. Since the overall power consumption grows rapidly from some 34 TWh in 2010 to 190 TWh in 2050, the relative hydro contributions decline.

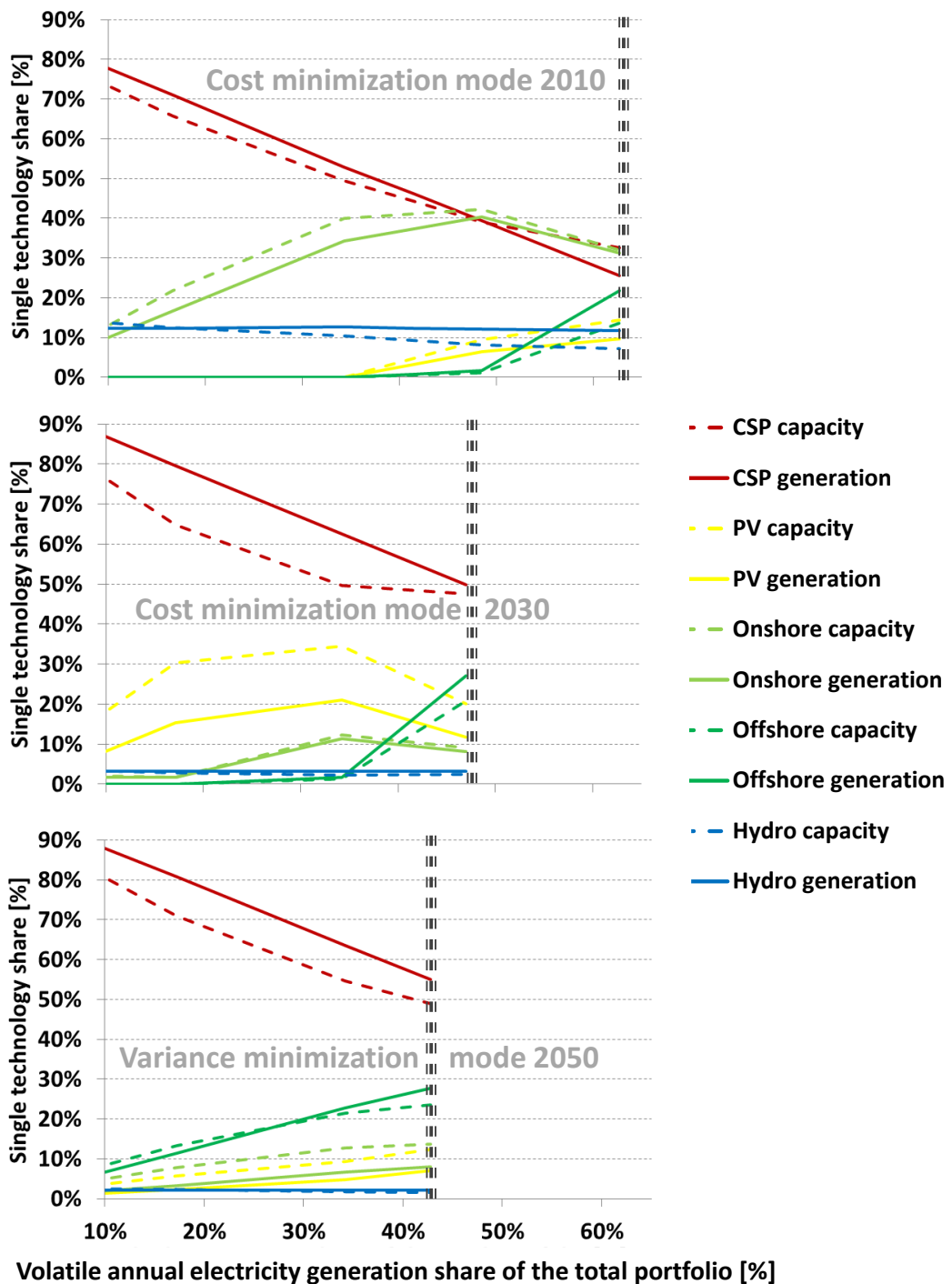


Figure 4.8.: Development of the shares of the installed capacities and generation as a function of the volatile annual electricity generation shares. Load, which is not met by the volatile generation (PV and wind) is satisfied by hydro and CSP. Due to this setup, CSP shares are very high for small volatile generation shares. The double-dashed vertical lines indicate the feasibility barriers: To the left, solutions are found that entirely obey the set of boundary conditions, to the right the surplus restriction cannot be met.

For the 2010 case, a descend of the CSP generation share from some 80% to approximately 25% can be observed for volatile annual electricity generation shares of 10% and 63%, respectively. The volatile annual electricity generation share of 10% in this case is entirely met by onshore wind plants, indicating that onshore wind is the cheapest option for harvesting these 10%. The remaining 10% are contributed by hydro power. Onshore wind remains the cheapest option for the volatile generation until a volatile annual electricity generation share of 34% is reached. This is the point where either the best sites for PV can generate electricity at less cost than the remaining onshore wind sites or the surplus of onshore wind would become too high. The latter would collide with the surplus restriction limiting the excess energy production to 2650 MW in the 2010 cases. Therefore PV enters into the portfolio. The same can be observed for offshore wind at this point. As both PV and offshore wind are now used besides onshore wind to satisfy the volatile annual electricity generation share, the linear ascend of onshore wind generation is discontinued and the slope is reduced accordingly. At a volatile annual electricity share of 48% offshore wind becomes increasingly important. The final single technology generation shares at the feasibility barrier are: 10% PV, 22% offshore wind, 32% onshore wind, 24% CSP and 12% hydro. As discussed earlier, for volatile annual electricity generation shares above the feasibility barrier, the occurring surplus generation can not be accommodated by the neighboring power grids. Therefore, no feasible solutions in terms of the established boundary conditions are obtained beyond this point.

In contrast to the 2010 cost minimization case, the 2030 cost minimization case sees a declining feasibility frontier. It is now found at some 47% in terms of the volatile generation share. As discussed in subsection 4.3.2.1 above, this is caused by a strong increase in peak load demand from some 5.6 GW in 2010 to some 21.5 GW in 2030, while transmission capacities merely rise to 3350 MW (see figure 4.4). Due to the cost evolution, all renewable technologies become cheaper. Combining the aspects annuity and resource availability, PV is now the most competitive volatile technology and therefore enters into the portfolio first. Onshore and offshore wind are used for higher volatile annual electricity generation shares for the same reasons as discussed above for PV (either the best sites can generate electricity at less cost than the remaining PV sites or the surplus of PV would become too high). The role of hydro is unchanged.

For the output variance minimization case in 2050, the third top performing optimization mode, the feasibility barrier drops again to some 43% of volatile power generation. Compared to the cost minimization modes, it can be observed that significant shares of all technologies are used from the very beginning, i.e. at a volatile annual electricity generation share of 10%. Also, the contributions of PV, on- and offshore wind increase linearly until the feasibility barrier is reached. This behavior is due to the fact that in the variance minimization mode, the greatest portfolio or smoothing effect of the volatile output is obtained by both spatial distribution of the installations and tapping different resources.

Performance of the CSP plants

The intermittent generation technologies PV and wind along with dispatchable hydro power are capable of reducing the overall hourly load thereby acting as fossil fuel savers in current energy systems. Figures 4.9 and 4.10 indicate exemplary winter and summer weeks resulting from the cost minimization mode for 2010, 2030 and 2050. It can be seen, how CSP meets the residual load, which is obtained after volatile generation by PV and wind plus dispatchable hydro power is deduced from the hourly load. Overall the following statements can be made: From 2010 to 2050, the relative contributions of onshore wind and hydro decrease, while those for offshore wind and PV increase. Moreover, demand increases drastically while the available net transfer capacities to the neighboring countries incline very moderately. The latter fact results in a decreasing transmission buffer in relative terms.

In the displayed cases, volatile generation merely consists of onshore wind in 2010, complemented by firm hydro power generation. As natural gas prices are comparatively cheap, the fossil share of the compensating CSP plants is higher than in the years 2030 and 2050. Vice versa the solar share increases over the same period. In the typical winter weeks, large parts of the CSP generation originate from co-firing, while in the summer months, the solar field can provide sufficient amounts of thermal energy to charge the thermal storage and to run the turbines almost completely, i.e. also during nighttime. Moreover during summer, periods are observed when the thermal storage is completely charged, which can be seen when the storage charge forms a constant plateau. When the storage levels decline, the CSP generation is at least partially if not completely run on stored energy. Furthermore in 2030 and 2050, when splitting up the CSP generation into an imaginary base load and a peak load band, the latter starts operation in the evening hours and during night, while most of the daytime load is covered by PV. This is due to the fact that during daytime, in the direct competition in terms of generation cost between CSP and PV, PV outperforms CSP. Therefore during daytime, the solar field can harvest energy, which is not directly converted into electricity, but which is used to charge the thermal storage.

4.3.3. Summary

Within the framework of the present chapter, a new feature is added to the REMix modeling environment: The plant siting module REMix-PlaSMo. It builds upon hourly power generation time series and installable capacities data provided by REMix-EnDaT. The overall goal of REMix-PlaSMo is the optimized siting of the volatile power plant portfolio's installation, consisting of PV, on- and offshore wind, against three objectives: minimization of the volatile portfolio's cost, of its output and residual load variance. The motivation for the approach and the methodology are discussed. A sound algebraic formulation is given. The tool is designed to be applicable for an arbitrary country, in this work the case is made for Morocco. The three optimization modes are employed separately for the years 2010, 2030 and 2050. The best performing optimization mode is identified in terms of the minimum overall net generation cost. For 2010 and 2030, the cost minimization and for 2050 the output variance minimization are obtained as top

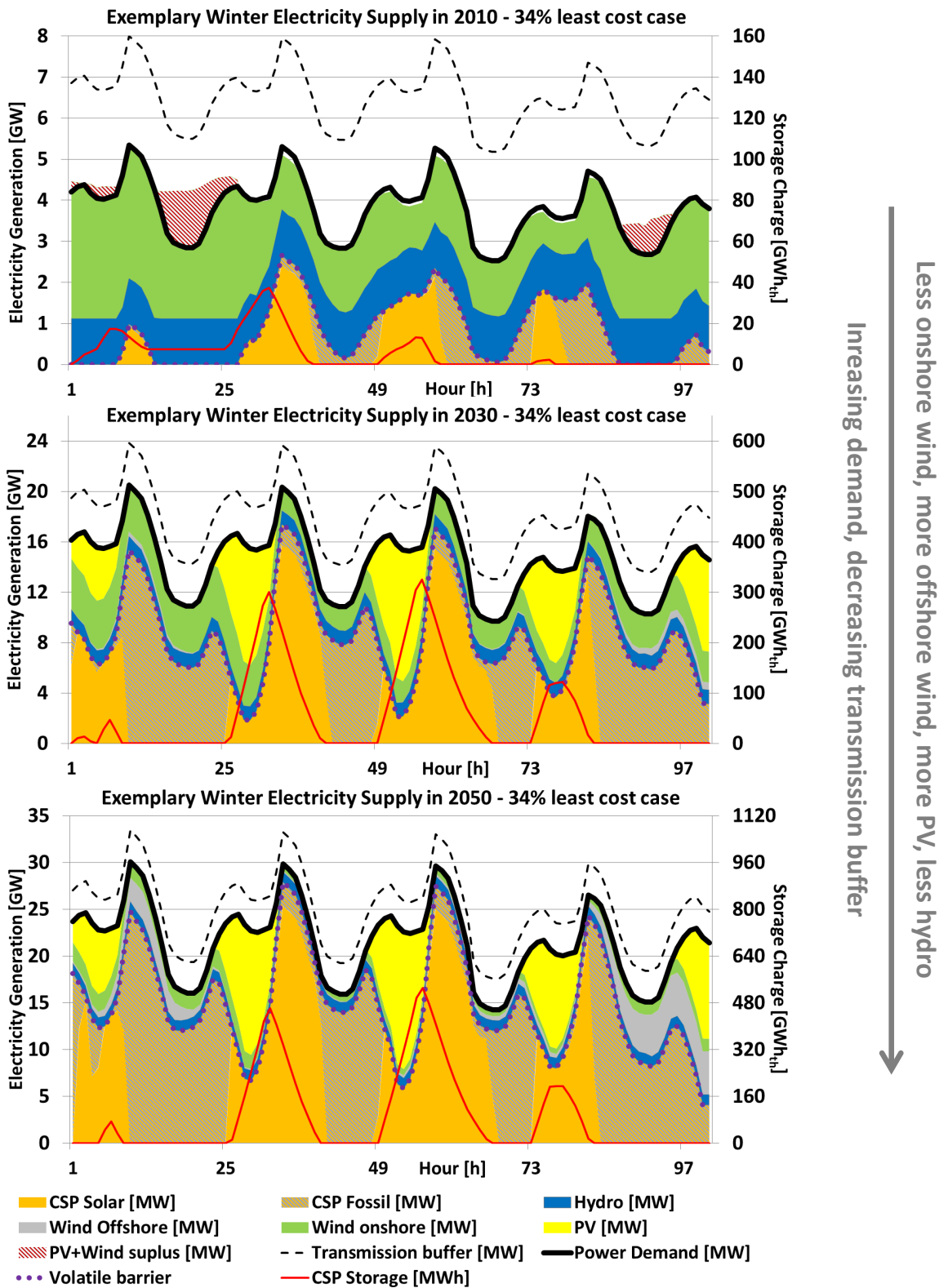


Figure 4.9.: Electricity supply for a winter week resulting from the optimizations depicted for the cost minimization case for the years 2010 (top), 2030 (center) and 2050 (bottom).

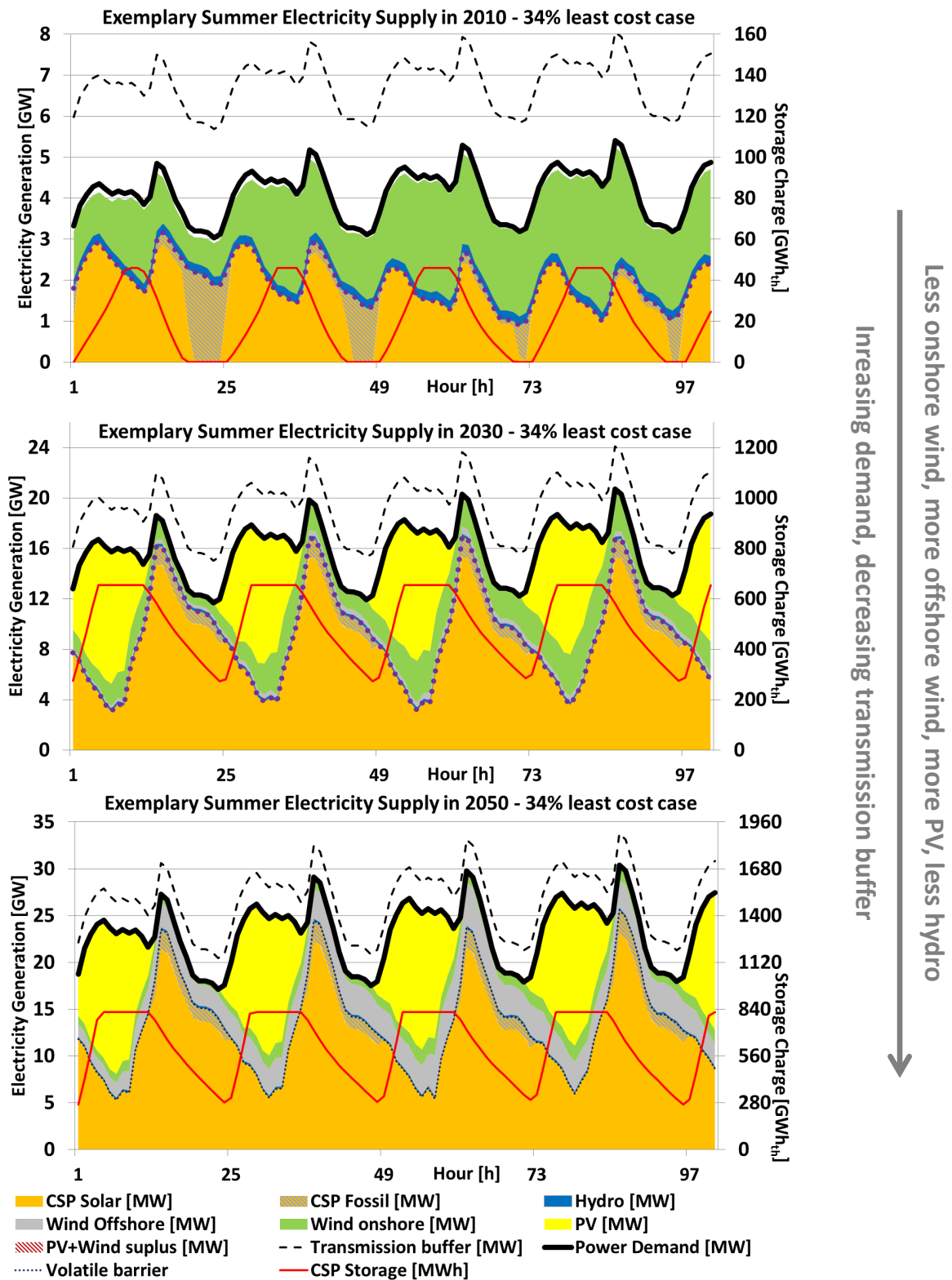


Figure 4.10.: Electricity supply for a summer week resulting from the optimizations depicted for the cost minimization case for the years 2010 (top), 2030 (center) and 2050 (bottom).

performing optimization modes. In 2050 the top performing results are very close: the cost minimization performed slightly less competitive than the output variance mode. The cheapest net generation cost for the top performing modes ranging between 10.1 and $10.5 \frac{\text{€ct}}{\text{kWh}}$ is obtained for a volatile share of the portfolio's overall generation of 34%. Compared to the cost and output variance minimization modes, an optimization of the residual load in terms of minimizing its variance and inducing a smoothed load band does not prove to be a favorable solution in terms of the overall portfolio's (i.e. PV, CSP and wind and hydro power) net generation cost. On the one hand, this residual load is to be covered using CSP with high solar multiples and full load hours, in turn inducing decreasing CSP generation cost. On the other hand in order to obtain smoothing effects on the residual load induced by the volatile generation portfolio, sites for PV and wind are chosen as to fulfill that goal rather than to minimize installation cost. These increased cost cannot be compensated by lower cost due to CSP plants with higher solar multiples.

The output variance minimization case should result in a residual load similar to a peak load band. This peak load is best met by photovoltaic rather than CSP. In 2050, it is nonetheless proven that the overall cost of the output variance minimization case is smaller compared to the cost minimization case. Keeping the very small differences of the results in mind, in summary, the very good overall performance of the least cost case is also a reasonable result in terms of a qualitative argumentation.

One major restriction implemented into the design of the case study is the limitation of surplus generation by the volatile portfolio. Besides storage, the power transmission grid can be used as a means of balancing power. In the case study carried out in this chapter, no electricity storage is considered, merely power transmission to Morocco's neighbors Algeria and Spain is implemented. In this investigation a power transmission capacity constraint is implemented, yielding the actual sum of the net transfer capacities to the neighboring countries. Due to the latter constraint, feasible solutions for the volatile portfolio shares amount to 67% in 2010 with a decreasing trend to 43% in 2050, predominantly caused by the fact that the peak load is assumed to increase a great deal from 5.6 GW in 2010 to some 31.3 GW in 2050 while transmission capacities are considered to only increase slightly from 2.65 to 3.35 GW. This constraint might attract criticism, however, any assumption on new transmission capacities had to face similar critique, which is why this conservative approach is chosen over a progressive scenario. There are certainly ways to further increase the volatile renewable shares if the following measures are taken, all of which capable of consuming surplus power: Active grid management is an option, in particular influencing the demand side using the full spectrum of available technologies and those, which are to be further developed: electricity storage using pumped hydro, compressed air, batteries and hydrogen/methane. Moreover targeted load shifting in the industrial sector, selective heating/cooling in the private sector and directed charging/discharging of electric cars might allow for using surplus power from volatile generation. For all of the latter options competitiveness is only given if the benefit of storage is not outperformed by the efficiency loss it suffers. Eventually, the possibility of an extension of power transmission capacities to other markets shall be mentioned as an option to increase grid stability which has already been implemented in the past.

5. REMix-OptiMo: Enhancements and application in a scenario validation study

Within the framework of the present chapter new features are added to the energy system optimization module REMix-OptiMo, the third fundamental tool of the REMix modeling environment. As indicated in figure 5.1, REMix-OptiMo uses data on installable capacities, hourly power generation and demand time series provided by REMix-EnDaT as input. Enhancements made to REMix-OptiMo, added for the purpose of a scenario validation, are discussed and presented in this chapter. Within this work,

- a new transmission model, discussed in section 5.2 and based on a DC¹-approximation of the AC² grid, is implemented improving the accuracy of inter-nodal power transmission.
- imports of firm capacity provided by CSP plants in the MENA³ region via high voltage direct current links (HVDC) are developed and included as summarized in subsection 5.3.2.2.

5.1. Overview on REMix-OptiMo

The original version of the optimization module REMix-OptiMo allows for optimizations of green-field energy systems, taking into account temporally and spatially resolved data on both electricity supply and demand, heat demand, transmission connections between energy regions aggregated within hubs using high voltage direct current power lines and storage as a means of load balancing. The basic version of this tool has been developed by Scholz [Sch12], who established the framework in order to compute least-cost energy supply portfolios for countries situated in the region Europe-Middle East-North Africa (EUMENA). Further work regarding the development of this model are the introduction of electric cars as a demand and supply option [Ten12], the implementation of demand side management issues and a complete overhaul of the overall structure of the operating interface, including input error query and scenario run administration. A side branch of the model deals with country specific solutions in order to investigate market introduction and renewable energy capacity expansion strategies [Fic12].

¹DC: direct current

²AC: alternating current

³MENA: Middle East and North Africa

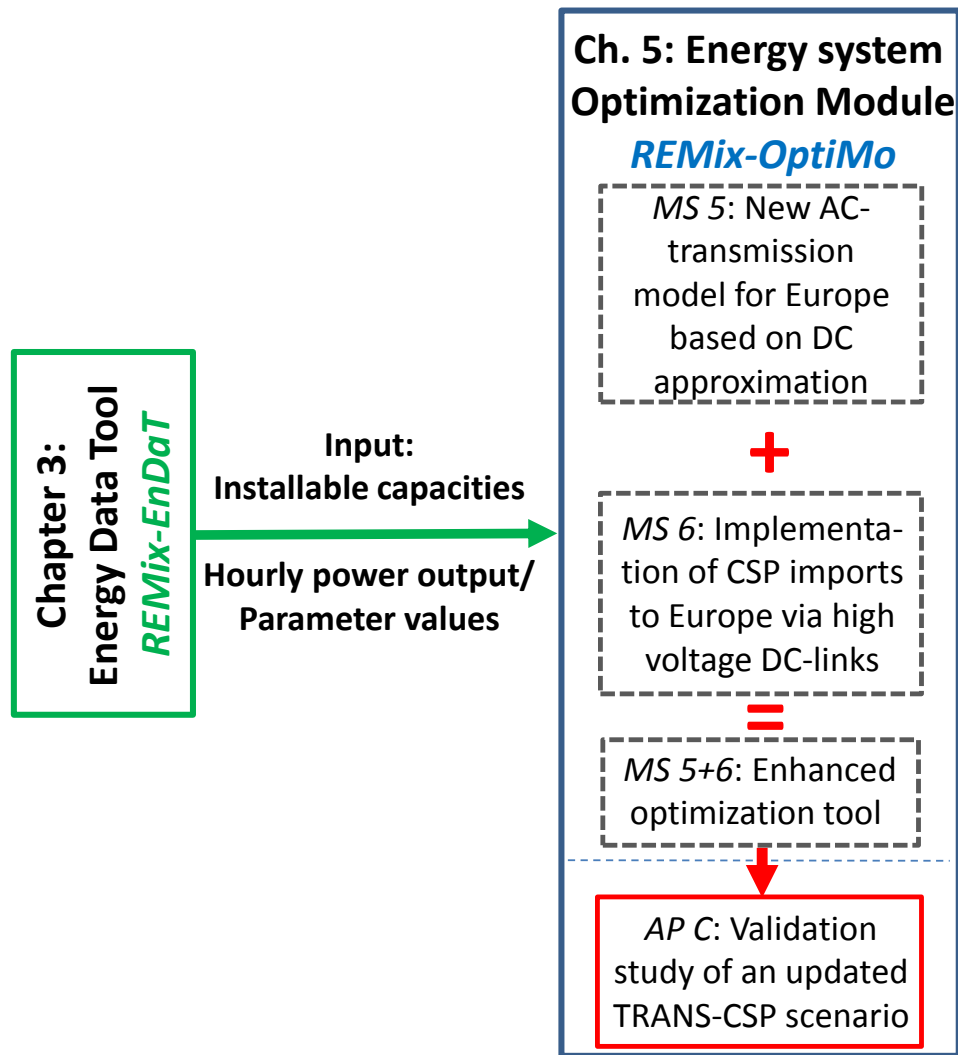


Figure 5.1.: Structure of the present chapter. The enhanced version of REMix-OptiMo resulting from the methodology section is used for a validation of an energy scenario.

OptiMo is implemented in the programming language GAMS [GAM12], which is capable of providing a sound environment for the modelization of optimization problems taking into account numerous boundary conditions. Within OptiMo, the variable of concern to be minimized is the overall cost of the entire energy system. Input to the model are data on electricity and heat demand and renewable power generation. The latter is provided on an hourly basis by a pre-assessment employing REMix-EnDaT (please see chapter 3), also capable of assessing the country specific installable capacities for each technology considered. Further input includes a vast database on technical and economic parameters both for renewable and conventional power generation. Electric cars as a demand and storage option which can consume and provide power when needed are also implemented. Moreover the technologies pumped storage, compressed air or hydrogen serve as an option for electricity storage. In the original model, power transmission is

enabled through high voltage direct current links between countries, each country being represented by one node.

The optimization itself is country based, i.e. all input data is cumulated on country level. For instance, time series data on renewable generation are aggregated for the entire node, inherently yielding a somewhat smoothed power curve, representing the integral of each technologies' hourly power generation over all sites a node is comprised of. Demand data is also available on a nodal basis. Transmission line lengths are determined according to the distances between the nodes' geographic centers of gravity. The most important restrictions are that demand be met for all time steps, and installed capacities of the renewable technologies, which can be flexibly chosen, must not exceed the installable capacities as derived by the pre-assessment in REMix-EnDaT. Eventually the solving algorithm is seeking a solution representing the least cost portfolio covering the energy demand of the entire region under consideration for one year.

5.2. Enhancing REMix-OptiMo: A new power transmission model

Within this work a new formulation to represent the power transmission between the nodes - generally representing entire countries - is implemented into the model. It is based on the DC-approximation of a full AC power flow, merely considering active power flows while neglecting voltage support and reactive power management. A thorough application of the latter is used by Heide [Hei10], his general approach is also used in this work. Stott et al. [SJA09] give a good discussion on both advantages and disadvantages of the DC-approach. In summary the most appealing characteristics are time-saving computation due to relatively simple approximations and assumptions, including non-iterative, unique solutions, and - even more important at this stage - its linearity.

Since neither active grid operation or management are represented nor data on power transmission distribution factors or the susceptance, conductance and shunt conductance are available for a thorough, in-depth electric simulation of the entire European transmission grids, the choice for a DC-approximation appears justified. In the following an overview of the physical relations eventually yielding the desired expression for the net hourly power flow $E_{i,j}^{flow}(h)$ on the line between two nodes i and j is given.

Any AC system containing resistances, capacitances and inductances can be described under the assumption of both sinusoidal voltages $U(t)$ and currents $I(t)$ with constant frequencies ω and the phases ϕ_U and ϕ_I by the complex valued expression for the latter as follows:

$$U(t) = U \cdot e^{j(\omega t + \Phi_U)} \quad (5.1)$$

$$I(t) = I \cdot e^{j(\omega t + \Phi_I)} \quad (5.2)$$

Expressing Ohm's Law with the complex admittance Y ⁴ yields:

$$I(t) = Y \cdot U(t) \quad (5.3)$$

where Y is a function of the conductance G and the susceptance B :

$$Y = G + jB \quad (5.4)$$

Using the complex relations (5.1) and (5.2) for the voltage and current and defining φ as the phase difference between the current's and the voltage's phases $\varphi = \Phi_U - \Phi_I$, the complex power \underline{S} is found as:

$$\underline{S} = U(t) \cdot I(t) \quad (5.5)$$

$$= U \cdot I \cdot e^{i\varphi} \quad (5.6)$$

Applying the trigonometric identity $e^{i\varphi} = \cos(\varphi) + i \sin(\varphi)$, finally an expression for the complex power \underline{S} using active power P and the reactive power Q is obtained [AWA06]:

$$\underline{S} = UI \cos(\varphi) + jUI \sin(\varphi) \quad (5.7)$$

$$= P + jQ \quad (5.8)$$

Transferring the above statement for \underline{S} to be eligible of representing the complex power at a node i of a power grid requires the introduction of the admittance matrix Y , indices for the nodes i and the links $i \rightarrow j$. In this notation, the entry of the admittance for the link $i \rightarrow j$ is given by $Y_{ik} = G_{ik} + jB_{ik}$. Thus, in steady state the complex power at each node i , S_i , is expressed as

$$S_i = P_i + jQ_i \quad (5.9)$$

$$= U_i \left(\sum_k Y_{ik} \cdot U_k \right)^* \quad (5.10)$$

Decomposing the above statement into real and imaginary parts yields a set of coupled equations for the average power P_{ik} and the reactive power Q_{ik} for a link $i \rightarrow j$ [Dut07]:

$$P_{ik} = U_i^2 G_{ik} - U_i U_k G_{ik} \cos(\Phi_{U_{ik}}) - U_i U_k B_{ik} \sin(\Phi_{U_{ik}}) \quad (5.11)$$

$$Q_{ik} = -U_i (B_{ik} + B_{ik}^{shunt}) + U_i U_k B_{ik} \cos(\Phi_{U_{ik}}) - U_i U_k G_{ik} \sin(\Phi_{U_{ik}}) \quad (5.12)$$

The non-linear relations presented above can be solved using an iterative process such as Newton's method [OO11], P and Q at an arbitrary point of a grid can be determined as long as all parameters for the voltage U , the susceptance G , the conductance B , the shunt conductance B^{shunt} and the differences of the voltage angles $\Phi_{U_{ik}}$ are known. Since that is not always the case, particularly for the present energy system model, the following approximations - which for the greater part result from empirical experience - are carried out [OO11; Dut07]:

⁴In AC circuits, for resistances R , capacities C and inductances L , Y equals: $Y = R^{-1}$, $Y = j\omega C$ and $Y = (j\omega L)^{-1}$.

1. The differences of the voltage angles $\Phi_{U_{ik}}$ are small and the impedances are dominated by the reactances, since the resistances are assumed to be small:
Hence

$$\cos(\Phi_{U_{ik}}) = 0 \quad (5.13)$$

$$\sin(\Phi_{U_{ik}} - \alpha_{U_{ik}}) = 0. \quad (5.14)$$

Also, for small voltage angle differences, the following general relation holds:

$$\sin(\Phi_{U_{ik}}) = \Phi_{U_{ik}} \quad (5.15)$$

2. Uniform voltages in the system are assumed, U_i and U_k therefore reduce to $U_i = 1$ and $U_k = 1$ [Sch09b]
3. The inductive part of the line dominates the admittances

The power between nodes i and j is then given by [WW96]:

$$P_{ik} = B_{ik} \cdot \Phi_{U_{ik}} \quad (5.16)$$

In vector notation this transfers to:

$$\vec{P} = B \cdot \vec{\Phi}_U \quad (5.17)$$

In other words: The susceptance along with the voltage's phase differences fully describe the system. This is known as the DC-approximation or the DC power flow of an AC grid.

Using Kirchhoff's current and potential laws for an arbitrary DC-grid, an expression similar to 5.17 is obtained as follows:

$$\vec{I} = Y \cdot \vec{U} \quad (5.18)$$

in complete accordance to Ohm's Law as introduced in relation (5.3), however this time without time dependencies. Again, Y is the admittance matrix, for the DC case it reduces to $Y = R^{-1}$. Eventually, for a link $i \rightarrow j$ the current I_{ij} is determined by:

$$I_{ij} = Y_{ij}(U_j - U_i) \quad (5.19)$$

$$= R_{ij}^{-1}(U_j - U_i) \quad (5.20)$$

In terms of their physical statements, equations (5.16) and (5.19) are identical, as can be seen by comparing the properties and structure of the matrices Y and B [Hei10]. In order to come up with a suitable expression for a linear optimization model, the following approach is presented in accordance with discussions by Heide [Hei10] and Bollobas [Bol98], who introduce a matrix K , representing the direction of a link between two nodes i and j , as follows:

$$K_{ij} = \begin{cases} 1 & \text{if the link initiates at node } i \text{ and terminates at node } j \\ -1 & \text{if the link initiates at node } j \text{ and terminates at node } i \\ 0 & \text{if none of the above applies} \end{cases} \quad (5.21)$$

The product of its transposition, i.e. K^T , and the potential \vec{U} , indicates the potential differences for all links, the latter always obey Ohm's law. Therefore the flow f_{ij} across a link $i \rightarrow j$ can be expressed as

$$f_{ij} = Y_{ij} \cdot (U_j - U_i) \quad (5.22)$$

Using matrix notation and bearing in mind that in this case $Y = R^{-1}$ yields:

$$\vec{f} = R^{-1} \cdot K^T \cdot \vec{U} \quad (5.23)$$

with the respective resistances of each link $R_{ij} \forall i = j$. Let now s_i represent the net flow at a node i . For all nodes this can be expressed in vector notation also employing relation (5.23) as follows:

$$\vec{s} = K^T \cdot \vec{f} \quad (5.24)$$

$$= K \cdot R^{-1} \cdot K^T \cdot \vec{U} \quad (5.25)$$

$$= Y \cdot \vec{U} \quad (5.26)$$

The last transformation uses the matrix Y , directly mapping from the potentials to the net flows space of each node. It has certain characteristics, whose specifics and solution strategies are beyond the scope of this work⁵. In order to solve equation (5.26), the Moore-Penrouse pseudoinverse Y^+ [SBP⁺08; Lux07] is used. Finally this gives:

$$\vec{U} = Y^+ \cdot \vec{s} \quad (5.27)$$

Combining equations (5.23) and (5.27), the final relation for the flow is obtained:

$$\vec{f} = B \cdot K \cdot Y^+ \cdot \vec{s} \quad (5.28)$$

This relation is solved for all links, giving an idea of the extent of balancing needs in the system. The resulting hourly flows must not exceed each link's respective net transfer capacities, which may differ in terms of the flow direction. In annex A.5, the values for the limiting net transfer capacities are presented in figures A.14 and A.15 for summer and winter months respectively. In this work, the average of both values is used for the net transfer capacity in zeroth approximation. Figure 5.2 gives an overview of all links included in the model along with the the net transfer capacities resulting from this approach.

In summary this approach allows for the implementation of an approximated AC power flow using the DC approximation. It can be considered valid, as long as in steady state the network has no significant voltage shifts between nodes and under the assumption of negligible resistances between the nodes [WW96; Hei10; VHVP⁺06].

⁵Heide [Hei10] gives a short review on the most important aspects of the latter.

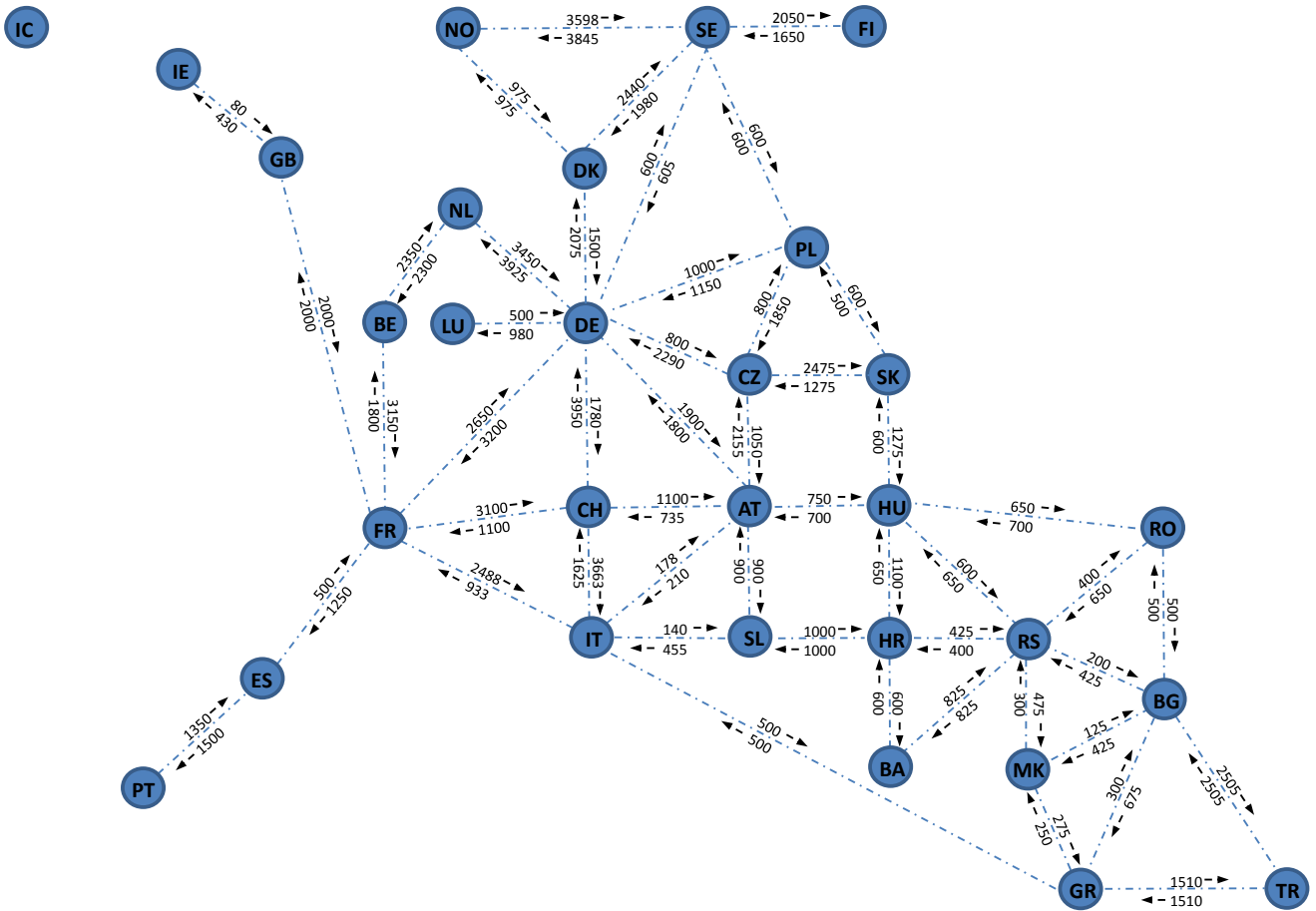


Figure 5.2.: Mean net transfer capacities according to ENTSO-e [Str12]. Displayed values indicate the average of the figures from summer 2010 and winter 2010/2011. All links are included in the model, the line lengths are approximated as the distances of the geographical centers.

5.3. Application of REMix-OptiMo: Validation of an updated TRANS-CSP scenario

As part of a case analysis employing the tools EnDaT and OptiMo discussed in chapters 3 and 5, an updated scenario pathway of the original TRANS-CSP study [TSK+06] considering novel power demand and updated figures on supply is validated against temporally resolved optimizations using REMix-OptiMo. The validated pathway is one out of three based on this updated scenario framework. For the validation process, the installed power plant capacities as provided by pathway #1 (indicated as TRANS-CSP update in figure 5.3) are used. Electricity imports from CSP plants located in North African countries are allowed, a total renewable coverage approaching 80% in 2050 is considered. For the assessment, three timesteps are considered: 2010, 2030 and 2050. They evidently differ in their figures for the installed capacities of the distinct technologies, economic and technical parameters and the possibility to allow for imports of electricity provided by CSP plants in the MENA⁶ region, introduced in 2020.

Since the backbone of the scenario update used here is the original release of the TRANS-CSP study, an overview on the fundamental approach and underlying assumptions according to [TSK+05; TSK+06; TMS07] are presented in section A.3. Building upon and extending the foundation of the original TRANS-CSP release, the approach and results of the update of the original scenario framework along with three new scenario pathways are presented and discussed in subsection 5.3.1. In subsection 5.3.2, the configuration of REMix-OptiMo for the validation run using pathway #1 out of the above mentioned scenario pathways is presented. Besides the description of the input data, an elaborate discussion on the implementation of electricity imports from North Africa and the Middle East to Europe is given in subsection 5.3.2.2.

Building upon the obtained framework, REMix-OptiMo is then used for the scenario validation. Results of the latter are summarized in subsection 5.3.3.

5.3.1. Approach and major outcomes of the new TRANS-CSP scenarios

As some of the data basis used for the original publication of the TRANS-CSP study in 2006 has changed, particularly figures on the installed renewable capacities but also values for the development of the demand, three new scenarios anticipating different overall boundary conditions but altogether based on the updated demand and supply framework are prepared by [Tri12]. Pathway #1 (TRANS-CSP update) uses the same goals as the original scenario, i.e. first and foremost a total share of 80% of electricity supply being covered with renewable generation, however, this time with recent figures on the power plant portfolios and updated demand until 2010. Also, high biomass shares and a nuclear phase out are considered. For pathway #2 (Island Europe) no nuclear phase out and merely “domestic” European renewable generation is considered, no electricity imports from MENA are taken into account. Pathway #3 (Maximum Renewable Energy Share) aims at a full supply with renewable generation by 2050 approaching 100%.

⁶MENA: Middle East and North Africa

All three pathways yield the complete set of constraints and boundaries of the original TRANS-CSP release discussed in section A.3, however figures for the electricity supply are implemented as follows: Figures for the years 2000 and 2010 are updated according to existing statistical data [BP12; IEA12; CIA10]. Short term estimates from 2010 to 2020 are taken from the National Renewable Energy Action Plans⁷ taken as reference by the countries assessed in the scenarios [BHV11]. Thereafter, the generation portfolio is evolved according to the scenario constraint's, as discussed in section A.3. As far as electricity demand is concerned, a continuous growth in demand exceeding 6000 TWh per annum by 2050 is forecast [ABBK⁺11], in sharp contrast to the original release's 4000 TWh in 2050 with a distinct saturation or even inflection point from around 2040 onwards. This significant increase is primarily due to an inclusion of electrical heating and mobility as "new" consumers. The latter are not taken into account within the approach for an estimated evolution of the original release's demand building upon an empirical top-down methodology by Trieb and Klann [TK06].

Pathway #3 (Maximum Renewable Energy Share) is the most demanding and challenging scenario in terms of anticipating an electricity system almost completely based on renewable resources. The major challenge during its creation is to successfully substitute the 20% of generation to boost the original 80% TRANS-CSP release to an updated 100% scenario. Also, a demand increase of some 50% is to be met. In pathway #1 and # 3 nuclear power phases out completely. Where feasible, domestic renewable generation is increased. In order to still provide sufficient amounts of firm capacities, both CSP imports from MENA rise from some 15% up to 25% and a significant amount of gas power plants is maintained even in the long run, i.e. until 2050. A comparison of the results of the different scenario assumptions for the installed capacities, electricity generation and related CO₂ emissions are presented in figure 5.3.

One major area of criticism against the original release of TRANS-CSP is the use of regressions based upon sets with limited amounts of data to come up with predictions of the real world, and in this respect particularly the evolution of electricity demand excluding power demand for eventual new consumers like the mobility and heat sectors [PJ]. Using demand data based on an external analysis provided by Amann et al. [ABBK⁺11] and backing up the overall scenario approach with an hourly power plant dispatch and thus electricity generation simulation based on the installed portfolio capacities as provided by pathway #1 (TRANS-CSP update), the fundamental feasibility of the suggested approach is to be assessed: Results of this investigation are presented in section 5.3.3.

⁷commonly abbreviated by the term NREAP

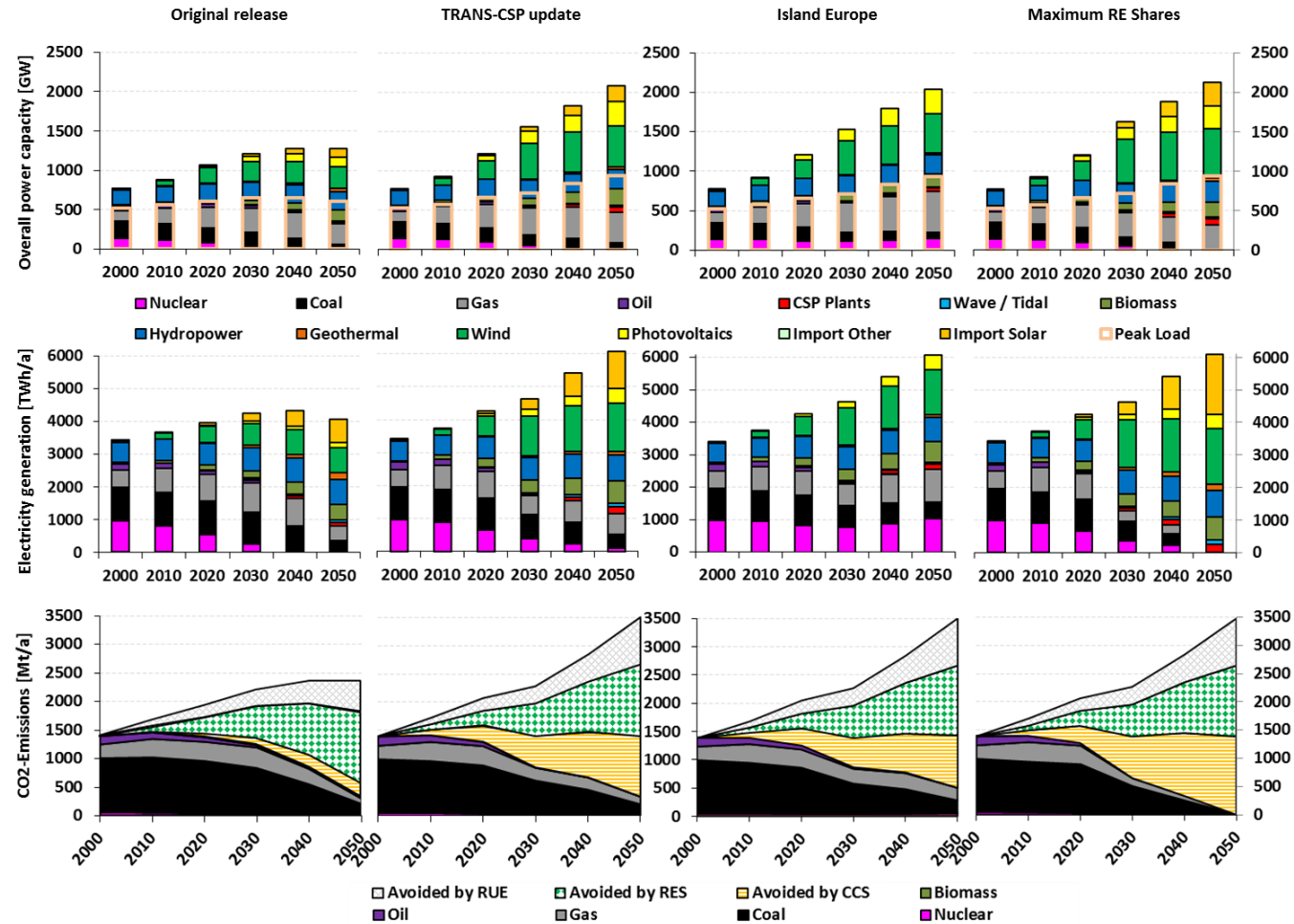


Figure 5.3.: Graphs indicating the overall installed capacities (top), electricity generation (center) and CO₂ emissions (bottom) for the total of 30 European countries assessed within the original release of TRANS-CSP [TSK+06] (left) and three new scenarios altogether based on updated figures for electricity consumption and supply: TRANS-CSP update (center-left), Island Europe (center-right) and Maximum Renewable Energy Share (right). For the three updated scenarios the overall demand increases from some 4000 TWh/a in 2050 (as used in the original release) to some 6000 TWh/a (as used in the new scenarios presented here) primarily caused by the inclusion of electromobility and electrical heating as loads.

5.3.2. Configuration of REMix-OptiMo for the validation simulations

5.3.2.1. Installed capacities, power generation, load and transmission

The entire simulation builds upon the energy model as described and amended in the present chapter. Both power generation and load data are aggregated on country levels, suggesting a power grid which is perfectly accessible and permeable within each country. Hourly input time series data for the technologies PV, CSP, on- and offshore wind and hydro power is provided by the REMix module EnDaT presented in chapter 3 using resources data of the year 2002 and bottom-up power plant models⁸. Since the power plant output of hydro power is conducted on a monthly basis, a polynomial fit is performed to obtain an hourly interpolation, yielding the boundary condition that the time integral over the raw (monthly) output and the interpolated output be identical. Full load hour data as provided by the pathway #1 results are included for biomass and geothermal power plants.

Load data is retrieved from ENTSO-e [Str12] for the year 2010. Power transmission between countries is included according to the discussion in section 5.2. It is based on a DC approximation of the existing AC power grid. Figures on existing links between the European countries which are part of ENTSO-e along with data on the net transfer capacities, which are used as the upper limits of feasible hourly power transmission, are used as provided by ENTSO-e [Str12].

For conventional power generation combined cycle gas turbines (CCGT), coal and nuclear power plants are implemented.

Tables 5.1 through 5.3 give an overview on the installed capacities used within the validation runs according to the updated scenario pathway #1.

Solar electricity imports via high voltage direct current links from 10 sites located in the MENA region using CSP plants for power generation are included in the model according to the following discussions in subsection 5.3.2.2.

⁸For hydro power, a top-down approach is carried out, please refer to sections 3.2.1.4 and 3.2.3 for further insight

2010 [GW]	Wind	PV	Geothermal	Biomass	CSP domestic	Wave	Hydro	Oil	Gas	Coal	Nuclear	CSP Import
Austria	1.0	0.1	0.0	1.0	0.0	0.0	10.7	0.3	6.3	1.5	0.0	0.0
Belgium	0.9	0.4	0.0	0.7	0.0	0.0	0.1	0.6	5.3	1.6	5.7	0.0
Bosnia-Herzegovnia	0.0	0.0	0.0	0.2	0.0	0.0	1.9	0.0	0.0	1.3	0.0	0.0
Bulgaria	0.4	0.0	0.0	0.0	0.0	0.0	1.9	0.2	0.5	4.7	2.8	0.0
Croatia	0.1	0.0	0.0	0.2	0.0	0.0	2.2	0.7	1.7	0.2	0.0	0.0
Czech Republic	0.2	0.7	0.0	0.4	0.0	0.0	1.9	0.6	2.1	5.7	5.0	0.0
Denmark	3.8	0.0	0.0	0.8	0.0	0.0	0.0	0.0	4.2	4.9	0.0	0.0
Finland	0.2	0.0	0.0	1.8	0.0	0.0	2.9	0.9	4.8	4.3	2.7	0.0
France	5.7	0.5	0.0	1.2	0.0	0.1	24.3	9.4	15.5	10.0	60.0	0.0
Germany	27.2	10.1	0.0	7.3	0.0	0.1	4.9	3.8	27.8	51.0	17.8	0.0
Greece	1.2	0.2	0.0	0.1	0.0	0.0	3.7	1.8	3.5	4.6	0.0	0.0
Hungary	0.3	0.0	0.0	0.4	0.0	0.0	0.1	0.5	4.2	2.1	1.5	0.0
Iceland	0.0	0.0	0.5	0.0	0.0	0.0	1.1	0.0	0.5	0.0	0.0	0.0
Ireland	1.4	0.0	0.0	0.1	0.0	0.0	0.3	0.3	2.9	1.8	0.0	0.0
Italy	5.8	1.5	0.7	2.5	0.0	0.0	20.4	13.1	34.1	6.3	0.0	0.0
Luxembourg	0.0	0.0	0.0	0.0	0.0	0.0	1.1	0.0	0.0	0.0	0.0	0.0
Macedonia	0.0	0.0	0.0	0.0	0.0	0.0	0.6	0.2	0.0	0.8	0.0	0.0
Netherlands	2.2	0.1	0.0	1.3	0.0	0.0	0.1	0.0	16.6	4.1	0.3	0.0
Norway	0.4	0.0	0.0	0.5	0.0	0.1	33.2	0.0	5.2	0.0	0.0	0.0
Poland	1.1	0.0	0.0	1.3	0.0	0.0	1.2	0.5	3.1	28.9	0.0	0.0
Portugal	3.9	0.2	0.0	0.7	0.0	0.0	3.8	2.1	3.3	1.8	0.0	0.0
Romania	0.5	0.0	0.0	0.0	0.0	0.0	6.5	0.0	5.7	6.9	1.3	0.0
Serbia & Montenegro	0.0	0.1	0.0	0.3	0.0	0.0	3.6	0.0	2.4	4.0	0.0	0.0
Slovakia	0.0	0.0	0.0	0.1	0.0	0.0	2.4	0.1	2.2	1.1	2.4	0.0
Slovenia	0.0	0.0	0.0	0.1	0.0	0.0	1.0	0.0	0.2	1.3	0.8	0.0
Spain	20.7	4.4	0.0	1.0	0.3	0.1	20.3	7.6	21.9	8.7	6.1	0.0
Sweden	2.2	0.0	0.0	2.3	0.0	0.0	14.1	0.0	7.3	0.4	10.0	0.0
Switzerland	0.0	0.1	0.0	0.5	0.0	0.0	13.2	0.0	1.9	0.0	3.0	0.0
Turkey	1.3	0.7	0.1	0.9	0.1	0.0	17.1	1.7	10.9	7.7	0.0	0.0
United Kingdom	5.2	0.0	0.0	2.7	0.0	0.5	2.7	2.7	22.2	37.3	8.8	0.0

Table 5.1.: Installed capacities according to the updated TRANS-CSP framework for pathway #1, which are used in the 2010 validation run.

2030 [GW]	Wind	PV	Geothermal	Biomass	CSP domestic	Wave	Hydro	Oil	Gas	Coal	Nuclear	CSP Import
Austria	5.4	2.9	0.1	2.4	0.0	0.0	12.2	0.0	8.4	0.0	0.0	0.0
Belgium	8.4	5.1	0.0	3.1	0.0	0.0	0.1	0.0	8.5	1.9	2.5	1.5
Bosnia-Herzegovnia	0.0	0.4	0.0	0.7	0.0	0.0	2.6	0.0	0.0	0.7	0.0	0.0
Bulgaria	5.6	1.4	0.0	0.5	0.0	0.0	2.3	0.0	3.6	2.6	1.0	0.5
Croatia	0.8	0.8	0.0	0.8	0.0	0.0	2.4	0.0	1.5	0.2	0.0	0.0
Czech Republic	9.0	3.1	0.0	2.3	0.0	0.0	2.4	0.0	5.3	4.0	3.0	1.5
Denmark	5.0	1.1	0.0	2.0	0.0	0.1	0.0	0.0	6.1	2.0	0.0	0.0
Finland	4.2	2.9	0.0	6.0	0.0	0.1	3.2	0.0	5.8	1.6	1.0	0.0
France	57.1	15.1	0.7	8.9	0.3	0.8	25.3	0.0	48.7	9.0	30.0	12.0
Germany	77.1	26.7	0.7	16.4	0.0	0.5	6.5	0.0	47.4	30.2	0.0	11.0
Greece	9.3	2.3	0.2	0.7	0.4	0.2	5.2	0.0	5.8	2.6	0.0	1.5
Hungary	5.9	1.9	0.3	1.2	0.0	0.0	0.1	0.0	3.8	1.5	0.5	2.0
Iceland	0.0	0.0	0.4	0.0	0.0	0.0	1.1	0.0	0.6	0.0	0.0	0.0
Ireland	4.2	1.6	0.0	0.8	0.0	0.2	0.3	0.0	3.7	1.6	0.0	0.0
Italy	41.4	19.4	1.5	8.1	0.9	0.2	21.7	0.0	44.7	4.0	0.0	11.0
Luxembourg	0.4	0.4	0.0	0.1	0.0	0.0	1.2	0.0	0.0	0.0	0.0	0.0
Macedonia	0.0	0.2	0.0	0.2	0.0	0.0	1.0	0.0	0.0	0.8	0.0	0.0
Netherlands	16.8	6.0	0.0	4.6	0.0	0.0	0.1	0.0	15.4	1.4	0.1	0.0
Norway	2.6	0.2	0.0	1.1	0.0	0.5	39.0	0.0	4.8	0.0	0.0	0.0
Poland	19.4	7.8	0.0	5.4	0.0	0.0	2.3	0.1	9.0	21.0	0.0	2.0
Portugal	5.0	1.7	0.1	1.7	1.1	0.3	5.5	0.0	4.5	1.7	0.0	0.0
Romania	4.0	2.4	0.0	2.6	0.0	0.0	7.0	0.0	9.8	1.6	1.0	2.0
Serbia & Montenegro	0.1	1.1	0.1	1.6	0.0	0.1	4.4	0.0	3.8	3.3	0.0	0.0
Slovakia	4.1	1.1	0.1	0.7	0.0	0.0	2.7	0.0	4.4	1.2	1.0	0.0
Slovenia	1.6	0.6	0.0	0.4	0.0	0.0	1.3	0.0	0.1	1.6	0.3	0.0
Spain	52.1	11.5	0.5	3.9	8.6	0.6	23.5	0.0	35.6	7.9	2.0	5.0
Sweden	12.8	3.3	0.0	6.7	0.0	0.1	14.0	0.0	6.1	0.0	4.7	0.0
Switzerland	6.0	2.5	0.0	1.1	0.0	0.0	13.2	0.0	5.9	0.0	2.0	0.0
Turkey	43.2	11.4	3.7	5.2	5.7	0.0	29.0	0.0	28.1	7.3	0.0	3.0
United Kingdom	50.0	15.9	0.0	6.4	0.0	4.8	4.2	0.0	29.1	22.0	2.5	6.0

Table 5.2.: Installed capacities according to the updated TRANS-CSP framework for pathway #1, which are used in the 2030 validation run.

2050 [GW]	Wind	PV	Geothermal	Biomass	CSP domestic	Wave	Hydro	Oil	Gas	Coal	Nuclear	CSP Import
Austria	6.3	5.9	0.2	9.2	0.0	0.0	12.6	0.0	9.4	0.0	0.0	0.0
Belgium	9.5	10.2	0.0	4.7	0.0	0.0	0.1	0.0	11.6	1.9	0.0	12.0
Bosnia-Herzegovnia	0.1	0.8	0.0	0.8	0.0	0.0	3.2	0.0	0.0	0.0	0.0	0.0
Bulgaria	6.5	2.8	0.0	2.6	0.0	0.0	2.6	0.0	5.0	2.0	0.0	3.0
Croatia	0.9	1.6	0.0	1.4	0.0	0.0	2.7	0.0	1.0	0.0	0.0	0.0
Czech Republic	10.5	6.3	0.0	4.4	0.0	0.0	2.6	0.0	3.7	3.8	0.0	6.0
Denmark	5.4	2.3	0.0	2.1	0.0	0.3	0.0	0.0	7.3	2.0	0.0	0.0
Finland	4.7	5.8	0.0	16.1	0.0	0.3	3.4	0.0	4.0	0.0	0.0	0.0
France	64.0	30.6	2.5	26.4	0.7	2.3	25.4	0.0	66.1	7.5	0.0	40.0
Germany	82.2	54.1	2.5	29.0	0.0	1.3	6.9	0.0	56.5	15.0	0.0	35.0
Greece	10.8	4.8	0.8	2.1	1.1	0.6	6.6	0.0	5.3	1.3	0.0	4.0
Hungary	6.8	3.8	1.3	3.2	0.0	0.0	0.2	0.0	4.5	1.0	0.0	4.0
Iceland	0.0	0.0	0.0	0.0	0.0	0.0	1.1	0.0	0.7	0.0	0.0	0.0
Ireland	4.8	3.2	0.0	2.5	0.0	0.6	0.3	0.0	3.5	0.7	0.0	3.5
Italy	65.3	39.4	3.6	15.4	1.7	0.6	22.6	0.0	57.9	2.3	0.0	25.0
Luxembourg	0.4	0.9	0.0	0.1	0.0	0.0	1.2	0.0	0.0	0.0	0.0	0.0
Macedonia	0.0	0.5	0.0	0.6	0.0	0.0	1.3	0.0	0.0	0.8	0.0	0.0
Netherlands	18.4	12.1	0.0	6.7	0.0	0.1	0.1	0.0	15.1	1.4	0.0	12.0
Norway	2.9	0.4	0.0	1.0	0.0	1.4	34.6	0.0	7.4	0.0	0.0	0.0
Poland	22.1	15.8	0.0	14.9	0.0	0.1	2.4	0.0	11.8	10.3	0.0	12.0
Portugal	5.6	3.5	0.5	3.9	4.3	1.0	6.1	0.0	2.3	0.7	0.0	0.0
Romania	4.6	4.8	0.0	8.2	0.0	0.0	7.8	0.0	10.4	1.3	0.0	4.0
Serbia & Montenegro	0.2	2.3	0.2	4.0	0.0	0.3	5.2	0.0	2.1	0.6	0.0	0.0
Slovakia	4.8	2.3	0.3	2.1	0.0	0.0	2.9	0.0	3.6	1.3	0.0	1.5
Slovenia	1.8	1.2	0.0	2.5	0.0	0.0	1.6	0.0	0.2	1.0	0.0	0.0
Spain	58.2	23.4	1.9	11.5	34.3	1.8	24.0	0.0	34.0	4.2	0.0	8.0
Sweden	14.4	6.6	0.0	16.1	0.0	0.3	14.0	0.0	3.4	0.0	0.0	0.0
Switzerland	6.9	5.0	0.0	1.8	0.0	0.0	13.2	0.0	7.8	0.0	0.0	0.0
Turkey	49.9	23.0	13.2	12.8	18.6	0.0	40.9	0.0	23.1	2.5	0.0	8.0
United Kingdom	55.8	32.3	0.0	7.0	0.0	13.2	4.3	0.0	47.3	7.5	0.0	22.0

Table 5.3.: Installed capacities according to the updated TRANS-CSP framework for pathway #1, which are used in the 2050 validation run.

5.3.2.2. Integration of CSP power from North African sites via HVDC links

For the purpose of enabling electricity imports from selected sites in North Africa and the Middle East, CSP plants along with high voltage direct current HVDC power transmission lines are included into the model topology of the optimization module REMix-OptiMo. Figures for installed electricity generation capacities of CSP as provided by Trieb et al. [TSPO12] change according to an update of the TRANS-CSP framework developed by Trieb [Tri12] and discussed in subsection 5.3.1. This update takes much higher electricity demand into account: in the original release of TRANS-CSP a demand of some 4000 TWh/a is to be covered in 2050 while in the update demand soars to some 6000 TWh/a for the same year. This is primarily caused by additional loads such as electric heating/cooling and electromobility, which are not considered in the original release of TRANS-CSP [TSK⁺06]. Moreover, three different pathways with differing boundary conditions are established, out of which pathway #1 is used both for the implementation of CSP imports to Europe as discussed here and the scenario check as discussed in chapter 5.3. This updated pathway has the same objectives as the original release of TRANS-CSP (e.g. 80% total renewable share in 2050).

To take account of the massive increase in demand, the following approach is carried out for an adjustment of the CSP importing scheme: The basic setup of the transmission corridors, their cost and efficiencies as a function of overhead line, sea cable and underground cable length including the respective loss are implemented according to the specifications provided by Trieb et al. [TSPO12; REA11]. However, the figures for the installed capacities of the CSP plants in MENA⁹ are scaled to obtain the installed capacities provided in scenario pathway #1. This method leaves the transmission corridors, attributed line loss and cost unaffected, thereby assuring the model's consistency. Figures for Ireland are attributed to UK, Greece to Bulgaria, Switzerland to Italy, Denmark to Germany and Slovakia to Hungary. It is assumed that the solar imports for the latter cases are transferred from the first import country to the final destination via the existing AC transmission grid, e.g. first import country UK, then transmission via AC line to final destination Ireland. Table 5.4 indicates the updated gross and net capacities from exporting to importing countries considered along with the loss occurring during the transmission. Figures for the latter are in the range from 6 to 17%, depending both on the line lengths and strictly speaking also their capacity utilization. Each connection is displayed in figure 5.4 and elaborated in further detail in table 5.5 indicating start and end points, line lengths as a function of terrain typology, year of anticipated implementation, net import capacity and loss.

⁹comprising the regions Middle East and North Africa

CSP Net Import / Export Capacity in 2050 [MW]	Morocco	Tunisia	Algeria	Libya	Egypt	Jordan	Saudi Arabia	Total Gross Import [MW]	Total Transmission Loss [MW]	Total Net Import [MW]
Germany	11000	7000	17000	x	x	x	x	39082	4082	35000
France	12000	13000	15000	x	x	x	x	44077	4077	40000
United Kingdom	14000	x	11500	x	x	x	x	28631	3131	25500
Spain	5000	x	3000	x	x	x	x	8475	475	8000
Italy	x	5000	11000	9000	x	x	x	26977	1977	25000
Belgium	12000	x	x	x	x	x	x	13520	1520	12000
Netherlands	12000	x	x	x	x	x	x	13438	1438	12000
Czech Republic	x	x	4500	3000	x	x	x	8282	782	7500
Romania	x	x	2000	x	x	2000	x	4515	515	4000
Greece / Bulgaria	x	x	x	x	7000	x	x	7897	897	7000
Hungary	x	x	x	4000	x	x	x	4404	404	4000
Poland	x	x	x	x	4000	6000	2000	13994	1994	12000
Turkey	x	x	x	x	x	3000	5000	8920	920	8000
Total Net Export [MW]	66000	25000	64000	16000	11000	11000	7000			200000
Total Transmission Loss [MW]	7506	2439	6721	1489	1554	1582	919		22213	
Total Gross Export [MW]	73506	27439	70721	17489	12554	12582	7919	222213		

Table 5.4.: Gross and net capacities of CSP plants referred to their respective exporting and importing countries. Due to transmission losses, gross and net capacities differ considerably for scenario pathway #1.

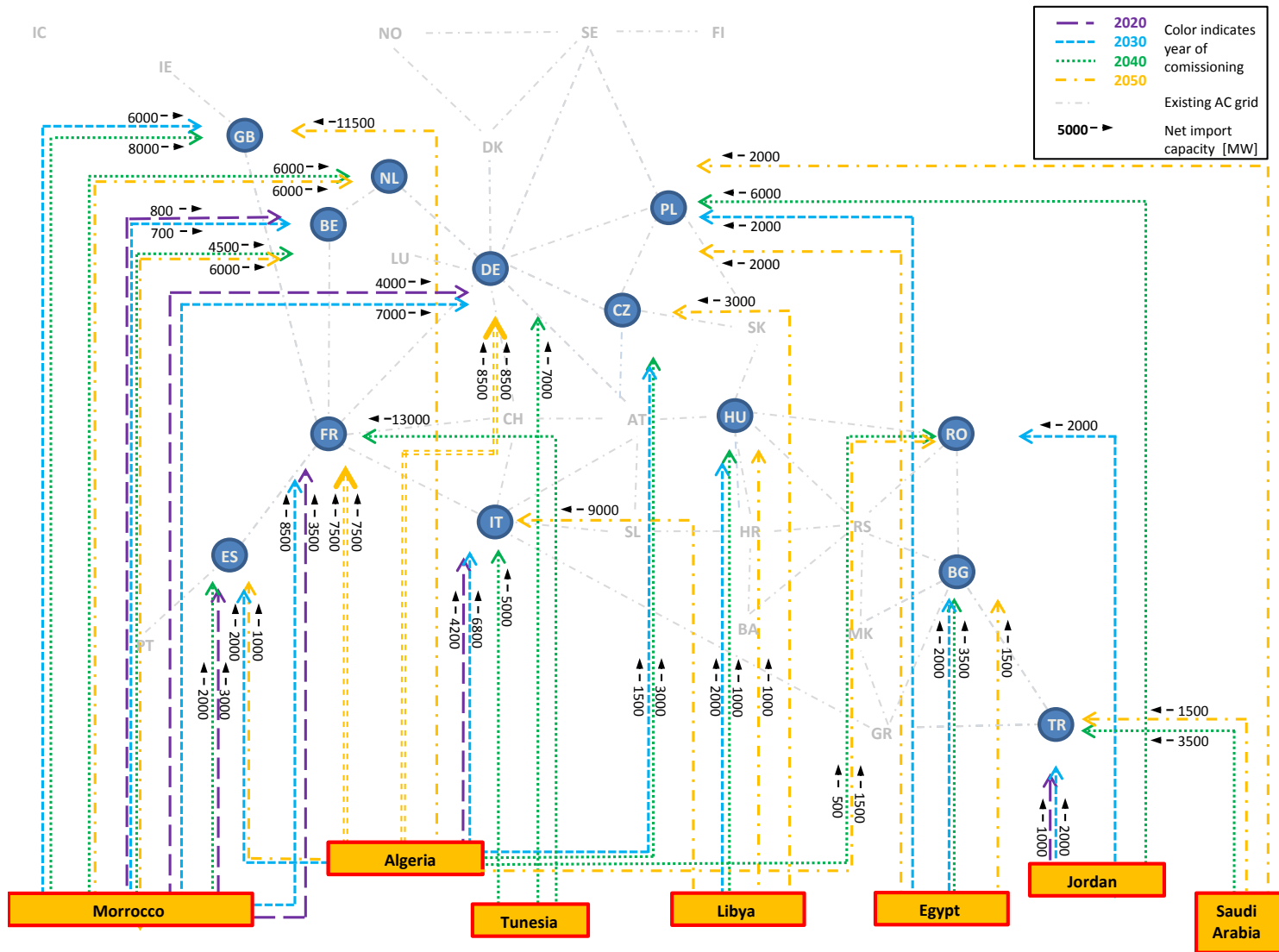


Figure 5.4.: CSP import capacities implemented into the REMix-OptiMo environment according to an updated framework of Trieb et al. [TSK⁺06]. The different colors indicate the year of commissioning of each respective line, indicated values next to the lines represent the net import capacities [MW], i.e. net feed-in at the terminal node after power transmission loss. Dashed grey lines show the existing AC grid.

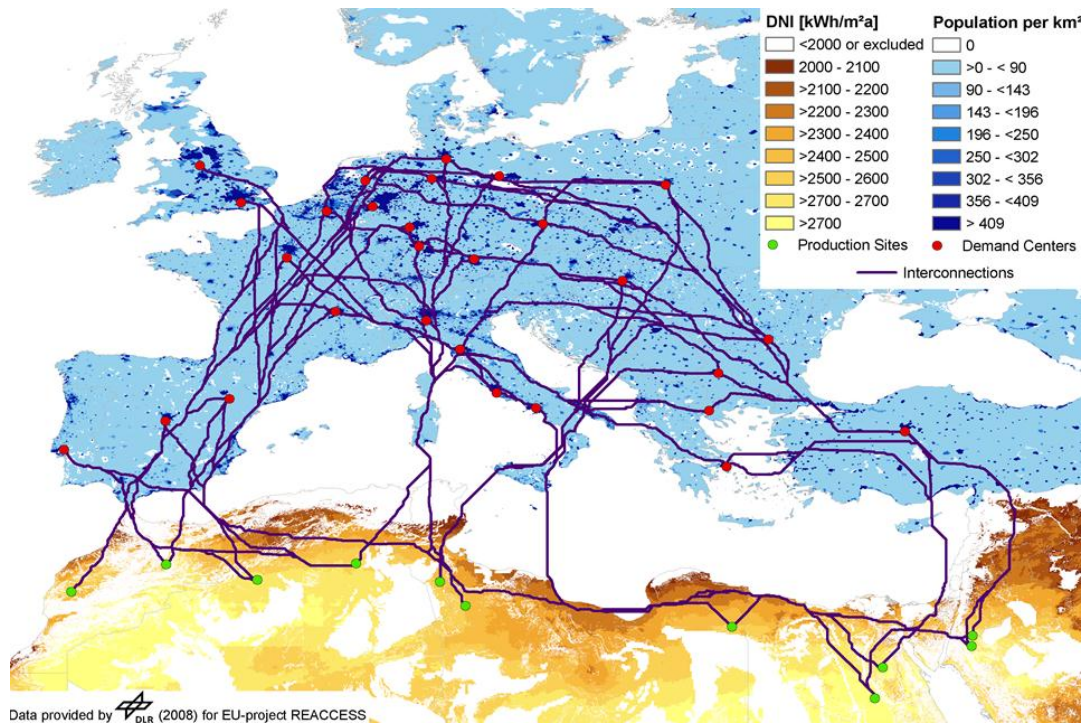


Figure 5.5.: Geographic illustration of CSP plant sites located in North Africa and the Middle East interconnected via high voltage direct current power lines to various centers of demand in Europe [TSPO12; REA11]. High population densities corresponding to the centers of demand and advantageous sites in terms of solar irradiance are connected.

Moreover, figure 5.5 gives a geographic overview of the sites envisaged for the installation of the CSP plants located in North Africa and the Middle East along with the centers of demand they are connected to and the respective transmission corridors. Within the model, each link is modeled as an autonomous power plant, with a virtual feed-in into the node in which the end point is located. Generation cost is taken into account as in an ordinary CSP plant as discussed in section A.4 with the add-on of the cost of the transmission lines. A summary on all cost values concerning these transmission lines is provided in annex A.6.

5.3.2.3. Optimization process and objective

As introduced in chapter 5, the energy modeling tool REMix-OptiMo uses the software package GAMS [GAM12] to compute least cost solutions for pre-defined energy systems. Two fundamentally differing approaches are feasible: First, the optimization is run on a green-field, i.e. hourly time series and maximum capacities for power plants along with hourly demand are known on a nodal basis, both dispatch and capacities to be installed are subject to the boundary conditions and further relations as presented in [Ten12]. Second, the installed capacities are provided beforehand and set constant, no additional construction of power plants is permitted. The existing portfolio is dispatched according

Import Country	Start Point	End Point	Overhead Line Length [km]	Underground Cable Length [km]	Sea Cable Length [km]	Total Length [km]	Start Year [a]	Net Import Capacity [MW]	HVDC Loss [MW]	HVDC Loss [%]
Germany	Morocco #1	Karlsruhe, Germany	2506	278	132	2917	2020	4000	560	14
	Morocco #2	Jülich, Germany	2075	231	149	2455	2030	7000	836	12
	Tunisia #1	Mainz, Germany	1634	182	344	2160	2040	7000	722	10
	Algeria #1	Hannover, Germany	2384	265	202	2851	2050*	8500	1156	14
	Algeria #2	Munich, Germany	1427	159	413	1998	2050	8500	807	9
France	Morocco #1	Paris, France	1957	217	132	2306	2020	3500	396	11
	Morocco #2	Paris, France	1611	179	149	1939	2030	8500	823	10
	Tunisia #1	Paris, France	1666	185	344	2195	2040	13000	1361	10
	Algeria #1	Lyon, France	1480	164	202	1847	2050*	7500	689	9
	Algeria #2	Lyon, France	1805	201	202	2208	2050	7500	808	11
United Kingdom	Morocco #1	London, UK	2125	236	282	2643	2030	6000	753	13
	Morocco #2	London, UK	1835	204	265	2304	2040	8000	887	11
	Algeria #1	Newcastle, UK	2196	244	308	2748	2050	11500	1491	13
Spain	Morocco #2	Madrid, Spain	853	95	16	964	2020	3000	180	6
	Algeria #1	Zaragoza, Spain	879	98	202	1179	2030	2000	120	6
	Morocco #2	Madrid, Spain	853	95	16	964	2040	2000	112	6
	Algeria #1	Zaragoza, Spain	879	98	202	1178	2050	1000	62	6
Italy	Algeria #2	Milano, Italy	1057	117	413	1587	2020	4200	323	8
	Algeria #2	Milano, Italy	1057	117	413	1587	2030	6800	522	8
	Tunisia #1	Firence, Italy	980	109	344	1432	2040	5000	356	7
	Libya #1	Roma, Italy	1305	145	312	1761	2050	9000	776	9
Poland	Egypt #1	Warszaw, Poland	2574	286	665	3525	2030	2000	316	16
	Jordan #1	Warszaw, Poland	3053	339	108	3500	2040	6000	997	17
	Egypt #2	Warszaw, Poland	2837	315	665	3817	2050*	2000	341	17
	Saudi Arabia #1	Warszaw, Poland	3130	348	108	3586	2050	2000	340	17
Turkey	Jordan #1	Ankara, Turkey	2050	205	0	2255	2020	1000	113	11
	Jordan #1	Ankara, Turkey	2050	205	0	2255	2030	2000	227	11
	Saudi Arabia #1	Ankara, Turkey	2100	210	0	2310	2040	3500	405	12
	Saudi Arabia #1	Ankara, Turkey	2100	210	0	2310	2050	1500	174	12
Czech Republic	Algeria #2	Prague, Czech Republic	1635	182	413	2230	2030	1500	158	11
	Algeria #2	Prague, Czech Republic	1635	182	413	2230	2040	3000	315	11
	Libya #1	Prague, Czech Republic	1629	181	344	2154	2050	3000	309	10
Belgium	Morocco #1	Brussels, Belgium	2232	248	132	2612	2020	800	101	13
	Morocco #1	Brussels, Belgium	2232	248	132	2612	2030	700	89	13
	Morocco #1	Brussels, Belgium	2232	248	132	2612	2040	4500	570	13
	Morocco #1	Brussels, Belgium	2232	248	132	2612	2050	6000	760	13
Netherlands	Morocco #2	Appledorn, Netherlands	2082	231	149	2462	2040	6000	719	12
	Morocco #2	Appledorn, Netherlands	2082	231	149	2462	2050	6000	719	12
Romania	Jordan #1	Bukarest, Romania	2154	239	108	2502	2030	2000	244	12
	Algeria #2	Bukarest, Romania	2255	251	413	2918	2040	500	68	14
	Algeria #2	Bukarest, Romania	2255	251	413	2918	2050	1500	203	14
Bulgaria	Egypt #2	Sophia, Bulgaria	1974	219	655	2849	2030	2000	256	13
	Egypt #2	Sophia, Bulgaria	1974	219	655	2849	2040	3500	449	13
	Egypt #2	Sophia, Bulgaria	1974	219	655	2849	2050	1500	192	13
Hungary	Libya #1	Budapest, Hungary	1388	154	712	2254	2030	2000	202	10
	Libya #1	Budapest, Hungary	1388	154	712	2254	2040	1000	101	10
	Libya #1	Budapest, Hungary	1388	154	712	2254	2050	1000	101	10

* start year is 2045 in the original scenario, allocated to 2050 for the validation run.

Table 5.5.: Overview on all lines with more elaborate data on line end points, lengths, import capacities and loss based on Trieb et al. [TSPO12; REA11]. Values of net import capacities are derived within an update of TRANS-CSP. All power plants indicated in red are added to the original framework to meet the massive demand increase.

to the merit order¹⁰. This method - used in the scenario validation - yields the set of constraints and equations established by Luca de Tena [Ten12] as discussed in annex A.4.

Both approaches use the Cplex solver [IBM], enabling the employment of “solution algorithms for linear, quadratically constrained and mixed integer programming problems. While numerous solving options are available, GAMS/Cplex automatically calculates and sets most options at the best values for specific problems.” [Cpl]. The overall objective function to be minimized in both running modes are the total annual cost.

5.3.3. Simulation results

Using REMix-OptiMo with the configuration as described in the previous subsection 5.3.2, the scenario validation simulations for TRANS-CSP pathway #1 are performed. The following discussion presents the results obtained. As the installed capacities are defined exogenously, the major focus of the assessment is directed on the dispatch of this portfolio, the role of imported CSP electricity and the capacity utilization of the AC-transmission grid.

Figure 5.6 gives an overview on the power generation in terms of an aggregation for all considered countries. Results of the scenario pathway and the REMix-OptiMo validation runs are compared. Key findings in this respect are:

Demand in all countries is met for each assessed hour using the power plant portfolio proposed by the scenario. This result is of major importance as it proves the feasibility of the approach chosen for the scenario development: First and foremost, the provision of 125% of firm capacity ensures system stability at all considered 8760 time steps.

The overall renewable shares differ slightly: The scenario anticipates values for the renewable shares of 30%, 60% and 80% for the three considered years 2010, 2030 and 2050 respectively. In the REMix-OptiMo runs, the overall renewable share is slightly inferior in 2010 with 27.9% and agrees completely in 2030 with 59.9%. In 2050, the overall renewable share obtained from REMix-OptiMo reaches a value of 73.3%, 6.4%-points less than anticipated in the scenario.

REMix-OptiMo results for electricity imports from CSP plants in the MENA region show good agreement with slightly inferior values compared to the propositions in the scenario, which anticipates solar shares of the total portfolio generation of 10% in 2030 and 18.6% in 2050. This compares to REMix-OptiMo results for the total generation shares of 7.2% in 2030 and 17.4% in 2050.

For some technologies, significant changes in power plant dispatch are observed. The above figures for the renewable and solar import shares are the results after all available technologies are dispatched. Looking at the usage of each single technology, as indicated in figure 5.6 along with table 5.6, the following items are observed in a direct comparison of the scenario and REMix-OptiMo results¹¹:

¹⁰the cheapest plants are chosen over more expensive ones subject to their availability.

¹¹As the year 2002 is used for the resources data for the entire region, using different resource years will impact the results. However, performing sensitivity runs is beyond the scope of the present work.

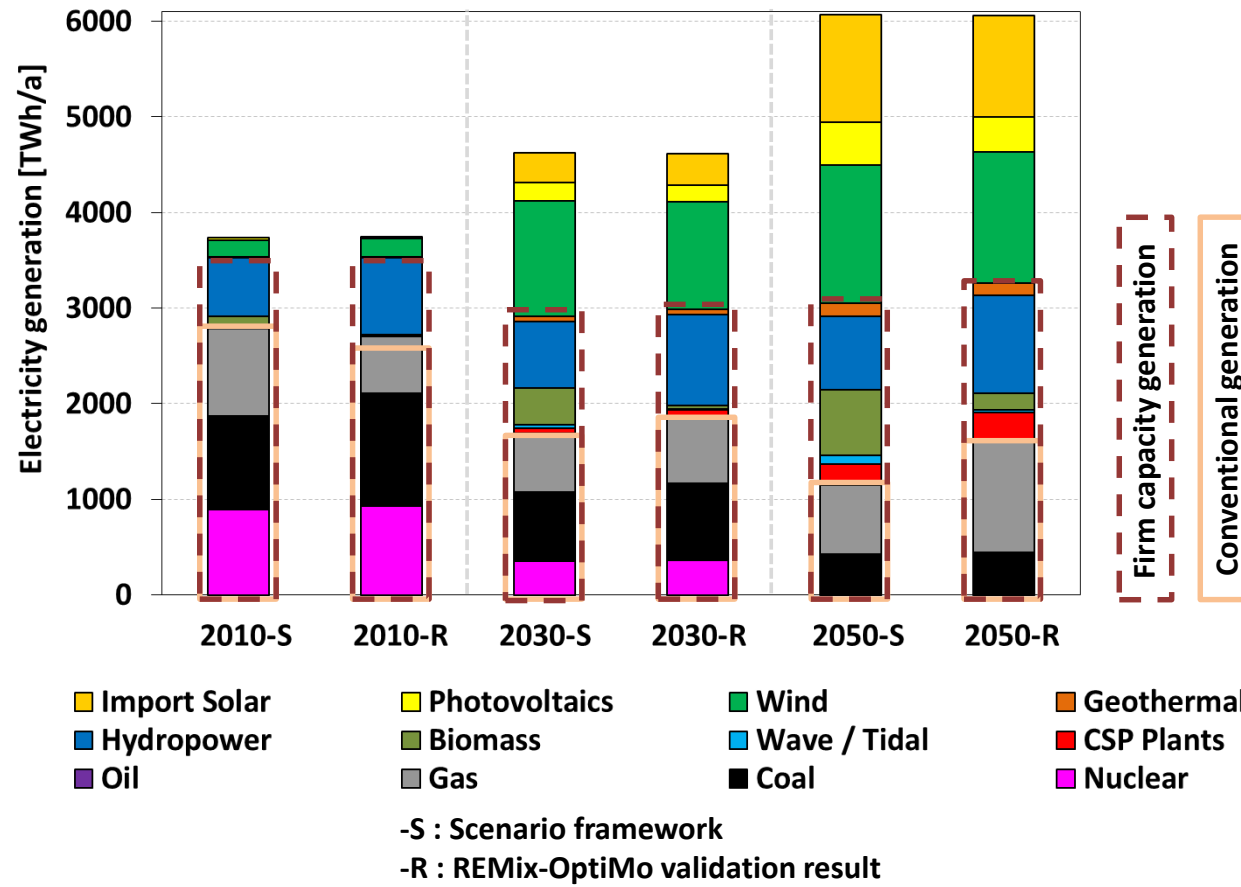


Figure 5.6.: Comparison of the aggregated results for all 30 countries considered. The validation simulations are carried out for 2010, 2030 and 2050. The columns present the results of the scenario (denoted with the 2010-S, 2030-S and 2050-S) and the REMix-OptiMo runs (denoted with 2010-R, 2030-R and 2050-R).

All values in [TWh]	2010-S	2010-R	R/S	2030-S	2030-R	R/S	2050-S	2050-R	R/S
Wind	180	191	6%	1203	1122	-7%	1453	1375	-5%
Photovoltaics	21	21	0%	197	177	-10%	443	363	-18%
Geothermal	8	8	0%	51	51	0%	130	130	0%
Biomass	125	12	-90%	380	33	-91%	685	169	-75%
CSP domestic	2	2	48%	60	83	40%	212	291	37%
Wave / Tidal	4	1	-68%	35	11	-67%	96	32	-67%
Hydropower	609	810	33%	703	957	36%	771	1026	33%
Gas / Oil	917	590	-36%	614	685	12%	724	1170	62%
Coal	974	1179	21%	720	802	11%	428	446	4%
Nuclear	896	933	4%	352	364	3%	0	0	0%
CSP Import	0	0	0%	308	333	0%	1127	1055	0%
Total	3736	3750	0%	4622	4619	0%	6070	6057	0%

Table 5.6.: Results of the REMix-OptiMo validation run compared in terms of technologies to the validated scenario. Positive (negative) deviations of the REMix-OptiMo results in [%] are indicated in red (blue), agreement in green. The results of the scenario are denoted with the 2010-S, 2030-S and 2050-S. The REMix-OptiMo runs are denoted with 2010-R, 2030-R and 2050-R.

- Little deviations are observed for wind power from 2010 through 2050.
- For PV identical results are obtained for 2010. For 2030 and 2050, moderate deviations between 10% and 18% are obtained.
- Due to modeling geothermal power with the full load hours from the scenario, identical results for their dispatch are achieved.
- In the REMix-OptiMo simulations, both biomass and wave power plants are much less used than anticipated in the scenario for all considered years.
- Domestic CSP plants are used more often, an increase of 48%, 40% and 37% is observed for 2010, 2030 and 2050 respectively.
- The use of hydro power is significantly higher in all three REMix-OptiMo runs.

- Gas/Oil plants are less dispatched in 2010 (-36%), and used more often in 2030 and 2050 (12% and 62%).
- Coal plants are dispatched more often in 2010, with a decreasing trend towards 2050 (21%, 11% and 4% respectively).
- Very good agreement is achieved for the dispatch of nuclear power.

Apart from presenting the REMix-OptiMo results on an aggregated level as performed above, in the following the power generation is displayed for each country separately. In figures 5.7 through 5.9 overviews on the composition of the power generation and the imports for each country along with the utilization of the AC transmission connections between the countries are given separately for the years 2010, 2030 and 2050. Each of these graphs is accompanied with tables providing the respective data for each country, presented in terms of the generation technologies (please see tables 5.7 through 5.9). Figures for the net import via the AC grid, the usage of pumped storage, the overall generation for domestic use and the resulting import-export balance are also presented. Moreover, the results for wind are decomposed into on- and offshore plants. All data indicated in brackets refer to the scenario results. As the key findings from the paragraph above result from an aggregation of all countries, its results are generally also valid within each respective country.

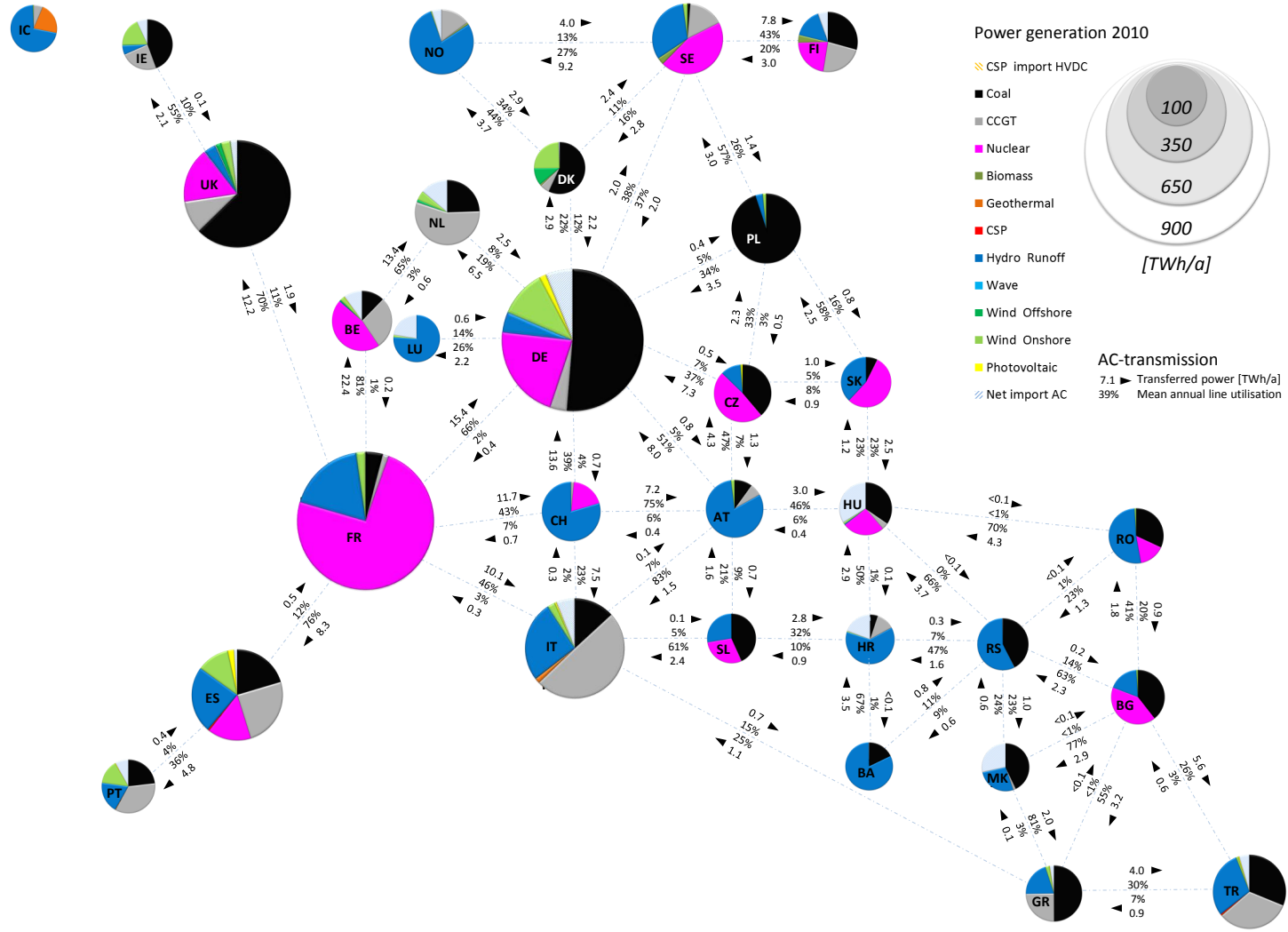


Figure 5.7.: Shares of power generation, AC and CSP imports displayed for each country for the year 2010. Data on AC transmission between the countries is presented in terms of overall transferred annual power $\left[\frac{TWh}{a}\right]$ and the connection's mean annual line utilization [%].

[TWh/a] 2010	CSP import HVDC	Coal	CCGT	Nuclear	Biomass	Geothermal	CSP	Hydro Runoff	Wave	Wind Offshore	Wind Onshore	Photovoltaic	Net import/AC	Pumped Storage	Generation for domestic use	Demand	Export-import balance	[TWh/a] 2010
Austria	0.0	7.4 (5.2)	5.2 (17.9)	0.0	0.0 (4.7)	0.0	0.0	60.3 (38.5)	0.0	0.0	1.4 (2.0)	0.1 (0.1)	0.0 (-1.5)	3.3	67.9	66.9	6.5 (1.5)	Austria
Belgium	0.0	11.5 (12.5)	26.6 (21.7)	42.9 (48.5)	0.0	0.0	0.0	0.4 (0.4)	0.0	0.5 (0.3)	2.2 (1.9)	0.3 (0.3)	9.5 (4.3)	2.0	84.5	92.9	-9.5 (-4.3)	Belgium
Bosnia Herzegovina	0.0	2.5 (4.5)	0.0	0.0	0.0 (0.8)	0.0	0.0	11.6 (6.0)	0.0	0.0	0.0	0.0 (0.0)	0.0 (-1.1)	0.7	10.4	10.2	3.7 (1.1)	Bosnia Herzegovina
Bulgaria	0.0	19.6 (18.0)	0.0 (3.8)	20.7 (14.1)	0.0 (0.0)	0.0	0.0	9.1 (3.2)	0.0	0.0	0.5 (0.8)	0.0 (0.0)	0.0 (-4.6)	1.5	35.8	35.4	14.2 (4.6)	Bulgaria
Croatia	0.0	1.1 (1.0)	2.5 (7.8)	0.0	0.0 (0.7)	0.0 (0.0)	0.0	12.7 (6.2)	0.0	0.0	0.1 (0.2)	0.0 (0.0)	4.0 (4.0)	0.5	16.4	20.0	-4.0 (-4.0)	Croatia
Czech Republic	0.0	29.9 (45.0)	0.1 (4.1)	37.4 (26.6)	0.0	0.0	0.0	8.8 (2.1)	0.0	0.0	0.4 (0.5)	0.6 (0.6)	0.0 (-10.0)	2.1	71.5	70.9	5.8 (10.0)	Czech Republic
Denmark	0.0	22.2 (17.0)	2.3 (7.4)	0.0	0.3	0.0	0.0	0.1 (0.1)	0.0 (0.1)	4.2 (2.8)	9.5 (6.9)	0.0	0.3 (0.6)	0.0	38.6	38.5	-0.3 (-0.6)	Denmark
Finland	0.0	26.9 (14.9)	21.4 (18.8)	20.2 (22.9)	3.8	0.0	0.0	14.4 (14.2)	0.0 (0.0)	0.0	0.3 (0.5)	0.0	4.9 (-11.9)	0.0	86.9	91.3	-4.9 (-11.9)	Finland
France	0.0	23.9 (35.0)	8.6 (60.8)	434.9 (396.0)	0.0	0.2 (0.2)	0.0	107.7 (69.0)	0.1 (0.4)	0.0	12.5 (11.9)	0.6 (0.6)	0.0 (-69.3)	9.3	512.4	510.0	76.1 (69.3)	France
Germany	0.0	318.2 (263.0)	24.1 (102.0)	134.0 (139.9)	0.2 (32.8)	0.0 (0.0)	0.0	28.8 (18.0)	0.0 (0.2)	0.0	67.3 (49.5)	9.5 (9.5)	38.5 (0.5)	11.8	582.1	615.4	-38.5 (-0.5)	Germany
Greece	0.0	33.2 (35.0)	16.5 (22.3)	0.0	0.0 (0.3)	0.0	0.0	13.4 (5.0)	0.0 (0.1)	0.0 (0.1)	1.5 (2.9)	0.2 (0.2)	1.6 (0.0)	1.4	64.8	65.9	-1.6 (0.0)	Greece
Hungary	0.0	15.1 (11.0)	1.8 (13.4)	11.3 (11.7)	0.0 (2.0)	0.0	0.0	0.3 (0.2)	0.0	0.0	0.5 (0.6)	0.0	14.7 (3.4)	2.3	28.9	42.3	-14.7 (-3.4)	Hungary
Iceland	0.0	0.0	0.4 (0.0)	0.0	0.0	1.4 (1.4)	0.0	4.6 (6.4)	0.0	0.0	0.0	0.0 (0.0)	0.0 (0.0)	0.0	6.5	7.8	0.0 (0.0)	Iceland
Ireland	0.0	12.6 (12.0)	6.8 (10.8)	0.0	0.1 (0.6)	0.0	0.0	1.6 (0.7)	0.0 (0.1)	0.1 (0.1)	5.2 (3.8)	0.0	2.0 (0.1)	0.5	26.5	28.2	-2.0 (-0.1)	Ireland
Italy	0.0	45.8 (29.0)	172.1 (200.9)	0.0	0.1 (8.6)	5.6 (5.6)	0.0	91.4 (42.1)	0.0	0.0	8.7 (11.6)	2.0 (2.0)	21.2 (43.2)	10.0	325.6	343.2	-21.2 (-43.2)	Italy
Luxembourg	0.0	0.0	0.0 (0.4)	0.0	0.0 (0.1)	0.0	0.0	5.6 (0.9)	0.0	0.0	0.1 (0.1)	0.0 (0.0)	1.6 (5.7)	0.0	5.7	7.2	-1.6 (-5.7)	Luxembourg
Macedonia	0.0	4.8 (5.0)	0.2 (2.1)	0.0	0.0 (0.2)	0.0	0.0	3.0 (1.7)	0.0	0.0	0.0	0.0 (0.0)	3.2 (0.1)	0.5	8.1	9.1	-3.2 (-0.1)	Macedonia
Netherlands	0.0	29.7 (30.0)	67.2 (57.6)	0.0 (2.5)	0.2 (6.0)	0.0	0.0	0.3 (0.1)	0.0 (0.0)	1.5 (0.9)	5.6 (4.2)	0.1 (0.1)	16.8 (18.9)	0.0	104.5	120.3	-16.8 (-18.9)	Netherlands
Norway	0.0	0.0	18.4 (0.0)	0.0	1.2 (2.4)	0.0	0.0	96.5 (149.2)	0.1 (0.2)	0.0	0.7 (1.0)	0.0 (0.0)	6.0 (-19.4)	1.4	116.9	133.4	-6.0 (19.4)	Norway
Poland	0.0	149.8 (140.0)	0.0 (11.3)	0.0	0.0 (6.0)	0.0	0.0	5.4 (2.3)	0.0 (0.0)	0.0	2.6 (2.4)	0.0	0.0 (-6.4)	3.0	156.6	155.6	1.2 (6.4)	Poland
Portugal	0.0	12.4 (14.8)	18.5 (15.8)	0.0	0.1 (2.4)	0.2 (0.2)	0.0	10.1 (9.7)	0.1 (0.2)	0.0	7.6 (8.6)	0.2 (0.2)	4.3 (0.9)	1.6	49.1	52.8	-4.3 (-0.9)	Portugal
Romania	0.0	19.9 (24.0)	0.0 (5.3)	9.5 (11.0)	0.0 (0.1)	0.0	0.0	32.3 (16.6)	0.0	0.0	0.6 (1.0)	0.0	0.0 (-0.7)	1.0	57.5	57.2	4.7 (0.7)	Romania
Serbia & Montenegro	0.0	14.8 (14.0)	0.0	0.0	0.0 (1.2)	0.0 (0.0)	0.0	20.0 (13.5)	0.0 (0.0)	0.0	0.0 (0.1)	0.1 (0.1)	0.0 (3.9)	1.2	33.2	32.8	1.8 (-3.9)	Serbia & Montenegro
Slovakia	0.0	2.4 (5.0)	0.1 (5.7)	18.1 (16.5)	0.0 (0.6)	0.0	0.0	12.7 (4.8)	0.0	0.0	0.0	0.0 (0.0)	0.0 (-2.6)	1.2	30.4	30.1	2.9 (2.6)	Slovakia
Slovenia	0.0	9.0 (6.5)	0.1	6.0 (5.8)	0.0 (0.3)	0.0	0.0	5.7 (4.2)	0.0	0.0	0.0	0.0 (0.0)	0.0 (-1.4)	0.3	15.6	15.4	5.2 (1.4)	Slovenia
Spain	0.0	59.8 (50.0)	72.9 (96.9)	45.1 (50.7)	0.1 (4.5)	0.0	1.6 (1.1)	69.9 (34.6)	0.0 (0.3)	0.0	34.1 (42.7)	6.6 (6.4)	3.4 (4.5)	7.0	290.3	291.7	-3.4 (-4.5)	Spain
Sweden	0.0	2.0 (1.5)	25.8 (0.0)	71.1 (64.0)	5.1 (10.5)	0.0	0.0	51.1 (68.2)	0.0 (0.0)	0.2 (0.2)	3.3 (4.6)	0.0	0.0 (0.3)	0.9	149.7	149.3	8.8 (-0.3)	Sweden
Switzerland	0.0	0.0	1.4 (8.1)	15.7 (25.4)	0.0 (2.1)	0.0	0.0	66.1 (38.2)	0.0	0.0	0.0 (0.1)	0.1 (0.1)	0.0 (-7.4)	2.6	67.4	66.7	15.9 (7.4)	Switzerland
Turkey	0.0	55.3 (40.0)	58.0 (75.4)	0.0	0.0 (3.3)	0.6 (0.6)	0.8 (0.5)	52.4 (47.3)	0.0	0.0 (0.1)	1.7 (2.9)	0.8 (1.0)	8.1 (3.4)	11.3	169.6	174.4	-8.1 (-3.4)	Turkey
UK	0.0	249.7 (140.0)	39.5 (146.9)	66.4 (60.7)	0.8 (12.3)	0.0	0.0	14.4 (5.1)	0.8 (2.1)	6.5 (4.8)	11.6 (10.2)	0.0 (0.0)	8.4 (14.2)	4.6	389.7	396.4	-8.4 (-14.2)	UK
[TWh/a] 2010	CSP import HVDC	Coal	CCGT	Nuclear	Biomass	Geothermal	CSP	Hydro Runoff	Wave	Wind Offshore	Wind Onshore	Photovoltaic	Net import/AC	Pumped Storage	Generation for domestic use	Demand	Export-import balance	[TWh/a] 2010

Table 5.7.: Country specific data as presented in figure 5.7 for the year 2010 on the power generation, AC and CSP imports, pumped storage utilization, domestic power generation, demand and the import-export balance. Values in brackets are taken from the scenario framework. All indicated numbers are in $\left[\frac{TWh}{a}\right]$.

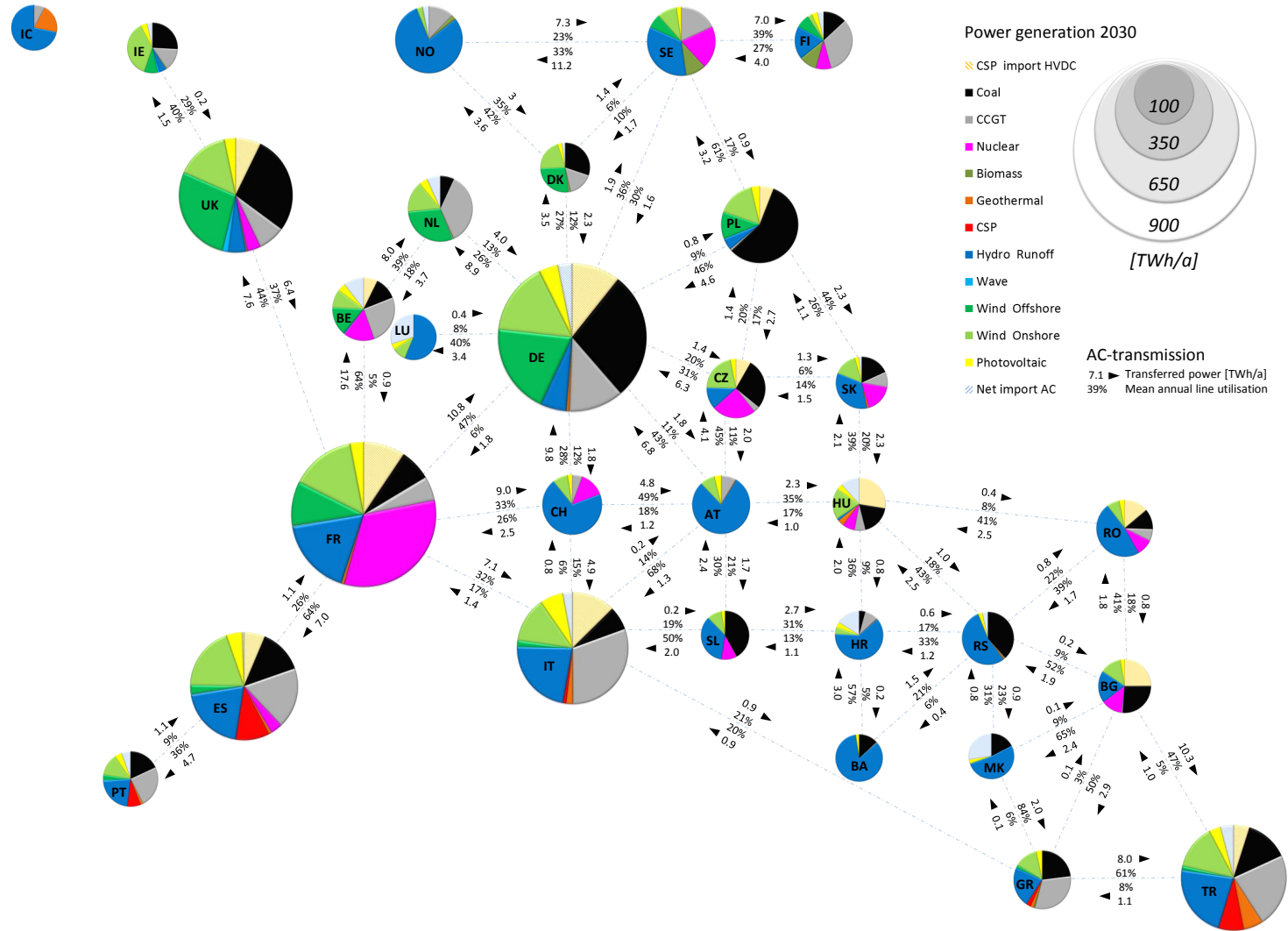


Figure 5.8.: Shares of power generation, AC and CSP imports displayed for each country for the year 2030. Data on AC transmission between the countries is presented in terms of overall transferred annual power $\left[\frac{TWh}{a}\right]$ and the connection's mean annual line utilization [%].

[TWh/a] 2030	CSP import HVDC	Coal	CCGT	Nuclear	Biomass	Geothermal	CSP	Hydro Runoff	Wave	Wind Offshore	Wind Onshore	Photovoltaic	Net import/AC	Pumped Storage	Generation for domestic use	Demand	Export-import balance	[TWh/a] 2030
Austria	0.0	0.0	7.5 (14.2)	0.0	0.0 (9.6)	0.3 (0.3)	0.0	68.7 (44.0)	0.0	0.0	7.3 (10.7)	3.4 (3.6)	0.0 (-1.5)	3.0	82.0	81.0	5.2 (1.5)	Austria
Belgium	8.6 (6.0)	13.6 (15.0)	29.7 (28.5)	18.6 (21.2)	0.2 (12.6)	0.0	0.0	0.6 (0.5)	0.0	16.9 (12.0)	10.9 (9.8)	4.8 (5.2)	12.4 (4.3)	2.0	95.4	115.2	-12.4 (-4.3)	Belgium
Bosnia Herzegovina	0.0	2.5 (3.6)	0.1 (0.3)	0.0	0.0 (3.0)	0.0	0.0	15.4 (8.0)	0.0	0.0	0.1 (0.1)	0.4 (0.5)	0.0 (-1.1)	0.7	14.6	14.4	3.8 (1.1)	Bosnia Herzegovina
Bulgaria	13.9 (7.0)	14.6 (13.0)	0.4 (3.4)	7.2 (5.1)	0.0 (1.8)	0.0	0.0	10.8 (3.8)	0.0	0.0	7.4 (11.8)	1.5 (1.9)	0.0 (-4.6)	1.0	24.6	38.2	17.2 (4.6)	Bulgaria
Croatia	0.0	0.9 (1.0)	2.0 (4.1)	0.0	0.0 (3.5)	0.1 (0.1)	0.0	14.1 (6.9)	0.0	0.0	1.0 (1.7)	0.8 (1.0)	3.7 (4.0)	0.5	19.0	22.3	-3.7 (-4.0)	Croatia
Czech Republic	7.6 (5.0)	25.3 (32.0)	3.1 (10.3)	22.2 (16.0)	0.0 (10.2)	0.0	0.0	11.0 (2.6)	0.0	0.0	19.6 (20.7)	2.9 (3.1)	0.0 (-10.0)	1.7	83.0	90.0	1.2 (10.0)	Czech Republic
Denmark	0.0	12.2 (10.0)	6.5 (2.4)	0.0	0.4 (9.8)	0.0	0.0	0.1	0.1 (0.4)	10.7 (8.3)	8.4 (7.4)	1.1 (1.2)	0.9 (0.6)	0.0	39.6	40.2	-0.9 (-0.6)	Denmark
Finland	0.0	11.5 (8.0)	28.7 (5.0)	7.4 (8.5)	8.8 (21.1)	0.0	0.0	16.3 (16.0)	0.0 (0.4)	6.7 (8.0)	2.4 (5.3)	2.8 (3.1)	3.1 (11.9)	0.0	84.6	87.3	-3.1 (-11.9)	Finland
France	61.6 (60.0)	45.8 (45.0)	35.4 (97.8)	212.3 (198.0)	0.1 (31.1)	4.5 (4.5)	0.0 (1.0)	113.2 (71.9)	1.0 (3.3)	65.0 (44.9)	95.3 (97.7)	19.8 (21.2)	0.0 (-69.3)	6.2	547.3	607.1	45.1 (69.3)	France
Germany	72.1 (60.0)	189.9 (170.0)	80.2 (73.1)	0.0	0.8 (65.7)	4.5 (4.5)	0.0	38.3 (23.9)	0.2 (1.9)	134.0 (109.5)	108.0 (133.8)	28.3 (30.3)	21.3 (0.5)	10.5	584.1	673.3	-21.3 (-0.5)	Germany
Greece	0.0	19.3 (20.0)	26.0 (16.6)	0.0	0.7 (2.4)	1.5 (1.5)	2.2 (1.5)	18.7 (6.9)	0.1 (0.8)	1.4 (2.1)	11.1 (20.6)	2.8 (3.7)	0.0 (0.0)	1.3	81.7	81.2	2.1 (0.0)	Greece
Hungary	14.6 (8.0)	9.8 (8.0)	3.5 (6.3)	4.0 (4.2)	0.0 (5.6)	2.1 (2.1)	0.0	0.8 (0.5)	0.0	0.0	10.0 (11.7)	1.9 (2.3)	6.2 (3.4)	1.8	32.1	52.0	-6.2 (-3.4)	Hungary
Iceland	0.0	0.0	0.5 (0.2)	0.0	0.0 (0.0)	1.3 (1.4)	0.0	4.6 (6.6)	0.0	0.0	0.0	0.0	0.0	0.0	6.4	7.9	0.0	Iceland
Ireland	0.0	9.3 (11.0)	5.2 (5.6)	0.0	0.3 (2.7)	0.0	0.0	1.6 (0.7)	0.4 (0.8)	3.1 (2.2)	13.3 (11.0)	1.5 (1.6)	1.3 (0.1)	0.6	34.7	35.7	-1.3 (-0.1)	Ireland
Italy	54.5 (65.0)	29.5 (20.0)	131.2 (92.7)	0.0	0.6 (28.4)	8.2 (8.2)	4.1 (3.0)	97.1 (44.8)	0.1 (0.8)	8.2 (10.7)	56.5 (80.8)	29.4 (31.5)	12.6 (43.2)	9.1	364.9	429.0	-12.6 (-43.2)	Italy
Luxemburg	0.0	0.0	0.0 (0.2)	0.0	0.0 (0.4)	0.0	0.0	5.7 (0.9)	0.0	0.0	1.0 (0.9)	0.4 (0.4)	3.0 (7.1)	0.0	7.1	10.0	-3.0 (-7.1)	Luxemburg
Macedonia	0.0	1.5 (2.8)	0.0	0.0	0.0 (1.1)	0.0	0.0	4.6 (2.5)	0.0	0.0	0.0 (0.1)	0.2 (0.3)	2.4 (-0.1)	0.5	6.5	6.8	-2.4 (0.1)	Macedonia
Netherlands	0.0	9.3 (10.0)	48.8 (26.1)	0.0 (0.5)	0.5 (18.4)	0.0	0.0	0.4 (0.2)	0.0 (0.2)	39.8 (32.2)	20.9 (21.4)	5.6 (6.0)	9.2 (18.9)	0.0	125.4	133.9	-9.2 (-18.9)	Netherlands
Norway	0.0	0.0	18.3 (1.7)	0.0	3.3 (5.6)	0.0	0.0	117.4 (163.6)	0.6 (2.0)	0.0	4.3 (6.7)	0.2 (0.2)	4.5 (-19.0)	1.1	144.1	160.8	-4.5 (19.0)	Norway
Poland	12.3 (10.0)	119.6 (105.0)	1.6 (10.1)	0.0	0.1 (24.3)	0.0	0.0	10.5 (4.4)	0.0 (0.2)	23.9 (13.6)	33.8 (30.7)	7.5 (8.0)	0.0 (-6.4)	2.5	188.4	199.9	8.6 (6.4)	Poland
Portugal	0.0	12.1 (14.0)	16.4 (8.4)	0.0	0.1 (6.1)	0.9 (0.9)	5.3 (4.0)	14.6 (14.1)	0.5 (1.4)	2.1 (1.8)	8.7 (11.8)	2.8 (3.0)	3.6 (0.9)	1.3	63.4	66.4	-3.6 (-0.9)	Portugal
Romania	10.2 (8.0)	8.5 (8.0)	4.9 (5.7)	6.9 (8.5)	0.0 (10.6)	0.0	0.0	34.9 (17.9)	0.0	0.0	5.3 (8.5)	2.3 (3.2)	0.0 (0.5)	0.7	60.9	70.8	2.0 (-0.5)	Romania
Serbia & Montenegro	0.0	17.5 (16.6)	0.2 (0.0)	0.0	0.2 (5.6)	0.3 (0.3)	0.0	24.6 (16.5)	0.0 (0.4)	0.0	0.2 (0.3)	1.1 (1.6)	1.6 (4.0)	1.0	44.1	45.3	-1.6 (-4.0)	Serbia & Montenegro
Slovakia	0.0	7.6 (6.0)	4.0 (10.9)	7.5 (6.9)	0.0 (3.2)	0.5 (0.5)	0.0	14.4 (5.5)	0.0	0.0	6.2 (9.7)	1.0 (1.5)	0.8 (-2.6)	1.1	41.2	41.5	-0.8 (2.6)	Slovakia
Slovenia	0.0	9.5 (8.1)	0.0	2.3 (4.3)	0.0 (1.4)	0.0	0.0	7.9 (5.8)	0.0	0.0	2.3 (1.8)	0.6 (0.6)	0.0 (-1.6)	0.3	18.6	18.4	4.0 (1.6)	Slovenia
Spain	25.9 (24.0)	54.1 (45.0)	74.2 (76.0)	14.3 (16.9)	0.4 (17.6)	3.3 (3.3)	41.2 (30.0)	80.8 (40.0)	0.4 (2.6)	11.4 (12.5)	78.5 (112.4)	19.6 (20.2)	2.3 (4.5)	5.5	378.4	405.0	-2.3 (-4.5)	Spain
Sweden	0.0	0.0	27.3 (0.0)	30.3 (30.0)	14.6 (26.7)	0.0	0.0	51.2 (68.0)	0.0 (0.4)	10.0 (10.6)	14.2 (21.7)	3.4 (3.6)	0.0 (-15.2)	0.8	146.3	145.9	4.7 (15.2)	Sweden
Switzerland	0.0	0.0	5.4 (18.9)	13.3 (17.0)	0.0 (4.9)	0.0	0.0	67.5 (38.2)	0.0	0.0	8.2 (12.6)	2.4 (2.6)	0.0 (-7.4)	2.1	87.6	86.8	9.2 (7.4)	Switzerland
Turkey	19.2 (15.0)	52.0 (38.0)	89.2 (74.6)	0.0	0.1 (18.1)	23.8 (23.8)	30.4 (20.0)	88.7 (80.1)	0.0	5.2 (8.0)	53.6 (87.8)	14.0 (19.4)	16.2 (3.4)	12.8	357.0	388.3	-16.2 (-3.4)	Turkey
UK	32.7 (40.0)	126.0 (110.0)	35.0 (21.2)	17.6 (16.9)	1.8 (29.0)	0.0	0.0	22.3 (7.9)	7.8 (19.0)	125.6 (105.3)	68.9 (71.9)	14.7 (15.8)	0.0 (14.2)	4.3	419.7	451.0	0.1 (-14.2)	UK
[TWh/a] 2030	CSP import HVDC	Coal	CCGT	Nuclear	Biomass	Geothermal	CSP	Hydro Runoff	Wave	Wind Offshore	Wind Onshore	Photovoltaic	Net import/AC	Pumped Storage	Generation for domestic use	Demand	Export-import balance	[TWh/a] 2030

Table 5.8.: Country specific data as presented in figure 5.8 for the year 2030 on the power generation, AC and CSP imports, pumped storage utilization, domestic power generation, demand and the import-export balance. Values in brackets are taken from the scenario framework. All indicated numbers are in $\left[\frac{TWh}{a}\right]$.

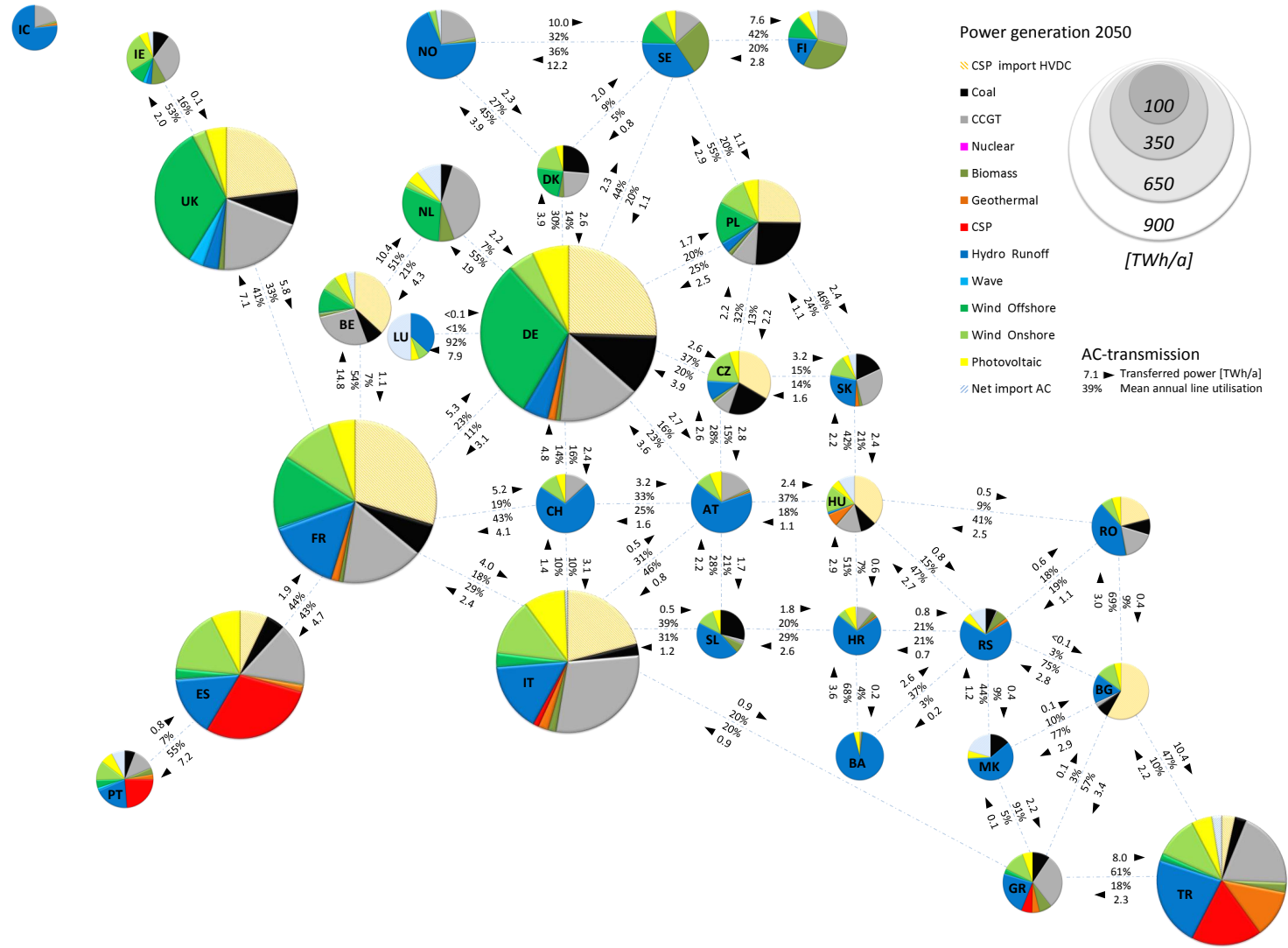


Figure 5.9.: Shares of power generation, AC and CSP imports displayed for each country for the year 2050. Data on AC transmission between the countries is presented in terms of overall transferred annual power $\left[\frac{TWh}{a}\right]$ and the connection's mean annual line utilization [%].

[TWh/a] 2050	CSP import HVDC	Coal	CCGT	Nuclear	Biomass	Geothermal	CSP	Hydro Runoff	Wave	Wind Offshore	Wind Onshore	Photovoltaic	Net import/AC	Pumped Storage	Generation for domestic use	Demand	Export-import balance	[TWh/a] 2050
Austria	0.0	0.0	19.5 (13.8)	0.0	1.1 (27.6)	0.9 (0.9)	0.0	70.9 (45.4)	0.0	0.0	8.9 (12.6)	7.0 (8.2)	0.0 (-1.5)	2.5	108.1	106.9	0.3 (1.5)	Austria
Belgium	68.0 (53.0)	13.9 (15.0)	49.5 (59.8)	0.0	3.2 (14.1)	0.0	0.0	0.6 (0.5)	0.0 (0.1)	19.5 (14.0)	12.6 (11.7)	9.9 (11.7)	7.6 (4.3)	0.9	109.3	184.2	-7.6 (-4.3)	Belgium
Bosnia Herzegovina	0.0	0.0	0.2 (0.0)	0.0	0.1 (3.8)	0.0	0.0	18.7 (10.0)	0.0	0.0	0.1 (0.1)	0.8 (1.1)	0.0 (-1.2)	0.8	14.1	13.8	5.8 (1.2)	Bosnia Herzegovina
Bulgaria	42.6 (12.0)	5.4 (12.0)	1.9 (3.7)	0.0	0.0 (7.7)	0.0	0.0	12.3 (4.4)	0.0	0.0	8.1 (13.9)	2.9 (4.3)	0.0 (-4.6)	0.6	11.2	53.4	19.5 (4.6)	Bulgaria
Croatia	0.0	0.0	2.4 (0.0)	0.0	0.8 (6.2)	0.2	0.0	15.4 (7.6)	0.0	0.0	1.2 (2.1)	1.6 (2.3)	0.3 (3.4)	0.4	21.7	21.8	-0.3 (-3.4)	Croatia
Czech Republic	40.2 (31.0)	26.1 (30.0)	10.7 (11.7)	0.0	2.2 (20.0)	0.0	0.0	12.0 (2.9)	0.0	0.0	22.9 (24.3)	6.0 (7.1)	0.0 (-10.0)	0.8	76.7	116.9	3.2 (10.0)	Czech Republic
Denmark	0.0	13.0 (12.0)	11.4 (3.2)	0.0	1.6 (10.6)	0.0	0.0	0.1	0.3 (1.2)	11.7 (9.4)	9.0 (8.3)	2.3 (2.7)	0.0 (0.6)	0.0	47.7	48.1	1.5 (-0.6)	Denmark
Finland	0.0	0.0	27.5 (2.9)	0.0	28.1 (40.3)	0.0	0.0	17.1 (16.8)	0.1 (1.1)	11.7 (14.1)	0.7 (1.6)	5.8 (6.9)	4.7 (11.9)	0.0	90.9	95.5	-4.7 (-11.9)	Finland
France	229.8 (190.0)	48.9 (45.0)	126.8 (194.0)	0.0	6.7 (79.1)	12.4 (12.4)	0.0	113.3 (72.0)	2.9 (9.2)	111.1 (79.1)	82.5 (88.4)	40.6 (47.8)	0.0 (-69.3)	3.6	522.5	749.9	22.7 (69.3)	France
Germany	220.0 (200.0)	95.6 (90.0)	129.5 (70.0)	0.0	7.4 (87.0)	12.4 (12.4)	0.0	40.3 (25.2)	0.6 (5.4)	258.1 (227.5)	42.1 (56.9)	57.9 (68.2)	0.0 (0.5)	7.6	624.3	843.1	19.6 (-0.5)	Germany
Greece	0.0 (20.0)	9.6 (10.0)	30.3 (9.4)	0.0	7.0 (7.2)	4.1 (4.1)	5.9 (4.0)	23.8 (8.8)	0.1 (2.2)	2.6 (3.8)	12.2 (22.9)	5.7 (8.2)	0.0 (0.0)	1.1	101.1	100.7	0.3 (0.0)	Greece
Hungary	29.0 (16.0)	7.0 (6.0)	11.7 (14.8)	0.0	0.3 (11.3)	5.7 (5.7)	0.0	1.1 (0.8)	0.0	0.0	11.8 (13.8)	3.8 (5.3)	7.6 (3.4)	1.5	41.3	77.1	-7.6 (-3.4)	Hungary
Iceland	0.0	0.0	1.2 (0.0)	0.0	0.1 (0.1)	0.1 (0.1)	0.0	4.6 (6.7)	0.0	0.0	0.0	0.0	0.0	0.0	6.0	6.6	0.0	Iceland
Ireland	0.0	5.5 (5.0)	17.8 (7.0)	0.0	5.0 (6.2)	0.0	0.0	1.6 (0.7)	1.2 (2.2)	5.5 (3.9)	13.7 (11.6)	3.1 (3.6)	1.9 (0.1)	0.4	53.5	55.3	-1.9 (-0.1)	Ireland
Italy	134.8 (155.0)	16.6 (14.0)	185.9 (91.6)	0.0	11.7 (46.1)	14.5 (14.5)	8.2 (6.0)	101.1 (46.6)	0.3 (2.3)	20.1 (26.2)	83.4 (123.3)	60.2 (70.9)	4.3 (43.2)	7.0	502.1	639.7	-4.3 (-43.2)	Italy
Luxemburg	0.0	0.0	0.0	0.0	0.0 (0.4)	0.0	0.0	5.8 (0.9)	0.0	0.0	1.2 (1.1)	0.9 (1.0)	7.9 (15.6)	0.0	7.9	19.0	-7.9 (-15.6)	Luxemburg
Macedonia	0.0	1.3	0.0 (1.1)	0.0	0.0 (2.6)	0.0	0.0	5.7 (3.4)	0.0	0.0	0.0 (0.1)	0.5 (0.7)	2.0 (-0.5)	0.5	7.6	7.3	-2.0 (0.5)	Macedonia
Netherlands	0.0 (65.0)	10.3 (10.0)	87.0 (26.8)	0.0	13.4 (20.0)	0.0	0.0	0.5 (0.2)	0.1 (0.6)	66.8 (56.6)	5.8 (6.3)	11.5 (13.6)	22.9 (18.9)	0.0	195.4	217.9	-22.9 (-18.9)	Netherlands
Norway	0.0	0.0	35.4 (0.0)	0.0	3.2 (5.2)	0.0	0.0	112.5 (178.0)	1.6 (5.5)	0.0	5.0 (7.9)	0.3 (0.4)	3.8 (-23.3)	0.7	158.0	173.6	-3.8 (23.3)	Norway
Poland	65.8 (67.0)	67.4 (62.0)	25.6 (7.0)	0.0	4.5 (52.1)	0.0	0.0	10.9 (4.5)	0.1 (0.6)	41.7 (24.1)	30.2 (28.1)	15.3 (18.0)	0.0 (-6.4)	1.9	191.7	257.0	3.9 (6.4)	Poland
Portugal	0.0	4.9 (6.0)	10.6 (2.1)	0.0	3.0 (13.6)	2.4 (2.4)	19.5 (15.0)	16.3 (15.8)	1.3 (3.9)	3.6 (3.2)	9.1 (12.8)	5.7 (6.7)	6.4 (0.9)	0.8	76.5	82.4	-6.4 (-0.9)	Portugal
Romania	20.0 (16.0)	8.3 (8.0)	16.4 (4.8)	0.0	0.4 (24.5)	0.0	0.0	39.0 (20.0)	0.0	0.0	6.2 (10.0)	4.7 (7.2)	0.2 (4.5)	0.5	75.0	95.1	-0.2 (-4.5)	Romania
Serbia & Montenegro	0.0	2.9	0.4 (3.4)	0.0	3.0 (10.0)	0.9 (0.9)	0.0	29.0 (19.5)	0.0 (1.1)	0.0	0.2 (0.3)	2.3 (3.6)	4.6 (4.0)	0.9	38.7	42.9	-4.6 (-4.0)	Serbia & Montenegro
Slovakia	0.0 (6.5)	10.0 (8.0)	15.6 (11.5)	0.0	1.1 (9.7)	1.4 (1.4)	0.0	15.2 (5.8)	0.0	0.0	7.2 (11.4)	2.1 (3.3)	2.8 (-2.6)	0.8	52.6	55.0	-2.8 (2.6)	Slovakia
Slovenia	0.0	6.3 (5.8)	0.7 (0.0)	0.0	1.4 (6.3)	0.0	0.0	9.8 (7.2)	0.0	0.0	2.6 (2.1)	1.2 (1.5)	0.0 (-1.4)	0.3	21.5	21.4	0.5 (1.4)	Slovenia
Spain	38.7 (55.0)	25.3 (25.0)	86.2 (49.0)	0.0	1.6 (40.4)	9.3 (9.3)	159.4 (120.0)	82.8 (41.0)	1.1 (7.2)	14.4 (16.0)	88.6 (130.0)	40.1 (45.6)	0.0 (4.5)	3.1	505.3	542.9	3.5 (-4.5)	Spain
Sweden	0.0	0.0	19.7 (0.0)	0.0	40.1 (48.2)	0.0	0.0	51.2 (68.0)	0.1 (1.1)	17.1 (18.6)	12.1 (19.3)	7.0 (8.2)	0.0 (-20.9)	0.4	144.6	142.5	2.7 (20.9)	Sweden
Switzerland	0.0	0.0	12.6 (29.6)	0.0	0.3 (8.0)	0.0	0.0	67.4 (38.3)	0.0	0.0	10.0 (14.9)	5.0 (5.9)	0.0 (-7.4)	1.7	90.7	89.2	4.5 (7.4)	Switzerland
Turkey	18.6 (45.0)	15.8 (15.0)	107.8 (45.0)	0.0	13.8 (44.7)	66.1 (66.1)	97.6 (65.0)	125.0 (112.9)	0.0	9.6 (14.2)	59.2 (98.6)	28.4 (43.7)	13.9 (3.4)	11.4	523.2	553.5	-13.9 (-3.4)	Turkey
UK	147.9 (180.0)	51.5 (45.0)	125.3 (66.1)	0.0	8.1 (31.4)	0.0	0.0	22.5 (7.9)	21.8 (52.8)	214.5 (185.5)	20.8 (22.6)	30.2 (35.5)	0.0 (14.2)	3.1	494.0	641.1	0.6 (-14.2)	UK
[TWh/a] 2050	CSP import HVDC	Coal	CCGT	Nuclear	Biomass	Geothermal	CSP	Hydro Runoff	Wave	Wind Offshore	Wind Onshore	Photovoltaic	Net import/AC	Pumped Storage	Generation for domestic use	Demand	Export-import balance	[TWh/a] 2050

Table 5.9.: Country specific data as presented in figure 5.9 for the year 2050 on the power generation, AC and CSP imports, pumped storage utilization, domestic power generation, demand and the import-export balance. Values in brackets are taken from the scenario framework. All indicated numbers are in $\left[\frac{TWh}{a}\right]$.

The overall capacity utilization of the AC transmission grid is decreasing. This result is of major interest as it proves the concept behind the idea of establishing an infrastructure for CSP electricity imports from the MENA region. As CSP provides firm capacity, power transmission requirements to neighboring countries for system balancing purposes decrease. This is indicated in figure 5.10, which gives an overview on the monthly mean power transmission. For reasons of clarity, merely the two nearest neighbors to Germany are displayed. It can be observed for instance, how the mean power transmission between France and Germany decreases from 2010 to 2050: In 2010 the monthly mean hourly imports from France to Germany are as high as some 2.6 GW during summer, this figure decreases to less than 0.9 GW in 2050. Starting 2030 with increasing impact towards 2050, the electricity flow is even reversed for some times in the year. These results indicate that a structural deficit of generation capacity in Germany in 2010 is improved greatly until 2050. The transmission line is less utilized, power flows start to become bi-directional. These bi-directional flows are extremely important for the usage of distribution effects of renewable generation.

Overall it can be concluded that the energy portfolio as provided by the analysed scenario pathway #1 is feasible of providing sufficient power to meet all loads performing the assessment on an hourly bases. Moreover, the transmission requirements between countries do not increase. On the contrary, the quality of the import-export balances improves significantly. Against these results, the validated scenario appears to offer a solid foundation for a development towards an increased use of renewable energies in Europe.

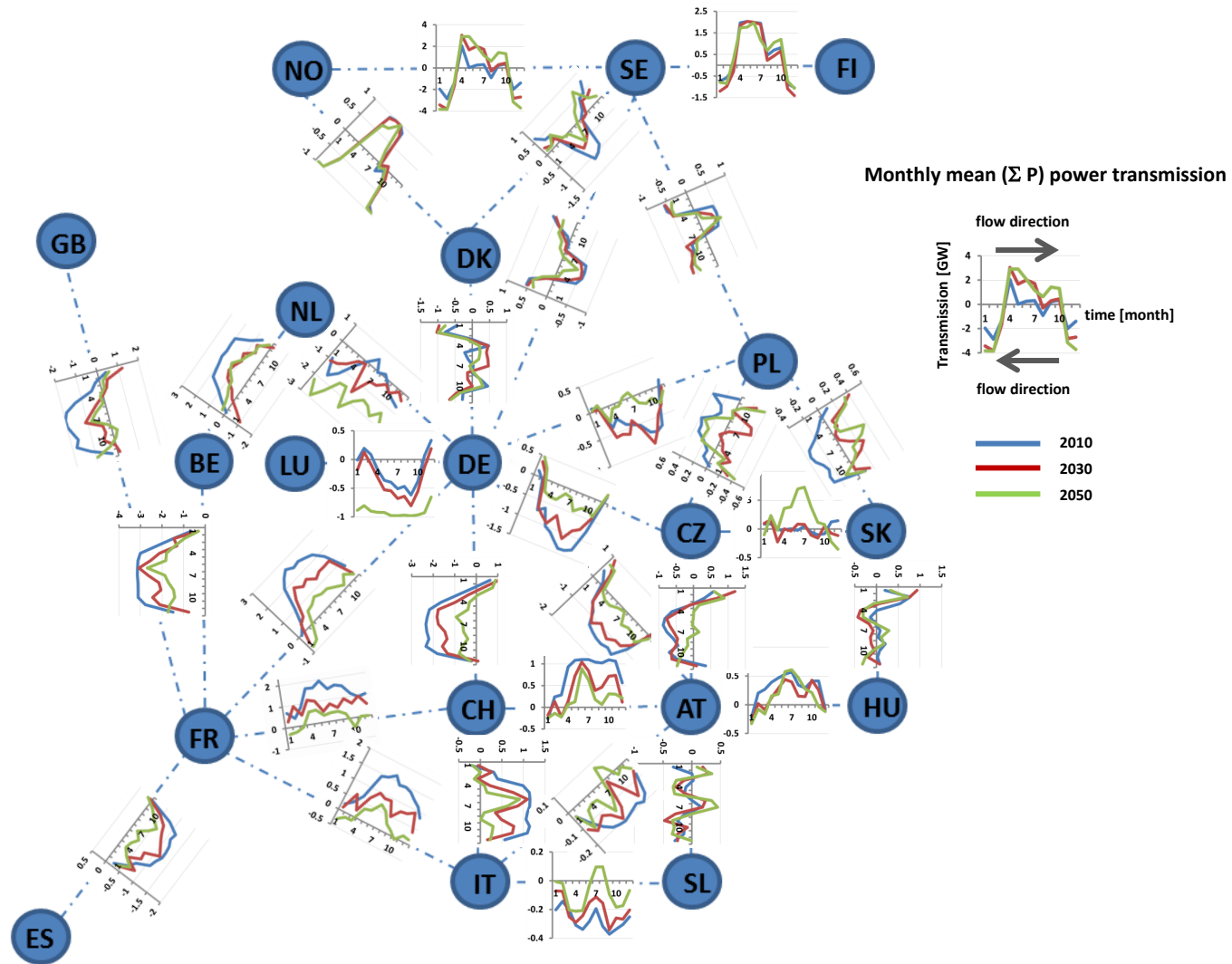


Figure 5.10.: Mean monthly bi-directional power transmission [GW] resulting from the REMix-OptiMo validation simulations. Data for the years 2010, 2030 and 2050 is indicated in blue, red and green, respectively. The presentation is limited to the second nearest neighbors of Germany for reasons of clarity.

5.4. Summary

In the present chapter the existing energy modeling tool REMix-OptiMo (abbreviating “Optimization Module”) along with the extensions amended as part of this work are discussed. The base version of REMix-OptiMo, developed by Scholz [Sch12] is used as the fundamental framework for these additions. REMix-OptiMo is capable of determining green-field least cost power plant portfolios using both renewable and conventional generation as well as plant dispatch. It is enhanced in order to be applicable for scenario validations. Within this work, a new AC-power transmission model is implemented. A thorough mathematical formulation and discussion are given. This amended framework is employed in a validation study of an updated TRANS-CSP scenario as established by Trieb [Tri12].

The general approach and outcomes of the scenario update are presented. The most significant change compared to the original TRANS-CSP release [TSK⁺06] is a drastic increase in the projected development of demand. While the original release assumes an electricity demand of some 4000 TWh/a in 2050, the updated framework uses figures of more than 6000 TWh/a. This is mainly due to the inclusion of electric heating/cooling and electric cars as loads. Employing the updated framework, also taking into account more recent figures for the setup of the generation portfolios according to the National Renewable Energy Action Plans [BHV11], three new scenario pathways are developed by Trieb [Tri12]. Out of these three, pathway #1, an update of the original TRANS-CSP scenario taking the updated framework as backbone, is used within a validation process. The setup of the amended tool REMix-OptiMo for this validation is presented. The option of using DC-imports of electricity originating in CSP plants located in MENA countries is implemented. Figures for the import capacities are corrected to be in line with scenario pathway #1.

Within the validation study, the overall feasibility of the scenario is checked for hourly time steps using the power plant portfolio as provided by the updated scenario pathway #1. The results of the simulation runs indicate that the anticipations and assumptions made provide a robust framework for a secure power supply. Transmission lines between countries appear to be less utilized comparing the results from 2010 over 2030 and 2050. This is an important contribution to the present public discussion on the extension of electricity grids, and somehow contradicting the need for severe grid expansions due to the increased use of renewable energies.

Future work has to be dedicated to sensitivity analyses in order to derive those portions of the portfolio, which can be waived: Are there capacities in the scenario which are barely used and can therefore be set aside? Which power plant portfolio’s would then represent an optimum in terms of providing both supply quality and reasonable cost? Moreover the simulation has to be run using different years of meteorological data in order to assess the impact on the results.

6. Key results, concluding remarks and outlook

Within the framework of the present thesis the energy modeling environment REMix, abbreviating "Renewable Energy Mix", **is significantly extended in terms of**

A enhancing the existing potential assessment tool REMix-EnDaT ("Energy Data Tool"), now enabling assessments of installable capacities, hourly power output, full load and cost potentials on a global scale for the technologies photovoltaics, concentrating solar, on- and offshore wind and hydro power: Land use data with the highest available resolution (300x300 m²) is used for the determination of suitable sites for power plant installation. A global long term inventory covering the period from 1984 to 2004 on solar irradiance, wind speed and river discharge is established at hourly time steps and a spatial resolution of 0.45° (50x50 km² at the equator). Considerable effort is devoted to solar irradiance, which also requires the highest processing effort. The results of the satellite based approaches for the establishment of the database are cross-checked with satellite-derived and ground station data. Overall, slightly lower annual means of the processed resources data are obtained compared to satellite-derived data. Global maps for the resulting long term annual averages are included to indicate the geographical occurrence of the resources. The present approach and obtained data within REMix-EnDaT **serve as input for energy modeling approaches as carried out in sections 4.3 and 5.3**, since temporal resolutions of one hour are sufficiently reflecting balancing effects. **For policy consultancy purposes, the data can be used as input to shape goals and scenarios for future energy systems** and to assess associated cost of a transition from today's supply to a future renewable power plant portfolio.

B adding the new plant siting optimization tool REMix-PlaSMo, capable of performing plant siting optimizations for the volatile technologies photovoltaics, on- and offshore wind according to three different operation modes: minimization of the portfolio's cost, of its output and residual load variances. The tool is globally operable on a country basis, data on installable capacities and hourly power generation being provided by REMix-EnDaT. Using CSP as the complementing technology, least cost energy supply configurations can be derived.

C enhancing the existing energy system optimization tool REMix-OptiMo ("Optimization Module") in terms of adding a new power transmission model based on the direct current approximation of the full alternating current flow. Also, electricity imports from concentrating solar power plants using high voltage direct current links are implemented.

These extensions of REMix are presented and discussed in depth in the methodology parts of chapters 3, 4 and 5. Together they contribute to the enhanced REMix modeling environment. The latter creates the foundation for three different application studies, each of which using the methodological enhancements developed within this work.

REMmix-EnDaT is used for the computation of **a world-wide potential assessment study in section 3.3 for the technologies photovoltaics, concentrating solar, on- and offshore wind and hydro power. Results are indicated on a global level in terms of full load and cost potentials.** For CSP, different plant layouts (solar multiples) are used to indicate the impact on the overall potential. Full load hours are indicated globally as maps, the overall results are presented in terms of 10 world regions. The discussion includes a sensitivity analysis on the major parameters as well as an overview on geographical resolution effects.

REMmix-PlaSMo is used in a country study conducted for Morocco in section 4.3. Considered technologies in this assessment are photovoltaics, on- and offshore wind on the one hand and hydro and concentrating solar power on the other hand. The assessment is carried out for 2010, 2030 and 2050. The key question is: **How can volatile (PV and wind) and firm capacities (CSP and to some extent hydro power) be best combined to achieve the least overall cost of the entire system and what is the resulting optimum share of volatile power generation?** To investigate this issue, the volatile generation portfolio is optimized with respect to minimizing its generation cost, portfolio output and resulting residual load variance. Key findings are: **An optimum volatile generation share is found for all considered years at a contribution of 34%. The overall portfolio's power generation cost remains stable between 10.1 and 10.5 $\left[\frac{\text{€ct}}{\text{kWh}}\right]$. The higher cost of the volatile generation portfolio resulting from optimized plant siting as to minimize the residual load's variance can not be compensated by CSP plants with high solar multiples. The best performing optimization for 2010 and 2030 is the cost minimization mode of the volatile portfolio. In 2050, the variance minimization mode yields slightly cheaper overall results, which is due to a cheaper CSP layout.**

REMmix-OptiMo is employed in a validation study of an externally provided energy scenario in a dynamical, i.e. hourly resolved energy system model. The discussion presented in section 5.3 gives an insight into the establishment of the scenario. Moreover, the configuration of REMmix-OptiMo is elaborated in detail. Special attention is given to the implementation of concentrating solar power plants providing import electricity from North African and Middle Eastern countries. The scenario validation runs are carried out for 2010, 2030 and 2050. Key findings include the **overall feasibility of the scenario framework: Demand in all countries is met for each assessed hour using the power plant portfolio proposed by the TRANS-CSP scenario. The overall resulting renewable shares differ slightly while for some technologies significant changes in power plant dispatch are observed. Results for electricity imports from CSP plants in the MENA region show good agreement with slightly lower values compared to the propositions in the scenario. Finally, the overall capacity utilization of the AC transmission grid**

is decreasing, contradicting the presently discussed need for a strong expansion of the electricity grids. These results are displayed in graphs indicating the annual power generation sum and shares on country level as well as monthly means for power transmission.

Overall the methodological development carried out in this work **has advanced the energy system modeling environment REMix as a whole, as all enhancements added are usable for further assessments other than the applications performed in this work.** During the development phase and beyond, several requests for potential analysis have been carried out, for instance for Africa, South Eastern Europe and South Korea. Optimized plant siting remains an issue also for further optimization analyses concerned with determining best quality at least cost power plant portfolios. Before this work's enhancements, only country averages for the volatile generation were used. The new AC power transmission model along with the implementation of CSP electricity imports is already scheduled to be employed in future research projects.

Future methodological work going beyond the scope of the present thesis to enhance the energy modeling environment has to **focus on the implementation of higher temporal and spatial resolutions for all modules REMix is comprised of.**

Higher spatial resolution of the resources data results in more accurate geographical distributions of potential estimates, in turn enhancing the significance of the potential assessments. Moreover, subdividing the energy system optimizations into smaller regions enhances the scientific information implied in the results.

Higher temporal resolution in combination with better spatial resolution of the resources data along with the implementation of more regions in the energy system model eventually will enable more accurate estimates for the role and issues related to the transmission grids, for instance critical deviations from the anticipated voltages and frequencies.

Concerning the optimization process, improvements are to be achieved in the overall approach and code design. The optimization itself has to be laid out to be operable on supercomputers to achieve both, less processing time and capability for more complex models. Currently the optimization is run for one year. Future work therefore has to develop algorithms considering long term developments optimizing the entire period of interest.

Overall, all of these efforts result in an improvement of the model in order to obtain more significant results for assessments conducted within the framework of policy consultancy and scientific research.

Bibliography

- [ABBK⁺11] AMANN, M. ; BERTOK, I. ; BORKEN-KLEEFELD, J. ; COFALA, J. ; HEYES, C. ; HÖGLUND-ISAKSSON, L. ; KLIMONT, Z. ; NGUYEN, B. ; POSCH, M. ; RAFAJ, P. ; SANDLER, R. ; SCHÖPP, W. ; WAGNER, F. ; WINIWARTER, W.: Cost effective control of air quality and green house gases in Europe: Modelling and policy applications. In: *Environmental Modelling and Software* 26 (2011), S. 1489–1501
- [AJ05] ARCHER, C.L. ; JACOBSON, M.Z.: Evaluation of global wind power. In: *Journal of geophysical research* 110 (2005)
- [AWA06] AKAGI, H. ; WATANABE, E.H. ; AREDES, M.: *Instantaneous power theory and applications to power conditioning*. John Wiley & Sons, Inc., 2006
- [Bad12] BADGER, J. *Resolution effects of wind data*. personal communication. 2012
- [BB05] BARTHOLOM, E. ; BELWARD, A. S.: GLC 2000: A new approach to global land cover mapping from earth observation data. In: *International Journal of Remote Sensing* 26 (2005), Nr. 9, S. 1959–1977
- [BCH96] BEYER, H.G. ; COSTANZO, C. ; HEINEMANN, D.: Modifications of the Heliosat procedure for irradiance estimates from satellite images. In: *Solar Energy* 56 (1996), Nr. 3, S. 207 – 212
- [BH81] BIRD, R.E. ; HULSTROM, R.L.: *A Simplified Clear Sky Model for Direct and Diffuse Insolation on Horizontal Surfaces*. Solar Energy Research Institute. 1981. – Available online at <http://rredc.nrel.gov/solar/pubs/PDFs/TR-642-761.pdf>; visited on November 12th 2012.
- [BHB03] BERNDES, G. ; HOOGWIJK, M. ; VAN DEN BROEK, R.: The contribution of biomass in the future global energy supply: A review of 17 studies. In: *Biomass and Bioenergy* 25 (2003), Nr. 1, S. 1 – 28
- [BHV11] BEURSKENS, L.W.M. ; HEKKENBERG, M. ; VETHMAN, P.: *Renewable Energy Projections as Published in the National Renewable Energy Action Plans of the European Member States*. Report ECN-E-10-069, Energy Research Centre of the Netherlands. 2011. – Available online at <http://www.ecn.nl/units/ps/themes/renewable-energy/projects/nreap>; visited on November 13th 2012.

- [Bib04] BIBERACHER, M.: *Modelling and optimization of future energy systems using spatial and temporal methods*, Institute for Physics, Experimental Plasma Physics, University of Augsburg, Diss., 2004
- [BMS⁺09] BEYER, H.G. ; MARTINEZ, J.P. ; SURI, M. ; TORRES, J.L. ; LORENZ, E. ; MÜLLER, S.C. ; HOYER-KLICK, C. ; INEICHEN, P.: *MESOR: Management and Exploitation of Solar Resource Knowledge*. D 1.1.3 Report on Benchmarking of Radiation Products. 2009. – Available online at http://www.mesor.org/docs/MESoR_Benchmarking_of_radiation_products.pdf; visited on November 13th 2012.
- [Bol98] BOLLOBÁS, B.: *Modern Graph Theory*. , 1998 (Graduate Texts in Mathematics Series)
- [BP12] *BP Statistical Review of World Energy*. Website. 2012. – Available online at <http://www.bp.com/statisticalreview>; visited on December 30th 2012.
- [BRC11] BOSILOVICH, M.G. ; ROBERTSON, F.R. ; CHEN, J.: Global Energy and Water Budgets in MERRA. In: *Journal of Climate* 24 (2011), S. 5721–5739
- [BSR12] *BSRN: Baseline Surface Radiation Network*. World Radiation Monitoring Center. 2012. – Available online at <http://www.bsrn.awi.de/>; visited on November 12th 2012.
- [BZ10] BRAND, B. ; ZINGERLE, J.: *The renewable energy targets of the Maghreb countries: Impact on electricity supply and conventional power markets*. EWI Working Paper, No. 10/02. 2010. – Available online at http://www.ewi.uni-koeln.de/fileadmin/user_upload/Publikationen/Working_Paper/EWI_WP_10-02_Renewable-Energy-Maghreb.pdf; visited on November 13th 2012.
- [Caf09] CAFLISCH, M. *Global Potentials for Concentrating Solar Power Electricity Generation*. Swiss Federal Institute of Technology - ETH Zürich. 2009
- [Cap01] CAPROS, P.: *The PRIMES Energy System Model - Summary Description*. European Commission Joule-III Programme. 2001. – Available online at <http://www.e3mlab.ntua.gr/manuals/PRIMsd.pdf>; visited on November 9th 2012.
- [CIA10] *The world factbook*. Central Intelligence Agency. 2010. – Available online at <http://www.cia.gov/library/publications/the-world-factbook>; visited on November 9th 2012.
- [CMA⁺86] CANO, D. ; MONGET, J. ; ALBUISSON, M. ; GUILLARD, H. ; REGAS, N. ; WALD, L.: A method for the determination of the global solar radiation from meteorological satellite data. In: *Solar Energy* 37 (1986), Nr. 1, S. 31 – 39

- [CMD⁺07] CLARKE, P. ; MUNAWWAR, S. ; DAVIDSON, A. ; MUNEER, T. ; KUBIE, J.: An investigation of possible improvements in accuracy of regressions between diffuse and global solar irradiation. In: *Building Service Engineering Research and Technology* 28(2) (2007), S. 189–197
- [COO03] *Forschungs und Entwicklungskonzept für emissionsarme fossil befeuerte Kraftwerke, Bericht der COORETEC-Arbeitsgruppen Nr. 527*. Bundesministerium für Wirtschaft und Arbeit. 2003
- [Cpl] *Cplex 12 - solver manual*. – Available online at <http://www.gams.com/dd/docs/solvers/cplex.pdf>; visited on November 22nd 2012.
- [CTDL77] COHEN-TANNOUJDI, C. ; DIU, B. ; LALOË, F.: *Quantum mechanics. (Mécanique quantique). Vol. 1-2*. Paris Wiley - Hermann XV, 1977 (Quantum Mechanics)
- [Czi05] CZISCH, G.: *Szenarien zur zukünftigen Stromversorgung, kostenoptimierte Variation zur Versorgung Europas und seiner Nachbarn mit Strom aus erneuerbaren Energien*, Fachbereich Elektrotechnik / Informatik der Universität Kassel, Diss., 2005
- [DB91] DUFFIE, J. A. ; BECKMAN, W. A.: *Solar Engineering of Thermal Processes*. Second. Wiley Interscience, 1991
- [DBW⁺12] DECKER, M. ; BRUNKE, M. ; WANG, Z. ; SAKAGUCHI, K. ; ZENG, X. ; BOSILOVICH, M.: Evaluation of the Reanalysis Products from GSFC, NCEP, and ECMWF Using Flux Tower Observations. In: *Journal of Climate* 25 (2012), S. 1916–1944
- [Deu09] *The CSP industry - an awaking giant*. Deutsche Bank global markets research. 2009
- [DFZ09] DOELL, P. ; FIEDLER, K. ; ZHANG, J.: Global-scale analysis of river flow alterations due to water withdrawals and reservoirs. In: *Hydrology and Earth System Sciences* 13 (2009), Nr. 12, S. 2413–2432
- [DLR14a] *German Aerospace Center - DLR: Windkraftforschung. Website. 2014*. – Available online at <http://www.dlr.de/dlr/Portaldata/1/Resources/bilder/portal/portal20131/windraeder.jpg>; visited on May 13th 2014.
- [DLR14b] *German Aerospace Center/RWE: Andasol-III-Heliostat. Website. 2014*. – Available online at <http://www.dlr.de/sf/Portaldata/73/Resources/images/aktuelles/2013/Andasol3Heliostat2Quelle-RWEhighres>; visited on May 13th 2014.

- [DM11] DENHOLM, P. ; MEHOS, M.: *Enabling Greater Penetration of Solar Power via the Use of CSP with Thermal Energy Storage*. National Renewable Energy Laboratory. 2011. – Available online at <http://www.nrel.gov/csp/pdfs/52978.pdf>; visited on November 13th 2012.
- [Doe10] DOELL, P. *Institute of Physical Geography, Goethe University Frankfurt, Frankfurt am Main, Germany*. personal communication. 2010
- [DSM07] *Digital soil map of the world*. FAO-UNESCO. 2007. – Available online at <http://www.fao.org/geonetwork/srv/en/metadata.show?id=14116>; visited on November 9th 2012.
- [Dut07] DUTHALER, C.L. *Power Transfer Distribution Factors: Analyse der Anwendung im UCTE-Netz*. Master Thesis, EEH - Power Systems Laboratory der ETH Zürich. 2007
- [Eco11] *Financing Renewable Energy in the European market*. Ecofys, Ernst and Young, Fraunhofer Association and Vienna University of Technology. 2011
- [EGP10] EWI ; GWS ; PROGNOSE: *Energieszenarien für ein Energiekonzept der Bundesregierung*. Bundesministerium für Wirtschaft und Technologie. 2010. – Available online at http://www.bmu.de/files/pdfs/allgemein/application/pdf/energieszenarien_2010.pdf; visited on November 13th 2012.
- [End12] *EU-Endorse Deliverable 3.4: Post-processing of surface solar irradiance*. EU - Seventh Framework Programme. 2012
- [Ene12] *Golden Rules for a Golden Age of Gas*. Website. 2012. – Available online at <http://www.enercon.de/dede/technologie%20.htm>; visited on November 13th 2012.
- [EPMS⁺11] EDENHOFER, O. ; PICHES-MADRUGA, R. ; SOKONA, Y. ; SEYBOTH, K. ; MATSCHOSS, P. ; KADNER, S. ; ZWICKEL, T. ; EICKEMEIER, P. ; HANSEN, G. ; SCHLÖMER, S. ; VON STECHOW, C.: *IPCC Special Report on Renewable Energy Sources and Climate Change Mitigation. Prepared by Working Group III of the Intergovernmental Panel on Climate Change*. Cambridge University Press. 2011. – Available online at <http://srren.ipcc-wg3.de/report>; visited on November 13th 2012.
- [ESJ82] ERBS, D.G. ; S.A., Klein ; J.A., Duffie: Estimation of the diffuse radiation fraction for hourly, daily and monthly average global radiation. In: *Solar Energy* 28 (1982), S. 293–302
- [Eur] *Orthographic projection of Europe*. Wikipedia - The free encyclopedia. – Available online at [http://de.wikipedia.org/wiki/Datei:Europe_\(orthographic_projection\).svg](http://de.wikipedia.org/wiki/Datei:Europe_(orthographic_projection).svg); visited on November 9th 2012.

- [EWE08] *Pure Power - Wind Energy Scenarios up to 2030*. European Wind Energy Association. 2008. – Available online at http://www.ewea.org/fileadmin/ewea_documents/documents/publications/reports/purepower.pdf; visited on November 13th 2012.
- [Fel] *The potential of wind energy to reduce carbon dioxide emissions*. Garrad Hassan. – pp.146
- [Fic12] FICHTER, T.: Optimized Integration of Renewable Energy Technologies into Jordan's Power Plant Portfolio. In: *Heat Transfer Engineering* submitted (2012)
- [FMR08] FRANKL, P. ; MENICHETTI, E. ; RAUGEI, M. *Technical data, costs and life cycle inventories of PV applications*. NEEDS, final report prepared for the European Commission. 2008
- [FS71] FINKELSTEIN, J.M. ; SCHAFER, R.E.: Improved goodness-of-fit tests. In: *Biometrika* 58 (1971), Nr. 3, S. 641 – 645
- [GAM12] *GAMS: General Algebraic Modeling System*. GAMS Development Corporation / GAMS Software GmbH. 2012. – Distribution 23.9.5 available online at <http://www.gams.com>; visited on November 12th 2012.
- [GEHW11] GREEN, M.A. ; EMERY, K. ; HISHIKAWA, Y. ; WARTA, W.: Solar Cell efficiency tables version 37. In: *Progress in Photovoltaics: Research and Applications* 19 (2011), Nr. 1, S. 84 – 92
- [GEMF09] GROSCHKE, M. ; EER, A. ; MÖST, D. ; FICHTNER, W.: Neue Anforderungen an optimierende Energiesystemmodelle für die Kraftwerkseinsatz- und zubauplanung bei begrenzten Netzkapazitäten. In: *Zeitschrift für Energiewirtschaft* 1 (2009), S. 14–22
- [Gil] GILS, Hans-Christian: *to be submitted (unpublished): Introduction of demand side management into the energy system modelling environment REMix*, Fakultät für Energie-, Verfahrens- und Biotechnik der Universität Stuttgart, Diss.
- [GLW04] *GLWD: Global lakes and wetlands database*. NASA - Goddard Space Flight Center. 2004. – Available online at http://gcmd.nasa.gov/records/GCMD_GLWD.html; visited on November 9th 2012.
- [GSSB11] GERLACH, A.-K. ; STETTER, D. ; SCHMID, J. ; BREYER, Ch. *PV and wind power - complementary technologies*. Proceedings of the 26th European Photovoltaic Solar Energy Conference. 2011

- [GVK97] GOETZBERGER, A. ; VOSS, B. ; KNOBLOCH, J.: *Sonnenenergie: Photovoltaik: Physik und Technologie der Solarzelle*. Second. Teubner, 1997 (Teubner Studienbücher). – ISBN 9783519132141
- [GWE10] *Global Wind energy outlook*. Greenpeace, Global Wind Energy Council. 2010. – Available online at http://www.ewea.org/fileadmin/ewea_documents/documents/publications/reports/purepower.pdf; visited on November 13th 2012.
- [H⁺08] HASSING, C. [u. a.]. *Technical data, costs and life cycle inventories of future offshore wind turbines*. NEEDS, final report prepared for the European Commission. 2008
- [HD07] HUNGER, M. ; DOELL, P.: Value of river discharge data for global-scale hydrological modeling. In: *Hydrology and Earth System Sciences Discussions* 4 (2007), Nr. 6, S. 4125–4173
- [Hei10] HEIDE, D.: *Statistical Physics of Power Flows on Networks with a high Share of Fluctuating Renewable Generation*, Fachbereich Physik der Universität Frankfurt, Diss., 2010
- [Hei12] HEIDE, D. *Update of the REMix modelling environment in terms of adding a new operation and configuration interface including error query and scenario management*. personal communication. 2012
- [HHH⁺03] HAMMER, A. ; HEINEMANN, D. ; HOYER, C. ; KUHLEMANN, R. ; LORENZ, E. ; MUELLER, R. ; BEYER, H.G.: Solar energy assessment using remote sensing technologies. In: *Remote Sensing of Environment* 86 (2003), Nr. 3, S. 423 – 432
- [HK12] HOYER-KLICK, C. *Comparison of various solar resource datasets*. personal communication. 2012
- [HKSS] HOYER-KLICK, C. ; SCHILLINGS, C. ; STETTER, D.: *Scaling in Solar Resource Assessments*. Energy Modelling Forum: Workshop on Climate Change Impacts and Integrated Assessment. – Snowmass, 2012
- [Hof02] HOFMAN, Y. *The potential of solar electricity to reduce CO₂ emissions*. Report no. PH4/14 for the Executive Committee of the IEA Greenhouse Gas R&D Programme. 2002
- [Hoo04] HOOGWIJK, M.: *On the global and regional potential of renewable energy sources*, Universiteit Utrecht, Diss., 2004
- [HPAB78] HALL, I.J. ; PRAIRIE, R.R. ; ANDERSON, H.E. ; BOES, E.C. *Generation of typical meteorological years for 26 SOLMET stations*. Sandia Laboratories Report SAND 78-1601. 1978

- [IBM] *CPLEX: High-performance mathematical programming solver for linear programming, mixed integer programming, and quadratic programming.* IBM ILOG CPLEX Optimizer. – Available online at <http://www-01.ibm.com/software/integration/optimization/cplex-optimizer/>; visited on November 22nd 2012.
- [IEA12] *Golden Rules for a Golden Age of Gas.* International Energy Agency. 2012. – Available online at <http://www.worldenergyoutlook.org/goldenrules/>; visited on November 13th 2012.
- [IMF10] *Deflators.* The International Monetary Fund. 2010. – Available online at <http://www.imf.org>; visited on November 13th 2012.
- [Iqb83] IQBAL, M.: *An introduction to solar radiation.* Academic Press, 1983
- [ISI12] *ISIS: Irradiance at the Surface derived from ISCCP cloud data.* German Aerospace Center DLR - Institute of Atmospheric Physics. 2012. – Available online at <http://www.pa.op.dlr.de/ISIS/>; visited on November 12th 2012.
- [JBMS09] JONKMAN, J. ; BUTTERFIELD, S. ; MUSIAL, W. ; SCOTT, G.: *Definition of a 5-MW Reference Wind Turbine for Offshore System Development.* National Renewable Energy Laboratory - Technical Report. 2009. – Available online at <http://www.nrel.gov/docs/fy09osti/38060.pdf>; visited on November 13th 2012.
- [JTAK06] JACOVIDES, C.P. ; TYMVIOS, F.S. ; ASSIMAKOPOULOS, V.D. ; KALTSOUNIDES, N.A.: Comparative study of various correlations in estimating hourly diffuse fraction of global solar radiation. In: *Renewable Energy* 31 (2006), S. 2492–2504
- [Kal03] KALOGIROU, Soteris A.: Generation of typical meteorological year (TMY-2) for Nicosia, Cyprus. In: *Renewable Energy* 28 (2003), Nr. 15, S. 2317 – 2334. – ISSN 0960–1481
- [KNK⁺09] KREWITT, W. ; NIENHAUS, K. ; KLEMMANN, C. ; CAPONE, C. ; STRICKER, E. ; GRAUS, W. ; HOOGWIJK, M. ; SUPERSBERGER, N. ; VON WINTERFELD, U. ; SAMADI, S. *Role and Potential of Renewable Energy and Energy Efficiency for Global Energy Supply.* 2009
- [Kol06] KOLB, G. *Proposed bench-scale tests to investigate recovery from salt freeze-up events in trough fields.* Trough Workshop in Lake Tahoe. 2006
- [KSW05] KALTSCHMITT, M. ; STREICHER, W. ; WIESE, A.: *Erneuerbare Energien: Systemtechnik, Wirtschaftlichkeit, Umweltaspekte.* Springer, 2005
- [KY89] KASTEN, F. ; YOUNG, A.T.: Revised optical air mass tables and approximation formula. In: *Applied Optics* 28(22) (1989), S. 4735–4738

- [Lai10] LAING, D. *CSP thermal storage systems loss*. personal communication. 2010
- [Lan10] *LandScan - global population distribution*. Oak Ridge National Laboratory. 2010. – Available online at <http://www.ornl.gov/sci/landscan>; visited on November 9th 2012.
- [LCV⁺05a] LECHON, Y. ; CABAL, H. ; VARELA, M. ; SAEZ, R. ; EHERER, C. ; BAUMANN, M. ; DWEKE, J. ; HAMACHER, T. ; TOSATO, G.C.: A global energy model with fusion. In: *Fusion Engineering and Design* 75-79 (2005), S. 1141 – 1144. – Proceedings of the 23rd Symposium of Fusion Technology
- [LCV05b] LEHNER, B. ; CZISCH, G. ; VASSOLO, S.: The impact of global change on the hydropower potential of Europe: a model-based analysis. In: *Energy Policy* 33 (2005), Nr. 7, S. 839 – 855
- [Lei10] *Leitstudie 2010 - Langfristszenarien und Strategien für den Ausbau erneuerbarer Energien in Deutschland bei Berücksichtigung der Entwicklung in Europa und global*. Bundesministerium für Umwelt, Naturschutz und Reaktorsicherheit. 2010. – Available online at http://www.bmu.de/erneuerbare_energien/downloads/doc/47034.php; visited on November 9th 2012.
- [LJ60] LIU, B.Y.H. ; JORDAN, R.C.: The interrelationship and characteristic distribution of direct, diffuse and total solar radiation. In: *Solar Energy* 4 (1960), S. 1–19
- [LMK09] LU, X. ; MCELROY, M.B. ; KIVILUOMA, J.: Global potential for wind-generated electricity. In: *Proceedings of the National Academy of Sciences of the United States of America* (2009)
- [Loh06] LOHMANN, S.: *Langzeitvariabilität der globalen und direkten Solarstrahlung für Solarenergieanwendungen*, Fakultät für Physik der Ludwig-Maximilians-Universität München, Diss., 2006
- [Lux07] VON LUXBURG, U. *A Tutorial on Spectral Clustering*. 2007
- [MEN11] *MENA Regional Water Outlook Part II: Desalination Using Renewable Energy (FINAL REPORT)*. Fichtner. 2011. – Available online at http://www.dlr.de/tt/Portaldata/41/Resources/dokumente/institut/system/projects/MENA_REGIONAL_WATER_OUTLOOK.pdf; visited on November 13th 2012.
- [MER12] *Modern Era Retrospective-analysis for Research and Applications MERRA*. National Aeronautics and Space Agency NASA - Modeling and Assimilation Data and Information Services Center. 2012. – Available online at <http://disc.sci.gsfc.nasa.gov/mdisc/>; visited on November 13th 2012.

- [MGG96] MESSNER, S. ; GOLODNIKOV, A. ; GRITSEVSKII, A.: A stochastic version of the dynamic linear programming model MESSAGE III. In: *Energy* 21 (1996), Nr. 9, S. 775 – 784. – ISSN 0360–5442
- [Mie08] MIE, G.: Beiträge zur Optik trüber Medien, speziell kolloidaler Metallösungen. In: *Annalen der Physik* 25(3) (1908), S. 377–445
- [MM06] MUNEER, T. ; MUNAWWAR, S.: Potential for improvement in solar diffuse irradiance. In: *Energy Conversion and Management* 47 (2006), S. 68–86
- [Mos12] MOSER, M. *CSP assessment tool*. personal communication. 2012
- [MT10] MOSER, M. ; TRIEB, F. *CSP power block efficiencies*. personal communication. 2010
- [MYM06] MUNEER, T. ; YOUNES, S. ; MUNAWWAR, S.: Discourses on solar radiation modeling. In: *Renewable and Sustainable Energy Reviews* 11 (2006), S. 551–602
- [OH76] ORGILL, J.F. ; HOLLANDS, K.G.T.: Correlation equation for hourly diffuse radiation on a horizontal surface. In: *Solar Energy* 19 (1976), S. 357–359
- [OO11] OEDING, D. ; OSWALD, B.R.: *Elektrische Kraftwerke und Netze*. Springer, 2011
- [P2G] *Verbundprojekt "Power2Gas"*. Zentrum für Sonnenenergie - und Wasserstoffforschung Baden-Württemberg. – Available online at <http://www.zsw-bw.de/themen/brennstoffe-wasserstoff/power-to-gas.html>; visited on December 29th 2012.
- [Pau07] PAUL, C. *Bilanzierungsmodell zur Bestimmung der regenerativen Stromüberschüsse der MENA Region im Jahr 2050*. Studienarbeit Nr. 2007-6, Universität Stuttgart. 2007
- [PJ] POSSOZ, L. ; JEANMART, H.: Comments on the electricity demand scenario in two studies from the DLR : MED CSP & TRANS CSP.
- [PL08] PALMINTIER, B ; LEVINE, J. *Spatial and temporal interactions of solar and wind resources in the next generation utility*. Proceedings of the American Solar Energy Society (ASES) Solar Conference. 2008
- [PLK⁺02] PRICE, H. ; LÜPFERT, E. ; KEARNEY, D. ; ZARZA, E. ; COHEN, G. ; GEE, R. ; MAHONEY, R.: Advances in Parabolic Trough Solar Power Technology. In: *Journal of Solar Energy Engineering* 124 (2002), Nr. 2, S. 109–125
- [Qua06] QUASCHNING, V.: *Regenerative Energiesysteme*. Hanser, 2006

- [RAA⁺10] RUIZ-ARIAS, J.A. ; ALSAMAMRA, H. [u. a.]: Proposal of a regressive model for the hourly diffuse solar radiation under all sky conditions. In: *Energy Conversion and Management* 51 (2010), S. 881–893
- [RBD90] REINDL, D.T. ; BECKMAN, W. A. ; DUFFIE, J. A.: Diffuse fraction correlations. In: *Solar Energy* 45 (1990), S. 1–7
- [RBW00] RIGOLLIER, C. ; BAUER, O. ; WALD, L.: On the clear sky model of the ESRA European Solar Radiation Atlas with respect to the heliosat method. In: *Solar Energy* 68 (2000), Nr. 1, S. 33 – 48
- [REA11] *REACCESS: Risk of energy availability common corridors for Europe Supply security*. EU - Seventh Framework Programme. 2011. – Available online at <http://reaccess.epu.ntua.gr/LinkClick.aspx?fileticket=ez26yrSc0cg%3d&tabid=721>; visited on November 9th 2012.
- [Rog00] ROGNER, H.-H.: *World Energy Assessment - energy and the challenge of sustainability, Chapter 5: Energy Resources*. United Nations Development Programme. 2000. – Available online at <http://www.ornl.gov/sci/landscan>; visited on November 9th 2012.
- [S99] SRENSEN, B. *Low energy consumption scenarios*. IPCC Expert Meeting on Mitigation and Stabilisation Scenarios. 1999
- [Sar09] *Assessment of Parabolic Trough, Power Tower, and Dish Solar Technology Cost and Performance Forecasts 2008*. Sargent&Lundy. 2009
- [SBP⁺08] SIMONSEN, I. ; BUZNA, L. ; PETERS, K. ; BORNHOLDT, S. ; HELBING, D.: Transient Dynamics Increasing Network Vulnerability to Cascading Failures. In: *Phys. Rev. Lett.* 100 (2008), May, S. 218701
- [Sch09a] SCHOLZ, Y. *Portfolio dispatch: Example using conventional and renewable power generation technologies*. personal communication. 2009
- [Sch09b] SCHWAB, A.J.: *Elektroenergiesysteme: Erzeugung, Transport, Übertragung und Verteilung elektrischer Energie*. Springer-Verlag GmbH, 2009
- [Sch12] SCHOLZ, Y.: *Renewable energy based electricity supply at low cost - Development of the REMix model and application for Europe*, Fakultät für Energie-, Verfahrens- und Biotechnik der Universität Stuttgart, Diss., 2012
- [SGS01] SEEBREGTS, A.J. ; GOLDSTEIN, G.A. ; SMEKENS, K.: *Energy / Environmental Modeling with the MARKAL Family of Models*. Proceedings of the OR2001 Conference, Energy and Environment Session. 2001. – Available online at <http://ftp.ecn.nl/pub/www/library/report/2001/rx01039.pdf>; visited on November 8th 2012.

- [SGS11] STETTER, D. ; GAMBA, N. ; SCHUELER, V. *Global GIS-based inventory of renewable resources in high spatial and temporal resolution*. Umweltbundesamt Dessau. 2011
- [SJA09] STOTT, B. ; JARDIM, J. ; ALSA: DC Power Flow Revisited. In: *IEEE Transactions on power systems* 24(3) (2009), S. 1290–1300
- [SKB12] SCHMID, E. ; KNOPF, B. ; BAUER, N.: *ReMIND-D: A Hybrid Energy-Economy Model of Germany*. Potsdam Institute for Climate Impact Research. 2012. – Available online at <http://www.pik-potsdam.de/research/sustainable-solutions/models/remind-d-documentation.html>; visited on December 30th 2012.
- [SOD] *SoDa - a project for the integration and exploitation of networked solar radiation databases*. Website. – Available online at <http://www.soda-is.com>; visited on November 13th 2012.
- [Sok04] *Sokrates-Projekt - AP 2.1*. Bundesministerium für Umwelt, Naturschutz und Reaktorsicherheit. 2004. – Available online at http://www.dlr.de/tt/Portaldata/41/Resources/dokumente/institut/system/projects/AP_2_1_Modellbildung.pdf; visited on November 9th 2012.
- [SOL12] *Solar Energy Mining SOLEMI*. German Aerospace Center DLR - The World Data Center for Remote Sensing of the Atmosphere. 2012. – Available online at http://wdc.dlr.de/data_products/SERVICES/SOLARENERGY/description.php; visited on November 12th 2012.
- [SRB12] *Surface Radiation Budget Release 3.0*. National Aeronautics and Space Agency NASA, Atmospheric Science Data Center. 2012. – Available online at http://eosweb.larc.nasa.gov/PRODOCS/srb/table_srb.html; visited on November 12th 2012.
- [SRU10] *100% erneuerbare Stromversorgung bis 2050: Klimaverträglich, sicher, bezahlbar*. Sachverständigenrat für Umweltfragen. 2010. – Available online at http://www.bmu.de/erneuerbare_energien/downloads/doc/47034.php; visited on November 9th 2012.
- [SSE12] *Surface Meteorology and Solar Energy: Methodology*. National Aeronautics and Space Agency NASA. 2012. – Available online at <http://eosweb.larc.nasa.gov/sse/documents/SSE6Methodology.pdf>; visited on November 12th 2012.
- [Ste07] STETTER, D. *Analyse und Optimierung des temperaturabhängigen Verhaltens von III-V Solarzellen*. Fakultät für Physik der Universität Karlsruhe (Karlsruhe Institute of Technology). 2007

- [Str11] STRACHAN, N.: *UKERC Energy Research Landscape: Energy Systems Modeling*. Website. 2011. – Available online at <http://ukerc.rl.ac.uk/Landscapes/Modelling.pdf>; visited on November 8th 2012.
- [Str12] STRACHAN, N.: *European Network of Transmission System Operators for Electricity*. Website. 2012. – Available online at <https://www.entsoe.eu/resources/ntc-values/ntc-matrix/>; visited on November 12th 2012.
- [Ten12] LUCA DE TENA, D.: *to be submitted (unpublished): Perspectives of electric/hybrid vehicles in a supply system with a high share of renewable energy sources*, Fakultät für Energie-, Verfahrens- und Biotechnik der Universität Stuttgart, Diss., 2012
- [TK] TRIEB, F. ; KLANN, U.: *Wind Turbine Economic Feasibility Calculator*. Website. – Available online at <http://www.windmeasurementinternational.com/windturbines/om-turbines.php>.; visited on December 30th 2010.
- [TK06] TRIEB, F. ; KLANN, U. *Modelling the future electricity demand of Europe, Middle East and North Africa*. DLR: Internal Report. 2006
- [TMS07] TRIEB, F. ; MÜLLER-STEINHAGEN, H.: *Sustainable Electricity and Water for Europe, Middle East and North Africa*. German Aerospace Center. 2007. – Available online at <http://www.dlr.de/tt>; visited on December 29th 2012.
- [Tri12] TRIEB, F. *Update of the original TRANS-CSP framework & establishment of three new scenario pathways*. personal communication. 2012
- [TSK⁺05] TRIEB, F. ; SCHILLINGS, C. ; KRONSHAGE, S. ; VIEBAHN, P. ; KABARITI, M. ; K.M., Daoud ; BENNOUNA, A. ; EL NOKRASCHY, H. ; HASSAN, S. ; YUSSEF, L.G. ; HASNI, T. ; EL BASSAM, N. ; SATOQUINA, H. *Concentrating Solar Power for the Mediterranean Region: MED-CSP*. German Federal Ministry of the Environment, Nature Conservation and Nuclear Safety. 2005
- [TSK⁺06] TRIEB, F. ; SCHILLINGS, C. ; KRONSHAGE, S. ; KLANN, U. ; VIEBAHN, P. ; MAY, N. ; WILDE, R. ; PAUL, C. ; KABARITI, M. ; BENNOUNA, A. ; EL NOKRASCHY, H. ; HASSAN, S. ; YUSSEF, L.G. ; HASNI, T. ; EL BASSAM, N. ; SATOQUINA, H. *Trans-Mediterranean Interconnection for Concentrating Solar Power: TRANS-CSP*. German Federal Ministry of the Environment, Nature Conservation and Nuclear Safety. 2006
- [TSO⁺09] TRIEB, F. ; SCHILLINGS, C. ; OSULLIVAN, M. ; PREGGER, T. ; HOYER-KLICK, C.: *Global Potential of Concentrating Solar Power*. In: *SolarPaces Conference* (2009)

- [TSPO12] TRIEB, F. ; SCHILLINGS, C. ; PREGGER, T. ; O’SULLIVAN, M.: Solar electricity imports from the Middle East and North Africa to Europe. In: *Energy Policy* 42 (2012), S. 341–353
- [Tur12] *Enercon E82 - 2MW wind turbine*. Website. 2012. – Available online at <http://www.enercon.de/de-de/62.htm>; visited on December 13th 2012.
- [Ung10] UNGER, T.: *Coordinated Use of Energy System Models in Energy and Climate Policy Analysis: Lessons Learned from the Nordic Energy Perspectives Project*. Profu, 2010
- [VHVP⁺06] VAN HERTEM, D. ; VERBOOMEN, J. ; PURCHALA, K. ; BELMANS, R. ; KLING, W.L.: Usefulness of DC power flow for active power flow analysis with flow controlling devices. In: *AC and DC Power Transmission, 2006. ACDC 2006. The 8th IEE International Conference on Power Transmission*, 2006. – ISSN 0537–9989, S. 58 – 62
- [VKTL08] VIEBAHN, P. ; KRONSHAGE, S. ; TRIEB, F. ; LECHON, Y. *Technical data, costs and life cycle inventories of solar thermal power plants*. NEEDS, final report prepared for the European Commission. 2008
- [Voo82] VAN DER VOORT, E.: The EFOM 12C energy supply model within the EC modelling system. In: *Omega* 10 (1982), Nr. 5, S. 507 – 523
- [WDP10] *World database on protected areas*. 2010. – Available online at <http://www.wdpa.org>; visited on November 9th 2012.
- [WEC10] *2010 Survey of Energy Resources*. World Energy Council - Conseil Mondial de l’Energie. 2010. – Available online at http://www.worldenergy.org/documents/ser_2010_report_1.pdf; visited on November 9th 2012.
- [WEO05] *World Energy Outlook*. International Energy Agency. 2005. – Available online at <http://www.worldenergyoutlook.org>; visited on December 29th 2012.
- [WEP09] *World Electric Power Plants Database*. PLATTS. 2009. – Available online at <http://www.platts.com/Products/worldelectricpowerplantsdatabase>; visited on November 9th 2012.
- [Wer12] WERNER, F. *Renewable Portfolio Optimization Strategies - A case study on Photovoltaics and Wind Energy in Germany*. Master Thesis, Lehrstuhl für Reaktorsicherheit und -technik der RWTH Aachen. 2012
- [WFBV10] WISSEL, S. ; FAHL, U. ; BLES, M. ; VOSS, A.: *Erzeugungskosten zur Bereitstellung elektrischer Energie von Kraftwerksoptionen in 2015*. Institut für Energiewirtschaft und Rationelle Energieanwendung der Universität Stuttgart - Arbeitsbericht. 2010. –

Available online at http://www.ier.uni-stuttgart.de/publikationen/arbeitsberichte/Arbeitsbericht_08.pdf; visited on November 13th 2012.

- [WIN12] *Earth's major wind systems*. National Aeronautics and Space Agency NASA. 2012. – Available online at <http://sealevel.jpl.nasa.gov/overview/climate-climatic.htmlsealevel.jpl.nasa.gov>; visited on November 12th 2012.
- [WM08] WILCOX, S. ; MARION, W.: *Users Manual for TMY3 Data Sets Users Manual for TMY3 Data Sets*. Website. 2008. – Available online at <http://www.nrel.gov/docs/fy08osti/43156.pdf>; visited on November 13th 2012.
- [Wor12] *Worldwatch Institute - Vital signs online*. Global hydropower installed capacity and use increase. 2012. – Available online at <http://vitalsigns.worldwatch.org/vs-trend/global-hydropower-installed-capacity-use-increase>; visited on May 13th 2014.
- [WRF12] *WRF: Weather Research and Forecasting*. National Center for Atmospheric Research (NCAR), National Oceanic and Atmospheric Administration, National Centers for Environmental Prediction (NCEP), Forecast Systems Laboratory (FSL), Air Force Weather Agency (AFWA), Naval Research Laboratory, University of Oklahoma and the Federal Aviation Administration (FAA). 2012. – Available online at <http://www.wrf-model.org/index.php>; visited on November 13th 2012.
- [WW96] WOOD, A.J. ; WOLLENBERG, B.F.: *Power Generation, Operation, and Control*. Wiley, 1996 (A Wiley Interscience publication)
- [YCT05] YOUNES, S. ; CLAYWELL, R. ; T., Muneer: Quality control of solar radiation data: Present status and proposed new approaches. In: *Energy* 30 (2005), S. 1533–1549

A. Annex

A.1. Physical principles of solar irradiance

Compared to other renewable energy sources¹, the sun is by far the predominant provider of energy to earth. By approximating its isotropically emitted energy originating from fusion processes as blackbody radiation, the law of Stefan-Boltzmann can be applied yielding an effective surface temperature of 5777 K, while its interior temperatures are estimated to be in the range of 8 to $40 \cdot 10^6$ K [DB91].

Moreover, according to this law, the radiative emission is determined by the temperature of the black body sun and the distance between its surface and the radiation receiver. The radiation intensity decreases with the inverse square of that distance. In particular, the spectral irradiance of the system sun-earth obeys the following formula [GVK97]:

$$I_{sc} = \pi r_{sun}^2 \frac{r_{earth}^2}{R_{sun-earth}^2} \sigma T_{sun}^4 \quad (\text{A.1})$$

The latter expression yields the average extraterrestrial radiation I_{sc} impacting earth. Apart from the radii of the sun r_{sun} and earth r_{earth} , the temperature at the surface of the black body sun T_{sun} are considered. Using an average value² of $1.496 \cdot 10^{11}$ m for the distance between the sun and the earth $R_{sun-earth}$ and taking into account that the radiation on earth can only be received within a solid angle of 0.54° , the irradiance at the top of the atmosphere amounts to $1.367 \frac{kW}{m^2}$, this figure is also referred to as the solar constant I_{sc} . The respective spectrum is called AM0, since no air mass is encountered at that point. Two effects influence the extraterrestrial radiation: According to various observations [DB91] variations in the range of $\pm 1.5\%$ with different periodicities are due to sunspot activities. From an engineering point of view, these variations are negligible, particularly bearing in mind that the influence of atmospheric effects are much more significant [DB91]. However, the interannual variation of the distance between the sun and earth $R_{sun-earth}$ which is due to the elliptical course of earth's orbit leads to a periodic deviation of $\pm 3\%$, which can be expressed by the solar excentricity factor ϵ_{solar} :

$$\epsilon_{solar} = 1 + 0.033 \cdot \cos\left(\frac{2\pi \cdot doy}{365}\right) \quad (\text{A.2})$$

with *doy* representing the day of year. Thus the extraterrestrial radiation at the top of the atmosphere I_{toa} is obtained by:

$$I_{toa} = \epsilon_{solar} \cdot I_{sc} \quad (\text{A.3})$$

¹geothermal or gravitational energy are further observable and tappable renewable resources occurring on earth.

²The distances at the perihel and aphel of earth's orbit are 1.475 and $1.525 \cdot 10^{11}$ m respectively.

By crossing earth's atmosphere constituting an optically active medium, the incident radiation I_{toa} is diminished and finally yields the global horizontal irradiance (GHI) at the surface I_{GHI} according to the law of Lambert-Beer:

$$I_{GHI} = I_{toa} \cdot \exp(-\tau_z) \quad (\text{A.4})$$

with τ_z representing the optical thickness of the atmosphere and z its depth:

$$\tau_z = \int_0^z k_{extinction} dz' \quad (\text{A.5})$$

$k_{extinction}$ is the extinction coefficient, which can be expressed as the sum of the absorption and scattering coefficients [Loh06]. The following scattering, absorption and accordingly (re-)emission effects are distinguished:

- Absorption of photons occurs if the energy of the incident light corresponds to an energy level of the electrons of the matter concerned, which can be derived according to the rules of quantum mechanics [CTDL77]. The absorption process transfers the energy of the photon to the electron, which in turn is excited to a higher energy state. Reemission occurs when an excited electron descends to an energetically inferior state by sending out a photon with an energy equal to the difference of its pre and post states. Different bands mainly due to absorption by water, oxygen and ozone can therefore be identified in the spectrum of the incident light³.
- Scattering effects lead to a decomposition of the irradiance into a diffuse and direct (beam) component. The energy and thus the wavelength of the scattered wave are not effected, merely their direction is changed. Depending on the wavelength and the size of the scattering particle, the incidenting light is subject to Rayleigh or Mie scattering [Loh06; Mie08].

An overview of earth's energy budget is depicted in figure A.1, further information can be retrieved from [SSE12].

³For calibrations and calculations based upon global horizontal irradiance the standard spectrum AM1.5g and for those based on beam normal irradiance the standard spectrum AM1.5d are used respectively [Ste07].

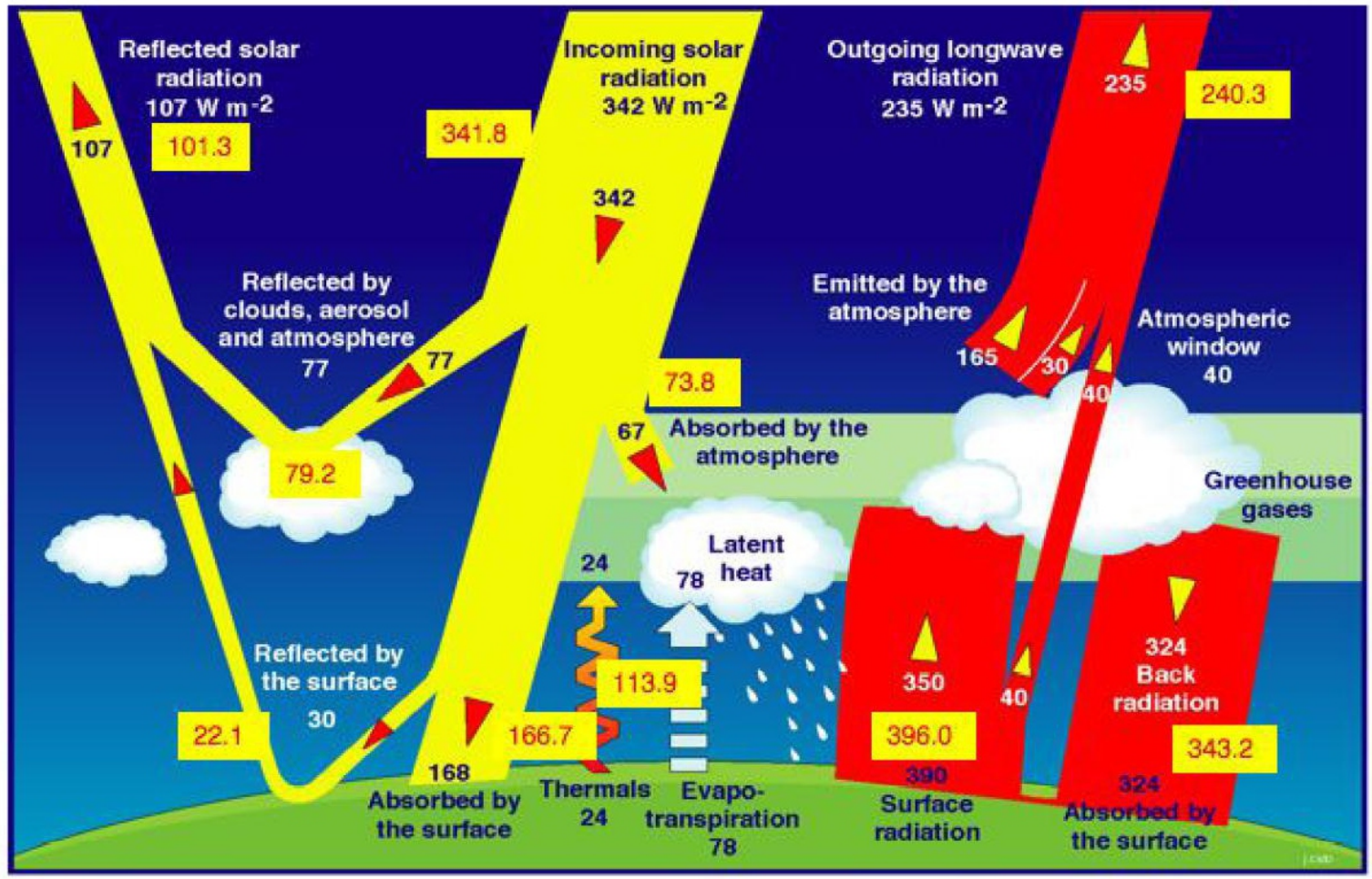


Figure A.1.: Description of the major components of earth's energy budget [SSE12]. Incoming irradiation is absorbed, scattered and reflected due to various mechanisms. The values indicated in yellow boxes (all in $[\frac{W}{m^2}]$) are derived from the NASA Solar Radiation Budget Release 3.0 [SRB12], serving as input for parts of the assessment within this work.

The irradiance received by the surface of earth is generally characterized by indicating horizontal and direct (beam) components of the direct (beam), diffuse and global irradiances. In order to compute the amount of radiation striking a tilted surface, both components diffuse and beam irradiance are required since the different physical nature of the latter determines as to how a projection on the surface has to be conducted [RAA⁺10]. The global horizontal irradiance (GHI) I_{GHI} is the sum of the beam horizontal irradiance (BHI) I_{BHI} and the diffuse horizontal irradiance (DHI) I_{DHI} :

$$I_{GHI} = I_{BHI} + I_{DHI} \quad (\text{A.6})$$

The beam normal irradiance (BNI) I_{BNI} is equal to the beam horizontal irradiance (BHI) I_{BHI} over the sine of the solar elevation angle $\alpha_{elevation}$, the latter representing the angle between the sun's position in the sky and the horizon:

$$I_{BNI} = \frac{I_{BHI}}{\sin(\alpha_{elevation})} \quad (\text{A.7})$$

A.2. Global potential assessment in terms of 10 OECD regions

A graphical overview of the world regions is given in figure 3.22 in subsection 3.3.2. In the following table A.1 each world region is presented in terms of the countries it is constituted of in accordance to the International Energy Agency's World Energy Outlook [WEO05] definition.

According to this definition, the following results for the respective world regions as presented in figures A.2 through A.11 are obtained for the full load hour and cost potentials.

World region	Constituting countries
OECD Europe	Austria, Belgium, Czech Republic, Denmark, Finland, France, Germany, Greece, Hungary, Iceland, Ireland, Italy, Luxembourg, the Netherlands, Norway, Poland, Portugal, Slovak Republic, Spain, Sweden, Switzerland, Turkey, United Kingdom
OECD North America	Canada, Mexico, United States of America (metropolitan US and Alaska)
OECD Pacific	Australia, Japan, New Zealand, South Korea
Transition Economies	Albania, Armenia, Azerbaijan, Belarus, Bosnia-Herzegovina, Bulgaria, Croatia, Cyprus, Estonia, Georgia, Kazakhstan, Kyrgyzstan, Latvia, Lithuania, the former Republic of Macedonia, Malta, Moldova, Romania, Russia, Serbia and Montenegro, Slovenia, Tajikistan, Turkmenistan, Ukraine, Uzbekistan
China	People's Republic of China (including Hong Kong)
India	India
Rest of developing Asia	Afghanistan, Bangladesh, Bhutan, Brunei, Cambodia, Chinese Taipei, Fiji, French Polynesia, Indonesia, Kiribati, Democratic People's Republic of Korea, Laos, Macao, Malaysia, Maldives, Mongolia, Myanmar, Nepal, New Caledonia, Pakistan, Papua New Guinea, Philippines, Samoa, Singapore, Solomon Islands, Sri Lanka, Thailand, Vanuatu, Vietnam
Latin America	Antigua and Barbuda, Argentina, Bahamas, Barbados, Belize, Bermuda, Bolivia, Brazil, Chile, Colombia, Costa Rica, Cuba, Dominica, Dominican Republic, Ecuador, El Salvador, French Guiana, Grenada, Guadeloupe, Guatemala, Guyana, Haiti, Honduras, Jamaica, Martinique, Netherlands Antilles, Nicaragua, Panama, Paraguay, Peru, St. Kitts-Nevis-Anguila, St. Lucia, St. Vincent and Grenadines, Suriname, Trinidad and Tobago, Uruguay, Venezuela
Africa	Algeria, Angola, Benin, Botswana, Burkina Faso, Burundi, Cameroon, Cape Verde, Central African Republic, Chad, Comoros, Congo, Democratic Republic of Congo, Cote d'Ivoire, Djibouti, Egypt, Equatorial Guinea, Eritrea, Ethiopia, Gabon, Gambia, Ghana, Guinea, Guinea-Bissau, Kenya, Lesotho, Liberia, Libya, Madagascar, Malawi, Mali, Mauritania, Mauritius, Morocco, Mozambique, Namibia, Niger, Nigeria, Réunion, Rwanda, Sao Tome and Principe, Senegal, Seychelles, Sierra Leone, Somalia, South Africa, Sudan, Swaziland, United Republic of Tanzania, Togo, Tunisia, Uganda, Zambia, Zimbabwe
Middle East	Bahrain, Iran, Iraq, Israel, Jordan, Kuwait, Lebanon, Oman, Qatar, Saudi Arabia, Syria, United Arab Emirates, Yemen

Table A.1.: World regions used for the potential assessments in this work [SGS11].

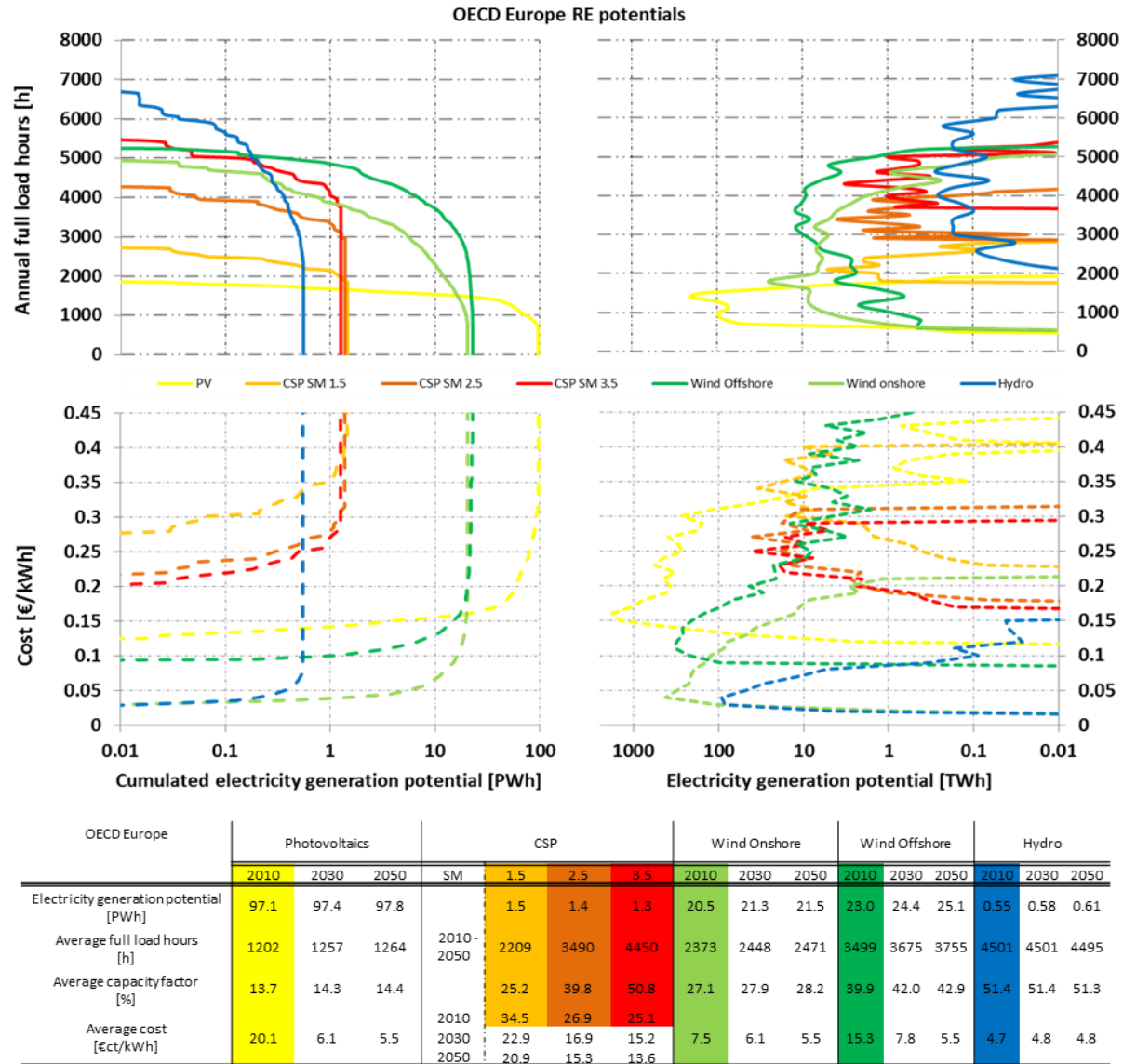
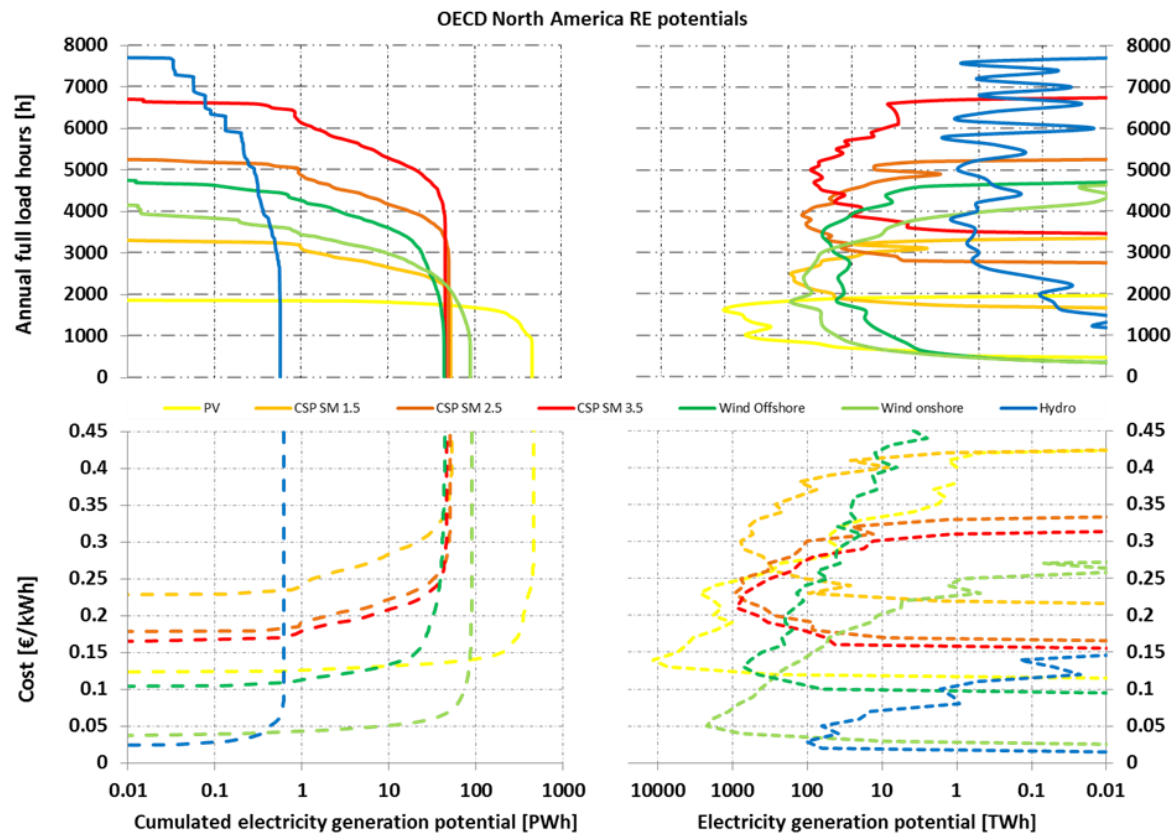
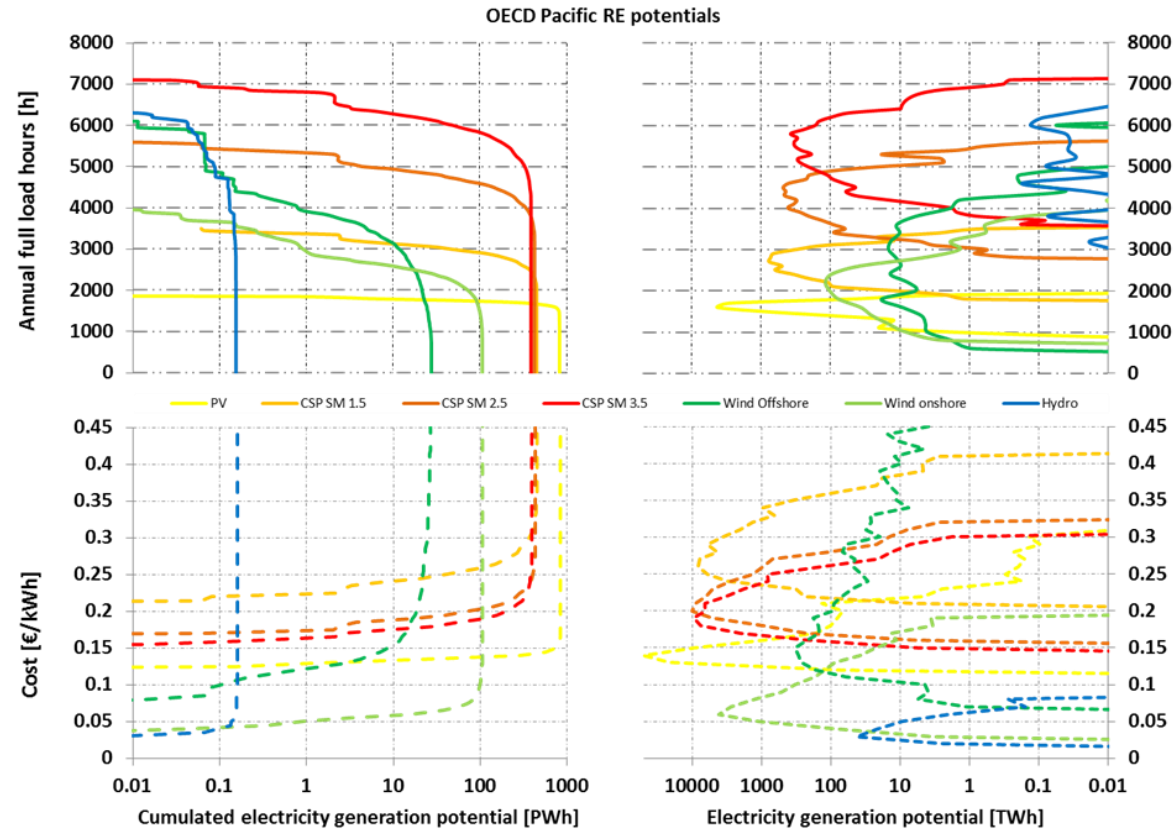


Figure A.2.: OECD Europe: Results of electricity generation potentials for the technologies photovoltaic, concentrating solar power, on- and offshore wind and hydro power. The two figures on the left are expressed in terms of cumulated potentials, the top graphs are indicated as a function of full load hours, the bottom graphs as a function of cost.



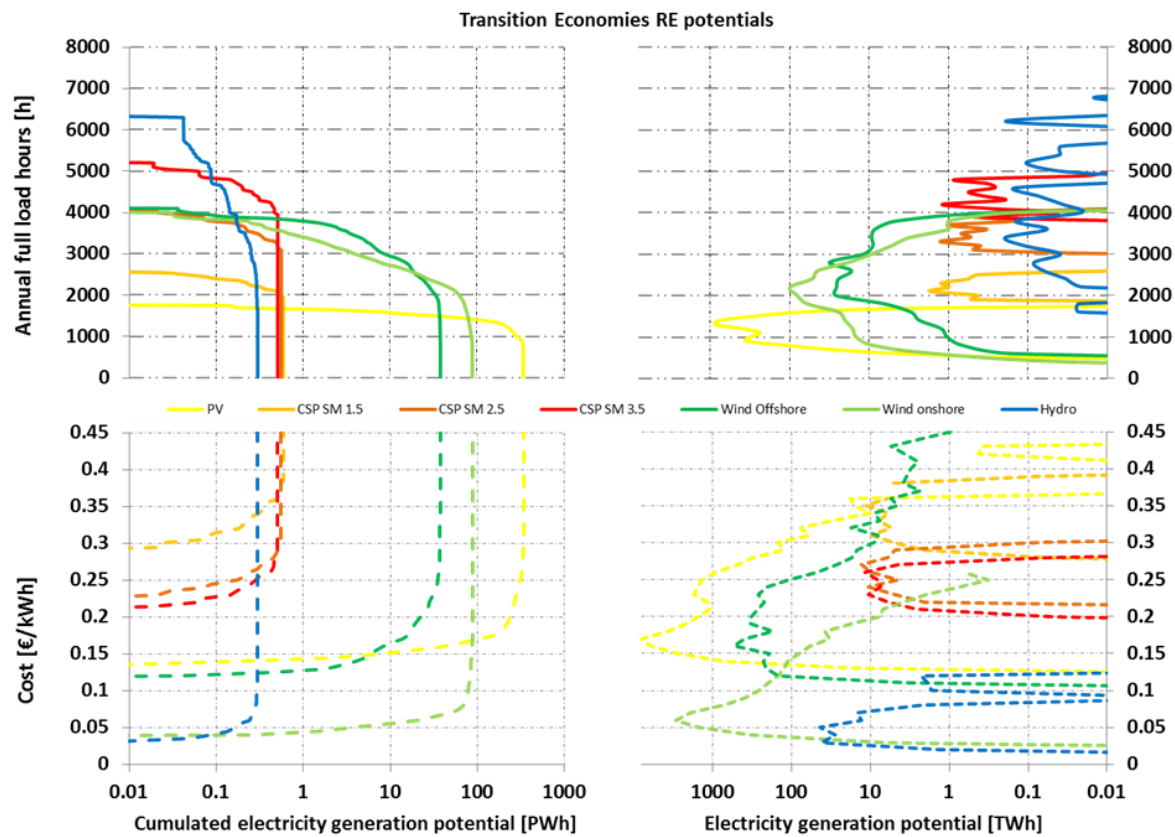
OECD North America	Photovoltaics			SM	CSP			Wind Onshore			Wind Offshore			Hydro		
	2010	2030	2050		1.5	2.5	3.5	2010	2030	2050	2010	2030	2050	2010	2030	2050
Electricity generation potential [PWh]	462.0	464.1	466.3		53	50	46	89.5	92.7	93.7	44.7	48.0	49.5	0.57	0.60	0.68
Average full load hours [h]	1406	1466	1476	2010-2050	2460	3886	4955	2213	2285	2307	2947	3124	3205	4931	4931	5109
Average capacity factor [%]	16.0	16.7	16.8		28.1	44.4	56.6	25.3	26.1	26.3	33.6	35.7	36.6	56.3	56.3	58.3
Average cost [€/kWh]	17.1	5.2	4.7	2010	31.1	24.3	22.6	7.6	6.2	5.7	18.3	9.3	6.5	4.3	4.3	4.4
				2030	20.7	15.3	13.7									
				2050	18.9	13.8	12.2									

Figure A.3.: OECD North America: Results of electricity generation potentials for the technologies photovoltaic, concentrating solar power, on- and offshore wind and hydro power. The two figures on the left are expressed in terms of cumulated potentials, the top graphs are indicated as a function of full load hours, the bottom graphs as a function of cost.



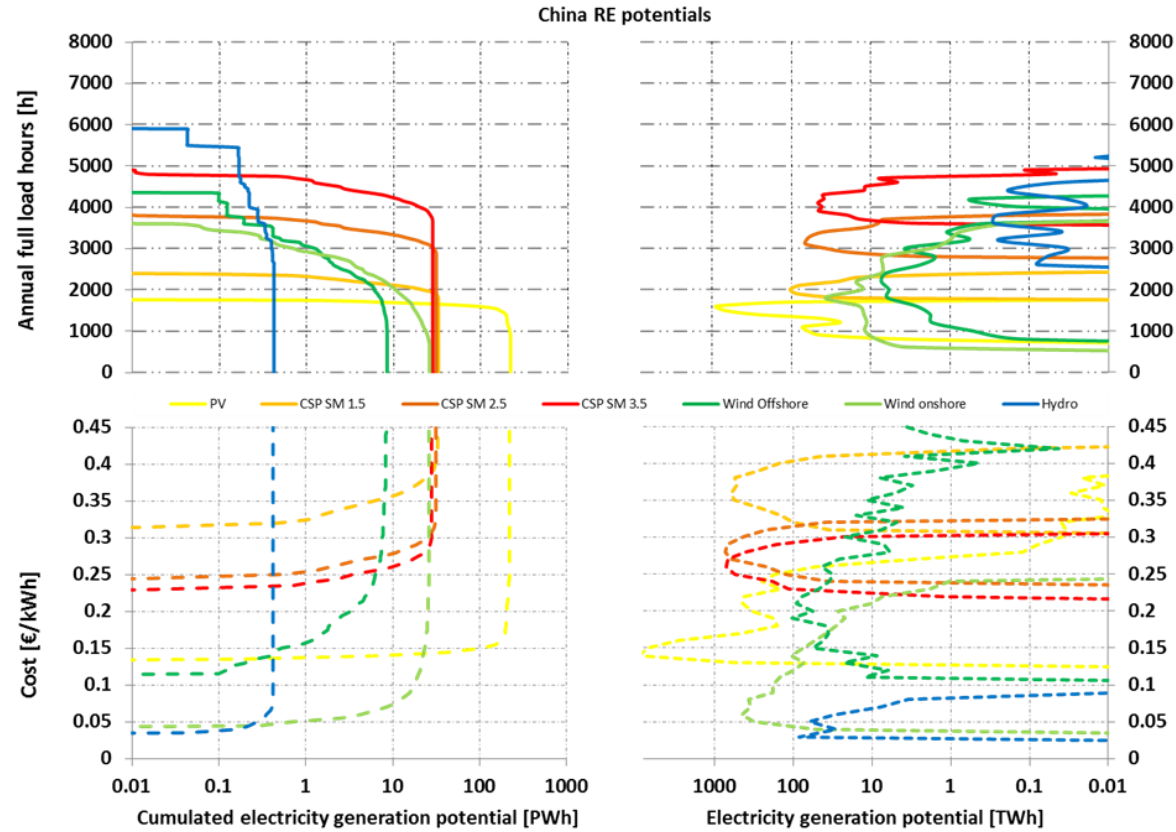
OECD Pacific	Photovoltaics			CSP			Wind Onshore			Wind Offshore			Hydro			
	2010	2030	2050	SM	1.5	2.5	3.5	2010	2030	2050	2010	2030	2050	2010	2030	2050
Electricity generation potential [PWh]	831.3	843.3	855.3		451.7	428.0	389.7	106.6	110.9	112.0	27.6	29.8	30.9	0.16	0.16	0.17
Average full load hours [h]	1620	1693	1717	2010-2050	2725	4304	5487	2147	2230	2256	2718	2902	2988	5170	5232	5232
Average capacity factor [%]	18.5	19.3	19.6		31.1	49.1	62.6	24.5	25.5	25.7	31.0	33.1	34.1	59.0	59.7	59.7
Average cost [€/kWh]	14.4	4.3	3.9	2010	28.0	21.8	20.3									
				2030	18.6	13.7	12.3	7.4	6.0	5.4	20.4	10.3	7.1	3.9	3.9	4.0
				2050	17.0	12.4	11.0									

Figure A.4.: OECD Pacific: Results of electricity generation potentials for the technologies photovoltaic, concentrating solar power, on- and offshore wind and hydro power. The two figures on the left are expressed in terms of cumulated potentials, the top graphs are indicated as a function of full load hours, the bottom graphs as a function of cost.



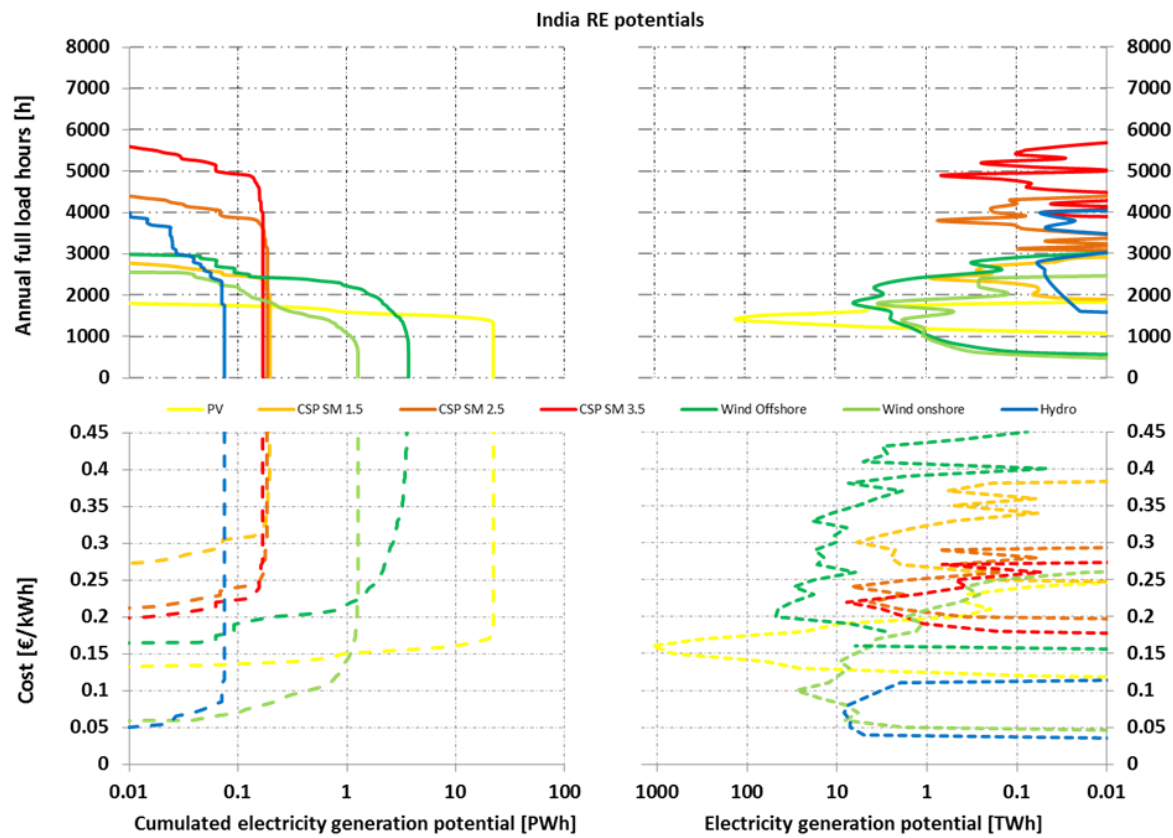
Transition Economies	Photovoltaics			SM	CSP			Wind Onshore			Wind Offshore			Hydro		
	2010	2030	2050		1.5	2.5	3.5	2010	2030	2050	2010	2030	2050	2010	2030	2050
Electricity generation potential [PWh]	341.0	341.3	341.6		0.6	0.6	0.5	88.4	91.5	92.5	38.0	40.8	42.2	0.30	0.31	0.33
Average full load hours [h]	1226	1279	1281	2010-2050	2244	3544	4519	2177	2249	2271	2619	2796	2879	4253	4253	4253
Average capacity factor [%]	14.0	14.6	14.6		25.6	40.5	51.6	24.8	25.7	25.9	29.9	31.9	32.9	48.5	48.5	48.5
Average cost [€/kWh]	19.3	5.9	5.4	2010	33.9	26.4	24.6	7.6	6.1	5.6	19.6	9.9	6.9	5.1	5.2	5.2
				2030	22.5	16.6	14.9									
				2050	20.6	15.0	13.3									

Figure A.5.: Transition Economies: Results of electricity generation potentials for the technologies photovoltaic, concentrating solar power, on- and offshore wind and hydro power. The two figures on the left are expressed in terms of cumulated potentials, the top graphs are indicated as a function of full load hours, the bottom graphs as a function of cost.



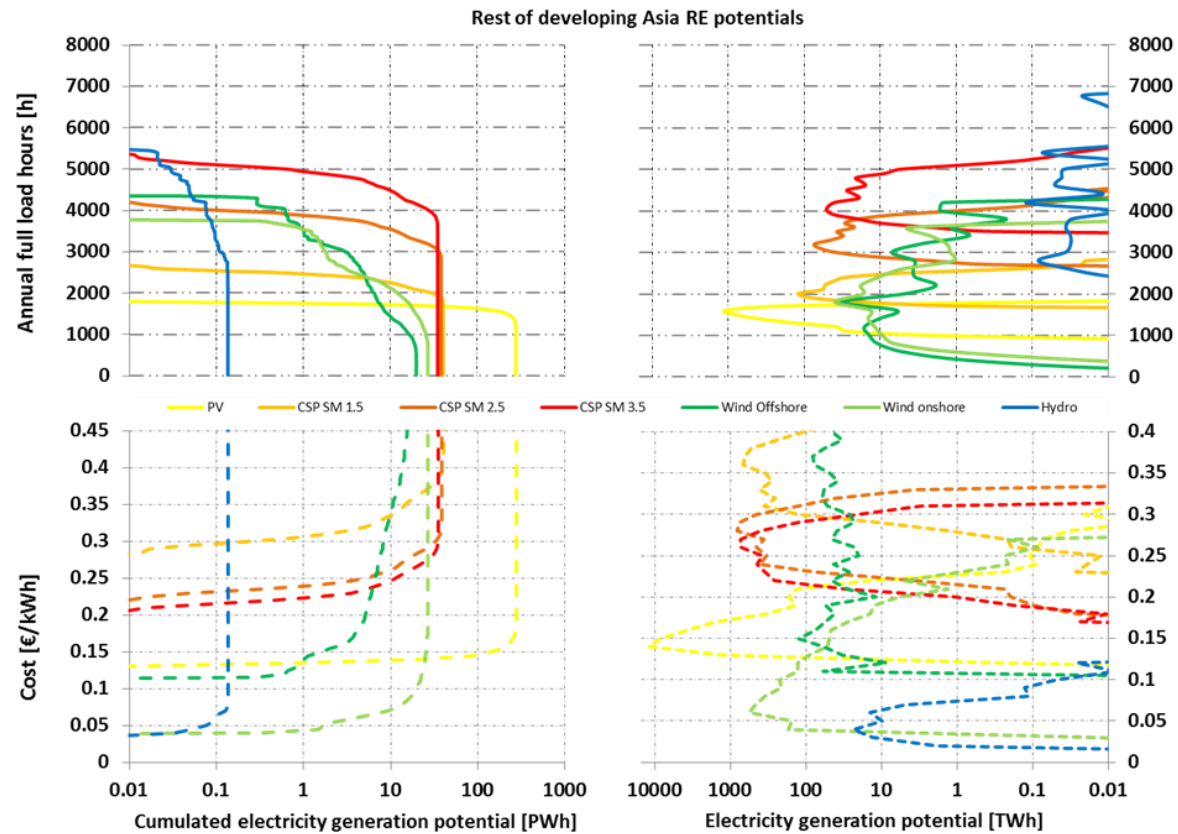
China	Photovoltaics			SM	CSP			Wind Onshore			Wind Offshore			Hydro		
	2010	2030	2050		1.5	2.5	3.5	2010	2030	2050	2010	2030	2050	2010	2030	2050
Electricity generation potential [PWh]	220.5	221.2	222.0		32.7	30.9	28.2	25.8	26.8	27.1	48.4	9.2	9.6	0.50	0.44	0.46
Average full load hours [h]	1486	1542	1547	2010-2050	2063	3259	4155	1858	1922	1941	2325	2500	2581	4445	4444	4445
Average capacity factor [%]	17.0	17.6	17.7		23.6	37.2	47.4	21.2	21.9	22.2	26.5	28.5	29.5	50.7	50.7	50.7
Average cost [€/kWh]	15.8	4.8	4.3	2010	36.8	28.7	26.7									
				2030	24.5	18.1	16.2	9.4	7.6	6.9	22.3	11.2	7.8	4.7	4.8	4.8
				2050	22.3	16.3	14.4									

Figure A.6.: China: Results of electricity generation potentials for the technologies photovoltaic, concentrating solar power, on- and offshore wind and hydro power. The two figures on the left are expressed in terms of cumulated potentials, the top graphs are indicated as a function of full load hours, the bottom graphs as a function of cost.



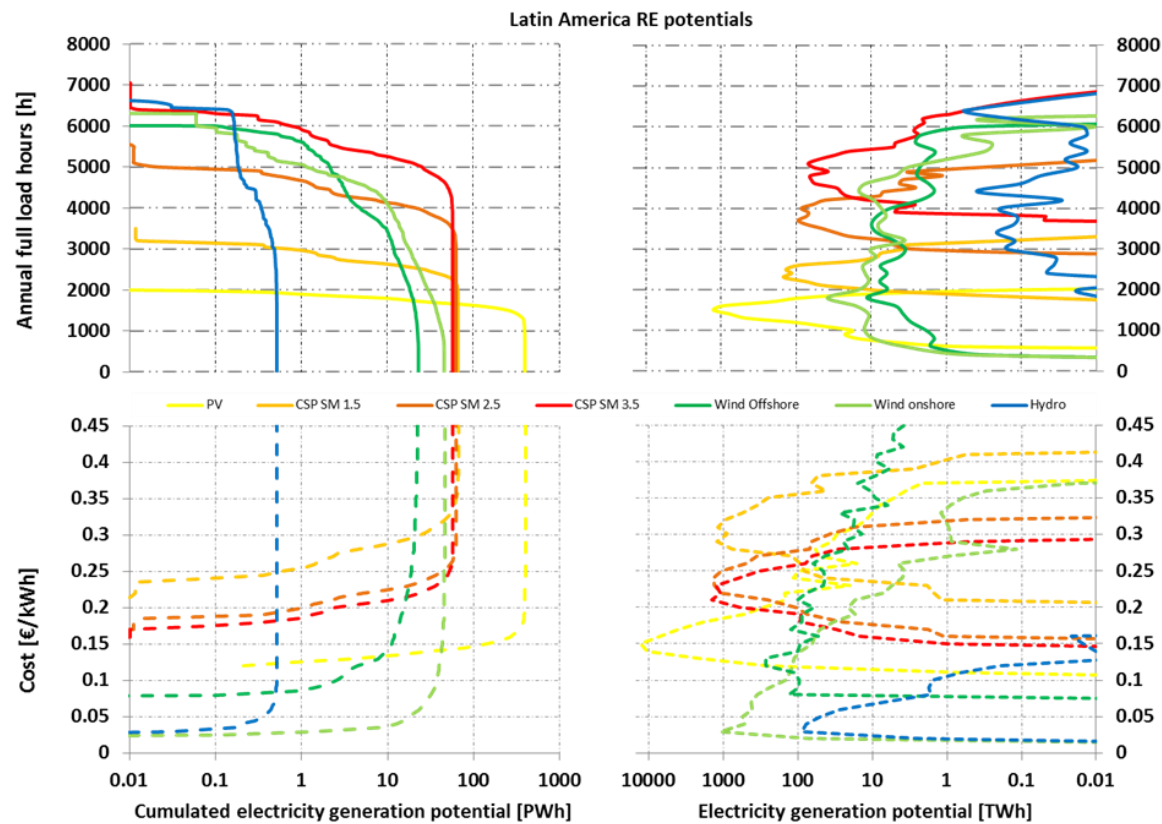
India	Photovoltaics			CSP			Wind Onshore			Wind Offshore			Hydro			
	2010	2030	2050	SM	1.5	2.5	3.5	2010	2030	2050	2010	2030	2050	2010	2030	2050
Electricity generation potential [PWh]	22.4	22.7	23.0		0.2	0.2	0.2	1.3	1.3	1.3	3.7	4.0	4.2	0.09	0.08	0.08
Average full load hours [h]	1428	1496	1516	2010-2050	2490	3933	5014	1431	1484	1500	1891	2052	2128	3016	3016	3016
Average capacity factor [%]	16.3	17.1	17.3		28.4	44.9	57.2	16.3	16.9	17.1	21.6	23.4	24.3	34.4	34.4	34.4
Average cost [€/kWh]	16.2	4.9	4.4	2010	30.6	23.8	22.2									
				2030	20.3	15.0	13.4	11.6	9.4	8.6	27.4	13.7	9.5	6.9	7.0	7.1
				2050	18.5	13.5	12.0									

Figure A.7.: India: Results of electricity generation potentials for the technologies photovoltaic, concentrating solar power, on- and offshore wind and hydro power. The two figures on the left are expressed in terms of cumulated potentials, the top graphs are indicated as a function of full load hours, the bottom graphs as a function of cost.



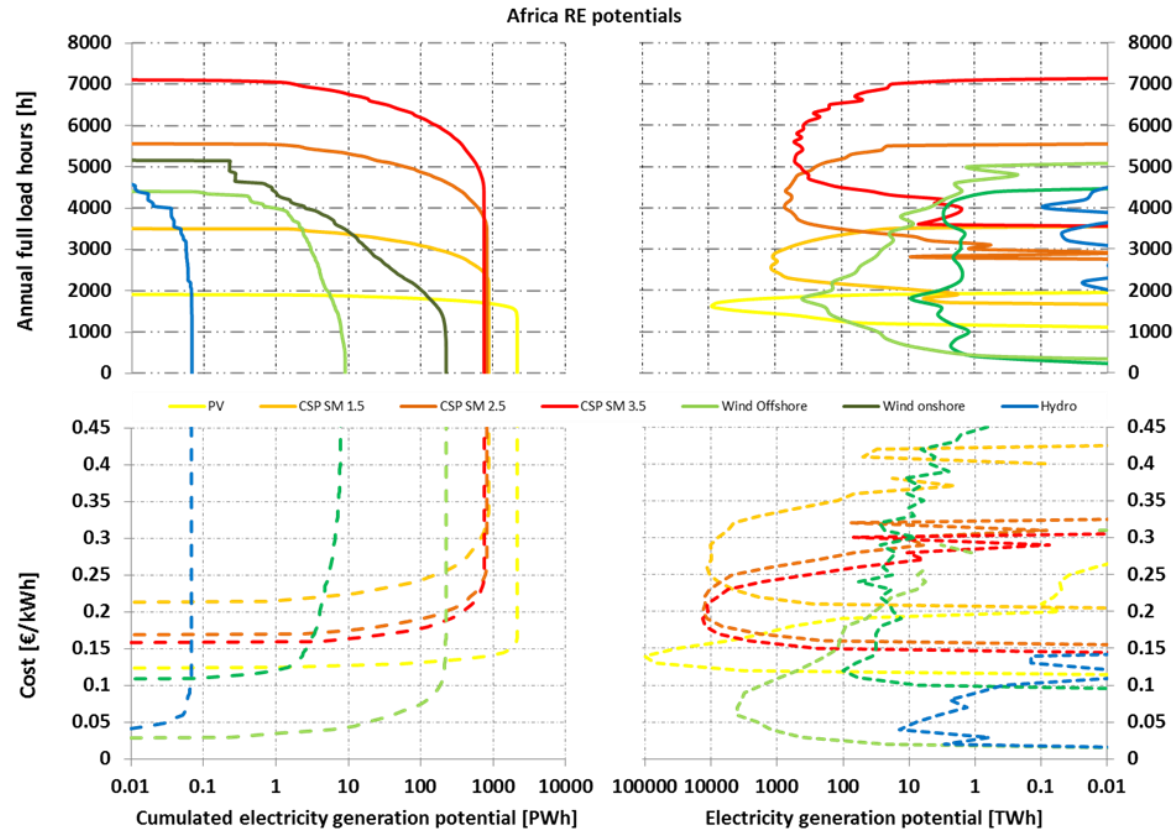
Rest of developing Asia	Photovoltaics			CSP				Wind Onshore			Wind Offshore			Hydro		
	2010	2030	2050	SM	1.5	2.5	3.5	2010	2030	2050	2010	2030	2050	2010	2030	2050
Electricity generation potential [PWh]	277.2	279.2	281.2		40.4	38.2	34.8	27.1	27.9	28.2	19.9	21.6	22.4	0.13	0.14	0.15
Average full load hours [h]	1523	1586	1597	2010-2050	2129	3362	4287	1942	2005	2024	1798	1929	1990	4163	4163	4163
Average capacity factor [%]	17.4	18.1	18.2		24.3	38.4	48.9	22.2	22.9	23.1	20.5	22.0	22.7	47.5	47.5	47.5
Average cost [€/kWh]	15.3	4.6	4.2	2010	35.8	27.9	26.0									
				2030	23.8	17.6	15.7	8.8	7.2	6.5	33.9	16.9	11.7	5.1	5.1	5.2
				2050	21.7	15.8	14.0									

Figure A.8.: Rest of developing Asia: Results of electricity generation potentials for the technologies photovoltaic, concentrating solar power, on- and offshore wind and hydro power. The two figures on the left are expressed in terms of cumulated potentials, the top graphs are indicated as a function of full load hours, the bottom graphs as a function of cost.



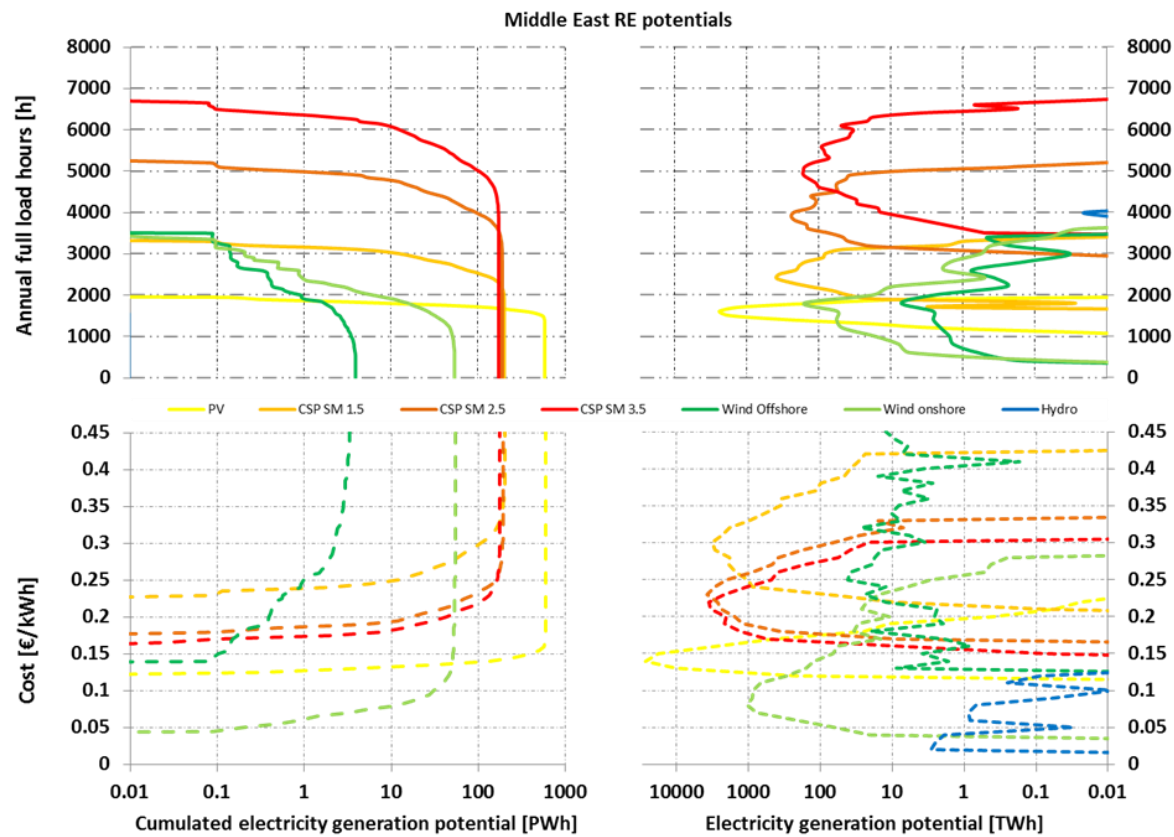
Latin America	Photovoltaics			SM	CSP			Wind Onshore			Wind Offshore			Hydro		
	2010	2030	2050		1.5	2.5	3.5	2010	2030	2050	2010	2030	2050	2010	2030	2050
Electricity generation potential [PWh]	399.5	403.4	407.6		66.4	62.9	57.3	45.8	47.5	48.0	23.0	25.0	25.9	0.52	0.54	0.57
Average full load hours [h]	1479	1545	1561	2010-2050	2448	3866	4929	2750	2825	2848	3117	3302	3388	4722	4722	4722
Average capacity factor [%]	16.9	17.6	17.8		27.9	44.1	56.3	31.4	32.2	32.5	35.6	37.7	38.7	53.9	53.9	53.9
Average cost [€/kWh]	15.8	4.8	4.3	2010	31.1	24.3	22.6	7.2	5.9	5.3	19.1	9.6	6.7	4.6	4.6	4.7
				2030	20.7	15.3	13.7									
				2050	18.9	13.7	12.2									

Figure A.9.: Latin America: Results of electricity generation potentials for the technologies photovoltaic, concentrating solar power, on- and offshore wind and hydro power. The two figures on the left are expressed in terms of cumulated potentials, the top graphs are indicated as a function of full load hours, the bottom graphs as a function of cost.



Africa	Photovoltaics			CSP			Wind Onshore			Wind Offshore			Hydro			
	2010	2030	2050	SM	1.5	2.5	3.5	2010	2030	2050	2010	2030	2050	2010	2030	2050
Electricity generation potential [PWh]	2167.7	2199.6	2231.6		871.8	826.1	750.5	224.9	233.8	236.5	9.0	9.8	10.2	0.07	0.07	0.08
Average full load hours [h]	1623	1696	1721	2010-2050	2751	4345	5540	2046	2119	2142	2427	2600	2680	3912	3911	3912
Average capacity factor [%]	18.5	19.4	19.6		31.4	49.6	63.2	23.4	24.2	24.5	27.7	29.7	30.6	44.7	44.7	44.7
Average cost [€/kWh]	14.4	4.3	3.9	2010	27.8	21.7	20.2									
				2030	18.5	13.6	12.2	8.2	6.7	6.0	26.6	13.4	9.3	5.5	5.6	5.7
				2050	16.8	12.3	10.9									

Figure A.10.: Africa: Results of electricity generation potentials for the technologies photovoltaic, concentrating solar power, on- and offshore wind and hydro power. The two figures on the left are expressed in terms of cumulated potentials, the top graphs are indicated as a function of full load hours, the bottom graphs as a function of cost.



Middle East	Photovoltaics			CSP				Wind Onshore			Wind Offshore			Hydro		
	2010	2030	2050	SM	1.5	2.5	3.5	2010	2030	2050	2010	2030	2050	2010	2030	2050
Electricity generation potential [PWh]	585.7	594.1	602.5		200.7	190.2	173.2	53.7	55.8	56.5	3.9	4.2	4.3	0.01	0.01	0.01
Average full load hours [h]	1584	1655	1679	2010-2050	2561	4045	5158	1607	1665	1683	1704	1830	1888	3238	3238	5332
Average capacity factor [%]	18.1	18.9	19.2		29.2	46.2	58.9	18.3	19.0	19.2	19.5	20.9	21.5	37.0	37.0	60.9
Average cost [€/kWh]	14.7	4.4	4.0	2010	29.8	23.3	21.7	10.1	8.2	7.5	32.2	16.2	11.3	5.0	5.1	5.1
				2030	19.8	14.6	13.1									
				2050	18.1	13.2	11.7									

Figure A.11.: Middle East: Results of electricity generation potentials for the technologies photovoltaic, concentrating solar power, on- and offshore wind and hydro power. The two figures on the left are expressed in terms of cumulated potentials, the top graphs are indicated as a function of full load hours, the bottom graphs as a function of cost.

A.3. Setup and major outcomes of the original TRANS-CSP release

The overall goal of the original release of the TRANS-CSP study - based on statistical data of 2002 and before - is to show the feasibility of a future energy supply for 30 European countries⁴ with high shares of domestic renewable generation and CSP imports via high voltage DC power transmission from countries in North Africa and the Middle East. It “comprises a comprehensive data base on the present and expected demand for electricity and firm power capacity, quantifies the available renewable energy sources and their applicability for power, provides scenarios of the electricity supply system until 2050 and evaluates the resulting socio-economic and environmental impacts for each of the analysed countries.” [TSK⁺06]. The scenario is not considered as a prediction of the future, but rather as a consistent pathway towards a long-term target defined by a set of criteria that describe a sustainable supply of electricity. This implies that it represents one out of many feasible options, it is not optimized in the sense of using a tool evaluating each possible transition path against a given objective. Boundary conditions - in the following referred to as guard rails - imposed by technical, economic, social and environmental constraints narrow down this pathway, which is to be free of any contradictions and inconsistencies. In this respect technical and economical constraints predominantly comprise the set of generation and transmission technologies available along with the amounts of renewable resources potentials which can be tapped. In the scenario the technologies are dispatched according to their cost, i.e. a merit-order approach is employed: First of all, non-polluting but fluctuating technologies such as wind and photovoltaics, foreseen to become more than competitive in the future and acting as fuel savers, are used. These technologies are complemented with more expensive while at the same time less volatile generation like hydro, biomass, concentrated solar and geothermal power. The resulting generation blend varies from country to country as a function of the respective available amounts of domestic renewable potentials and the demand structure. The residual load to be covered is met by ideally stored fossil fuels which are expected to become much more expensive compared to today’s cost in the long run. Figure A.12 gives an overview on the employed technologies as well as on the criteria for sustainability included within the scenario setup.

The evolution of renewable electricity generation cost over time is considered in terms of learning rates resulting in learning curves, a theory which is commonly used for any capital goods, i.e. also being eligible for renewable generation capacities. Fossil fuel price assumptions are in line with IEA figures [WEO05]. Political constraints are utterly excluded from any impact on the scenario, however, policy and decision makers in favor of a development towards an extended use of renewable energies are encouraged to estab-

⁴Iceland, Norway, Sweden, Finland, Denmark, Ireland, United Kingdom, Portugal, Spain, France, Belgium, Netherlands, Luxembourg, Germany, Austria, Switzerland, Italy, Poland, Czech Republic, Hungary, Slovakia, Slovenia, Croatia, Bosnia-Herzegovina, Serbia-Montenegro, Macedonia, Greece, Romania, Bulgaria and Turkey. MENA and the remaining Southern European countries are analysed within [TSK⁺05].

Criteria for Energy Sustainability:	Technology Portfolio:
<ul style="list-style-type: none"> ✓ Inexpensive low electricity cost no long term subsidies ✓ Secure diversified and redundant supply power on demand based on undepletable resources available or at least visible technology ✓ Compatible low pollution climate protection low risks for health and environment fair access 	<ul style="list-style-type: none"> ✓ Coal, Lignite ✓ Oil, Gas ✓ Nuclear Fission, Fusion ✓ Concentrating Solar Power (CSP) ✓ Geothermal Power (Hot Dry Rock) ✓ Biomass ✓ Hydropower ✓ Wind Power ✓ Photovoltaic ✓ Wave / Tidal <div style="text-align: right; margin-top: 10px;"> <ul style="list-style-type: none"> } ideally stored energy } storable energy } fluctuating energy </div>

Figure A.12.: Sustainability criteria narrowing down the TRANS-CSP target function and technical constraints imposed by the available portfolio of technologies and resources for power generation as considered in the TRANS-CSP scenario [TMS07].

lish frameworks capable of providing a stimulating environment for the developments anticipated within the scenario. Against this background the most severe implications are to be expected for the approval of storage and grid infrastructure as they face a series of acceptance challenges by the public.

Besides these “soft” delimiters, the following “hard” boundaries are imposed while generating the scenario:

A Resource restrictions:

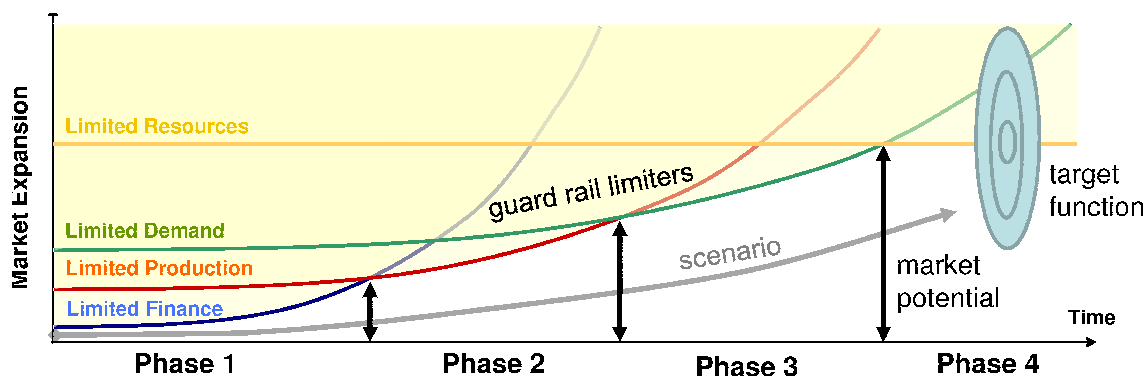
Renewable power generation is limited by the tappable potentials. A pre-analysis step gives an estimate for the latter data, tools such as REMix-EnDaT as presented in chapter 3 are capable of providing the desired information.

B Supply security:

Meeting the loads is to be assured throughout the year, i.e. sufficient reserves for unforeseeable break-downs or meteorological conditions impacting volatile renewable power generation are to be provided. For the TRANS-CSP scenario, a minimum firm capacity of 125% in terms of the peak load is therefore imposed enabling flexible dispatch of electricity and secure grid operation at any time.

C Plant portfolios:

The generation portfolios are comprised of plants with differing ages. Therefore, old plants are decommissioned, their capacities being replaced with state-of-the-art technology yielding the sustainability criteria as depicted in figure A.12 and potential limitations of production capacities for these replacements / new investments. Moreover, it is to be anticipated that the overall cost of the electricity blend tends towards year 2000 levels in the long run.



- Phase 1: Technology cost is high and expansion requires preferential investment and support
- Phase 2: Prices have become competitive but production capacities are still limited
- Phase 3: Production capacity catches up and the market is limited by demand
- Phase 4: As demand grows the availability of resources may become the main limiter

Figure A.13.: Criteria narrowing down the TRANS-CSP target function and technical constraints imposed by the available portfolio of technologies and resources for power generation as considered in the TRANS-CSP scenario [TMS07].

D Stable grid management:

Apart from up- or downramping firm capacity, merely storage or power transmission are eligible for balancing supply and demand. The former is subject to limitations between countries represented by the net transfer capacities - see the discussion on a new transmission model implemented within this work in section 5 for further insight. Any kind of energy storage is naturally associated with loss, which is why as little storage capacity as technically feasible is used.

Implementing the above discussed constraints, different implementation phases within the scenario can be identified, each of which facing a specific set of constraints as indicated in figure A.13. Overall, this results in the following major outcomes of the original release of TRANS-CSP⁵:

Secure power supply largely based upon renewable resources

An initial reported overall renewable share of approximately 20% in the year 2000 will evolve to about 80% in 2050. In order to keep the power grid within secure boundaries of system operation, quickly reacting fossil fired backup power plants are considered along with the implementation of today's transmission network between European countries and a yet to be constructed power supply via high voltage direct current power lines originating in CSP plants located in countries of the MENA region.

⁵In large parts this summary is based on the the executive summary of the TRANS-CSP study [TSK+06].

Economic benefits of going renewable compared to business as usual

Against the background of fossil fuel prices expected to increase continually, a fundamental strategic change of today's fossil fuel based towards a renewable based energy system could become cost effective within a time period of less than 15 years. Since renewable generation is still not competitive with conventional technologies - particularly if their external cost remain unconsidered - the necessary political frameworks are to be installed such as a feed-in-tariff systems like the German or Spanish Renewable Energy Acts. As the initial subsidies - although implemented for a limited period of time - lead to decreasing energy supply cost in the long run, any money devoted to a radical change of the current energy infrastructure can be considered as an investment rather than a subsidy.

Firm capacity provided by CSP

The key idea underlying the entire scenario is the concept of a local supply with renewable energy sources to the largest possible extent. However, increasing shares of renewable generation require a mix of measures to complement volatile supply building upon ideally stored fossil energy, affordable and efficient electricity storage and a very powerful grid infrastructure to compensate fluctuations of supply and demand. When it comes to providing renewable firm capacity (hydro, biomass, geothermal), the potentials in Europe are rather limited. Therefore the concept anticipates the installation of firm base, medium and peak load CSP capacities in 10 carefully selected - both in terms of resource availability and transmission corridors - locations in the MENA region effectively complementing local renewable generation via high voltage DC links. Building upon fossil plants to provide the same kind of system stability would violate the sustainability guard rails for the scenario construction as energy supply is to be diversified, both among technologies and regions, remain affordable and environmentally friendly. Some 60 TWh of CSP power generation in 2020 or 2025 could be ramped up to figures as high as 700 TWh by 2050, taking advantage of abundant solar irradiance conditions and little power transmission loss in the range between 10 and 15% leading to average kWh prices of about 0.05 €ct in terms of year 2000 price levels.

Severe reduction of green house gas emissions, little land use

A total reduction of CO₂ emissions to one quarter (25%) compared to year 2000 levels could be attained while land use for the implementation of a renewable based energy system would not consume more spaces than an estimated 1% of European land - approximately the figure that is currently used for the traffic infrastructures.

Positive economic and political implications

A realization of the presented TRANS-CSP concept would not only lead to a secure energy supply for Europe, but also help to reduce dependencies on fossil fuels in the MENA countries. Against estimated significant increases in energy consumption in these countries - both due to population and economic growth - stress on fossil fuel prices is not expected to lessen. Therefore there is a mutual interest in the large scale

implementation of renewables on all continents bordering on the Mediterranean Sea, complemented by CSP plants, which could furthermore offer the option of desalination using waste heat. Based on a new energy partnership, economic development and the establishment of stable, respectful and equal relations could culminate in a Community for Energy, Water and Climate Security. Even under the conservative assumptions of the original TRANS-CSP study, it is shown that an extended use of renewable energy in the power sector results in a medium term stabilization of electricity costs within two decades. In the long run (2050) renewable power could become the least cost option worldwide.

In summary it can be concluded that the original release of the TRANS-CSP study provides a framework of a feasible transition path from the year 2000's to 2050's energy supply system for 30 European countries. Focus is laid both on local supply with renewable generation to the greatest possible extent and to guarantee stable grid operation on the provision of adequate amounts of firm capacity, parts of which being contributed by the connection of concentrating solar power plants situated in the MENA region with centers of demand all over Europe. In the year 2050, 15% of Europe's power supply are estimated to originate from these CSP imports, while an overall renewable electricity supply share - also including locally available power generation tapping renewable resources - of 80% is foreseen. Costs for electricity are stabilized and green house gas emissions are limited in line with the 2°C goal recommended by IPCC [EPMS+11]. Nuclear power is phased out suffering from poor competitiveness as do lignite and fusion power - if ever available. This is caused by increasing shares of volatile generation leading to a reduced dispatch of the contemporary base load plant portfolio to some 2000 annual full load hours. Nonetheless, these plants along with gas fired stations remain part of the portfolio forming a cold reserve, which is quickly accessible in case of unpredictable power shortages using precious fossil fuel. Artificially created renewable fuels could be provided by renewable energy in the long run, using technologies such as power-to-gas [P2G]. The remaining capacity gap due to decommissioning of fossil plants is closed by firm power provided by stored hydro, biomass, geothermal and imported concentrating solar power from MENA. Only countries such as Spain, Portugal, Italy, Greece and Turkey export noteworthy domestic CSP potentials. In order to avoid excessive surpluses, i.e. for economic reasons, volatile generation is limited by the peak load.

A.4. REMix-OptiMo equations and boundary conditions used in this work

In order to provide a thorough insight into the model structure of the simulations carried out and discussed in section 5.3, this review gives a summary on the relations and constraints used within REMix-OptiMo. All of the presented equations in the following subsections have been developed by Scholz and Luca de Tena [Sch12; Ten12]. For the sake of the present work, bearing in mind that a validation of an updated Trans-CSP scenario is anticipated, merely the equations of concern are discussed, i.e. possible contributions of electromobility, combined heat and power and hydrogen as a means of storage are not included. Furthermore, any new - green field - installations of power plants are excluded, in turn reducing the number of degrees of freedom of the simulations. All equations which impose boundary conditions are denoted with the equality symbol " $\stackrel{!}{=}$ ", all others with the ordinary symbol " $=$ ".

Electricity power balance

Among the most important constraints, electricity demand has to be met in each region for any time step t . Equation (A.8) includes the latter implication, yielding that the sum of conventional, renewable power and imported CSP power generation originating from 10 plant sites in North Africa and the Middle East, $E_{node}^{conventional\ tech, gen}(t)$, $E_{gen,node}^{renewable\ tech, gen}(t)$ and $E_{node}^{CSP, import}(t)$, respectively, has to be capable of meeting the demand $E_{node}^{demand}(t)$. Moreover, the term $E_{node}^{not\ supplied}(t)$ representing any demand not supplied is also introduced to model unexpected or unavailable power plant outages. Finally incoming and leaving power transmission between nodes $E_{node}^{AC, in}(t)$ and $E_{node}^{AC, out}(t)$ as described in section 5.2 is also taken account of:

$$\begin{aligned}
 & \sum_{conventional\ tech} E_{node}^{conventional\ tech, gen}(t) + \sum_{renewable\ tech} E_{node}^{renewable\ tech, gen}(t) \\
 & + \sum_{import\ plants} E_{node}^{CSP, import}(t) + E_{node}^{not\ supplied}(t) \stackrel{!}{=} \\
 & E_{node}^{demand}(t) - E_{node}^{AC, in}(t) + E_{node}^{AC, out}(t)
 \end{aligned} \tag{A.8}$$

Electricity generation using photovoltaic, wind and wave power

Photovoltaic, wind and wave power are represented using one similar model syntax which is discussed in the following sections.

Feasible electricity generation

First of all, a feasible power output $E_{node}^{PV, wind, waves, feas\ gen}(t)$ is derived for each time step t using the installed capacities for each of these technologies on a nodal basis $P_{node}^{PV, wind, waves, inst}$ according to the scenario framework. Furthermore an input time

series normalized to one MW $T_{node}^{PV,wind,waves, normed}(t)$ provided by REMix-EnDaT is employed to represent the hourly availability of each technology. The former parameters are multiplied with each node's average annual full load hours⁶ $flh_{node}^{PV,wind,waves}$ in order to obtain:

$$E_{node}^{PV,wind,waves, feas\ gen}(t) = P_{node}^{PV,wind,waves, inst} \cdot T_{node}^{PV,wind,waves, normed}(t) \cdot flh_{node}^{PV,wind,waves} \quad (A.9)$$

Net electricity generation

By subtracting any surplus of renewable power generation $E_{node}^{PV,wind,waves, surplus}(t)$ which cannot be used from the feasible hourly power time series $E_{node}^{PV,wind,waves, feas\ gen}(t)$, the net power generation of photovoltaic, wind and waves $E_{node}^{PV,wind,waves, gen}(t)$ is derived as follows:

$$E_{node}^{PV,wind,waves, gen}(t) = E_{node}^{PV,wind,waves, feas\ gen}(t) - E_{node}^{PV,wind,waves, surplus}(t) \quad (A.10)$$

Total operational cost

The operational cost $C_{node}^{PV,wind,waves, op}$ for photovoltaic, wind and waves are composed of variable and fixed contributions $C_{node}^{PV,wind,waves, var}$ and $C_{node}^{PV,wind,waves, fixed}$, respectively, which can primarily be attributed to maintenance:

$$C_{node}^{PV,wind,waves, op} = C_{node}^{PV,wind,waves, var} + C_{node}^{PV,wind,waves, fixed} \quad (A.11)$$

Variable operational cost

Variable operational cost $C_{node}^{PV,wind,waves, var}$ arise as a product of the total generated electricity

$$\sum_t E_{node}^{PV,wind,waves, gen}(t)$$

and the specific operation and maintenance cost $c_{OM}^{PV,wind,waves, var}$:

$$C_{node}^{PV,wind,waves, var} = \sum_t E_{node}^{PV,wind,waves, gen}(t) \cdot c_{OM}^{PV,wind,waves, var} \quad (A.12)$$

Fixed operational cost

Fixed operational cost $C_{node}^{PV,wind,waves, fixed}$ are determined by multiplying the total investment cost derived as the product of installed capacity and installation specific cost $P_{node}^{PV,wind,waves, inst} \cdot c_{inst}^{PV,wind,waves}$ by a constant factor $f_{OM}^{PV,wind,waves}$:

$$C_{node}^{PV,wind,waves, fixed} = f_{OM}^{PV,wind,waves} \cdot P_{node}^{PV,wind,waves, inst} \cdot c_{inst}^{PV,wind,waves} \quad (A.13)$$

⁶The average full load hours are a result of the potential assessment carried out with REMix-EnDaT, for each node an average of the full load hours is used.

Investment cost

The annuity investment cost, i.e. the cost which arises each year of the depreciation period, $C_{node}^{PV,wind,waves, inv}$, are estimated by the installed capacity $P_{node}^{PV,wind,waves, inst}$, the installation-specific cost $c_{inst}^{PV,wind,waves}$ and the annuity factor $AF_{p,n}^{PV,wind,waves}$ (with the interest rate p and the depreciation period n):

$$C_{node}^{PV,wind,waves, inv} = AF_{p,n}^{PV,wind,waves} \cdot P_{node}^{PV,wind,waves, inst} \cdot c_{inst}^{PV,wind,waves} \quad (A.14)$$

Concentrating Solar Power

Available thermal energy for steam generation provided by the solar field and co-firing

Thermal energy in CSP plants either originates directly from the solar field or from a co-firing unit, enabling operation using gas as in any ordinary conventionally fuelled power plant. In order to derive the thermal energy output for a specific node $E_{node}^{CSP, thermal}(t)$, each node's installed CSP capacity (according to the scenario assumptions) $P_{node}^{CSP, inst}$ is multiplied by a time series curve for one year normalized to one MWh $T_{node}^{CSP, normed}(t)$ and the average number of full load hours in the node⁷ flh_{node}^{CSP} . To take account of the possibility of conventional co-firing, the term $E_{node}^{CSP, co-firing}(t)$ is introduced. Overall the following relation is obtained:

$$E_{node}^{CSP, thermal}(t) = P_{node}^{CSP, inst} \cdot T_{node}^{CSP}(t) \cdot flh_{node}^{CSP} + E_{node}(t)^{CSP, co-firing} \quad (A.15)$$

Energy balance of the power plant

To ensure that electricity generation is limited by the amount of available thermal energy, the energy balance limitation is introduced to the model. The thermal energy which is required for a given capacity in MW_{el} is derived by the quotient of rated capacity $P_{el, node}^{CSP, rated}$ over the efficiency of power generation η_{el}^{CSP} :

$$\frac{P_{el, node}^{CSP, rated}}{\eta_{el}^{CSP}} \quad (A.16)$$

The amount of thermal energy converted into electricity has to be equal or smaller to the available thermal energy according to the previous paragraph $E_{node}^{CSP, thermal}(t) \pm$ the thermal energy from or to the thermal storage $E_{node}^{CSP, storage}(t)$. Any thermal energy which is discharged from the storage device is multiplied by the round-trip efficiency $\eta_{round\ trip}^{CSP, storage}$ to take account of loss during the charging and discharging process. Any excess thermal energy is expressed in terms of possible electricity generation and subtracted. Finally

⁷Both time series data as well as an assessment on the average full load hours are provided by REMix-EnDaT as discussed in chapter 3.

the following equation holds:

$$\begin{aligned} \frac{P_{el, node}^{CSP, rated}}{\eta_{el}^{CSP}} &\stackrel{!}{\leq} E_{node}^{CSP, thermal}(t) \\ &+ E_{node}^{CSP, storage}(t) \cdot \eta_{round trip}^{CSP, storage} \\ &- \frac{E_{node}^{CSP, thermal surplus}(t)}{\eta_{el}^{CSP}} \end{aligned} \quad (A.17)$$

Generator capacity constraint

The generation capacity $P_{node}^{CSP, gen}$ in each node is limited by the installed capacity $P_{node}^{CSP, inst}$ multiplied by an availability factor $f_{av}^{CSP, gen}$ taking into account maintenance periods or any non-scheduled downtimes:

$$P_{node}^{CSP, gen} \stackrel{!}{\leq} P_{node}^{CSP, inst} \cdot f_{av}^{CSP, gen} \quad (A.18)$$

Thermal storage energy balance

The storage energy balance demands that the change of the storage level between two time steps $E_{node}^{CSP, storage level}(t) - E_{node}^{CSP, storage level}(t-1)$ be identical with the balance of charging and discharging with thermal energy $E_{node}^{CSP, storage in}(t) - E_{node}^{CSP, storage out}(t)$:

$$\begin{aligned} E_{node}^{CSP, storage in}(t) - E_{node}^{CSP, storage out}(t) &\stackrel{!}{=} \\ E_{node}^{CSP, storage level}(t) - E_{node}^{CSP, storage level}(t-1) \end{aligned} \quad (A.19)$$

Storage limitation

The stored thermal energy $E_{node}^{CSP, storage level}(t)$ must not exceed the installed capacity of the storage $P_{node}^{CSP, storage, inst}$ for a given node:

$$E_{node}^{CSP, storage level}(t) \stackrel{!}{\leq} P_{node}^{CSP, storage, inst} \quad (A.20)$$

Round trip storage balance Over the course of the entire calculation period, it is to be ensured that the storage's energy content in the first and last time steps be identical:

$$E_{node}^{CSP, storage level}(t=0) \stackrel{!}{=} E_{node}^{CSP, storage level}(t=8759) \quad (A.21)$$

Storage installation

The installed storage capacity $P_{node}^{CSP, storage, inst}$ is derived by multiplying the installed solar field capacity $P_{node}^{CSP, solar field, inst}$ by the storage factor $f_{storage, node}^{CSP}$ and the share of the solar field's capacity exceeding the turbine's rated power capacity. The latter is derived as a function of the solar multiple. The storage factor determines the number of (full load) hours the solar field's thermal energy can be charged into the storage device:

$$P_{node}^{CSP, storage, inst} = P_{node}^{CSP, solar field, inst} \cdot f_{storage, node}^{CSP} \cdot \frac{f_{SM, node}^{CSP} - 1}{f_{SM, node}^{CSP}} \quad (A.22)$$

Co-firing

The total thermal energy using gas for steam generation in a CSP plant $\sum_t E_{node}^{CSP, co-firing}(t)$ is limited by a fraction $f_{co-firing\ max}^{CSP}$ of the thermal output of the solar field :

$$\sum_t E_{node}^{CSP, co-firing}(t) \leq P_{node}^{CSP\ solar\ field, inst} \cdot T_{node}^{CSP, normed}(t) \cdot flh_{node}^{CSP} \cdot f_{co-firing\ max}^{CSP} \quad (A.23)$$

Solar field installation

The installed solar field capacity $P_{node}^{CSP\ solar\ field, inst}$ has to equal the generator's thermal energy demand $\frac{P_{node}^{CSP\ power\ block, inst}}{\eta_{el}^{CSP}}$ times the solar multiple of the system $f_{SM, node}^{CSP}$:

$$P_{node}^{CSP\ solar\ field, inst} \stackrel{!}{=} \frac{P_{node}^{CSP\ power\ block, inst} \cdot f_{SM, node}^{CSP}}{\eta_{el}^{CSP}} \quad (A.24)$$

Total operational cost

The total annual operational cost of a CSP plant $C_{node}^{CSP, op}$ are derived as the sum of variable $C_{node}^{CSP, var}$ and fixed $C_{node}^{CSP, fixed}$ operational cost:

$$C_{node}^{CSP, op} = C_{node}^{CSP, var} + C_{node}^{CSP, fixed} \quad (A.25)$$

Variable operational cost

Variable operational cost arise due to co-firing with gas. They are composed of both output-specific purchasing cost for gas and cost for emission certificates:

$$C_{node}^{CSP, var} = \sum_t E_{node}^{CSP, co-firing}(t) \cdot (c_{gas} + f_{spec\ emission\ gas} \cdot c_{certificate}) \quad (A.26)$$

Fixed operational cost

Fixed operational cost are determined by multiplying the total investment cost of the field, storage and power block expressed in terms of their respective installed capacities $P_{node}^{CSP\ component, inst}$ by a constant factor f_{OM}^{CSP} to take account of maintenance:

$$\begin{aligned} C_{node}^{CSP, fixed\ op} &= f_{OM}^{CSP} \cdot \\ & (P_{node}^{CSP\ solar\ field, inst} \cdot c_{inst}^{CSP\ solar\ field} \\ & + P_{node}^{CSP\ storage, inst} \cdot c_{inst}^{CSP\ storage} \\ & + P_{node}^{CSP\ power\ block, inst} \cdot c_{inst}^{CSP\ power\ block}) \end{aligned} \quad (A.27)$$

Investment cost

The investment cost are estimated by the annuity $AF_{p,n}^{CSP}$ (with the interest rate p and the depreciation period n) of the sum of the investment cost for the solar field, the storage and the power block's total cost:

$$\begin{aligned}
C_{node}^{CSP, inv} &= AF_{p,n}^{CSP} \cdot \\
& (P_{node}^{CSP solar field, inst} \cdot C_{inst}^{CSP solar field} \\
& + P_{node}^{CSP storage, inst} \cdot C_{inst}^{CSP storage} \\
& + P_{node}^{CSP power block, inst} \cdot C_{inst}^{CSP power block})
\end{aligned} \tag{A.28}$$

Hydro Power

Feasible electricity generation

In accordance with the discussion in section A.4, a feasible hourly power time series $E_{node}^{hydro, feas gen}(t)$ is derived using the installed capacity on a nodal basis $P_{node}^{hydro, inst}$ according to the scenario framework. It shall be noted that merely run-off plants are considered within the scenario validation, e.g. the installed capacities provided by the scenario framework are estimated to be utterly made up of river run-off plants. Furthermore an input time series $T_{node}^{hydro}(t)$ provided by REMix-EnDaT is employed to represent the hourly resource characteristics. The former parameters are multiplied with each node's average annual full load hours flh_{node}^{hydro} . Since hourly electricity generation is sought, the entire expression is divided by the generation efficiency η_{el}^{hydro} in order to obtain:

$$E_{node}^{hydro, feas gen}(t) = \frac{P_{node}^{hydro, inst} \cdot T_{node}^{hydro, normed}(t) \cdot flh_{node}^{hydro}}{\eta_{el}^{hydro}} \tag{A.29}$$

Net electricity generation

By subtracting any surplus of renewable power generation $E_{node}^{hydro, surplus}(t)$ which cannot be used from the feasible hourly power time series $E_{node}^{hydro, feas gen}(t)$, the net power generation $E_{node}^{hydro, gen}(t)$ is derived as follows:

$$E_{node}^{hydro, gen}(t) = E_{node}^{hydro, feas gen}(t) - E_{node}^{hydro, surplus}(t) \tag{A.30}$$

Generator capacity constraint

The generation $E_{node}^{hydro, gen}(t)$ in each node is limited by the installed capacity $P_{node}^{hydro, inst}$ multiplied by an availability factor $f_{av}^{hydro, gen}$ taking into account maintenance periods or any non-scheduled downtimes:

$$E_{node}^{hydro, gen}(t) \leq P_{node}^{hydro, inst} \cdot f_{av}^{gen, hydro} \tag{A.31}$$

Minimum run-off constraint

To consider that a minimum water volume always has to pass the hydro power barrier, the factor $f_{min run off}^{hydro}$ is introduced thus implicating for the power generation

$E_{node}^{hydro, gen}(t)$:

$$E_{node}^{hydro, gen}(t) \stackrel{!}{\geq} P_{node}^{hydro, inst} \cdot f_{min\ run\ off}^{hydro} \quad (A.32)$$

Fixed operational cost

Fixed operational cost $C_{node}^{hydro, fixed}$ are determined by multiplying the total investment cost $P_{node}^{hydro, inst} \cdot c_{inst}^{hydro}$ by a constant factor f_{OM}^{hydro} :

$$C_{node}^{hydro, fixed} = f_{OM}^{hydro} \cdot P_{node}^{hydro, inst} \cdot c_{inst}^{hydro} \quad (A.33)$$

Investment cost

The investment cost $C_{node}^{hydro, investment}$, obtained by the installed capacity $P_{node}^{hydro, inst}$ and the installation-specific cost c_{inst}^{hydro} , are estimated by their annuity factor $AF_{p,n}^{hydro}$ (with the interest rate p and the depreciation period n):

$$C_{node}^{hydro, investment} = AF_{p,n}^{hydro} \cdot P_{node}^{hydro, inst} \cdot c_{inst}^{hydro} \quad (A.34)$$

Biomass

Generation constraint

The generation $E_{node}^{biomass, gen}(t)$ in each node is limited by the installed capacity $P_{node}^{biomass, inst}$ multiplied by an availability factor $f_{av}^{biomass, gen}$ taking into account maintenance periods or any non-scheduled downtimes:

$$E_{node}^{biomass, gen}(t) \stackrel{!}{\leq} P_{node}^{biomass, inst} \cdot f_{av}^{biomass, gen} \quad (A.35)$$

Biomass consumption

The consumption of biomass $E_{node}^{biomass, fuel\ consumption}(t)$ in each node is derived as the quotient of power generation $E_{node}^{biomass, gen}(t)$ over the net efficiency of biomass power plants $\eta_{el}^{biomass}$:

$$E_{node}^{biomass, fuel\ consumption}(t) = \frac{E_{node}^{biomass, gen}}{\eta_{el}^{biomass}} \quad (A.36)$$

In summary, $E_{node}^{biomass, fuel\ consumption}(t)$ represents the chemical energy content, which has to be provided to the power plant to yield the anticipated electricity generation.

Exogenously defined full load hours

For the sake of the anticipated scenario validation, the full load hours for biomass power plants in each node are provided according to the scenario assumptions. The following boundary condition holds: The total power generation in a given node, expressed as the discrete sum over all time steps of the product of the consumption of biomass $E_{node}^{biomass, fuel\ consumption}$ and the net efficiency of biomass power plants $\eta_{el}^{biomass}$

equals the annual power generation expressed in terms of the product of the installed capacity $P_{node}^{biomass, inst}$ with the respective node's full load hours flh_{node}^{hydro} :

$$\sum_t E_{node}^{biomass, fuel\ consumption}(t) \cdot \eta_{el}^{biomass} \stackrel{!}{=} P_{node}^{biomass, inst} \cdot flh_{node}^{biomass} \quad (A.37)$$

Feasible hourly electricity generation

The hourly power output $E_{node}^{biomass, gen}(t)$ which can be obtained using biomass plants is expressed in terms of the product of the installed capacity $P_{node}^{biomass, inst}$ with the respective node's full load hours $flh_{node}^{biomass}$ over 8760 hours in a year:

$$E_{node}^{biomass, gen}(t) \stackrel{!}{\leq} \frac{P_{node}^{biomass, inst} \cdot flh_{node}^{biomass}}{8760} \quad (A.38)$$

Biomass availability constraint

The annual biomass consumption

$$\sum_t E_{node}^{biomass, fuel\ consumption}(t)$$

must not exceed the biomass potential $E_{node}^{biomass, potential}$:

$$\sum_t E_{node}^{biomass, fuel\ consumption}(t) \leq E_{node}^{biomass, potential} \quad (A.39)$$

Operational cost

The total operational cost of a biomass power plant $C_{node}^{biomass, op}$ is derived as the sum of an operation and maintenance - thereby fixed -component $C_{node}^{biomass, fixed}$ on the one hand, which is made up of the product of the specific investment cost $c_{inst}^{biomass}$, the installed capacity $P_{node}^{biomass, inst}$ and the operation and maintenance factor $f_{OM}^{biomass}$, and the variable operational cost for the biomass fuel itself $C_{node}^{biomass, var}$ on the other hand, expressed in terms of the specific fuel cost $c_{fuel}^{biomass}$ times the total fuel consumption

$$\begin{aligned} & \sum_t E_{node}^{biomass, fuel\ consumption}(t) : \\ C_{node}^{biomass, op} &= C_{node}^{biomass, fixed} + C_{node}^{biomass, var} \\ &= c_{inst}^{biomass} \cdot P_{node}^{biomass, inst} \cdot f_{OM}^{biomass} \\ & \quad + c_{fuel}^{biomass} \cdot \sum_t E_{node}^{biomass, fuel\ consumption}(t) \end{aligned} \quad (A.40)$$

Investment cost

The investment cost $C_{node}^{biomass, inv}$, obtained by the installed capacity $P_{node}^{biomass, inst}$ and the installation-specific cost $c_{inst}^{biomass}$, are estimated by their annuity factor $AF_{p,n}^{biomass}$ (with the interest rate p and the depreciation period n):

$$C_{node}^{biomass, investment} = AF_{p,n}^{biomass} \cdot P_{node}^{biomass, inst} \cdot c_{inst}^{biomass} \quad (A.41)$$

Geothermal Power

Geothermal power plants are capable of providing both electricity and heat, e.g. for district heating systems. Although the general approach of REMix is set up to model heat output, within the scope of the validation runs no heat demand is considered at all. This implicitly leads to an exclusive electric power output of the geothermal power plant, i.e. all resources are used to run the power generators.

Feasible hourly electricity generation

The hourly electricity output $E_{node}^{geothermal, gen}(t)$ is therefore a function of the installed capacity $P_{node}^{geothermal, inst}$. To take account of the scenario assumptions, the potential hourly electricity output is scaled by the node's respective full load hours $flh_{node}^{geothermal}$:

$$E_{node}^{geothermal, gen}(t) \leq P_{node}^{geothermal, inst} \cdot \frac{flh_{node}^{geothermal}}{8760} \quad (\text{A.42})$$

Operational cost

The operational cost of a geothermal power plant $C_{node}^{geothermal, op}$ is derived as the expenses due to operation and maintenance - also referred to as the fixed cost - which is made up of the product of the specific investment cost $C_{inst}^{geothermal}$, the installed capacity $P_{node}^{geothermal, inst}$ and the operation and maintenance fraction $f_{OM}^{geothermal}$:

$$C_{node}^{geothermal, fixed} = C_{inst}^{geothermal} \cdot P_{node}^{geothermal, inst} \cdot f_{OM}^{geothermal} \quad (\text{A.43})$$

Investment cost

The investment cost $C_{node}^{geothermal, inv}$, obtained by the installed capacity $P_{node}^{geothermal, inst}$ and the installation-specific cost $C_{inst}^{geothermal}$, are estimated by their annuity factor $AF_{p,n}^{geothermal}$ (with the interest rate p and the depreciation period n):

$$C_{node}^{geothermal, inv} = AF_{p,n}^{geothermal} \cdot P_{node}^{geothermal, inst} \cdot C_{inst}^{geothermal} \quad (\text{A.44})$$

Conventional Power Generation

Conventional power plants are altogether modeled with identical equations, however for each technology the respective parameters are used.

Feasible hourly electricity generation

The hourly electricity output $E_{node, year class}^{conventional tech, gen}(t)$ is modelled as a function of the installed capacity $P_{node, year class}^{conventional tech, inst}$ multiplied by the ratio of net over gross efficiencies $\frac{\eta_{net, year class}^{conventional tech}}{\eta_{gross, year class}^{conventional tech}}$. Finally, to take account of maintenance and unscheduled downtimes, an

availability factor $f_{av, year class}^{conventional tech}$ is used:

$$E_{node, year class}^{conventional tech, gen}(t) \stackrel{!}{\leq} P_{node, year class}^{conventional tech, inst} \cdot \frac{\eta_{net, year class}^{conventional tech}}{\eta_{gross, year class}^{conventional tech}} \cdot f_{av, year class}^{conventional tech} \quad (\text{A.45})$$

Fuel consumption

In order to derive the fuel consumption $E_{node, year class}^{conventional tech, fuel consumption}(t)$ in terms of the required chemical energy equivalent, the hourly electricity generation $E_{node, year class}^{conventional tech, gen}(t)$ is divided by the net efficiency of the power plant $\eta_{net, year class}^{conventional tech}$. Additionally, ramping up is accompanied by an increased fuel consumption which is modelled as the product of the number of power plants of concern $N_{plants, year class}^{conventional tech}$, the average capacity of one power block $P_{average, year class}^{conventional tech, inst}$ and the average fuel consumed for starting up one plant with such a mean capacity $E_{node, year class}^{start up, conventional tech, fuel consumption}(t)$:

$$E_{node, year class}^{start up, conventional tech, fuel consumption}(t) = \frac{E_{node, year class}^{conventional tech, gen}(t)}{\eta_{net, year class}^{conventional tech}} + N_{plants, year class}^{conventional tech} \cdot P_{average, year class}^{conventional tech, inst} \cdot E_{node, year class}^{start up, conventional tech, fuel consumption}(t) \quad (\text{A.46})$$

Number of power plants which are ramped up

The number of plants which are ramped up $N_{started plants, year class}^{conventional tech}$ is determined by the difference of the number of plants currently running $N_{plants, year class}^{conventional tech}(t)$ to those, which were in operation in the previous time step $N_{plants, year class}^{conventional tech}(t-1)$:

$$N_{started plants, year class}^{conventional tech} = N_{plants, year class}^{conventional tech}(t) - N_{plants, year class}^{conventional tech}(t-1) \quad (\text{A.47})$$

Number of plants in operation

The number of plants in operation $N_{plants, year class}^{conventional tech}(t)$ is expressed as the quotient of power output $E_{node, year class}^{conventional tech, gen}(t)$ over average block size $P_{average, year class}^{conventional tech, inst}$:

$$N_{plants, year class}^{conventional tech}(t) = \frac{E_{node, year class}^{conventional tech, gen}(t)}{P_{average, year class}^{conventional tech, inst}} \quad (\text{A.48})$$

Operated power plants at the beginning and the end of the considered run time

The number of operating plants at the beginning of the simulation run $N_{plants, year class}^{conventional tech}(t = 0)$ is to remain identical to the number of running plants at the end $N_{plants, year class}^{conventional tech}(t = 8759)$:

$$N_{plants, year class}^{conventional tech}(t = 0) \stackrel{!}{=} N_{plants, year class}^{conventional tech}(t = 8759) \quad (A.49)$$

Total operational cost

The total cost for conventional power plants $C_{total}^{conventional tech}$ are made up of the three components fuel and CO₂ certificates $C_{fuel+CO_2}^{conventional tech}$, wear and tear $C_{wear}^{conventional tech}$ and finally maintenance $C_{maintenance}^{conventional tech}$:

$$C_{total}^{conventional tech} = C_{fuel+CO_2}^{conventional tech} + C_{wear}^{conventional tech} + C_{maintenance}^{conventional tech} \quad (A.50)$$

Cost for fuel and CO₂ certificates

Cost due to fuel are represented by the product of fuel consumption $E_{node, year class}^{conventional tech, fuel consumption}(t)$ times specific fuel cost $c_{fuel type}^{conventional tech}$. The emission certificate's related cost are derived by the product of the fuel consumption $E_{node, year class}^{conventional tech, fuel consumption}(t)$, the specific emissions $f_{emission}^{fuel type}$, the specific certificate cost $c_{certificate}^{pollutant}$ and an expression considering the share of emission which is captured $(1 - f_{CCS}^{year})$. CCS cost is modelled as the product of fuel consumption $E_{node, year class}^{conventional tech, fuel consumption}(t)$, specific CCS cost c_{CCS}^{year} and the share of emissions, which is captured f_{CCS}^{year} . Altogether, the following relation holds:

$$C_{fuel+CO_2}^{conventional tech} = E_{node, year class}^{conventional tech, fuel consumption}(t) \cdot (c_{fuel type}^{year} + f_{emission}^{fuel type} \cdot c_{certificate}^{pollutant} \cdot (1 - f_{CCS}^{year}) + c_{CCS}^{year} \cdot f_{CCS}^{year}) \quad (A.51)$$

Cost for wear and tear

Wear and tear cost $C_{wear}^{conventional tech}$ are estimated as the product of the number of start-ups for the entire time period

$$\sum_t N_{started plants, year class}^{conventional tech}(t),$$

their average block size $P_{average, year class}^{conventional tech, inst}$ and the installation-specific wear and tear cost

$c_{wear\&tear, year class}^{conventional tech}$:

$$C_{wear}^{conventional tech} = \sum_t N_{started plants, year class}^{conventional tech}(t) \cdot P_{average, year class}^{conventional tech, inst} \cdot c_{wear\&tear, year class}^{conventional tech} \quad (A.52)$$

Cost for maintenance

Cost due to maintenance are the product of the installed capacity $P_{node, year\ class}^{conventional\ tech, inst}$, the installation-specific maintenance cost $c_{maintenance, year\ class}^{conventional\ tech}$ and the fraction of the total investment $f_{maintenance, year\ class}^{conventional\ tech}$:

$$C_{maintenance}^{conventional\ tech} = P_{node, year\ class}^{conventional\ tech, inst} \cdot c_{maintenance, year\ class}^{conventional\ tech} \cdot f_{maintenance, year\ class}^{conventional\ tech} \quad (A.53)$$

Investment cost

The investment cost $C_{node}^{conventional\ tech, inv}$, obtained by the installed capacity $P_{node, year\ class}^{conventional\ tech, inst}$ and the installation-specific cost $c_{inst, year\ class}^{conventional\ tech}$, are estimated by their annuity factor $AF_{p, n, year\ class}^{conventional\ tech}$ (with the interest rate p and the depreciation period n):

$$C_{node}^{conventional\ tech, inv} = AF_{p, n, year\ class}^{conventional\ tech} \cdot P_{node, year\ class}^{conventional\ tech, inst} \cdot c_{inst, year\ class}^{conventional\ tech} \quad (A.54)$$

A.5. ENTSO-e net transfer capacities

From		IE/NI	GB	MA	PT	ES	FR	BE	NL	LU	DE	DKw	DKe	NO	SE	FI	CH	IT	AT	SI	PL	CZ	SK	HU	GR	RO	HR	BA	RS	ME	MK	AL	BG	UA	LV	LT	EE	BY	RU	Maximum Import in MW						
To	IE/NI		410																																											
	GB	80																																												
MA					900 MA																																									
PT					1200																																									
ES				600 MA		1200																																								
FR			2000			500		1300			3200						1100	870																												
BE							2900		2200																																					
NL								2300			4000			700 NL																													3850 (4)			
LU											980																																			
DE (4)							2600		3900	NRL	1500 (4)	550		600	4400	1600					1200 (4)	2100 (4)																								
DKw (4)											950 (4)		950 (4)	340 (4)																																
DKe (4)											550			1300																																
NO									700 NO				950 (4)	370 (4)	3700 (4)																															
SE											600	370 (4)	1700	3545 (4)	3700 (4)	1650 (4)						0 (4)																								
FI														2050 (4)																																
CH							3000				2060								1440	540 (4)																										
IT (4)							2400																																							
AT																																														
SI																																														
PL (4)																																														
CZ																																														
SK																																														
HU																																														
GR																																														
RO																																														
HR																																														
BA																																														
RS																																														
ME																																														
MK																																														
AL																																														
BG																																														
UA																																														
LV																																														
LT																																														
EE																																														
BY																																														
RU																																														
Maximum Export in MW									3850 (4)		8500 (4)																																			

Figure A.14.: Indicative values for summer 2010 net transfer capacities [MW] according to ENTSO-e [Str12]. Data is based on a working day, peak hours (non-binding values). ENTSO-e member countries are indicated in blue, others in grey. Values indicated in green are either different estimates (lower value on top, country specifying higher value at the bottom) or availability of only one data source (value indicated along with country providing the NTC data). Footnotes are not discussed here as they refer to information not used in this work.

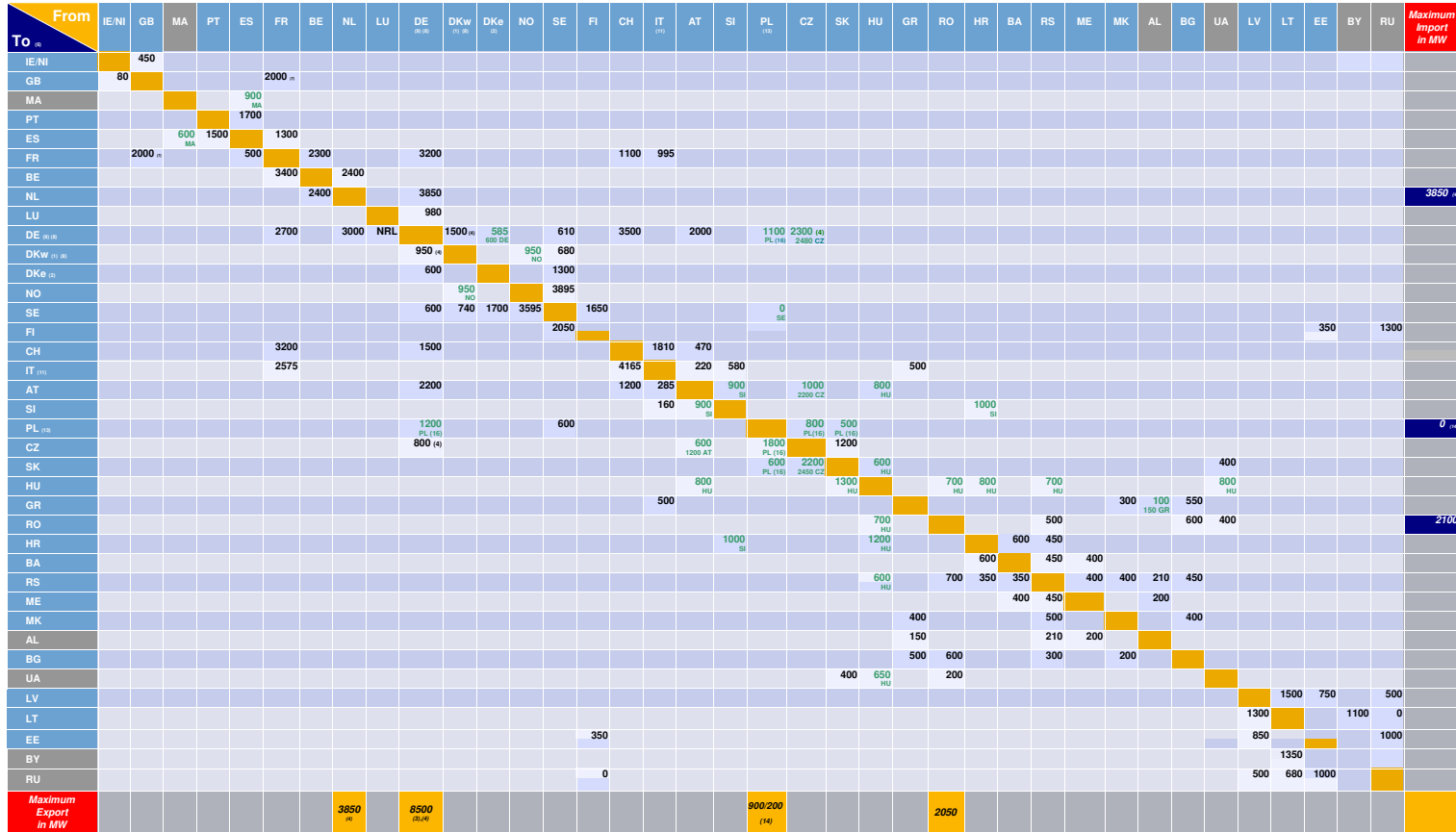


Figure A.15.: Indicative values for winter 2010/2011 net transfer capacities [MW] according to ENTSO-e [Str12]. Data is based on a working day, peak hours (non-binding values). ENTSO-e member countries are indicated in blue, others in grey. Values indicated in green are either different estimates (lower value on top, country specifying higher value at the bottom) or availability of only one data source (value indicated along with country providing the NTC data). Footnotes are not discussed here as they refer to information not used in this work.

A.6. Model parameters for HVDC transmission from MENA to Europe

Year		2010	2020	2030	2040	2050
Cost OL-600 kV	[€/(MW km)]	140	135	130	125	120
Cost SC-600 kV	[€/(MW km)]	975	938	900	863	825
Cost UC-600 kV	[€/(MW km)]	829	797	765	734	701
Cost per Station (x2)	[€/MW]	120000	108000	102000	96000	90000
Gross Capacity HVDC Link						
Gross Capacity HVDC Link	[MW]	4000	4000	4000	4000	4000
Length OL-600 kV	[km]	1600	1600	1600	1600	1600
Investment OL-600 kV	[M€]	896	864	832	800	768
Length SC	[km]	200	200	200	200	200
Investment SC-600 kV	[M€]	780	750	720	690	660
Length UC	[km]	200	200	200	200	200
Investment UC-600 kV	[M€]	663	638	612	587	561
Investment Stations (2)	[M€]	960	864	816	768	720
Overall Cost of HVDC Link	[M€]	3299	3116	2980	2845	2709
Line Losses						
Line Losses OL-600 kV	[%/1000 km]	4.5	4.5	4.5	4.5	4.5
Line Losses SC-600 kV	[%/1000 km]	2.7	2.7	2.7	2.7	2.7
Line Losses UC-600 kV	[%/1000 km]	3.5	3.5	3.5	3.5	3.5
Losses per Station (x2)	[%]	0.7	0.7	0.7	0.7	0.7

Table A.2.: Parameters used for the economic model of the HVDC links connecting MENA to Europe [TSPO12].

A.7. Parameter discussion

In this paragraph a direct excerpt from the investigations carried out by the author in [SGS11] is given regarding a parameter discussion for the technologies photovoltaic, CSP and wind power. The major goal is to enable a better insight in the technical and economic parameters used within the present work. Each section contains a technology-specific discussion on the respective parameters.

Photovoltaic

- Module efficiency η^{PV} and efficiency of the remaining plant (q-factor) q^{PV} :
There is a great variety of photovoltaic technologies with module efficiencies ranging from 8 to 18%. According to Kaltschmitt et al. [KSW05] monocrystalline silicon power plants, currently the predominant technology with a market share above 80% [FMR08], can reach module efficiencies of 16% and q-factors of 73%/78% (for decentralised/centralised systems, respectively). In the present work a module efficiency of some 16% in 2010 [KSW05] and a moderate increase up to 18% [Qua06] by 2030 after which it remains stable for the period until 2050 is assumed. The q-factor is assumed to amount to about 81% in 2010 with an increase to up to some 85% by 2050. These values as well as technological improvement appear to be in reasonable ranges, particularly considering the development over the course of the past decades and today's laboratory efficiencies [GEHW11]. Frankl et al. [FMR08] estimate much higher efficiencies for 2050 of up to 25% for mass market applications, thus the efficiencies used in this work are considered to be conservative values.
- Loss factor f_{loss}^{PV} :
This factor represents loss due to inclination and shadowing effects. Following the discussion of Quaschnig [Qua06], who assesses both pitched and flat roofs for different orientations, annual losses amount to about 10% for centralised and 15% for roof-tops.
- Availability factor f_{av}^{PV} :
Unlike other technologies, photovoltaic systems do not have any moving parts resulting in very little break down or maintenance periods. From the literature no values taking these effects into account could be derived, therefore we assume a very limited time for maintenance as well as breakdown purposes (particularly against the background that maintenance could be carried out during night times) and assume an availability factor of 98%.
- Investment cost C_{inv}^{PV} , fixed cost $C_{node}^{PV, fixed}$ and variable cost $C_{node}^{PV, variable}$:
Investment cost are generally distinguished between centralised and decentralised systems. For this study, cost from Leitstudie [Lei10] are considered. Krewitt et al. [KNK+09] compare PV cost projections of multiple authors and works. The results

of this study (updated with IMF deflators to 2010 prices) indicate that Leitstudie [Lei10] values are in the lower range of the other estimates. Fixed operation cost (operation and maintenance) per year are considered to amount to 1% of the total investment cost while assuming no variable operation cost [Lei10].

- Interest rate p :
The interest rate represents factors such as the risk associated to an investment. Leitstudie [Lei10] estimates the interest rate to amount to 6% while Ecofys [Eco11] gives a range between 7.5 and 8.3% for their low and high risk assessments, respectively. In this study an interest rate of 6% will be assumed, which represents an optimistic value compared to the studies mentioned above.
- Lifetime of the power plant N :
Leitstudie [Lei10] estimates the economic lifetime to amount to 20 years throughout the period from 2010 to 2050. Frankl et al. [FMR08] estimate module lifetimes in 2050 of at least 30 years for the mass market technologies. For both mono- and multicrystalline silicon based modules, lifetimes of at least 40 years are estimated. Therefore the anticipated 20 years can be considered as a conservative figure.

Concentrating Solar Power

- Efficiencies of the power block and the thermal storage:
The power block of a concentrating solar thermal power plant consisting of the turbines to convert heat into movement and the generators to convert the movement into electricity is laid out as in any conventional power plant. State-of-the-art efficiencies of steam power plants are in the order of 47% (hard coal) and 43% (lignite) [COO03]. Leitstudie [Lei10] estimates an efficiency of 46% in 2010 with an increase to some 51% in 2050 for hard coal plants. The turbines are designed for temperatures of 530°C and pressures of 140 bar. CSP power plants cannot reach the efficiency figures mentioned above as the maximum temperature attains 377°C at pressures of 100 bar. Also, the turbine might run in partial load more often. Therefore power block efficiencies of some 37% are assumed [MT10]. Furthermore, the thermal storage systems lose 1% of the stored heat per day [Lai10]. Taking into account that usually the storage is not used for long periods exceeding a couple of days, an efficiency of 95% appears to be reasonable [Lai10].
- Availability factor f_{av}^{CSP} :
Concentrating solar power is a mature technology: No major technology breakthroughs are needed for massive deployment today. The conventional part of a CSP power plant can be compared to any other steam power plant with high availabilities which are merely reduced by maintenance periods. Moreover the solar field can always be maintained during nighttime. Following that discussion, we assume an availability factor of 95% to be a reasonable figure.

- Investment cost C_{inv}^{CSP} , fixed cost $C_{node}^{CSP, fixed}$ and variable cost $C_{node}^{CSP, variable}$.
Investment cost distinguish between cost for the solar field, power block and thermal storage. According to Trieb et al. [TSO⁺09] the sum of the total investment for all components, which is used in this assesment, is based on a scenario of world-wide CSP expansion adopted by Viebahn [VKTL08] as optimistic/realistic scenario. It starts with 354 MW solar power capacity installed in 2005 and expands to 5000 MW by 2015, 150000 MW by 2030 and 500000 MW by 2050. The CSP cost model considers current oil-cooled parabolic trough technology with molten salt storage and steam cycle power block with dry cooling tower as reference. The figures for the single components are in good agreement with Sargent and Lundy [Sar09] where the share of the solar field is estimated to account for 68% of the total investment cost. No variable costs are considered, however for maintenance fixed operation costs of 2.5% p.a. of the total investment cost are assumed [Deu09]. These projections are also consistent with Leitstudie figures [Lei10].
- Lifetime of the power plant N:
Leitstudie [Lei10] estimates the economic lifetime to amount to 25 years throughout the period from 2010 to 2050. This is consistent with Trieb et al. [TSO⁺09]. Kolb [Kol06] gives a figure for an expected lifetime of 30 years. Deutsche Bank [Deu09] estimates the technical lifetime to amount to at least 25 to 30 years. An economic lifetime of 25 years [Lei10], which is used in this assessment, therefore appears to be within the estimates which are currently discussed.
- Installation density:
The installation density is determined considering the total area which is occupied by a CSP plant with a specified power capacity. Distances between the troughs, service roads, cooling devices and the power block are considered. For this assesment, the area-specific installable capacity of the solar field is derived using data from [Sok04]. In this case, an area of 0.5 km² is occupied by the power plant with a heat output from the solar field amounting to some 90 MW when illuminated with 800 $\frac{W}{m^2}$, the reference irradiance for specifying the installable capacity. Thus, the area-specific installable capacity of the solar field is determined to be 176.2 $\frac{MW}{km^2}$. Please note that this is the heat capacity per km², expressed by the thermal capacity density factor.

Wind Power

- Nominal capacity wind turbine:
Lu et al. [LMK09] use 2.5 and 3.6 MW for on- and offshore deployment, respectively, in 2009. Archer and Jacobsen [AJ05] use a 1.5 MW onshore turbine in their assessment. In this work we will refer to Leitstudie [Lei10], which uses 1.95 and 4.5 MW for on- and offshore deployment, respectively, in 2010. For onshore wind power, the values are rather conservative as 7.5 MW onshore power plants are already available for construction [Ene12], for offshore deployment, the scenario

development until 2050 can be considered to be feasible, but not conservative, as the largest offshore capacities currently being installed do not exceed 5 MW. Jonkman et al. [JBMS09] use hub heights of 90 and rotor diameters of 126 m in 2009, in this work hub heights ranging from 112 to 132 m (onshore) and 80 to 140 m (offshore) are used. Hub heights of 135 m are already on the market for onshore systems (e.g. Enercon E-126), so that the figures used in this work's scenario years can be considered conservative. For rotor diameters a range from 77 to 130 m (onshore) and 96 to 192 m (offshore) are considered. These values are in line with Leitstudie [Lei10]. Hassing et al. [H+08] even indicate higher figures for hub heights and rotor diameters, which underlines that the figures used in this work are moderate.

- Availability factor f_{av}^{wind} :
According to Leitstudie [Lei10], in this work an overall availability both for on- and offshore plants of 95% is considered. Unlike the case for PV or CSP, wind power plants can also operate during night time, which is why maintenance cannot be deferred to periods with no resource availability. On the other hand, maintenance time which requires a complete shut down of a plant is overseeable, therefore the assumption made in this work appears reasonable.
- Investment cost C_{inv}^{wind} , fixed cost $C_{node}^{wind, fixed}$ and variable cost $C_{node}^{wind, variable}$:
Several studies indicate that the onshore investment cost values in this assessment (according to Leitstudie [Lei10]) can be considered to be reasonable. EWI, GWS and Prognos [EGP10], the European wind Energy Association [EWE08] and Greenpeace [GWE10] use figures that represent the anticipated development in this assessment from 2010 through 2050 as indicated in the overview of table A.3:

2010	2020	2030	2040	2050	Source
	1048	1003	977	967	[EWI]
1331	1039	988	948	907	[Leitstudie]
1300	895	854			[EWEA]
1327	1240	1216	1204	1200	[GWEO]
1329	1208	1116	1068	1036	[GWEO]
1328	1172	1093	1037	1006	[GWEO]
1300	1019	954	943	943	[Energy Revolution]
1300 - 2275					[IPCC]

2010	2020	2030	2040	2050	Source
3327	2117	1815	1512	1311	[Leitstudie]
	2443	1700	1501	1374	[EWI]
2438	1354	1300			[EWEA]
2265	1745	1571		1484	[IEA-ETP]
3251	2243	1902	1712	1636	[Energy Revolution]
3467 - 5418					[IPCC]

Table A.3.: Investment cost for onshore (top table) and offshore wind plants (bottom table) in $\left[\frac{\text{€}}{\text{kW}}\right]$ according to different authors. In this assessment, values from Leitstudie [Lei10] are used. Investment cost are expressed in terms of 2010 price levels using deflators from the International Monetary Fund [IMF10].

For onshore wind 4% and for offshore wind 5.5% of the total investment cost are estimated to arise per annum [Lei10] as fixed cost due to operation and maintenance. No variable cost are considered. Other sources suggest values in the range of 1.5% through 3% [TK] so that the values used in this assessment are considered conservative. To derive the uncertainty of investment cost, a sensitivity analysis is carried out considering the top and bottom investment cost values of the tables presented above for the respective scenario years.

- Lifetime of the power plant N:
Economic lifetimes both for on- and offshore wind power plants are considered to amount to 18 years [Lei10].
- Area-specific installable capacity:
In order to derive this parameter, the necessary distance between the wind power plants must be determined. High distances between wind turbines reduce turbulence and the negative effects associated with it (e.g. material stress or lower electricity yield), whereas low distances lead to higher installation densities (in $[\frac{W}{m^2}]$). The distance between the turbines is given as a multiple of the rotor diameter, the so called distance factor $f_{distance}^{wind}$. According to Kaltschmitt et al. [KSW05], values for $f_{distance}^{wind}$ lie between 6 and 15 when no wind direction is prevalent and with a prevalent wind direction, $f_{distance}^{wind}$ is chosen between 8 and 10 in the prevalent wind direction and between 4 and 5 normal to it, resulting in a much denser formation. When area availability is limited, smaller distance factors are sometimes chosen. Here, $f_{distance}^{wind}$ was set to 6 without distinguishing between different wind directions [Sch12]. Future developments of wind technology suggest that both nominal capacities as well as turbine diameters will increase, causing an increase in the distances needed in order to reduce interferences. In this study, nominal capacities and rotor diameters are determined as to maintain the area specific installable capacity at a constant value throughout the scenario years. Using this approach yields identical area-specific installable capacities' figures for all scenario years of some $10.4 \frac{MW}{km^2}$. This value is comparatively high compared to other assessments using figures between 4 and $9 \frac{MW}{km^2}$, which is primarily due to higher distance factors used.

List of Figures

1.1. Outline of the intended workflow for this thesis. Dashed boxes indicate amendments or new developments (milestones MS 1 to MS 6). Enhancements to the tools REMix-EnDaT and REMix-OptiMo are made. REMix-PlaSMo is a new feature within the REMix modelling environment. These three REMix modules are eventually employed in three applications (AP A to AP C).	4
2.1. Historical development of the energy modeling environment REMix (Renewable Energy Mix). It is composed of the three major modules EnDaT, PlaSMo and OptiMo. Major contributions to these modules are highlighted in green (EnDaT), yellow (PlaSMo) and blue (OptiMo). Adjacent components are highlighted in purple and red.	8
2.2. Setup of the energy modeling environment REMix (Renewable Energy Mix). It is composed of the three major modules EnDaT, PlaSMo and OptiMo. Enhancements to REMix added within the present work are highlighted in red. Credits: CSP plant photo [DLR14b], wind plant photo [DLR14a], portfolio dispatch graph [Sch09a].	11
3.1. Structure of the present chapter.	13
3.2. Processing chain in order to determine the installable capacity of one specific technology for a given pixel. First of all the suitable sites are found and their total share of the pixel is derived. Second, the area of the pixel is calculated as a function of its geographic position (latitude). Third, these two items are combined to come up with the suitable area for power plant installation. Using the latter along with the area-specific installation density yields the installable capacity (source for globe image: [Eur]).	15
3.3. Results for suitable shares for power plant installation using the approach discussed in this section. The color code ranges from 0 (0% suitable) to 1 (100% suitable). White areas are completely excluded.	17
3.4. Various global maps used within the tool REMix-EnDaT, from top to bottom: Identification of countries and their exclusive economic zones, distances to settlements [<i>km</i>], terrain slopes [$^{\circ}$] and elevations [<i>m</i>] with respect to sea level.	19

3.5. Processing chain for computation of GHI data. Clear sky GHI data, provided by DLR and data from NASA SRB release 3.0 [SRB12] were combined in order to determine hourly global horizontal irradiance data with a spatial resolution of $0.45^\circ \times 0.45^\circ$	25
3.6. Annual average of global horizontal irradiance resulting from the 22 year data set processed in this work, covering a time frame from 1984 through 2005. The values presented are displayed in $\left[\frac{kWh}{m^2 \cdot a}\right]$. Overall, solar irradiance is naturally higher the closer the site is located to the equator. Furthermore, the height above sea level and regional weather patterns also impact on the incidenting irradiance at ground level.	26
3.7. Map indicating the stations used for cross-checks of both processed GHI and BNI data as well as for the generation of hourly BNI data using an empirical approach. Data is kindly provided by the Baseline Surface Radiation Network BSRN [BSR12]. Abbreviations represent Alice Springs (ASP), Barrow (BAR), Bermuda (BER), Billings (BIL), Bondville (BON), Boulder (BOU), Cambourne (CAM), Carpentras (CAR), Chesapeake Light (CLH), Cocos Islands (COC), De Aar (DAA), Darwin (DAR), Desert Rock (DRA), South Great Plains (E13), Florianopolis (FLO), Fort Peck (FPE), Ilorin (ILO), Kwajalein (KWA), Lauder (LAU), Lindenberg (LIN), Lerwick (LER), Momote (MAN), Nauru Island (NAU), Palaiseau Cedex (PAL), Payerne (PAY), Rock Springs (PSU), Regina (REG), Sede Boqer (SBO), Solar Village (SOV), Sioux Falls (SXF), Tamanrasset (TAM), Tateno (TAT), Toravere (TOR), Xianghe (XIA).	28
3.8. Scatter plot derived from cross-checking the processed NASA GHI data set with ground station measurements of the BSRN network. A correlation coefficient of 0.9 and a root mean bias deviation of -3.94% are achieved, indicating very good agreement between the assessed data.	29
3.9. Distribution functions of BNI annual sums for a window comprising Southern Europe and the Middle East / North Africa provided by Hoyer-Klick [HKSS]. High resolution data provided by SOLEMI [SOL12] is aggregated from 1 km to 100 km in order to obtain comparable values. A qualitative agreement can be observed between NASA [SRB12] and SOLEMI data [SOL12]. However, ISIS data [ISI12; Loh06] yields distributions which are out of the range of the other benchmarks.	30
3.10. Processing chain for computation of BNI data as used in approach (i-B). Clear sky BNI data, provided by DLR and data from NASAs SRB release 2.5 [SRB12] are combined in order to determine hourly beam normal irradiance data with a spatial resolution of $0.45^\circ \times 0.45^\circ$	33
3.11. Exemplary scatter plot of clearness index over diffuse fraction for the BSRN station Billings. Means (indicated in red) and standard deviations of the diffuse fraction are determined and interpolated for ten bins, yielding a corridor of quality checked data between the lower and upper boundaries indicated in green.	35

3.12. BNI long term annual average provided by NASA SRB 3.0 [SRB12]. This map is used as reference for the cross-check to the five BNI data sets established in this work.	36
3.13. Comparison of the five processed beam normal irradiance data sets (physical (i-A), physical (i-B), empirical (ii-A), empirical (ii-B), empirical (iii)) to 18 BSRN ground stations and to NASA SSE 6.0/SRB 3.0 annual BNI sum [SRB12]. For the former the four indicated figures beneath the distribution graphs on the left are derived as an average for the 18 sites: Satellite data mean, mean bias deviation, root mean bias error and correlation. For the latter the overall map deviation is determined. It is indicated beneath the distribution graphs on the very right. Data set (ii-B) is chosen for further assessments in this work.	37
3.14. Final BNI long term annual average as obtained by empirical approach ii-B. This data set is the best performer in cross-checks with BSRN ground measurements and NASA BNI annual average.	38
3.15. Illustration of earth's major wind systems according to [WIN12]	39
3.16. Annual average of the resulting wind speed at a height of 50 m out of the 22 year wind speed data set processed within this work. Indicated values are displayed in $\left[\frac{m}{s}\right]$. Good average wind speeds are generally found in regions with little roughness lengths such as water bodies or deserts. On the other hand, regions with high surface roughness length values, e.g. forests, result in inferior average wind speeds.	41
3.17. Annual long term average of the river discharge in $\left[\frac{km^3}{a}\right]$ based on data of the WaterGap model [HD07; DFZ09] and processed within this work. The major river systems can be identified.	43
3.18. Cascade of different potential classes, all of which being assessed in this work except for economic and tapped potentials. It can be seen how the energy content narrows down from theoretical towards tapped potentials.	49
3.19. Approach used in this work to determine the typical meteorological year for one site.	54
3.20. Different possible plant layouts of a CSP plant can be expressed in terms of the solar multiple [TSO+09].	56
3.21. The full load hours of a CSP plant are a function of the irradiance and the solar multiple [TSO+09].	57
3.22. World regions for which the assessments are carried out.	58
3.23. Results for full load hours for photovoltaic power plants in 2010. Top: Theoretically achievable full load hours without any land exclusion criteria. Bottom: Remaining surfaces with respective full load hours after land exclusion.	59

3.24. Results for full load hours for concentrating solar power plants in 2010. The figures refer to the full load hours of the solar field. Top: Theoretically achievable full load hours without any land exclusion criteria. Bottom: Remaining surfaces with respective full load hours after land exclusion and minimum resource boundary condition of an annual beam normal irradiance (BNI) sum of $1800 \frac{kWh}{m^2 \cdot a}$	60
3.25. Results for full load hours for onshore and offshore wind power plants in 2010. Top: Theoretically achievable full load hours without any land exclusion criteria. Bottom: Remaining surfaces with respective full load hours after land exclusion and minimum resource boundary condition of an annual mean wind speed of $4 \frac{m}{s}$	61
3.26. Results of global electricity generation potentials for the technologies photovoltaic, concentrating solar power, on- and offshore wind and hydro power. The two figures on the left are expressed in terms of cumulated potentials, the top graphs are indicated as a function of full load hours, the bottom graphs as a function of cost. All graphs refer to the year 2010.	63
3.27. Results of the potential assessment for the regions (from top to bottom) OECD Europe, OECD North America, OECD Pacific, Transition Economies and China. Figures for electricity generation, average full load hours and capacity factors as well as cost are displayed. The analysis is carried out for the years 2010, 2030 and 2050.	66
3.28. Results of the potential assessment for the regions (from top to bottom) India, Rest of developing Asia, Latin America, Africa and Middle East. Figures for electricity generation, average full load hours and capacity factors as well as cost are displayed. The analysis is carried out for the years 2010, 2030 and 2050.	67
3.29. Sensitivity analysis focusing on the deviations of the resulting full load hours after performing a single technical parameter variation. All parameters except for the rotor diameter of wind plants show a linear behavior. For CSP, an initial solar multiple at 100% of 2.5 is considered.	72
3.30. Results of multiple sensitivity analyses focusing on the deviations of the resulting cost per kWh after performing a single economic parameter variation. Particularly full load hours have the greatest impact on the resulting cost estimations.	73
3.31. Accumulation of highly resolved data to a coarse pixel according to Hoyer-Klick [HKSS], displayed values in $\left[\frac{kWh}{pixel \cdot a} \right]$. Since solar annual irradiance sums behave rather homogeneous over great distances, the average value of a coarse pixel represents well the distribution of its highly resolved counterparts.	75
3.32. Comparison of the effect of accumulation on the annual beam normal irradiance sums provided by Hoyer-Klick [HKSS]. The coarser the data - from top to bottom - the more details are lost.	76

3.33. Comparison of coarsely and highly resolved wind data according to Badger [Bad12]. The resolution is indicated in italic figures. Next to each graph, the average value and the mean of the windiest 50% are displayed, the latter in red. With increasing spatial resolution, i.e. from 10 km to 100 m, the mean values increase.	77
4.1. Structure of the present chapter.	82
4.2. Anticipated effects on the residual load using the optimization modes for variance minimization of the output (left) and the residual load (right).	84
4.3. Processing chain for the determination of the overall cost of a portfolio only consisting of PV, CSP, wind and hydro power. Hourly load and hydro power generation data (top left and right) are used to determine a "90% load" and a "CSP load A" according to the "10% rule". These 10% are intended to be met by firm capacity provided by hydro and - if necessary - by CSP, to ensure stable power grid operation. The "90% load" data serves as input to the volatile "PlaSMo" runs (bottom left), which are carried out with cumulated PV and wind shares in the range of 10 to 80% of annual (90%) power demand using three modes: least cost, output variance and residual load variance minimization. "CSP load A" resulting from the "10% rule" and the residual load curves of each respective run - "Residual (CSP) load B" - are summed up to obtain a "Final residual load A+B", in turn being met with an optimized "CSP layout" (center right). Eventually, for each run the overall "cost per kWh" are determined (bottom right).	90
4.4. Load duration curves for Morocco for the years 2010, 2030 and 2050. A sharp increase in peak load demand is visible. For the original load cases, it rises from about 5.6 GW in 2010 to more than 31 GW projected for 2050. Also, annual electricity consumption, i.e. the integral of each of the curves presented, rises from about 34 TWh in 2010 to approximately 190 TWh in 2050. 10% of this load is to be met with firm capacity provided by hydro and - for all cases when hydro cannot provide sufficient power - CSP.	91
4.5. Net generation cost of the portfolio comprised of PV, wind, CSP and hydro as a function of the volatile annual electricity generation share.	94
4.6. Comparison of the CSP plant layouts for the optimum volatile annual electricity generation in the case least cost and variance minimization in 2050. The latter case has higher net generation cost.	95
4.7. Net generation cost of the volatile portfolio (top) and CSP (bottom).	96

4.8.	Development of the shares of the installed capacities and generation as a function of the volatile annual electricity generation shares. Load, which is not met by the volatile generation (PV and wind) is satisfied by hydro and CSP. Due to this setup, CSP shares are very high for small volatile generation shares. The double-dashed vertical lines indicate the feasibility barriers: To the left, solutions are found that entirely obey the set of boundary conditions, to the right the surplus restriction cannot be met.	98
4.9.	Electricity supply for a winter week resulting from the optimizations depicted for the cost minimization case for the years 2010 (top), 2030 (center) and 2050 (bottom).	101
4.10.	Electricity supply for a summer week resulting from the optimizations depicted for the cost minimization case for the years 2010 (top), 2030 (center) and 2050 (bottom).	102
5.1.	Structure of the present chapter. The enhanced version of REMix-OptiMo resulting from the methodology section is used for a validation of an energy scenario.	106
5.2.	Mean net transfer capacities according to ENTSO-e [Str12]. Displayed values indicate the average of the figures from summer 2010 and winter 2010/2011. All links are included in the model, the line lengths are approximated as the distances of the geographical centers.	111
5.3.	Graphs indicating the overall installed capacities (top), electricity generation (center) and CO ₂ emissions (bottom) for the total of 30 European countries assessed within the original release of TRANS-CSP [TSK ⁺ 06] (left) and three new scenarios altogether based on updated figures for electricity consumption and supply: TRANS-CSP update (center-left), Island Europe (center-right) and Maximum Renewable Energy Share (right). For the three updated scenarios the overall demand increases from some 4000 TWh/a in 2050 (as used in the original release) to some 6000 TWh/a (as used in the new scenarios presented here) primarily caused by the inclusion of electromobility and electrical heating as loads.	114
5.4.	CSP import capacities implemented into the REMix-OptiMo environment according to an updated framework of Trieb et al. [TSK ⁺ 06]. The different colors indicate the year of commissioning of each respective line, indicated values next to the lines represent the net import capacities [MW], i.e. net feed-in at the terminal node after power transmission loss. Dashed grey lines show the existing AC grid.	121
5.5.	Geographic illustration of CSP plant sites located in North Africa and the Middle East interconnected via high voltage direct current power lines to various centers of demand in Europe [TSPO12; REA11]. High population densities corresponding to the centers of demand and advantageous sites in terms of solar irradiance are connected.	122

5.6.	Comparison of the aggregated results for all 30 countries considered. The validation simulations are carried out for 2010, 2030 and 2050. The columns present the results of the scenario (denoted with the 2010-S, 2030-S and 2050-S) and the REMix-OptiMo runs (denoted with 2010-R, 2030-R and 2050-R).	125
5.7.	Shares of power generation, AC and CSP imports displayed for each country for the year 2010. Data on AC transmission between the countries is presented in terms of overall transferred annual power $[\frac{TWh}{a}]$ and the connection's mean annual line utilization [%].	128
5.8.	Shares of power generation, AC and CSP imports displayed for each country for the year 2030. Data on AC transmission between the countries is presented in terms of overall transferred annual power $[\frac{TWh}{a}]$ and the connection's mean annual line utilization [%].	130
5.9.	Shares of power generation, AC and CSP imports displayed for each country for the year 2050. Data on AC transmission between the countries is presented in terms of overall transferred annual power $[\frac{TWh}{a}]$ and the connection's mean annual line utilization [%].	132
5.10.	Mean monthly bi-directional power transmission [GW] resulting from the REMix-OptiMo validation simulations. Data for the years 2010, 2030 and 2050 is indicated in blue, red and green, respectively. The presentation is limited to the second nearest neighbors of Germany for reasons of clarity.	135
A.1.	Description of the major components of earth's energy budget [SSE12]. Incoming irradiation is absorbed, scattered and reflected due to various mechanisms. The values indicated in yellow boxes (all in $[\frac{W}{m^2}]$) are derived from the NASA Solar Radiation Budget Release 3.0 [SRB12], serving as input for parts of the assessment within this work.	159
A.2.	OECD Europe: Results of electricity generation potentials for the technologies photovoltaic, concentrating solar power, on- and offshore wind and hydro power. The two figures on the left are expressed in terms of cumulated potentials, the top graphs are indicated as a function of full load hours, the bottom graphs as a function of cost.	162
A.3.	OECD North America: Results of electricity generation potentials for the technologies photovoltaic, concentrating solar power, on- and offshore wind and hydro power. The two figures on the left are expressed in terms of cumulated potentials, the top graphs are indicated as a function of full load hours, the bottom graphs as a function of cost.	163
A.4.	OECD Pacific: Results of electricity generation potentials for the technologies photovoltaic, concentrating solar power, on- and offshore wind and hydro power. The two figures on the left are expressed in terms of cumulated potentials, the top graphs are indicated as a function of full load hours, the bottom graphs as a function of cost.	164

A.5. Transition Economies: Results of electricity generation potentials for the technologies photovoltaic, concentrating solar power, on- and offshore wind and hydro power. The two figures on the left are expressed in terms of cumulated potentials, the top graphs are indicated as a function of full load hours, the bottom graphs as a function of cost.	165
A.6. China: Results of electricity generation potentials for the technologies photovoltaic, concentrating solar power, on- and offshore wind and hydro power. The two figures on the left are expressed in terms of cumulated potentials, the top graphs are indicated as a function of full load hours, the bottom graphs as a function of cost.	166
A.7. India: Results of electricity generation potentials for the technologies photovoltaic, concentrating solar power, on- and offshore wind and hydro power. The two figures on the left are expressed in terms of cumulated potentials, the top graphs are indicated as a function of full load hours, the bottom graphs as a function of cost.	167
A.8. Rest of developing Asia: Results of electricity generation potentials for the technologies photovoltaic, concentrating solar power, on- and offshore wind and hydro power. The two figures on the left are expressed in terms of cumulated potentials, the top graphs are indicated as a function of full load hours, the bottom graphs as a function of cost.	168
A.9. Latin America: Results of electricity generation potentials for the technologies photovoltaic, concentrating solar power, on- and offshore wind and hydro power. The two figures on the left are expressed in terms of cumulated potentials, the top graphs are indicated as a function of full load hours, the bottom graphs as a function of cost.	169
A.10. Africa: Results of electricity generation potentials for the technologies photovoltaic, concentrating solar power, on- and offshore wind and hydro power. The two figures on the left are expressed in terms of cumulated potentials, the top graphs are indicated as a function of full load hours, the bottom graphs as a function of cost.	170
A.11. Middle East: Results of electricity generation potentials for the technologies photovoltaic, concentrating solar power, on- and offshore wind and hydro power. The two figures on the left are expressed in terms of cumulated potentials, the top graphs are indicated as a function of full load hours, the bottom graphs as a function of cost.	171
A.12. Sustainability criteria narrowing down the TRANS-CSP target function and technical constraints imposed by the available portfolio of technologies and resources for power generation as considered in the TRANS-CSP scenario [TMS07].	174
A.13. Criteria narrowing down the TRANS-CSP target function and technical constraints imposed by the available portfolio of technologies and resources for power generation as considered in the TRANS-CSP scenario [TMS07].	175

A.14.Indicative values for summer 2010 net transfer capacities [MW] according to ENTSO-e [Str12]. Data is based on a working day, peak hours (non-binding values). ENTSO-e member countries are indicated in blue, others in grey. Values indicated in green are either different estimates (lower value on top, country specifying higher value at the bottom) or availability of only one data source (value indicated along with country providing the NTC data). Footnotes are not discussed here as they refer to information not used in this work.	191
A.15.Indicative values for winter 2010/2011 net transfer capacities [MW] according to ENTSO-e [Str12]. Data is based on a working day, peak hours (non-binding values). ENTSO-e member countries are indicated in blue, others in grey. Values indicated in green are either different estimates (lower value on top, country specifying higher value at the bottom) or availability of only one data source (value indicated along with country providing the NTC data). Footnotes are not discussed here as they refer to information not used in this work.	192

List of Tables

3.1. Overview on the final exclusion criteria to determine suitable areas for power plant installation.	18
3.2. Data used for the determination of the area-specific installation capacities (top) and the resulting values (bottom) according to Scholz [Sch12].	20
3.3. Summary of the different data sets presented above. The Solar Radiation Budget data sets (releases 2.5 and 3.0) [SRB12] provided by NASA were chosen for the further analyses.	24
3.4. Fitting coefficients according to Ruiz et al. [RAA ⁺ 10] for the models (ii-A) and (ii-B).	34
3.5. Overview of existing reanalysis data sets. Wind speed data from the Modern Era Retrospective-analysis for Research and Applications - MERRA - product [MER12] is used in this work.	40
3.6. Technical parameters used in this work, according to Scholz [Sch12].	44
3.7. Hub heights used for the calculation of the resulting wind speed according to Scholz [Sch12].	47
3.8. Values used in this thesis for the determination of the arising cost based on Scholz [Sch12].	51
3.9. Initial parameters used for the sensitivity analysis, corresponding to the 100% cases.	71
5.1. Installed capacities according to the updated TRANS-CSP framework for pathway #1, which are used in the 2010 validation run.	116
5.2. Installed capacities according to the updated TRANS-CSP framework for pathway #1, which are used in the 2030 validation run.	117
5.3. Installed capacities according to the updated TRANS-CSP framework for pathway #1, which are used in the 2050 validation run.	118
5.4. Gross and net capacities of CSP plants referred to their respective exporting and importing countries. Due to transmission losses, gross and net capacities differ considerably for scenario pathway #1.	120
5.5. Overview on all lines with more elaborate data on line end points, lengths, import capacities and loss based on Trieb et al. [TSPO12; REA11]. Values of net import capacities are derived within an update of TRANS-CSP. All power plants indicated in red are added to the original framework to meet the massive demand increase.	123

5.6.	Results of the REMix-OptiMo validation run compared in terms of technologies to the validated scenario. Positive (negative) deviations of the REMix-OptiMo results in [%] are indicated in red (blue), agreement in green. The results of the scenario are denoted with the 2010-S, 2030-S and 2050-S. The REMix-OptiMo runs are denoted with 2010-R, 2030-R and 2050-R.	126
5.7.	Country specific data as presented in figure 5.7 for the year 2010 on the power generation, AC and CSP imports, pumped storage utilization, domestic power generation, demand and the import-export balance. Values in brackets are taken from the scenario framework. All indicated numbers are in $[\frac{TWh}{a}]$	129
5.8.	Country specific data as presented in figure 5.8 for the year 2030 on the power generation, AC and CSP imports, pumped storage utilization, domestic power generation, demand and the import-export balance. Values in brackets are taken from the scenario framework. All indicated numbers are in $[\frac{TWh}{a}]$	131
5.9.	Country specific data as presented in figure 5.9 for the year 2050 on the power generation, AC and CSP imports, pumped storage utilization, domestic power generation, demand and the import-export balance. Values in brackets are taken from the scenario framework. All indicated numbers are in $[\frac{TWh}{a}]$	133
A.1.	World regions used for the potential assessments in this work [SGS11].	161
A.2.	Parameters used for the economic model of the HVDC links connecting MENA to Europe [TSPO12].	193
A.3.	Investment cost for onshore (top table) and offshore wind plants (bottom table) in $[\frac{\text{€}}{kW}]$ according to different authors. In this assessment, values from Leitstudie [Lei10] are used. Investment cost are expressed in terms of 2010 price levels using deflators from the International Monetary Fund [IMF10].	199

Erklärung über die Eigenständigkeit der Dissertation

Ich versichere, dass ich die vorliegende Arbeit mit dem Titel

”Enhancement of the REMix energy system model:
Global renewable energy potentials,
optimized power plant siting
and scenario validation”

selbstständig verfasst und keine anderen als die angegebenen Quellen und Hilfsmittel benutzt habe. Aus fremden Quellen entnommene Passagen und Gedanken sind als solche gekennzeichnet.

Declaration of Authorship

I hereby certify that the dissertation entitled

”Enhancement of the REMix energy system model:
Global renewable energy potentials,
optimized power plant siting
and scenario validation”

is entirely based on my own work except where stated otherwise. Passages and ideas from other sources have been clearly indicated.

Stuttgart, 28.12.2012

Daniel Stetter

Curriculum Vitae

Daniel Stetter

born on November 28th, 1980

in Heidelberg, Germany

2009-2012	PhD candidate	University of Stuttgart and German Aerospace Center DLR Visiting Scientist at Ecole Nationale Supérieure des Mines de Paris, France
2011	Diploma for Graduates in Economics	University of London International Programmes / London School of Economics and Political Science, UK
2007	Master of Science in Physics	Karlsruhe Institute of Technology, Germany Master Thesis on III-V multi-junction solar cells at Fraunhofer ISE Academic exchange with Institut National des Sciences Appliquées INSA Lyon, France
2000	Baccalaureat	Gymnasium Walldorf, Germany
1998	Honorary High School Diploma	Port Townsend High School, WA, USA Scholar of the 14th Congress-Bundestag Youth Exchange

